

Copyright
by
Christopher Scott Spaeth
2011

**The Dissertation Committee for Christopher Scott Spaeth Certifies that this is the
approved version of the following dissertation:**

**cAMP and Oxidative Mechanisms of Plasmalemmal Sealing and the Effects on
Rapid and Long Lasting Repair of Severed Axons *in vivo* by Polyethylene Glycol.**

Committee:

George Bittner, Supervisor

Jennifer Morgan

Harold Zakon

Adela Ben-Yakar

Kevin Dalby

**cAMP and Oxidative Mechanisms of Plasmalemmal Sealing and the Effects on
Rapid and Long Lasting Repair of Severed Axons *in vivo* by Polyethylene Glycol.**

by

Christopher Scott Spaeth, BSc

Dissertation

Presented to the Faculty of the Graduate School of

The University of Texas at Austin

in Partial Fulfillment

of the Requirements

for the Degree of

Doctor of Philosophy

The University of Texas at Austin

May 2011

Dedication

This dissertation is dedicated to my parents, for their continuous and unwavering support.

Acknowledgements

This work would not be possible without the support, advice, assistance and encouragement of many individuals, including financial support from the Lone Star paralysis institute awarded to Dr. George Bittner. First and foremost, I would like to thank my adviser, Dr. George Bittner, who gave me the opportunity and the tools to succeed. Under Dr. Bittner's guidance, I grew out of my former immaturity, and learned how to effectively undertake and complete multiple projects. I will always be indebted to Dr. Bittner, since he taught me what it means to be a researcher. Dr. Bittner's direct and honest critiques, sprinkled with healthy doses of humor, are something I would like to emulate. I would also like to thank my committee members, Dr. Harold Zakon, Dr. Jennifer Morgan, Dr. Adela Ben-Yakar, and Dr. Kevin Dalby, for always being available for questions and advice, for listening to me when I needed someone to talk to, and for helping direct my research to meaningful and unambiguous results. I would also like to thank Dr. Bing Zhang, who taught me what hard work truly means, and demonstrated what it looked like.

I have been fortunate to work closely with very talented colleagues and co-authors, who helped with experiments, listened to my (sometimes crazy) ideas, read and edited my papers and grants, and made my working experience much better just by being present. For these, and many other reasons, I would like to thank Josh Britt, Aleksej Zuzek, Lauren Figard, Taylor Robison, Rip Wilcott, Jerry Fan, Cody Estler, Jackie Kane, Yasmeen Jaber, and Andrew Trang. I would also like to thank Dr. Tim Schallert for his help with animal work and writing papers, and Dr. Francisco Gonzalez-Lima for his gift of Methylene Blue and providing helpful comments on experiments.

My family has been incredibly patient and understanding during my graduate career. They have heard about both good and bad, and understood all the times I forget to return their calls, forgave me for all the missed holidays and birthdays, and despite all my shortcomings as a son and brother, still invited me home whenever I had time. To my parents Phil and Carol and my sisters Jill and Jenn – I could not have finished my thesis without your support. I would also like to thank Matt Talboo, for his understanding ear, worthwhile advice, and for reminding me that missing too many NFL games makes me cranky.

Last, but certainly not least, I would like to thank my fiancée, Elaine Boydston, who helped with experiments, read and edited my papers and grants, and provided me with more support than any one person would be expected to, both inside and outside of the laboratory.

**cAMP and Oxidative Mechanisms of Plasmalemmal Sealing and the Effects on
Rapid and Long Lasting Repair of Severed Axons *in vivo* by Polyethylene Glycol.**

Publication No. _____

Christopher Scott Spaeth, Ph.D.
The University of Texas at Austin, 2011

Supervisor: George Bittner

Traumatic neuronal injury inevitably causes plasmalemmal damage, and sometimes leads to axonal severance. For any eukaryotic cell to survive following traumatic injury, the plasmalemma must be repaired (sealed). Plasmalemmal sealing occurs via a Ca^{2+} -dependent accumulation of vesicles or other membranous structures that form a plug at the damage site. Using uniquely identified and damaged rat hippocampal B104 cells that extend neurites with axonal properties, or rat sciatic nerves, plasmalemmal sealing is assessed by exclusion of an extracellular dye from each damaged B104 cell, or sciatic nerves *ex vivo*.

B104 cells with neurites transected nearer ($<50\ \mu\text{m}$) to the soma seal at a lower frequency and slower rate compared to cells with neurites transected farther ($>50\ \mu\text{m}$) from the soma. Sealing in B104 cells is enhanced by 1) increased [cAMP], 2) increased PKA activity, 3) increased Epac activity, 4) H_2O_2 and 5) Poly-ethylene glycol (PEG). Sealing is decreased by 1) PKA inhibition, 2), Botulinum toxins A, B, E, 3) Tetanus toxin 4), NEM, 5) Brefeldin A, 6) nPKC inhibition, 7) DTT, 8) Melatonin and 9) Methylene Blue. Substances (NEM, Bref A, PKI, db-cAMP, PEG) that affect plasmalemmal sealing

in B104 cells *in vitro* have similar effects on plasmalemmal sealing in rat sciatic nerves *ex vivo*. Based on data from co-application of enhancers and inhibitors of sealing, I propose a plasmalemmal sealing model having four partly redundant, parallel pathways mediated by 1) PKA, 2) Epac, 3) cytosolic oxidation and 4) nPKCs. The identification and confirmation of these pathways may provide novel clinical targets for repairing and/or recovery from traumatic injury.

The fusogenic compound PEG rapidly repairs axonal continuity of severed axons, potentially by rejoining severed proximal and distal axons. PEG-fusion is influenced by plasmalemmal sealing, since unsealed axons are easier to PEG fuse. I demonstrate that PEG restores morphological continuity, and improves behavioral recovery following crush-severance to sciatic nerves in rats *in vivo*. Co-application of Mel or MB prior to PEG application further improves PEG fusion (as measured by electrophysiology) and behavioral recovery following crush-severance *in vivo*. These PEG data may provide novel clinical techniques for rapidly repairing axonal severance.

Table of Contents

List of Tables:	xiv
List of Figures:	xv
 Chapter 1: General Introduction:	 1
Traumatic Injury:	1
Plasmalemmal Sealing:	3
Membrane Fusion Proteins:	4
cAMP in survival and regeneration of damaged axons:	7
Protein Kinase activated by cAMP:	9
Exchange protein activated by cAMP:	10
Convergence/Divergence of PKA and Epac activities:	13
Oxidative Enhancement of Plasmalemmal Sealing:	13
Polyethylene Glycol:	16
Summary:	18
 Chapter 2: A Model for Repairing Plasmalemmal Damage:	 22
Abstract:	22
Introduction:	23
Methods:	25
B104 cells:	25
Cell Culture:	25
Transection of Neurites of B104 cells:	26
Microscopy and Imaging:	26
Assessment of Plasmalemmal sealing:	27
Pharmacological Reagents:	28
Statistical Analysis:	29
Validation of our single dye assessment for plasmalemmal sealing:	31
Results:	32

PC Time determines Plasmalemmal sealing:	33
Plasmalemmal sealing depends upon transection distance from the soma:	35
Increasing cAMP, PKA activity, or Epac activity increases frequency and rate of sealing:	36
Ca ²⁺ independent sealing produced by cAMP analogs:	37
cAMP cannot fully substitute for Ca ²⁺ in plasmalemmal sealing:	38
Inhibiting PKA activity decreases frequency and rate of plasmalemmal sealing:	39
Epac activation partly overcomes PKA inhibition:	40
nPKC inhibition decreases frequency and rate of plasmalemmal sealing:	41
Melatonin decreases frequency of plasmalemmal sealing:	41
Discussion:	42
Supplemental List of Plasmalemmal sealing references:	57

Chapter 3: Pathways for plasmalemmal repair mediated by PKA, Epac and cytosolic oxidation in rat B104 cells *in vitro* and sciatic axons *ex vivo*:

60

Abstract:	60
Introduction:	61
Materials and Methods:	63
B104 cells:	63
Cell culture:	63
Transection of neurites of B104 cells:	64
Microscopy and imaging:	64
Assessment of plasmalemmal sealing:	65
Pharmacological reagents:	65
Western Blotting:	66
Statistics:	66
Sealing of cut rat sciatic axons <i>ex vivo</i> :	68

Surgical procedures:	68
Nerve treatments:	68
Results:	69
Plasmalemmal sealing <i>in vitro</i> in rat B104 cells with singly transected neurites:	69
Epac1 and 2 and PKA are expressed in B104 cells:	70
Sealing is increased by cBiMPS, Epac-cAMP, db-cAMP and H ₂ O ₂ :	70
Sealing is decreased by BoNT A/E, B, TeNT, Bref A, and NEM:	71
Three pathways that enhance plasmalemmal sealing:	73
A PKA pathway for plasmalemmal sealing:	74
An Epac pathway for plasmalemmal sealing:	75
A cytosolic oxidation pathway for plasmalemmal sealing:	77
PKA, Epac, and cytosolic oxidation pathways each converge on NSF:	78
Plasmalemmal sealing <i>ex vivo</i> in rat sciatic nerves with doubly transected axons:	79
Discussion:	80
Chapter 4: Cytosolic oxidation enhances plasmalemmal repair of B104 cells:	102
Abstract:	102
Introduction:	102
Methods:	103
Results:	104
Methylene Blue indicates cytosolic oxidation following plasmalemmal damage:	104
H ₂ O ₂ increases sealing at early time points:	104
H ₂ O ₂ leads to cell death at later time points:	105
PKA inhibition prevents H ₂ O ₂ from increasing sealing:	106

DTT, Mel, MB decrease plasmalemmal sealing in Ca ²⁺ free saline:	107
DTT, Mel, MB decrease plasmalemmal sealing in Ca ²⁺ containing saline:	107
Discussion:	107
Supplemental Methods:	113
B104 cells:	113
Cell Culture:	113
Transection of neurites:	114
Microscopy and Imaging:	114
Assessment of plasmalemmal sealing:	115
Pharmacological reagents:	115
Statistical analysis:	117
 Chapter 5: Polyethylene Glycol Rapidly Restores Axonal Integrity and Improves Behavioral Recovery After Sciatic Nerve Crush Injury:	 117
Abstract:	117
Introduction:	118
Methods:	121
Subjects:	121
Surgical Procedures:	122
Electrophysiological recording of CAPs across a lesion site:	123
Intra-axonal dye diffusion across a lesion site:	124
Behavioral tests:	125
Foot fault test:	126
Sciatic Functional Index:	127
Video recordings:	128
Statistical analysis:	128
Results:	128
CAP assessments of axonal continuity:	129
Intra-axonal dye diffusion across a lesion site:	131

Foot Fault Assymetry Scores:	131
Video Recordings:	133
Sciatic Functional Index:	134
Discussion:	135
 Chapter 6: Polyethylene glycol repair of severed axons: behavioral recovery and in vitro mechanisms:	 147
Abstract:	147
Introduction:	147
Results:	148
Animals:	149
Morphological assessment of axonal continuity:	149
Physiological assessment of axonal continuity:	150
Sciatic Functional index:	150
Foot Fault test:	151
Plasmalemmal sealing:	152
Sciatic nerves:	153
Different PEG concentrations increase sealing:	153
Melatonin and Methylene Blue sealing time course:	154
PEG sealing unaffected by inhibitors of sealing:	155
Discussion:	155
Supplemental Materials and Methods:	161
Animal subjects:	161
Surgical Procedures:	162
Electrophysiological recording of CAPS across a lesion site:	163
Intra-axonal dye diffusion across a lesion site:	163
Behavioral tests:	164
Foot Fault Test:	164
Sciatic functional index:	165
B104 cells:	165
Cell Culture:	166

Transection of neurites of B104 cells:	166
Microscopy and imaging:	167
Assessment of plasmalemmal sealing:	167
Pharmacological Reagents:	168
Statistics:	169
Chapter 7: General Discussion	171
Plasmalemmal sealing summary:	171
Pathways of plasmalemmal sealing:	173
Proteins targeted by toxins/inhibitors affect sealing:	174
PKA and Epac pathways of sealing:	175
Oxidation-dependent pathways of sealing:	177
Proteins predicted to affect sealing:	177
Evolutionary origins of proteins required for plasmalemmal sealing:	181
Role of plasmalemmal sealing in PEG fusion:	182
Conclusions and potential clinical relevance:	184
References	185
Vita	206

List of Tables

Table 2.1: PC time, not PT time or dye exposure time, determines sealing time of B104 cells:	50
Table 2.2: Effect of test substances on the time constant (τ) and rate constant (k) of sealing:	52
Supplemental Table 2.1A: Number of cells and dishes used to obtain the data points for all figures for cells transected nearer to ($< 50 \mu\text{m}$) the soma:	56
Supplemental Table 2.1B: Number of cells and dishes used to obtain the data points for all figures for cells transected farther from ($> 50 \mu\text{m}$) the soma:	56
Table 3.1: Sealing constants (τ , k) and R^2 for exponential fits of sealing PC times:	88
Table 3.1 A: Number of cells and dishes used to obtain the data points for all figures for cells transected nearer to ($< 50 \mu\text{m}$) the soma:	96
Table 3.1 B: Number of cells and dishes used to obtain the data points for all figures for cells transected farther from ($> 50 \mu\text{m}$) the soma:	97
Table 4.1A: Rates of increasing sealing for different H_2O_2 concentrations:	109
Table 4.1B: Rates of declining sealing for different H_2O_2 concentrations:	109
Table 5.1: Number of rats, and treatments groups, for behavioral testing or dye diffusion assays:	141

List of Figures

Figure 1.1: Model of plasmalemmal sealing:	21
Figure 2.1: Brightfield and fluorescent images typical of those used to assess plasmalemmal sealing:	49
Figure 2.2: Sealing frequency (%) plotted versus PC time (min); cAMP analogs increase sealing:	51
Figure 2.3: Sealing of cAMP analogs at 0 PC; post-cAMP sealing; PKA inhibition decreases sealing:	53
Figure 2.4: Epac partly overcomes PKA inhibition; Mel and nPKC η decrease sealing:	54
Figure 2.5: Model of plasmalemmal sealing:	55
Figure 3.1: Western Blots of Epac isoforms, PKA; Images of sciatic nerves used for sealing studies:	89
Figure 3.2: PKA, Epac, and H ₂ O ₂ increase sealing; PKA and Epac, but not H ₂ O ₂ increase sealing at 0 PC:	90
Figure 3.3: BoNT A or TeNT decrease sealing; Epac, not PKA, partly overcomes BoNTA/TenT:	91
Figure 3.4: NEM or Bref decrease sealing; PKA, not Epac partly bypasses Bref A; neither bypass NEM:	92
Figure 3.5: Bref A prevents Epac from bypassing Bont A, TenT:	93
Figure 3.6: H ₂ O ₂ bypasses Bref A, not BoNT A, TeNT, NEM; All sealing pathways cannot bypass or further decrease NEM during sealing:	94
Figure 3.7: Model of Plasmalemmal Sealing:	95
Supplemental Figure 3.1: Higher BoNT A or TeNT do not further decrease sealing; BoNT B exhibits same effect on sealing as TeNT:	98
Supplemental Figure 3.2: Bref A pretreatment or higher NEM	

concentration does not further decrease sealing:	99
Supplemental Figure 3.3: BoNT E has same effect as BoNT A; Bref A does not further decrease effect of BoNT A or TeNT:	100
Supplemental Figure 3.4: H ₂ O ₂ bypasses Bref A, not BoNT A, TeNT, NEM further from the soma:	101
Figure 4.1: Images typical of those used to asses sealing; including undamaged cell exhibiting “blebbing”:	110
Figure 4.2: Effect of H ₂ O ₂ on sealing; PKI prevents H ₂ O ₂ from increasing sealing:	111
Figure 4.3: Mel, MB, DTT decrease sealing in Ca ²⁺ -free saline, Ca ²⁺ containing saline, or both:	112
Figure 5.1: Mechanisms of axonal repair by polyethylene glycol (PEG) and increasing strength of extracellular matrix (ECM) by fibrin glue:	142
Figure 5.2: Compound Action potentials (CAP) of rat sciatic nerves:	143
Figure 5.3: Intra-axonal dye diffusion percentages by treatment; images of sciatic nerves with or without dye diffusion:	144
Figure 5.4: Foot Fault Assymetry Scores:	145
Figure 5.5: Sciatic Functional Index Scores:	146
Figure 6.1: Model of PEG fusion; Images of sciatic nerves:	157
Figure 6.2: CAP amplitudes, SFI and FF scores:	158
Figure 6.3: Sealing in sciatic nerves; different PEG concentrations affect sealing; Mel or MB decrease sealing up to 60 min PC:	159
Figure 6.4: Cells transected in Ca ²⁺ ; PEG cannot substitute for Ca ²⁺ ; PEG sealing unaffected by substances that inhibit sealing:	160

Chapter 1: Introduction

In this thesis, I present a model of plasmalemmal sealing based on both data I have collected, and other reports of plasmalemmal sealing, or related pathways that are involved in vesicle trafficking and membrane fusion. Confirmation of this model would significantly improve knowledge of neuro-protective plasmalemmal sealing mechanisms required for survival of all cells and the evolutionary origin of proteins involved in membrane fusion and exocytosis. Since plasmalemmal sealing is so important for cell survival, multiple, redundant pathways have evolved to ensure that sealing occurs. Greater understanding of proteins and pathways involved in plasmalemmal sealing should also suggest new clinical treatments for traumatic nerve injury and neurodegenerative disorders. Furthermore, plasmalemmal sealing plays an important role during PEG-fusion of proximal and distal severed axonal halves. Combinatorial studies involving PEG and substances/proteins that affect plasmalemmal sealing could lead to further improvements in behavioral recovery following cut or crush injury to peripheral or central neurons.

Traumatic injury

Plasmalemmal damage inevitably occurs following traumatic injuries, such as axonal severance, or muscle tearing. For example, plasmalemmal damage in muscle plays a role in the etiology of muscular dystrophy, as muscles are not able to efficiently repair minor plasmalemmal disruptions following normal walking, and the muscle cells begin to die (Cai, et al., 2009a). Plasmalemmal disruptions play a role in ischemic nerve

death due to stroke, and neurodegenerative disorders, such as ALS, Parkinson's, and Alzheimer's disease (Bansal and Campbell, 2004). Plasmalemmal repair (sealing) is a necessary first step for cell survival. Increasing plasmalemmal sealing can decrease the severity or symptoms associated with damage caused by traumatic injury (Nehrt, et al., 2010; Britt, et al., 2010).

A consequence of plasmalemmal damage is the influx of extracellular solution, including Ca^{2+} and various other ions, through the damage site, and the death of the damaged cell. Extracellular Ca^{2+} flowing through the lesion site activates repair (sealing) pathways (Yawo and Kuno, 1985; Krause *et. al.*, 1994; Steinhart *et. al.*, 1994; Blanchette, *et. al.*, 1999; Eddleman, *et. al.*, 2000). However, this increase in internal free Ca^{2+} concentration ($[\text{Ca}^{2+}]_i$) also initiates processes that lead to axonal degeneration or cell death, often via apoptosis (Schlaepfer and Bunge, 1973; Nguyen, *et. al.*, 2005). Those neurons that do not quickly repair plasmalemmal damage do not survive or regenerate axonal processes (Yoo, *et. al.*, 2003, 2004). Thus, sealing is often neuroprotective. However, plasmalemmal sealing does not *guarantee* neuronal survival after injury. Neurons that seal plasmalemmal damage at sites nearer to the soma are less likely to survive than neurons that seal plasmalemmal damage at sites further from the soma (Ramon y Cajal, 1928; Loewy and Shader, 1977; Lucas, et al., 1985, 1990; Yoo, et al., 2004; Nguyen, et al., 2005). In this way, increasing the rate of sealing should decrease the severity of the symptoms of plasmalemmal damage by decreasing the probability of extracellular Ca^{2+} from initiating apoptosis.

Plasmalemmal Sealing

Prior to 1994, textbooks (Kandel, et al., 1990) and research publications (Spira et al., 1993) assumed that minor damage to the plasmalemma was sealed by spreading of plasmalemmal lipids and complete transection was sealed by collapse and fusion of plasmalemmal leaflets. In 1994, we (Krause et al., 1994) showed that either lesion type, in several invertebrate axons, sealed by an accumulation of membrane-bound structures (mostly vesicles). Steinhart et al. (1994) showed a similar sealing mechanism in sea urchin eggs and mammalian epithelial cells. Data from our lab using invertebrate giant axons or mammalian axons, and other labs using sea urchin eggs or mammalian non-neuronal cells, consistently show that plasmalemmal sealing requires various proteins, many of whose isomers are Ca^{2+} -dependent and involved in membrane fusion in synapses or the Golgi apparatus: synaptobrevin (Yoo, et al., 2003), syntaxin (Detrait, et al., 2000a, b), synaptophilin (Yoo, et al., 2003), synaptotagmin (Detrait, et al., 2000a,b; Shen, et al., 2005), calpains (Godell, et al., 1997), dysferlin (Bansal and Campell, 2004), Annexin A1 (McNeil, et al., 2006), Caveolin 3 (Mellgren, et al., 2006), Fetuin A (Mellgren, et al., 2007), TRIM proteins (Cai, et al., 2009a, b, c), PKA, and PKC (Shen and Steinhardt, 2005; Shen, et al., 2005).

Large diameter invertebrate cells that can be individually identified have been observed to seal plasmalemmal damage by Ca^{2+} -dependent production of vesicles that form a plug, often at a partially- constricted cut end (Krause, et al., 1994; Steinhardt, et al., 1994; Blanchette, et al., 1999; Eddleman, et al., 1997, 1998; Terasaki, et al., 1997).

Following axonal damage or complete axonal transection (dashed line in **Fig. 1**), vesicles from nearby undamaged membrane (Eddleman, et al., 1997), lysosomes (Reddy, et al., 2001) and/or myelin delaminations (Ballinger, et al., 1997) migrate (arrows in Fig. 1), accumulate, and pack tightly at the damage site. These vesicles interact with each other and with undamaged membrane to reduce the influx (straight and curved arrows in Fig. 1) of extracellular Ca^{2+} and other ions until a seal is restored. Complete plasmalemmal repair takes about 24 hours for earthworm giant axons, at which time vesicles are no longer observed at the original lesion site and a continuous plasmalemma is restored (Lichstein, et al., 2000).

Individual mammalian axons, neuronal or other cell types, are much more difficult to image and view vesicle interactions, but biochemical data show that the same proteins are involved in mammalian cells as in invertebrate giant axons (Detrait, et al., 2000a,b; Yoo, et al., 2003), and many other cell types, such as plants (Idone, et al., 2008), fibroblasts (Togo, 2006), and sea urchin eggs (Steinhardt, et al., 1994). For a complete list of proteins and preparations that confirm vesicle mediated plasmalemmal sealing, see the supplemental sealing list at the end of Chapter 2 (Spaeth, et al., 2010). Thus, similar mechanisms are likely involved in the repair of all eukaryotic cells. No study has yet investigated whether interactions between the proteins listed above or below are involved in plasmalemmal sealing or their role in pathways necessary to form a plasmalemmal seal.

Membrane Fusion Proteins

Membrane traffic and fusion occurs in all eukaryotic cells in all intracellular compartments (see Sudhof, et al., 2004). Although different pathways perform varied intracellular functions, the basic mechanism of action in all these pathways is the same: vesicles, or membrane, possibly endocytosed from a larger membrane source, traffic to, and fuse with, the target. Due to this similarity, all vesicle trafficking and membrane fusion pathways likely evolved from the same precursor pathway (see Rothman and Sudhof, 2009). Thus, studying plasmalemmal sealing may provide important insights into the fundamental nature of membrane fusion and vesicle fusion in all intracellular compartments.

Plasmalemmal sealing requires the fusion of two distinct membranes, which may be a vesicle, an organelle, or an undamaged plasmalemmal leaflet. Plasmalemma and all other membranes in eukaryotic cells are composed of lipids, which contain a hydrophobic tail (mostly hydrocarbons) and a hydrophilic head (typically a phospholipid group). The hydrophobic groups interact with each other to form a very stable membrane (see Kandel, et al., 2000). Once formed, the addition of new lipid groups, such as membrane fusion or insertion, requires the energetically unfavorable interaction of hydrophobic lipids using specialized membrane fusion proteins (for review see Rizo, 2005). These proteins overcome the activation energy barrier to actively drive membrane fusion.

Many proteins act in concert to fuse two disparate membranes together. Studies using very specific neurotoxins elucidated much of our understanding of the function of these proteins. Early studies of vesicle fusion and membrane traffic in neurotransmission identified three proteins: VAMP (Vesicle Associated Membrane Protein)/synaptobrevin

(Sudhof, et al., 1989), SNAP-25 (Oyler, et al., 1989), and syntaxin (Inoue, et al., 1992). VAMP /synaptobrevin binds to vesicles (Chapman, et al., 1994). In contrast, SNAP-25, characterized by centrally located palmitoylated cysteines, and syntaxin, characterized by hydrophobic C-terminal amino acids, both bind to target membranes (Sudhof, et al., 1993), but not exclusively. The function of these proteins remained unknown until Sollner and colleagues (1993) published an important paper proposing a model of membrane fusion termed “the SNARE hypothesis,” with SNARE standing for Soluble N-ethyl maleimide REceptor proteins. The SNARE hypothesis suggests that SNAP-25 binds to syntaxin on the target membrane, creating a binding site for VAMP/synaptobrevin (Sollner, et al, 1993). This complex, termed the 20S SNARE complex, brings the vesicle close to target membrane (trans-SNARE complex). Binding of SNAP (Soluble N-ethyl maleimide Attachment Proteins) isomers to the 20S SNARE complex recruits NSF (N-ethyl maleimide Sensitive Factor), an ATPase which provides the energy necessary to fuse the vesicle and target membrane together (Garcia, et al., 1995), and also provides the energy necessary for the vesicles to endocytose back to the cytosol (Parnas, et al., 2006).

Evidence supporting the SNARE hypothesis originates from studies using bacterial Botulinum (BoNT) or Tetanus (TeNT) neurotoxins specific for each of these SNARE proteins, as well as a potent inhibitor of NSF. BoNTs and TeNTs are composed of two different subunits: a heavy chain, and a light chain (Singh, et al., 2000). The heavy chain binds to specific extracellular ganglioside receptors, which actively transport the toxin into the cell. Once in the cytosol, the heavy chain remains bound to the now

internalized receptor, and the light chain dissociates. The light chain possesses catalytic activity, and cleaves target proteins at specific amino acid residues. All bacterial toxins cleave their targets with nano-molar specificity (Singh, et al., 2000). Botulinum toxin (BoNT) A and E specifically cleave SNAP-25 (Chapman, et al., 1993; Blasi, et al., 1993); Botulinum toxin B, D, F, G, and Tetanus toxin (TeNT) cleave some VAMP/synaptobrevin isoforms (Galli, et al, 1998); and BoNT C1 specifically cleaves syntaxin and SNAP-25 (Link, et al., 1992). As an example of the potency of any of these toxins, one molecule of toxin can decrease neurotransmission in an entire nerve terminal (Chapman, et al., 1993). Interestingly, despite decreasing exocytosis and membrane fusion, these toxins do not initiate any structural changes in, or excessive cell death of, nerve terminals, demonstrating the specificity of each toxin (Singh, et al., 2000). As an additional example of the role of toxins in membrane traffic, BoNTs prevent neurite outgrowth, causing the distal end of growing neurites to branch (Coffield and Yan, 2009). The observed branching probably due to an inability to deliver enough new membrane to growth cones since BoNTs decreased vesicular traffic. The NSF inhibitor N-ethyl maleimide (NEM) specifically binds to NSF, and at 1 mM, eliminates nearly all NSF activity (Rodriguez, et al., 1994). All of these toxins or inhibitors decrease neurotransmission, suggesting that they all decrease membrane fusion.

cAMP in survival and regeneration of damage axons

Activation of exocytosis and membrane fusion proteins occurs through second messenger signaling pathways, such as cAMP, which also promotes neuronal survival

and axon regeneration in mammalian and invertebrate models (Chierzi, et al, 2005; Murray and Shewan, 2008). Adenylate cyclase (AC) activity creates cAMP by cyclizing AMP, with both cytosolic and membrane AC isoforms activated by Ca^{2+} . Therefore, damage-induced Ca^{2+} influx through a site of plasmalemmal disruption (Nguyen, et al, 2005) almost certainly increases [cAMP]. Increased [cAMP] increases neuronal survival and axon regeneration in mammalian spinal cords, effectively overcoming the growth inhibition of myelin associated glycoprotein (MAG) (Qui, et al, 2002). [cAMP] can be increased in spinal axons by pre-lesioning DRG neurons, which also leads to increased survival and axon regeneration (Cai, et al, 2001). In other animal models of regeneration, increased [cAMP] increases the regenerative capacity of transected retinal axons in Goldfish (Rodgers, et al, 2005). Additionally, high [cAMP] stimulates growth of neurons on an inhibitory substrate, whereas low cAMP concentration inhibits growth of neurons (Qui, et al 2002). All these, and other data, demonstrate an important role for cAMP in neuron survival and regeneration.

Some of the effects of cAMP in neuronal survival (and other cellular processes) following injury are due to activation of PKA (Rodgers et al, 1999; Qui et al, 2002; Sudhof, 2004). For example, many synaptic vesicle proteins are activated by cAMP through PKA (for review see Sudhof 2004). Other pathways directly activated by cAMP are less clearly defined. One is the stimulation of Epac (de Rooij, et al., 1998) and the other is a PKA and Epac independent pathway that activates integrins (Ivins, et al., 2004). Neuronal survival after injury may be increased by Epac (Shewan and Murray, 2008). Therefore, the cAMP dependent increase in neuronal survival after plasmalemmal

damage may be due, in part, to an increase in the plasmalemmal sealing rate via cAMP activation of PKA and Epac.

Protein Kinase Activated by cAMP (PKA)

cAMP binds many different intracellular targets, and the most well-known target of cAMP is PKA. PKA was discovered in 1970 in a screen for proteins that bound to cyclic nucleotides (Gilman, 1970), and controls many different intracellular processes, ranging from vesicle trafficking to transcription (for review, see Sudhof, et al., 2004; Taylor, et al., 2005). PKA is a 4 subunit protein, with two catalytic domains, required for binding ATP and transferring a phosphate to specific amino acids on a target protein (typically serines or threonines) (Taylor, et al., 1995). The two regulatory subunits of PKA sequester the catalytic sites from intracellular targets. Binding of cAMP to the cyclic nucleotide binding (CNB) domains of the regulatory subunits changes their conformation and releases the catalytic subunits. The small endogenous protein PKI (protein kinase inhibitor) further inhibits PKA by allosterically inhibiting the cAMP binding site on the regulatory subunits, thereby preventing the activation of PKA catalytic subunits (Knighton, et al., 1991; Dalton and Dewey, 2006). The broad expression of PKA subunits and isoforms in all cell types investigated demonstrates the importance of PKA signaling (for review, see Taylor, et al., 2005).

Since PKA can be activated by very small increases in [cAMP] (Dunn, et al., 2009), PKA-activation of target proteins depends on the strict subcellular localization of PKA, mediated by A-kinase anchoring proteins (AKAPs) (Glantz, et al., 1992). Thus,

AKAPs control specific activities of PKA in different intracellular compartments. For example, PKA localized to the plasma membrane affects hyperpolarization via phosphorylation of specific potassium channels (Gervasi, et al., 2007). In contrast, Golgi bound AKAPs regulate specific Golgi structure, but surprisingly, increased PKA activity does not increase anterograde traffic to the plasma membrane (Mavillard, et al., 2009)

PKA phosphorylation activates many proteins important in vesicle targeting and fusion, including regulated exocytosis via targeting of proteins to intracellular compartments (Gervasi, et al., 2007), the synaptic vesicle cycle (for reviews, see Sudhof et al., 1995, 2004) and plasmalemmal sealing (Shen, et al., 2005). PKA phosphorylation of synapsins prevents vesicle attachment to the actin cytoskeleton, thus increasing vesicle motility (Menegon, et al., 2005). Once vesicles are free of the cytoskeleton, PKA phosphorylation of rabphilins stabilizes the Rab-family of vesicle motor proteins (Deak, et al., 2006). Upon reaching the target membrane, PKA phosphorylation of SNAP-25 increases SNAP-25 binding to syntaxin (Bronk, et al., 2007). PKA phosphorylation of alpha-SNAP increases NSF binding to the 20S complex, which increases membrane fusion by recruiting NSF (Nagy, et al., 2004). PKA phosphorylation of NSF increases ATPase activity, thereby increasing membrane fusion (Garcia, et al., 1995). Even in the absence of Ca^{2+} , PKA increases spontaneous transmitter release in *Drosophila* through a synaptobrevin-dependent pathway (Yoshihara et al., 1999, 2000). Increased PKA activity also increases survival following traumatic nerve injury (Rodger, et al., 2005) suggesting increased PKA activity may be neuroprotective.

Exchange Protein Activated by cAMP (Epac)

Epac is a recently discovered, multi-functional cAMP- activated guanine exchange factor that increases exocytosis and vesicle traffic in many different cell types and subcellular compartments (for review, see Holz, et al., 2005). Epac, or cAMP-GEF, was originally identified by searching for cAMP-dependent, PKA-independent proteins that activate Rap1 GTPase (deRoos, et al., 1998). A screen for proteins with cyclic nucleotide binding domains revealed 2 Epac isoforms, Epac1 and Epac2, both with broad expression, especially in the central and peripheral nervous system, as well as in pancreatic, cardiac, liver, kidney, and muscle cells (see Holz, et al., 2005). Similar to PKA, Epac isoforms are spatially regulated by binding to AKAPs (Bos, 2006).

The different domains of Epac proteins explain the multiplicity of Epac function. Both Epac isoforms contain a C-terminal CDC25 homology domain, where nucleotide exchange activity occurs. The Ras exchange motif (REM) stabilizes the CDC25 tertiary structure. A Ras Association (RA) domain separates the REM from the CDC25 domains, and is important for interactions at the plasmalemma. The N-terminal contains a Dishevelled, Ecl10, Pleckstrin (DEP) domain, required for plasma membrane binding. Near the DEP is one (Epac1) or 2 (Epac2) cyclic nucleotide binding domains (CNB). The Epac CNB domains bind cAMP with lower affinity than the CNB on the regulatory subunits of PKA (Christenson, et al., 2003). The N-terminal domain CNB of Epac2 binds cAMP with very low affinity. Due to the broad overlap of Epac 1 and 2 isoforms across many tissues, and relatively little difference in Epac1 or Epac2 actions in these tissues, both PKA and Epac-dependent activities can be modulated by changes in

intracellular [cAMP] (de Rooij, et al., 1998, 2000). In this way, a small increase in [cAMP] activates PKA only, a larger increase in [cAMP] activates PKA and Epac1 activity, and a further increase in [cAMP] activates PKA, Epac1 and Epac2.

Epac isoforms principally exchange guanine nucleotides (GEF activity) during Rab-family dependent vesicle motility in many different intracellular compartments (Branham, et al., 2009). Much evidence supports the role for Epac in vesicle motility. For example, Epac isoforms increase neurotransmitter during hippocampal synaptic potentiation (Gelinas, et al., 2007), and increases glutamatergic release in the rat Calyx of Held synapse during inflammatory pain responses (Hucho, et al, 2005). Epac isoforms are also involved in dense core vesicle exocytosis (Hatakeyama, et al., 2007), delivery of membrane during growth cone extension (Murray and Shewan, 2008), plasma membrane activation of Rap1 (Li, et al., 2006), stimulation of exocytosis in mouse melanocytes (Sedej, et al., 2005), and increasing Ca^{2+} -dependent vesicle accumulation in PC12 cells (Hatakeyama, et al, 2007). Additionally, Epac1 rearranges microtubules in response to increased [cAMP], which increases vesicle traffic (Sehrawat, et al., 2008). During constitutive secretion, Epac isoforms bind to Rap1 GTPase, a protein required for anterograde Golgi traffic (Wu, et al., 2000). The bacterial toxin Brefeldin A (Bref A) has recently been reported to inhibit Epac activity during long term synaptic depression, confirming a role for Epac-dependent Golgi activation in synaptic compartments (Ster, et al., 2009).

Epac may stimulate vesicle exocytosis by interacting with a variety of vesicle-bound proteins. During constitutive secretion, Epac isoforms bind Rap1 GTPase, a

protein localized on both trans-Golgi stacks and the plasma membrane (Niimura, et al., 2009). Additionally, the Epac1-piccolo interaction increased insulin secretion in pancreatic cells. Piccolo is vesicle bound mammalian Ca^{2+} sensor (Fujimoto, et al., 2002). The Epac2- Rim2 interaction increases evoked excitatory potentials in mouse neurons (Ster, et al., 2009). Rim2 is a plasma membrane bound binding partner for Rab3, a GTPase which plays a central role in Ca^{2+} -dependent exocytosis (for review see Fukuda, 2008). Epac1 binds Rab3 during the acrosome reaction, a Ca^{2+} dependent pathway for membrane fusion of male gametes (Branham, et al., 2009). Taken together, these data suggest that Epac isoforms stimulate vesicle exocytosis as the GEF required for Ca^{2+} -dependent Rab3 activity in both synaptic and Golgi compartments.

Epac may also activate membrane fusion. Epac isoforms interact with Munc13/Sec1, a protein critical for the priming stage of vesicle fusion (Kwan, et al., 2007). Thus, Epac may affect plasmalemmal sealing by stimulating Rab3-dependent vesicle exocytosis and Sec1/Munc13-dependent membrane fusion, partly in synergy with PKA and partly independent of PKA (Hochbaum, et al., 2008; Nijholt, et al., 2008). How PKA and Epac-pathways interact is unclear (Borland, et al., 2009), but these data suggest that Epac might help seal plasmalemmal damage, possibly in combination with PKA.

Convergence/Divergence of PKA and Epac activities

Recently, dissection of cAMP-dependent pathways demonstrates distinct roles for both PKA and Epac. For example, during insulin secretion, genetic truncation of SNAP-25 prevents cAMP from increasing large dense core vesicle exocytosis. Investigation of

cAMP-dependent insulin secretion revealed that both Epac1 and PKA stimulated readily releasable dense core vesicles but not reserve pool vesicles (Vikman, et al., 2009). Thus, both PKA and Epac exocytotic pathways share SNAP-25 as a target in INS-12 cells. However, during neurite extension in primary mouse neurons, Epac1, but not PKA enhanced neurite outgrowth following damage (Murray and Shewan, 2008). In PC12 cells, Ca^{2+} induced vesicle exocytosis is differentially stimulated by PKA and Epac 2, since Epac activation requires significantly more free internal [cAMP] than PKA (Hatakeyama, et al., 2007). Additionally, PKA and Epac differentially activated the cytokines tumor necrosis factor beta (TNF- β), interleukin 1 beta (IL-1 β), and interleukin 10 (IL-10) in microglial cultures (Liu, et al., 2010). In the adrenal cortex, PKA, but not Epac2 or the splice variant Epac2B, initiate the production of adrenal steroids, however both PKA and Epac2B regulate cell shape, actin organization, and cell motility (Niimura, et al., 2009). Taken together, these data suggest that cAMP exerts effects through both PKA and Epac, which have both convergent and divergent activities. Therefore, it is likely that PKA and Epac exhibit both convergent and divergent actions during cAMP-dependent plasmalemmal sealing.

Oxidative Enhancement of Plasmalemmal Sealing

Cytosolic oxidation also influences plasmalemmal sealing. After plasmalemmal damage, Ca^{2+} and other substances diffuse into the cell through the damage site, and intracellular substances flow out. These intracellular events shift the cytosolic redox environment to a more oxidized level (McNeil, 2009) and activates proteins (Sod family,

glutathiones, thioredoxins) responsible for maintaining the intracellular redox environment. Cytosolic oxidation leads to an accumulation of vesicles, stimulated in muscle by the TRIM protein mitsigumin 53 (mg53, Cai, et al., 2009 a,b). These vesicles might undergo Ca^{2+} -dependent membrane fusion in plasmalemmal sealing.

In addition to the cytosolic oxidation, lipid and cholesterol groups may also be oxidized following plasmalemmal damage. Increased membrane cholesterol groups reduced spontaneous excitatory potential, but increased evoked excitatory potentials, suggesting the importance of cholesterol in exo- and endocytosis (Ma, et al., 2010). Furthermore, an additional oxygen moiety on cholesterol, known as an oxy-sterol, resulting from kainite induced plasmalemmal damage, increased vesicle accumulation (Ma, et al., 2010). These oxy-sterol induced-vesicles require an influx of Ca^{2+} for complete fusion. Thus, oxidation of the cytosol and cholesterol may also be important for enhancing Ca^{2+} dependent plasmalemmal sealing.

Neurons are very sensitive to changes to the intracellular reducing potential and cytosolic oxidation may be a secondary effect of plasmalemmal damage. Proteins such as glutathiones, thioredoxins, super-oxide dismutases, and catalases (Celsi, et al., 2009) all help maintain the intracellular reducing environment. Improper functioning of these proteins leads to neuronal death. For example, mutated super-oxide dismutase (hSod1) is responsible for nearly 10% of all familial ALS (Barber and Shaw, 2009). This phylogenetically ancient oxidation-dependent damage control pathway may then have been co-opted to serve in other damage control pathways, especially those involved in neurodegenerative disorders.

Polyethylene glycol (PEG)

In the last several decades, various procedures have improved the number and specificity of PNS axons that re-establish connections following severance, but not the outgrowth rate or time for PNS axons to re-establish those connections. For example, nerve grafts (Jeng and Coggeshall, 1986; Lago et al. 2007), connective tissue matrices (Herbert et al., 1996; Lore et al., 1999; Bozkurt et al., 2007), and nerve growth guides (Aebischer et al., 1990; Kalbermatten et al. 2009) have all been reported to improve regeneration of severed PNS axons whose proximal ends grow into these exogenous structures at 1-2 mm/day.

We have developed a novel technique to improve the speed (time course) and specificity of acute and chronic axonal repair by directly applying PEG solutions to the lesion site of severed axons (Fig. 1B-E). We initially used PEG solutions whose direct application to the lesion site in Ca^{2+} -containing salines repaired 3% of invertebrate giant axons (Bittner et al., 1986). We then developed techniques using Ca^{2+} -free hypotonic salines containing a Ca^{2+} -chelator (EGTA) followed by 50% PEG w/v in distilled water that consistently (80-100%) repaired the severed ends of myelinated or unmyelinated CNS giant axons in invertebrates (Krause and Bittner, 1990; Krause et al., 1991; Lore et al., 1999). Since large-diameter invertebrate axons are individually identifiable morphologically and evoke unique behaviors, these papers convincingly demonstrated that “PEG-fusion” produces acute (within minutes) morphological and physiological continuity and behavioral recovery *in vitro and vivo*. Furthermore, such PEG-fusion also

produced chronic (permanent) repair *in vivo* if a PEG-based hydrogel glue was applied to the lesion site at the time of PEG application to strengthen the ECM – or the animal was anesthetized for a day or two by cooling to prevent muscle and limb movement, but not some ECM repair (Lore et al., 1999). We also showed that severed distal stumps survive for months in most invertebrates (Hoy et al, 1967; Bittner et al., 1974; Kennedy and Bittner, 1974; Birse and Bittner, 1981; Bittner and Brown, 1981; Bittner, 1991). Furthermore, surviving severed ends of earthworm axons can be PEG-fused days to weeks after severance (Lore et al., 1999).

In contrast to a few large-diameter invertebrate axons, many small diameter mammalian axons that are not uniquely identifiable run parallel to each other in PNS and CNS nerves or nerve tracks in endothermic animals that cannot be safely anesthetized for days by cooling or drugs. Nevertheless, PEG fusion can re-establish the continuity of some crush-severed axons *in vitro* in rat sciatic nerves as measured by the restored conduction of CAPs and the intra-axonal diffusion of fluorescent dye across the lesion site (Lore et al., 1999). PEG acutely repairs mammalian PNS axons for up to 24 hours after crush-severance *in vitro and in vivo* (Stavisky et al., 2005). That is, even in mammals, PEG-repair procedures do not have to be begun immediately after injury because Ca^{2+} -free hypotonic salines containing a Ca^{2+} -chelator (EGTA) can open previously sealed ends of severed axons and flush out vesicles so that the axons can still be PEG-fused. Furthermore, we have also developed techniques (cooling, direct application of melatonin to the injury site, subcutaneous injections of cyclosporin A) to *retard* axonal Wallerian degeneration of severed mammalian axons for up to 6 days and

increase the survival time and/or success rate of PEG-fusion for *many* days (Sea et al., 1995; Sunio and Bittner, 1997; Marzullo et al., 2002; Stavisky et al., 2005). Extending the time in which axons can be successfully PEG-fused after axonal severance has important clinical implications, as it is not always possible to treat nerve injuries immediately after they occur in humans. These reports demonstrated that PEG applied days after axonal severance can acutely restore continuity to some severed ends *in vitro* and *in vivo*, but did not examine if such repair was specific or chronic, i.e. if severed proximal and distal axonal ends of appropriate functional/behavioral specificity were rejoined or if such acute repair was long-lasting.

Summary

This PhD thesis is composed of 5 additional chapters. Chapter 2 demonstrates that rat hippocampal B104 cells efficiently model plasmalemmal damage in a manner consistent with previous published preparations. Furthermore, pharmacological activators, or inhibitors, can be specifically targeted to intracellular proteins and/or events in B104 cells, and can provide important information about the pathways and proteins involved in plasmalemmal sealing. Data from Chapter 2 suggests that Ca^{2+} -dependent cAMP activation of PKA and/or Epac isoforms strongly influences plasmalemmal sealing. These data provide the first evidence that the Ca^{2+} -requirement for sealing can be partly bypassed. Additionally, PKA or nPKC inhibition, and Melatonin, all decrease sealing, suggesting that multiple pathways influence sealing. Much of these data were

accepted for publication by the Journal of Neuroscience and printed in the November 24th issue as Spaeth, et al., 2010.

Chapter 3 is a continuation of the sealing studies from Chapter 2. Since PKA, Epac, and cytosolic oxidation all increase plasmalemmal sealing, using toxins or inhibitors that specifically affect their target, I demonstrate that sealing requires membrane fusion proteins involved in neurotransmitter release SNAP-25 and synaptobrevin, as well as Golgi-vesicular traffic, and N-ethylmaleimide sensitive factor (NSF). Both PKA and cytosolic oxidation pathways require SNAP-25 and synaptobrevin, whereas the Epac pathway requires Golgi-vesicular traffic, and only partly requires SNAP-25 and synaptobrevin. All three pathways require NSF.

Chapter 4 investigates the role of cytosolic oxidation during plasmalemmal sealing. This chapter suggests that sealing is increased by many [H₂O₂], however high [H₂O₂] lead to eventual cell death. Consistent with this observation, decreasing cytosolic oxidation, using the reducing agent DTT, the anti-oxidant Melatonin, or the redox indicator Methylene blue, decreases sealing. The decrease in sealing occurs whether or not these substances are present when Ca²⁺ is present.

Chapter 5 extends previous *in vitro* studies of PEG in mammalian sciatic axons to *in vivo* studies. Here, we demonstrate that following complete sciatic crush severance injuries, PEG application restores electrophysiological and morphological continuity, as measured by electrical conductance of compound action potentials and the diffusion of dye across the site of plasmalemmal damage. We also demonstrate that PEG increases behavioral recovery following crush-severance injuries to sciatic nerves as measured by

two tests: the sciatic functional index (SFI) and a foot fault (FF) asymmetry score. Much of this Chapter was published in the Journal of Experimental Physiology as Britt, et al., 2010.

Chapter 6 further extends *in vitro* and *in vivo* studies of behavioral recovery due to the fusogenic compound PEG, and further demonstrates that PEG may seal some proximal axons that are not fused to distal axons. This chapter demonstrates that the behavioral recovery observed following PEG treatment of crush-severed sciatic nerves can be further enhanced by treatment with MB or Mel prior to PEG application. Furthermore, PEG increases sealing in sciatic nerves *ex vivo* and B104 cells, even when Ca^{2+} is not present. The increase in sealing due to PEG does not require membrane fusion proteins, or cytosolic oxidation.

Chapter 7 provides a discussion of all the data presented herein, summarizing the interpretations of all previous chapters. Additionally, new targets required for plasmalemmal sealing will be proposed. Finally, I will suggest how understanding plasmalemmal sealing can lead to increased PEG fusion, which is a potentially new therapeutic method for repairing, or decreasing the severity of, traumatic nerve injury, and neurodegenerative disorders.

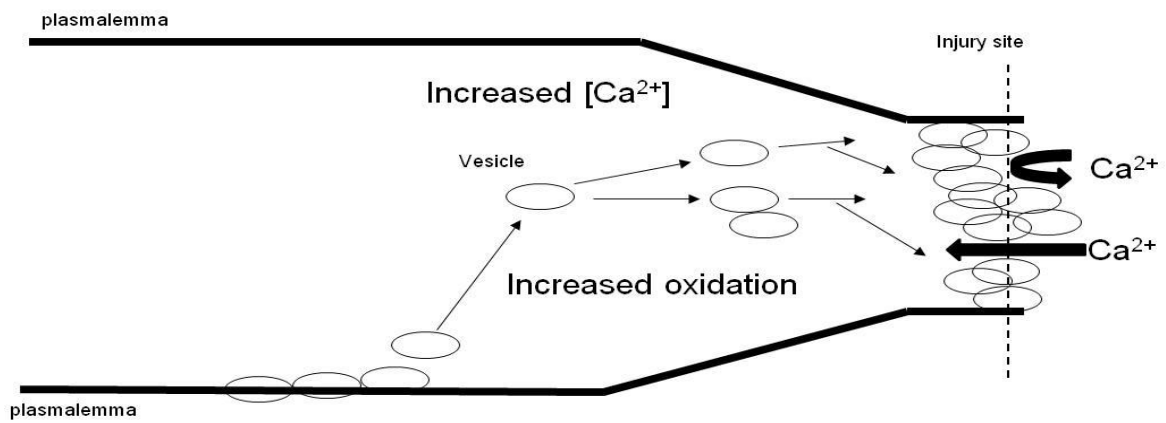


Figure 1.1: Model of plasmalemmal sealing. See text for details.

Chapter 2: A Model for Repairing Plasmalemmal Damage*

Significant portions of this chapter have been published as Spaeth, et al., 2010

Abstract

Plasmalemmal repair is necessary for survival of damaged eukaryotic cells. Ca^{2+} influx through plasmalemmal disruptions activates calpain, vesicle accumulation at lesion sites, and membrane fusion proteins; Ca^{2+} influx also initiates competing apoptotic pathways. Using the formation of a dye barrier (seal) to assess plasmalemmal repair, we now report that B104 hippocampal cells with neurites transected nearer ($<50\ \mu\text{m}$) to the soma seal at a lower frequency and slower rate compared to cells with neurites transected farther ($>50\ \mu\text{m}$) from the soma. Analogs of cAMP, including protein kinase A (PKA)-specific and Epac-specific cAMP, each increase the frequency and rate of sealing and can even initiate sealing in the absence of Ca^{2+} influx at both transection distances. Furthermore, Epac activates a cAMP-dependent, PKA-independent, pathway involved in plasmalemmal sealing. The frequency and rate of plasmalemmal sealing are decreased by a small molecule inhibitor of PKA targeted to its catalytic subunit (KT5720), a peptide inhibitor targeted to its regulatory subunits (PKI), an inhibitor of a novel PKC (an nPKC pseudosubstrate fragment), and an antioxidant (melatonin). Given these and other data, we propose a model for redundant parallel pathways of Ca^{2+} -dependent plasmalemmal sealing of injured neurons mediated in part by nPKCs, cytosolic oxidation, and cAMP activation of PKA and Epac. We also propose that the evolutionary origin of these pathways and substances was to repair plasmalemmal damage in eukaryotic cells. Greater

understanding of vesicle interactions, proteins, and pathways involved in plasmalemmal sealing should suggest novel neuroprotective treatments for traumatic nerve injuries and neurodegenerative disorders.

Introduction

Traumatic injury to any eukaryotic cell, including neurons, inevitably produces plasmalemmal damage, and rapid repair (sealing) of this damage is necessary for cell survival (Schlaepfer, 1973; Fishman and Bittner, 2003). Ca^{2+} influx through plasmalemmal disruptions initiates processes that lead to cell death, often via apoptosis (Schlaepfer and Bunge, 1973; Nguyen et al., 2005). However, such Ca^{2+} influx also leads to competing processes that activate plasmalemmal sealing pathways (Fishman and Bittner, 2003), sometimes before the internal Ca^{2+} concentration becomes toxic (Nguyen et al., 2005). Sealing is especially important for adult neurons, since they typically cannot proliferate. Thus, increasing the rate of sealing may increase the probability of cell survival following plasmalemmal damage and, for neurons, may increase the likelihood of axonal regeneration. Confocal and EM images show that giant invertebrate axons seal plasmalemmal damage by Ca^{2+} -dependent production of vesicles that form a plug, often at a partially constricted cut end (Krause et al., 1994). After plasmalemmal disruption, vesicles from nearby undamaged membrane (Eddleman et al., 1997, 1998), lysosomes (Reddy et al., 2001), and/or myelin delamination (Ballinger et al., 1997) migrate, accumulate, and pack tightly at the damage site. These vesicles interact with each other and undamaged membrane to reduce the influx of extracellular Ca^{2+} and other ions until a

seal is restored. Complete plasmalemmal repair takes approximately 24 h for earthworm giant axons, at which time vesicles are no longer observed at the original lesion site and a continuous plasmalemma is restored (Lichstein et al., 2000). Similar micromorphological images are difficult to obtain from small-diameter unmyelinated or myelinated mammalian axons or other mammalian cell types. Although many proteins and molecules influence plasmalemmal sealing, to date no study has described possible molecular pathways involved in plasmalemmal sealing.

To investigate pathways of plasmalemmal sealing, we transected neurites of individual B104 hippocampal cells and assessed repair (sealing) of the damaged plasmalemma by formation of a barrier to extracellular dye. Cells transected $<50\ \mu\text{m}$ (nearer) from the soma always sealed at a slower rate compared to cells transected $>50\ \mu\text{m}$ (farther) from the soma. Increasing cAMP concentration or specifically activating protein kinase A (PKA) or Epac via target-specific cAMP analogs all produced similar increases in plasmalemmal sealing. Furthermore, all three cAMP analogs increased sealing in the absence of Ca^{2+} , suggesting that cAMP, PKA, and Epac act downstream of Ca^{2+} to induce plasmalemmal sealing. Plasmalemmal sealing is decreased by inhibiting PKA or novel protein kinase C (nPKC) or by an antioxidant (melatonin). These and other data have enabled us to develop a model of plasmalemmal sealing that involves redundant, parallel pathways initiated by Ca^{2+} influx. Because *in vivo*, *ex vivo*, and *in vitro* biochemical and dye exclusion data from many different preparations and many diverse phyla, including B104 cells, show that isomers of the same proteins and processes are likely involved in plasmalemmal sealing (see supplemental list, available at

www.jneurosci.org as supplemental material), we suggest that the evolutionary origin of such proteins in eukaryotes was to repair plasmalemmal damage. Therefore, identifying plasmalemmal sealing pathways in neurons may provide insights into sealing in other cell types.

Methods

B104 cells: B104 cells derived from a CNS neuroblastoma (Bottenstein and Sato, 1979) have often been used as a model system to study neuronal function in vitro (Toda et al., 1999; Tan et al., 2003; Yoo et al., 2003, 2004; Nguyen et al., 2005; Miller et al., 2006). B104 cells extend neurites that have properties typical of nerve axons such as generation of action potentials, smooth (but not rough) endoplasmic reticulum, release of neurotransmitter, and regeneration of severed neurites. These cells have easily identifiable cell bodies and neurites, allowing precise identification of individually damaged cells at their injury site (Detrait et al., 2000b; Yoo et al., 2003, 2004). Unlike some other model neuronal cell lines (e.g., PC12 cells), B104 cells do not require growth factor supplements to fetal bovine serum to proliferate (Detrait et al., 2000b; Yoo et al., 2003). Data on sealing of B104 cells are consistent with similar data on sealing from at least 20 other preparations from many phyla and different cell types (see supplemental sealing list, page 73).

Cell culture: As described previously (Nguyen et al., 2005), B104 cells were grown in 75 cm² vented cap flasks (BD Falcon; BD Biosciences) in a humidified incubator at 37°C in 5% CO₂ and in 4 ml of "cell growth medium: consisting of a 1:1 mixture of Dulbecco's modified Eagle's medium and Ham's F12 (DMEM:F-12, HyClone)

supplemented for growth with 10% heat-inactivated fetal bovine serum (FBS; HyClone) and 1% antibiotics (10,000 U of penicillin/ml and 10 mg/ml streptomycin; Sigma-Aldrich). The cell growth medium was changed every 2 days. Cultures were passaged at 80% confluency, and cells were then either subcultured in a vented cap flask or seeded at 2000 cells/cm² in cell growth media on Petri dishes coated with poly-D-lysine (Sigma-Aldrich) to prevent cells from detaching during solution changes and/or neurite transection. After 24 h, the growth media was replaced with serum-free DMEM:F12 (Hyclone) to allow the B104 cells to differentiate. B104 neurites were transected 24–48 h after replacing the cell growth media with serum-free DMEM:F12.

Transection of neurites of B104 cells: Before transecting neurites, the solution (DMEM:F12) in the Petri dish was washed out twice with a Ca²⁺-free phosphate-buffered saline (referred to as "Ca²⁺-free saline," PBS^{-/-}; HyClone). All neurites were transected in Ca²⁺-free saline using a broken, pulled glass, microcapillary tube ("micro-knife") that was placed on a micromanipulator (Narishige Instruments) and quickly drawn across the surface of the Petri dish, etching a score line that showed the path of the knife. We were able to uniquely and individually identify each transected cell by the relation of the transected neurite to its soma and to the score mark on the plate (see Fig. 2.1). In some experiments, 3 kDa fluorescein dextran (Invitrogen) was added to the Ca²⁺-free saline before transecting neurites to confirm that the score line could be reliably used to uniquely identify individual cells.

Microscopy and imaging: For all experiments, B104 cells were observed under an inverted Zeiss ICM-405 fluorescent microscope with a 40x long focal distance lens.

Transected cells were imaged through a hole cut out of the bottom of a plastic dish covered by a thin glass coverslip using a Leica DM IRBE outfitted with a 40x lens and a Leica DFC350 FX fluorescence camera at the University of Texas core microscopy facility. Cells with neurites obviously transected $<50\ \mu\text{m}$ from the soma were counted as transected "nearer to" the soma, and those with neurites transected $>50\ \mu\text{m}$ from the soma were counted as transected "farther from" the soma. No further observations were made on any cell whose transection distance was not clearly definable.

Assessment of plasmalemmal sealing: We used the most reliable measure of plasmalemmal repair (dye exclusion) to assay plasmalemmal sealing (Blanchette et al., 1999; Detrait et al., 2000a,b). Other measures of sealing, such as intracellular recordings of membrane potential or input resistance (Krause et al., 1995), vibrating probe measurements of cell currents (Eddleman et al., 2000), preloading cells with Ca^{2+} -sensitive dyes, or fluorescence extinction of membrane-bound dyes (Togo et al., 2003), all have much more ambiguous interpretations as measures of plasmalemmal sealing. To date, electron microscopic images in any preparation have insufficient resolution to assess the status of plasmalemmal repair (Fishman and Bittner, 2003).

To assess plasmalemmal repair, we first transected 10–130 cells in Ca^{2+} -free saline within 10 min. The time elapsed after a neurite is transected in Ca^{2+} -free saline is defined as the post-transection time (PT time). The Ca^{2+} -free saline was then replaced with a phosphate-buffered saline containing 1 mM Ca^{2+} (" Ca^{2+} -saline." PBS+/+; HyClone) to initiate the sealing process (Detrait et al., 2000b; Yoo et al., 2003). The time elapsed after exposing cells to Ca^{2+} -saline is defined as the "post- Ca^{2+} addition time" (PC

time). Thus, unless otherwise noted, all cells on a given Petri dish have the same PC time, but each cell has a different PT time.

At various PC times (0–60 min PC), 3 kDa Texas Red dextran (Invitrogen) was added to the Ca^{2+} -saline to assess the formation of a plasmalemmal seal. At 0 min PC, Texas Red dextran was typically added at the same time as Ca^{2+} -saline to investigate whether cells with transected neurites excluded dye before Ca^{2+} addition. For all experiments, the dye was thoroughly washed out with Ca^{2+} -saline after a 10 min exposure to Texas Red dextran, and was sealing assessed. Transected cells that excluded Texas Red dextran were counted as "sealed" (Fig. 2.1 C). Cells that did not exclude Texas Red dextran were counted as "not sealed" (Fig. 2.1 F). Nearby undamaged cells did not take up Texas Red dextran (Fig. 2.1 A, C; cell identified by arrows).

Previous studies of sealing using dye exclusion in many preparations have used fluorescent dyes of various molecular weights (600 Da–10 kDa) and showed that higher molecular weight dyes are excluded faster than lower molecular weight dyes (Detrait et al., 2000a; Yoo et al., 2003), which are excluded faster than ions having even lower molecular weights than the smallest dye (Krause et al., 1994; Eddleman et al., 2000). We confirmed that Texas Red dyes of higher molecular weights (10 kDa) are excluded from B104 cells with transected neurites faster than dyes of lower molecular weight. For example, cells transected nearer to the soma and assessed for sealing at 5 min PC with 10 kDa Texas Red dextran (108 cells, 2 Petri dishes) sealed at a significantly [$p < 0.001$, Cochran-Mantel-Haenszel (CMH χ^2 test)] higher frequency (80%) than cells assessed for sealing with 3 kDa Texas Red dextran (272 cells, 15 Petri dishes; 45%). To avoid

variation in observed sealing frequency or time due to the molecular weight of the dye, we consistently used 3 kDa Texas Red dextran to assess sealing in all other experiments.

Pharmacological reagents: We used pharmacological agents to quickly inhibit or activate a target protein to avoid complications of compensatory pathways that may result from gene knock-outs or chronic applications of pharmacological inhibitors (Steinberg, 2008). All pharmacological reagents were typically dissolved in distilled water and added to Ca^{2+} -free saline immediately before neurites were transected to backload cells with each reagent during transection. Dibutyryl-cAMP (db-cAMP, 1 mM, 491.37 Da; Sigma-Aldrich) was used to increase intracellular cAMP concentration. Two structurally different, small molecule inhibitors of PKA were used to verify PKA inhibition: KT5720 (1 mM, 537.6 Da; AG Scientific) and PKI (50 μM , 1868 Da; Sigma-Aldrich; a generous gift from Drs. Michael Markham and Harold Zakon, University of Texas, Austin, TX). PKI is very specific for PKA (Dalton and Dewey, 2006). Sp-5,6-Dichloro-1-D-ribofuranosylbenzimidazole-3',5'-monophosphorothioate (8 μM), referred to as cBiMPS (419.2 Da; Biomol), was used to specifically activate PKA and not other cAMP targets (Christensen et al., 2003). 8-(4-Chlorophenylthio)-2'-O-methyladenosine-cAMP (8 μM), referred to as Epac-cAMP (507.82 Da; Tocris Biosciences), was used to activate Epac and not other cAMP targets (Enserink et al., 2002; Christensen et al., 2003). Melatonin (2 mM; Sigma-Aldrich) was used to decrease cytosolic oxidation following plasmalemmal damage. An nPKC pseudosubstrate fragment (7 μM , 2 kDa; EMD Chemicals) was used to specifically inhibit nPKC (Liu et al., 2006; Barros et al., 2009).

Statistical analyses: We obtained data from individual, uniquely identified B104

cells that all received similar, well-specified, neurite transections as plasmalemmal injuries in a tightly controlled environment. [Other studies of plasmalemmal sealing based on the averaged response of a population of different cell types that receive unknown or variable injuries almost always present statistical measures of a population of indistinguishable cells, each with an unspecified injury, to obtain data that often have more ambiguous interpretations (Mellgren et al., 2007).] For each experimental treatment group, at a given PC time the data were pooled for all cells (n) from all Petri dishes (N). See supplemental Table 1, A and B for “n” and “N” values for each data set at each PC time point in all figures presented in this paper. "Sealing frequency" is defined as the percentage of a set of individually-transected and uniquely identified cells that exclude 3 kDa Texas Red dye (sealed) at a given PC time. The CMH χ^2 test for independence was used to determine whether the differences between the sealing frequency at a given PC time for different experimental treatments was statistically significant ($p < 0.05$), as described previously (Agresti, 1996; Detrait et al., 2000b; Yoo et al., 2003, 2004).

GraphPad Prism was used to fit the sealing frequency for all PC times of a given control or test substance to a one-phase exponential equation (eq 1.1),

$$y(t) = Y_{\max} * (1 - e^{-kt}), \quad (1)$$

where $y(t)$ is the sealing frequency (%) of cells examined at a given PC time (t), Y_{\max} is the maximum plateau sealing frequency (%) of cells for that control or test substance, e is Euler's constant, t is a given PC time (min), and k is the rate constant (min^{-1}) of a given exponential equation. The rate constant k is the reciprocal of the time constant (τ , min)

defined as the elapsed PC time needed to achieve 63.2% (reciprocal of Euler's constant) of the observed maximum (plateau) sealing.

The solid and dashed lines on all graphs were calculated by GraphPad Prism according to Eq. 1 and represent the exponential equations fitted to the sealing frequencies at all PC times for all data sets. The time constants were calculated according to Eq. 1 and $\tau = 1/k$. The maximum sealing frequency (plateau) was always reached within 60 min PC.

Sealing time constants or rate constants for two experimental conditions were normalized and compared by using Fisher's Z transformation (FZT). Two sealing constants were considered significantly different if p was <0.05 , using a Z table. We also calculated R^2 values for the exponential equation defining each time constant to determine how closely the exponential equations modeled the observed data (see Table 2.2).

Validation of our single dye assessment method for plasmalemmal sealing

We confirmed that we can reliably identify individual B104 cells with transected neurites by their relationship to the score mark on a Petri dish by adding 3 kDa fluorescein dextran to the Ca^{2+} -free saline before transecting a set of neurites. We then added 3 kDa Texas Red dextran at 0 min PC (i.e., after neurite transection) to assess sealing. As reported previously (Yoo et al., 2003, 2004; Nguyen et al., 2005), cells with transected neurites identified by their relationship to the score mark were always filled with fluorescein dextran (Fig. 2.1 B,E), whether or not they excluded Texas Red dextran. Nearby undamaged cells did not take up fluorescein dextran or Texas Red dextran (i.e.,

these cells had an undamaged plasmalemma) (Fig. 2.1 A–C, cells identified by arrows).

We observed no significant ($p > 0.05$, CMH χ^2) difference in the percentage of cells that excluded Texas Red dextran (sealing frequency) identified as transected because they contained fluorescein dextran at 0 min PC (0%, 45 cells from 2 dishes) compared to the percentage of cells that excluded dye identified as transected solely by their relation to the score mark (0%, 131 cells from 4 dishes). That is, we could reliably identify transected cells by their relationship to the score mark without having to use a second fluorescent dye (fluorescein dextran) to confirm that those neurites were indeed transected.

As further confirmation of the validity of our single-dye assessment technique, when transection distance was not taken into account, the percentage of cells that sealed in the present study at 5, 20, and 60 min PC was not significantly ($p > 0.05$, CMH χ^2) different than that in previous studies in which fluorescein dextran was used as an additional indicator of cells that were transected, but transection distance was not noted (Yoo et al., 2003; 2004; Nguyen et al., 2005). Hence, in all protocols described below, we used a single dye (Texas Red dextran) to assess dye exclusion as a measure of plasmalemmal sealing of transected B104 neurites. This single dye assessment technique allowed us to transect the neurites of a greater number of uniquely identified cells within 10 min on a single Petri dish and to more rapidly assess their ability to seal.

Results

In all experiments, cells were transected in Ca^{2+} -free saline for 10 min, at which time the solution in the dish (Ca^{2+} -free saline) was replaced with Ca^{2+} -saline (1 mM Ca^{2+}). Any experimental compounds were added to the Ca^{2+} -free saline during neurite transection. At various times post- Ca^{2+} addition (PC time), dye was added and sealing was typically assessed after 10 min of dye exposure.

PC time determines plasmalemmal sealing

The time at which a cell is transected during the 10 min transection period, PT time, does not affect the sealing frequency of B104 cells, while the time elapsed since Ca^{2+} addition determines sealing frequency. For a given transection distance, cells with longer PT times, up to 10 min PT, did not seal at a significantly ($p > 0.05$, CMH χ^2) different frequency compared to cells with shorter PT times (Table 2.1). These and all other data in Table 2.1 confirmed that the frequency and rate of sealing in B104 cells was determined by PC time and not the time of neurite transection, as was previously reported for this and other preparations (Blanchette et al., 1999; Detrait et al., 2000b; Yoo et al., 2004). Hence, unless otherwise stated, all measures of sealing by B104 cells in this article are given in PC times. The data in Table 2.1 also show that the sealing frequency does not depend on the length of time cells are exposed to Texas Red dextran in Ca^{2+} -saline before sealing is assessed. For example, bathing cells in Texas Red dextran for 2 or 10 min did not affect the sealing frequency at 5 min PC, suggesting that Texas Red dextran very rapidly entered and filled all transected cells after the dye was added to Ca^{2+} -saline.

Thus, if a cell excludes dye at a given PC time, it is a reliable indicator that the cell had sealed before dye addition. Since dye exposure time did not affect the observed sealing frequency, in all other experiments below we exposed cells to Texas Red dextran for 10 min to more brightly label the score marks on the plastic Petri dishes.

We also examined whether sealing frequency was affected by the time at which cells were imaged after the dye was washed out. We transected cells as described above and added Texas Red dextran at 5 min PC. We then maintained the cells in Ca^{2+} -saline-containing dye for 10 min on one Petri dish, after which cells were immediately imaged and the sealing frequency (48%, 30 cells) was noted. On another Petri dish, we imaged the cells at 60 min after the dye was washed out and the sealing frequency was again noted (49%, 25 cells). There was no significant ($p > 0.95$, CMH χ^2) difference in the sealing frequency between cells on these two Petri dishes. Furthermore, when we reexamined the first Petri dish after 60 min, the same cells continued to exclude dye and the percentage of cells that excluded dye remained unchanged (48%, 30 cells). Therefore, the time at which cells are imaged after dye is washed out (up to 60 min PC) does not affect sealing frequency.

To confirm that sealing was initiated by Ca^{2+} influx at 0 min PC rather than by any residual Ca^{2+} remaining in the Ca^{2+} -free saline or released from nearby cells, we transected B104 cells in 0.5 mM EGTA. This EGTA concentration reduces extracellular Ca^{2+} to $<10^{-6}$ M, which is too low to initiate plasmalemmal sealing (Yoo et al., 2003) but not low enough to produce plasmalemmal damage for up to 10 min, since cells without transected neurites (undamaged cells) did not take up Texas Red dextran after 10 min of

exposure to 0.5 mM EGTA. Cells transected nearer to or farther from the soma in 0.5 mM EGTA did not have a significantly different sealing frequency compared to control sealing at 5 min PC ($p > 0.05$, CMH χ^2 , data not shown). Considering all our data, when neurites are transected in Ca^{2+} -free saline and subsequently exposed to Ca^{2+} -saline-containing dye, control sealing frequency is determined by PC time and not by PT time, the time of dye exposure, the time at which cells are observed following dye washout, or by the residual Ca^{2+} remaining in the Petri dish following solution changes.

Plasmalemmal sealing depends upon transection distance from the soma

We observed a significantly lower control sealing frequency for cells with neurites transected nearer to the soma ($<50\ \mu\text{m}$) compared to cells transected farther from the soma ($>50\ \mu\text{m}$) at all PC times between 1 and 10 min PC ($p < 0.01$ to $p < 0.001$, CMH χ^2) (Fig. 2.2 A). Control sealing was complete between 5 and 10 min PC for cells transected farther from the soma and by 20 min PC for cells transected nearer to the soma. Furthermore, control sealing of cells transected nearer to the soma had a significantly slower rate (longer time constant) compared to cells transected farther from the soma ($p < 0.001$, FZT) (Table 2.2). As described in subsequent sections, cells transected nearer to the soma always sealed at a significantly lower frequency and a significantly slower rate compared to cells transected farther from the soma for all test substances used in this study (Table 2.2). R^2 values in Table 2.2 also show that a single exponential equation very closely models the observed sealing data for control or test substances.

Increasing cAMP, PKA activity, or Epac activity increases frequency and rate of sealing

Because cAMP, PKA, and Epac are involved in vesicle mediated processes (Hatakeyama et al., 2007) and axon regeneration (Cai et al., 2001; Chierzi et al., 2005; Murray and Shewan, 2008), we hypothesized that Ca^{2+} influx through a damaged plasmalemma increases cAMP concentration, which activates PKA and Epac and leads to repair of plasmalemmal damage. (This hypothesis implies that PKA and Epac act downstream of cAMP, which acts downstream of Ca^{2+} during plasmalemmal sealing.)

We first examined the effects of increased cAMP concentration by transecting cells in 1 mM db-cAMP, a membrane-permeable analog of cAMP (Qiu et al., 2002). The sealing frequency following neurite transection nearer to the soma at 0, 1, and 5 min PC was significantly increased by 1 mM db-cAMP compared to control sealing ($p < 0.01$, CMH χ^2) (Fig. 2.2B). Furthermore, cells with neurites transected nearer to the soma in 1 mM db-cAMP sealed at a significantly faster rate compared to control sealing ($p < 0.01$, FZT) (Table 2.2). At 10 and 20 min PC, 1 mM db-cAMP did not significantly increase the sealing frequency of cells compared to control sealing, because sealing was almost complete by 10 min PC ($p > 0.05$, CMH χ^2). Similarly, 1 mM db-cAMP significantly increased the sealing frequency (at 0, 1, and 2.5 min PC) and increased the rate of sealing for cells with neurites transected farther from the soma compared to control sealing. Cells transected nearer to or farther from the soma in 50 μM db-cAMP sealed at a significantly greater frequency and faster rate compared to control sealing at 5 and 20 min PC ($p < 0.01$, CMH χ^2 ; data not shown), indicating that 1 mM db-cAMP likely saturated all

relevant cAMP targets.

We next examined whether increased PKA or Epac activity enhanced plasmalemmal sealing. With the exception of cells transected farther from the soma at 0 min PC (see below), cAMP analogs that activate PKA (cBiMPS) or Epac (Epac-cAMP) had nearly the same effect as db-cAMP. Specifically, 8 μ M cBiMPS or 8 μ M Epac-cAMP significantly increased the sealing frequency ($p < 0.05$, CMH χ^2) (Fig. 2.2 B,C) and rate ($p < 0.01$, FZT) (Table 2.2) compared to control sealing for cells transected nearer to and farther from the soma. These data are consistent with our hypothesis that cAMP activates PKA and Epac during plasmalemmal sealing.

Ca²⁺ independent sealing produced by cAMP analogs

In all previous studies and in our current studies presented above (Table 2.1, Fig. 2.2 A), Ca²⁺ influx has been necessary to initiate sealing of plasmalemmal damage (see list in supplemental list, available at www.jneurosci.org as supplemental material). In contrast, Figure 2. 2, B and C, show that this Ca²⁺ requirement can be bypassed by 1 mM db-cAMP, 8 μ M cBiMPS, or 8 μ M Epac-cAMP. That is, when cells are transected in Ca²⁺-free saline containing one of these three cAMP analogs, some cells seal before Ca²⁺ addition (i.e., at 0 min PC).

To further examine whether cAMP analogs can initiate plasmalemmal sealing in the absence of Ca²⁺, we transected cells in Ca²⁺-free saline containing 0.5 mM EGTA and one of these cAMP analogs and evaluated sealing without ever exposing these cells to Ca²⁺ (i.e., after transecting neurites in Ca²⁺-free saline, dye was added to the Ca²⁺-free

saline). We observed no significant ($p > 0.05$, CMH χ^2) difference in the sealing frequency between cells transected in a cAMP analog and never exposed to Ca^{2+} compared to cells transected in a cAMP analog and exposed to Ca^{2+} at 0 min PC (Fig. 2.3 A, compare gray bars to black bars). Furthermore, B104 cells sealed at a significantly ($p < 0.05$, CMH χ^2) higher frequency at 0 min PC in 1 mM db-cAMP compared to the other two cAMP analogs, whether or not cells were exposed to Ca^{2+} (Fig. 2.3 A). All these data are consistent with an ability of cAMP-activated proteins to initiate neuroprotective plasmalemmal sealing in the absence of Ca^{2+} and are consistent with our hypotheses that PKA and Epac act downstream of Ca^{2+} during plasmalemmal sealing.

cAMP cannot fully substitute for Ca^{2+} requirements during plasmalemmal sealing

We examined whether cAMP can completely substitute for Ca^{2+} by comparing the sealing frequency and rate initiated by 1 mM db-cAMP at various "post-cAMP times" in cells never exposed to Ca^{2+} to sealing initiated by Ca^{2+} saline (control sealing) at various PC times. The sealing frequency and rate in 1 mM db-cAMP without Ca^{2+} was significantly less than the frequency ($p < 0.01$, CMH χ^2) and rate ($p < 0.01$, FZT) of control sealing (Fig. 2.3 B, compare post-cAMP curves to PC curves). When cells were deprived of Ca^{2+} for >20 min, even in the presence of 1 mM db-cAMP, we observed membrane blebbing (plasmalemmal breakdown) and a decrease in sealing frequency at 20 min post-cAMP time compared to control sealing. These data suggest that cAMP cannot completely substitute for Ca^{2+} in plasmalemmal sealing and that exposure to Ca^{2+} -free solutions for >15 min has deleterious effects on membrane integrity and cell viability.

Inhibiting PKA activity decreases plasmalemmal sealing frequency and rate

Because activating PKA increased the ability of B104 cells to seal (Fig. 2.2 B,C), we hypothesized that inhibiting PKA would decrease the ability of cells to seal. We therefore inhibited PKA with KT5720, a membrane-permeant, small molecule, PKA inhibitor that blocks the ATP binding site of PKA (Davies et al., 2000). Since KT5720 is soluble in DMSO but not in distilled water or Ca^{2+} -free saline, we first transected B104 cells in 312 mM DMSO as a vehicle control. Except for one data point at 20 min PC for cells transected farther from the soma, the sealing frequency of cells following transection in 312 mM DMSO was not significantly different from control sealing in which cells are transected in Ca^{2+} -free saline ($p > 0.05$, CMH χ^2 ; data not shown). Likewise, cells transected nearer to, or farther from, the soma in 312 mM DMSO did not seal at a significantly different rate compared to control sealing ($p > 0.05$, FZT; Table 2.2).

To examine whether inhibiting PKA decreases sealing, we transected cells in 1 mM KT5720 dissolved in DMSO. Specifically, 1 mM KT5720 significantly decreased the sealing frequency of cells following transection nearer to the soma at all PC times compared to control sealing ($p < 0.001$, CMH χ^2) (Fig. 2.3 C). Furthermore, 1 mM KT5720 significantly decreased the sealing rate compared to control sealing ($p < 0.001$, FZT) (Table 2.2). We obtained similar results for neurites transected farther from the soma in 1 mM KT5720 (Fig. 2.3 D).

Since KT5720 has been reported to inhibit protein kinases other than PKA in cell lysates (Davies et al., 2000), we examined the effect of PKI, a structurally dissimilar

peptide inhibitor that binds to the regulatory subunit and more specifically inhibits PKA (Dalton and Dewey, 2006). Compared to control sealing, both 50 μ M PKI and 1 mM KT5720 decreased the frequency and the rate of sealing to a similar extent for neurites transected nearer to or farther from the soma at all PC times investigated, suggesting that the primary effect of both compounds is to inhibit PKA (Fig. 2.3 C,D). When cells were transected in greater (2x) concentrations of either inhibitor or in both inhibitors at the same time, we did not observe a further decrease in sealing frequency, suggesting that both inhibitors are inhibiting PKA to the maximum possible extent at the concentrations tested (data not shown).

Epac activation partly overcomes PKA inhibition

To further investigate the role of Epac in plasmalemmal sealing, we inhibited PKA with 50 μ M PKI while simultaneously increasing Epac activity with 8 μ M Epac-cAMP (Fig. 2.4 C,D). Despite a consistent, significant decrease in the sealing frequency at all PC times compared to control sealing (Fig. 2.4 C), the rate of sealing for cells transected nearer to the soma in 8 μ M Epac-cAMP and 50 μ M PKI was not significantly different from the rate of control sealing ($p > 0.05$, FZT) (Table 2.2). Similar results for the frequency and rate of sealing were observed for cells transected farther from the soma in 8 μ M Epac-cAMP and 50 μ M PKI compared to control sealing (Fig. 2.4 D, Table 2.2). Thus, when PKA is inhibited, Epac activation is able to restore the rate but not the frequency of sealing to control levels.

Cells transected in 8 μ M Epac-cAMP with 50 μ M PKI sealed at a significantly

higher frequency ($p < 0.01$, CMH χ^2) and significantly faster rate ($p < 0.01$, FZT) compared to cells transected nearer to or farther from the soma in 50 μM PKI (Fig. 2.4C,D). Thus, Epac activation is able to partially bypass PKA inhibition, suggesting that plasmalemmal sealing has an Epac-dependent, PKA-independent component.

nPKC inhibition decreases frequency and rate of plasmalemmal sealing

PKC isozymes are involved in vesicle exocytosis and plasmalemmal sealing in invertebrate and non-neuronal preparations (Togo et al., 2003), and novel PKC (nPKC) isozymes are involved in cell wall maintenance in yeast (Arellano et al., 1999). To investigate whether nPKCs might affect plasmalemmal sealing, we inhibited an nPKC isozyme using an nPKC pseudosubstrate fragment (Steinberg, 2008). We examined cells transected farther from the soma, because this transection distance is a more sensitive measure of sealing (Fig. 2.4). At 5, 10, and 20 min PC, cells transected farther from the soma in 7 μM pseudosubstrate fragment sealed at a significantly ($p < 0.001$) lower frequency (CMH χ^2) and a significantly slower rate ($p < 0.01$, FZT) compared to control sealing (Fig. 2.4 C). These data suggest that nPKC facilitates plasmalemmal sealing.

Melatonin decreases frequency of plasmalemmal sealing

Cytosolic oxidation after traumatic injury enhances plasmalemmal sealing in muscle cells (Cai et al., 2009a,b), and melatonin acts as an antioxidant by scavenging free oxygen radicals (Millán-Plano et al., 2010). To investigate whether plasmalemmal sealing might be affected by an antioxidant, we transected neurites of B104 cells in 2 mM

melatonin, the maximum concentration that could be dissolved in distilled water. As seen for other test substances (i.e., KT5720, or PKI), melatonin significantly ($p < 0.01$, CMH χ^2) (Fig. 2.4 D) reduced the sealing frequency for cells transected nearer to or farther from the soma at 5 min PC compared to control sealing. Lower concentrations of melatonin (0.48 mM; data not shown) showed similar effects nearer to ($p < 0.05$, CMH χ^2) and farther from ($p < 0.01$, CMH χ^2) the soma compared to control sealing.

Discussion

Vesicles, plasmalemmal sealing, and cell survival

Before 1994, authors of textbooks (e.g., Kandel et al., 1991) and research publications (Spira et al., 1993) assumed that minor plasmalemmal damage was sealed by spreading of plasmalemmal lipids and that complete cellular or axonal transection was sealed by collapse and fusion of plasmalemmal leaflets. In 1994, we (Krause et al., 1994) showed that in several invertebrate neuronal preparations, either lesion type sealed by an accumulation of membrane-bound structures (mostly vesicles); Steinhardt et al. (1994) also reported a similar sealing mechanism in sea urchin eggs and mammalian epithelial cells. Damage-induced vesicles may continuously pack more densely and/or fuse with each other and nearby undamaged membrane to form a plug that retards the influx/efflux of smaller and smaller particles (Fishman and Bittner, 2003). Alternatively, these vesicles may interact in the vicinity of the damage site to form a "wound vesicle" or "membrane patch" that suddenly seals the membrane disruption (McNeil, 2009). Data from at least 20 different preparations from many phyla (see supplemental references list, available at

www.jneurosci.org as supplemental material) consistently show that plasmalemmal sealing requires (isomers of) the same proteins, many of which are Ca^{2+} dependent and associated with cytoskeletal elements and/or vesicle trafficking/fusion in synapses and/or the Golgi apparatus (for reviews, see Fishman and Bittner, 2003; McNeil, 2009).

The consistent decrease in sealing frequency and rate observed for B104 cells transected nearer to the soma compared to cells transected farther from the soma (Figs. 2.2 – 2.4) may be partly because the diameter of a neurite (or axon) of a B104 (or other neuronal) cell measured nearer to the soma is often larger than the diameter of that same neurite measured farther from the soma (Lucas et al., 1985; 1990). Thus, vesicles probably require more time to accumulate to seal plasmalemmal damage of a larger diameter neurite or axon. Additionally, the potentially greater Ca^{2+} influx through a damage site nearer to the soma has a shorter diffusion distance to reach the soma and so may produce greater increases in somal Ca^{2+} , thus increasing the probability of cell death (Nguyen et al., 2005).

Model of plasmalemmal sealing

Because rapid repair of plasmalemmal damage is necessary for their survival, all eukaryotic cells may have evolved multiple parallel pathways to ensure rapid plasmalemmal sealing occurs, as shown in Figure 2.5 and as discussed below. cAMP increases plasmalemmal sealing (Fig. 2B,C), but cannot completely substitute for Ca^{2+} (Fig. 2.3 B)

cAMP increases vesicular interactions in Golgi trafficking, growth cone

extension, and transmitter release at synapses (Yoshihara et al., 2000; Sedej et al., 2005; for review see Hannila and Filbin, 2008). cAMP and cAMP activated proteins increase plasmalemmal sealing at PC times up to 20 min, including at 0 min PC, even when the bathing solution contains no Ca^{2+} (Fig. 2.2 B,C). That is, increased cAMP concentration or increased PKA or Epac activity can partly bypass the requirement for Ca^{2+} in plasmalemmal sealing. A similar result has been reported for *Drosophila* neurons, where increased cAMP concentration can partly bypass the Ca^{2+} requirements of membrane fusion proteins for vesicle exocytosis at presynaptic release sites (Yoshihara et al., 1999, 2000). However, cAMP cannot completely substitute for Ca^{2+} during plasmalemmal sealing, since Ca^{2+} produces higher sealing frequencies than cAMP or cAMP analogs at all PC times (Fig. 2.3 A). These data suggest the existence of other redundant Ca^{2+} -dependent pathways parallel to cAMP pathways, such as diacylglycerol (DAG) activation of nPKCs (see below) (Fig. 2.5).

PKA activation increases sealing (Fig. 2B,C); PKA inhibition decreases sealing (Fig. 2.4 A,B)

PKA activates many proteins important for membrane fusion and vesicle trafficking, such as SNAP-25 (Bronk et al., 2007), syntaxin (Nagy et al., 2004), synaptobrevin isoforms (Yoshihara et al., 1999, 2000), NSF (Garcia et al., 1995), and synapsin (Menegon et al., 2006). Most of these membrane fusion proteins are more abundant along axolemmal walls compared to nerve terminals (Tao-Cheng et al., 2000), suggesting that they may play a role in plasmalemmal repair. PKA may increase sealing

by activating these and other membrane fusion and vesicle trafficking proteins, whereas PKA inhibition likely prevents activation of these proteins.

Epac activation increases sealing (Fig. 2.2 B,C), partly independent of PKA (Fig. 2.4 A,B)

Epac isoforms are involved in vesicle formation (Hatakeyama et al., 2007), exocytosis (Sedej et al., 2005), and neuronal survival after damage (Murray and Shewan, 2008). Epac may increase plasmalemmal sealing by stimulating vesicle traffic by binding to Rim2 and piccolo (Fujimoto et al., 2002) and exchanging guanine nucleotides for Rab3 (Branham et al., 2009). Epac increases membrane fusion by activating Sec1/Munc13 (Kwan et al., 2007) or SNARE proteins (Sedej et al., 2005). Inhibition of trans-Golgi traffic using the bacterial toxin brefeldin A decreases the influence of Epac on synaptic transmission, suggesting that Epac isoforms activate Rab3A exocytosis in both synaptic and Golgi trafficking pathways (Ster et al., 2009). That is, Epac pathways likely activate proteins in the PKA pathway (e.g., Rab3A, mUNC proteins, SNAREs) (Hochbaum et al., 2008), but also may activate parallel (redundant) Ca^{2+} -dependent pathways important for plasmalemmal sealing (Fig. 2.5).

nPKC inhibition decreases plasmalemmal sealing (Fig. 2.4C)

nPKCs activate many vesicle-mediated processes, such as cell wall maintenance and repair during yeast fission (Arellano et al., 1999), axonal growth cone turning, transport of β_1 integrins, and neurite extension through phosphorylation of MARCKS and

GAP43 (Sivasankaran et al., 2004; Gatlin et al., 2006; Sisková et al., 2006; Korshunova et al., 2007; Tsai et al., 2007). Inhibition of nPKC isozymes inhibits such vesicle-mediated processes and thus likely decreases the ability of vesicles to seal a damaged plasmalemma. nPKC isozymes are activated by binding of DAG to their regulatory subunits. Intracellular DAG concentration is increased by damage-induced Ca^{2+} influx that activates calpain to cleave and activate phospholipase C. [Calpains are Ca^{2+} -dependent proteases necessary for plasmalemmal sealing in many preparations (Godell et al., 1997; Mellgren et al., 2007).]

Melatonin decreases sealing (Fig. 2.4 D)

The diffusion of Ca^{2+} and other substances into or out of a cell at a site of plasmalemmal damage oxidizes the cytosol (McNeil, 2009). Cytosolic oxidation activates proteins (Sod family, glutathiones, thioredoxins) responsible for maintaining the intracellular redox environment and cell survival (Circu et al., 2009). In muscle, cytoplasmic oxidation activates the TRIM protein mitsigumin 53 (MG53), which stimulates vesicle accumulation (Cai et al., 2009a,b). These vesicles likely undergo Ca^{2+} -dependent membrane fusion. Vesicle accumulation by damage-induced TRIM protein activation may also occur in neurons, since neuronal TRIM proteins increase vesicle accumulation in growth cones (van Diepen et al., 2005). Thus, the antioxidant melatonin may decrease sealing by reducing the formation of oxidation-induced vesicles.

Because melatonin decreases plasmalemmal sealing at 5 min PC, we hypothesize that other antioxidants or reducing agents may also impair sealing, whereas oxidizing

agents may facilitate plasmalemmal sealing. Since cytosolic oxidation plays an important role in neurodegenerative disorders such as amyotrophic lateral sclerosis (Circu et al., 2009), a more complete understanding of how oxidation affects neurons, especially following plasmalemmal damage, may provide key insights into the etiology of neurodegenerative disorders.

Evolutionary origin of membrane fusion proteins was to seal plasmalemmal damage

Similar cellular/molecular mechanisms of plasmalemmal sealing occur in all eukaryotic cells and use protein isomers that have likely undergone a conservative evolution (see Supplemental Sealing List, page 73). Since eukaryotic cells likely evolved a plasmalemmal membrane before membrane-enclosed organelles (Gerhart and Kirchner, 1997), we suggest that the first evolved role of membrane fusion proteins activated by PKA, Epac, PKC, or cytosolic oxidation was likely to seal plasmalemmal damage. Membrane fusion proteins were likely then co-opted in eukaryotic evolution for use in Golgi trafficking and subsequently, as suggested by Südhof and Rothman (2009), for transmitter release. Therefore, a better understanding of the molecular pathways of plasmalemmal sealing is likely to increase our understanding of vesicle interactions and membrane fusion in the Golgi apparatus, exocytosis, and synaptic transmission.

Clinical importance of plasmalemmal sealing

Repair of plasmalemmal damage is necessary but not sufficient for survival of eukaryotic cells, including B104 cells (Schlaepfer, 1973; Bittner and Fishman, 2000;

Nguyen et al., 2005). For example, neurons that seal plasmalemmal disruptions at sites nearer to the soma are less likely to survive compared to neurons that seal damage at sites farther from the soma (Ramon y Cajal, 1928; Loewy and Shader, 1977; Lucas et al., 1985, 1990; Yoo et al., 2004; Nguyen et al., 2005). Limiting Ca^{2+} influx by increasing the rate of plasmalemmal sealing could increase the survival rate of injured neurons (i.e., provide neuroprotection), potentially increasing behavioral recovery following traumatic injury to the CNS or PNS neurons (Britt et al., 2010; Nehrt et al., 2010). Increasing plasmalemmal sealing also decreases the adverse affects of treadmill climbing in normal mice and in a mouse model of muscular dystrophy (Bansal and Campbell, 2004). A more complete understanding of plasmalemmal repair may lead to new clinical treatments to better treat conditions involving plasmalemmal damage, including traumatic injury, neurodegenerative diseases, stroke or other ischemic conditions, and muscular degenerative disorders.

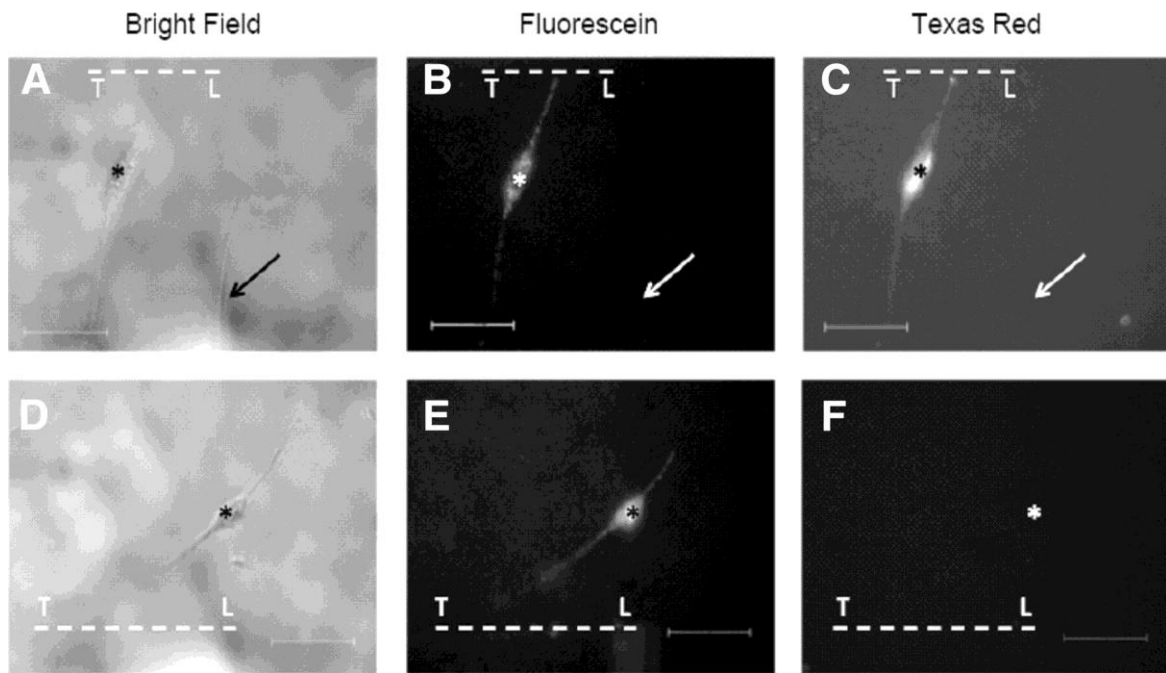


Figure 2.1 A–F: Bright-field (A, D) and fluorescence (B, C, E, F) images typical of those used to assess dye uptake or exclusion by B104 cells having a transected neurite. Bright-field images (A, D) were taken after transecting a neurite, marked by a score line [transection line (T - - -L)], in Ca^{2+} -free saline containing fluorescein dextran. After 10 min in Ca^{2+} -free saline, the cells were bathed in Ca^{2+} -saline for 5 min, at which time Texas Red dextran was added to the Ca^{2+} -saline. The cells were then imaged for fluorescein (B, E) and Texas Red (C, F) emission. The presence of fluorescein emission in B and E (cells marked with asterisk) shows that these cells took up fluorescein dye through a damaged plasmalemma (transected neurite). The presence of Texas Red emission (C) shows that this cell (marked with asterisk) did not exclude dye and therefore did not form a plasmalemmal seal. The absence of Texas Red emission (F) shows that this cell (location of cell marked with asterisk) excluded dye and therefore had formed a plasmalemmal seal. The uninjured cell (indicated by arrows, A–C) did not take up either dye and therefore shows no emission. Scale bars in all panels represent 50 μm .

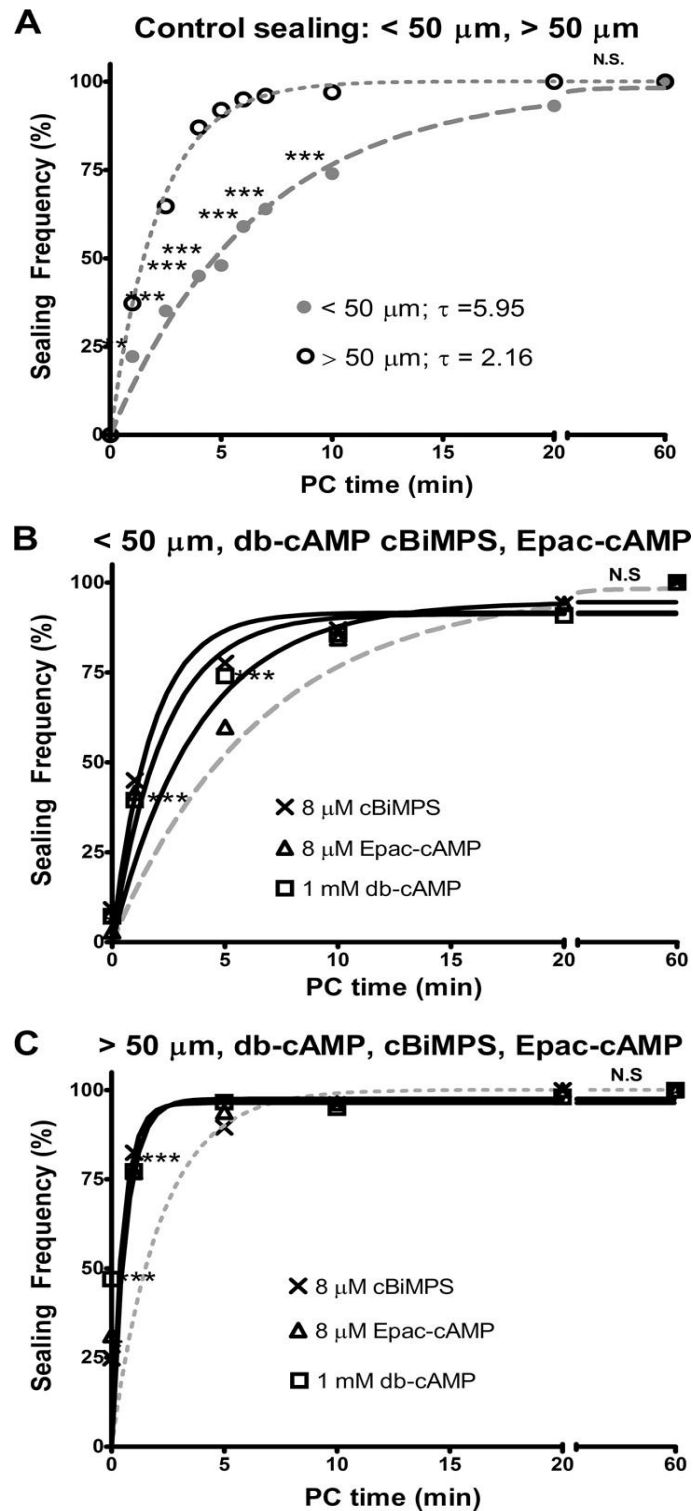
PT time (min)	PC time (min)	Dye exposure time (min)	Sealing frequency <50 μm (<i>n</i> , <i>N</i>)	Sealing frequency >50 μm (<i>n</i> , <i>N</i>)
1–2	5	10	48% (38, 2)	92% (25, 2)
9–10	5	10	52% (50, 2)	88% (26, 2)
1–2	5	2	48% (42, 2)	94% (18, 2)
9–10	5	2	46% (46, 2)	91% (22, 2)

Table 2.1: PC time, not PT time or dye exposure time, determines sealing time of

B104 cells

PT time is post-transection time (min). PC time is the time (min), after adding Ca^{2+} -saline, when Texas Red dextran was added to the bath solution. Dye exposure time is time (min) when B104 cells were bathed in Ca^{2+} -saline that contained Texas Red dextran. Sealing frequency is percentage of individually damaged, uniquely identifiable B104 cells with neurites transected <50 μm or >50 μm from the cell body that excluded Texas Red dextran. Numbers in parentheses (*n*,*N*) are the total number (*n*) of B104 cells with a transected neurite examined in a set (*N*) of identically treated Petri dishes. The sealing frequency of B104 cells was significantly different when transection distance or PC time was varied, but not when PT time or dye exposure time was varied.

Figure 2.2. A–C, Sealing frequency (%) plotted versus PC time (min). Sealing frequency



increases as PC time increases following neurite transection nearer to (<50 μm ; **A, B**) or farther from (>50 μm ; **A, C**), the soma. In this and subsequent figures, each line represents the sealing frequency for control sealing (dotted or dashed lines) or test substances (solid lines) fitted to Eq. 2.1 by GraphPad Prism (see Materials and Methods). **A**, Control sealing for neurites transected nearer to (dashed gray line, filled circles) or farther from (dotted gray line, open circles) the soma in Ca^{2+} -free saline and then exposed to Ca^{2+} at 0 min PC. **B**, **C**, Neurites transected in 1 mM db-cAMP (open squares), 8 μM cBiMPS (crosses), or 8 μM Epac-cAMP (open triangles) in Ca^{2+} -free saline and then exposed to Ca^{2+} at 0 min PC. In **A–C**, the x-axis is interrupted between 20 and 60 min PC so that differences in sealing frequencies from 0 to 20 min PC can more easily be observed. In **B** and **C** and subsequent figures, control sealing curves from Fig. 3A are replotted as dashed (<50 μm) or dotted (>50 μm) lines without data points to compare the effects of test substances (e.g., db-cAMP) to control sealing. The total number of cells transected to obtain each data point (n) varied from 40 to 403 on a total number (N) of Petri dishes (2–15). These numbers (n, N) are given in supplemental Table 2.1, A and B. N.S., No significant difference, $p > 0.95$.

Test substance	<50 μm τ (min)	<50 μm k (min^{-1})	R^2 < 50 μm	> 50 μm τ (min)	>50 μm k (min^{-1})	R^2 > 50 μm
Control	5.95	0.168	0.9865	2.16	0.461	0.9970
db-cAMP	1.98**	0.503**	0.9877	0.622**	1.61**	0.9976
db-cAMP (no Ca^{2+}) [#]	11.62***	0.086***	0.9455	3.98**	0.251**	0.9877
cBiMPS	1.24**	0.805**	0.9413	0.497**	2.01**	0.8231
Epac-cAMP	2.89**	0.345**	0.9141	0.628**	1.59**	0.7933
DMSO	7.59	0.131	0.9798	2.15	0.461	0.9856
KT5720	20.1***	0.049***	0.9769	9.91***	0.10***	0.9769
PKI	25.9***	0.038***	0.9972	10.7***	0.093***	0.9676
Epac-cAMP plus PKI	7.37	0.138	0.9795	3.35	0.298	0.9404
nPKC γ PSF				6.59**	0.152***	0.9618

Table 2.2: Effect of test substances on the time constant (τ) and rate constant (k) of sealing: Statistical comparisons of rate constants (k , min^{-1}) or exponential time constants (τ , min) for sealing of B104 cells transected nearer to (<50 μm) or farther from (>50 μm) the soma. Cells transected nearer to the soma and bathed in a given test substance always sealed at a slower rate compared to cells transected farther from the soma and bathed in the same test substance. R^2 < 50 μm or R^2 > 50 μm represents the goodness of fit values obtained from a single exponential model to fit the sealing frequency at all PC times for control sealing or for sealing in a given test substance. Asterisks indicate the level of significant difference between sealing time constants or rate constants for a given test substance compared to control sealing. Significance levels for this and all other tables and figures are indicated beside each value as follows: no asterisk = $p > 0.05$ and $p < 0.95$; single asterisk (*) = $p < 0.05$; double asterisk (**) = $p < 0.01$; and triple asterisk (***) = $p < 0.001$. [#]Initial increase in sealing frequency.

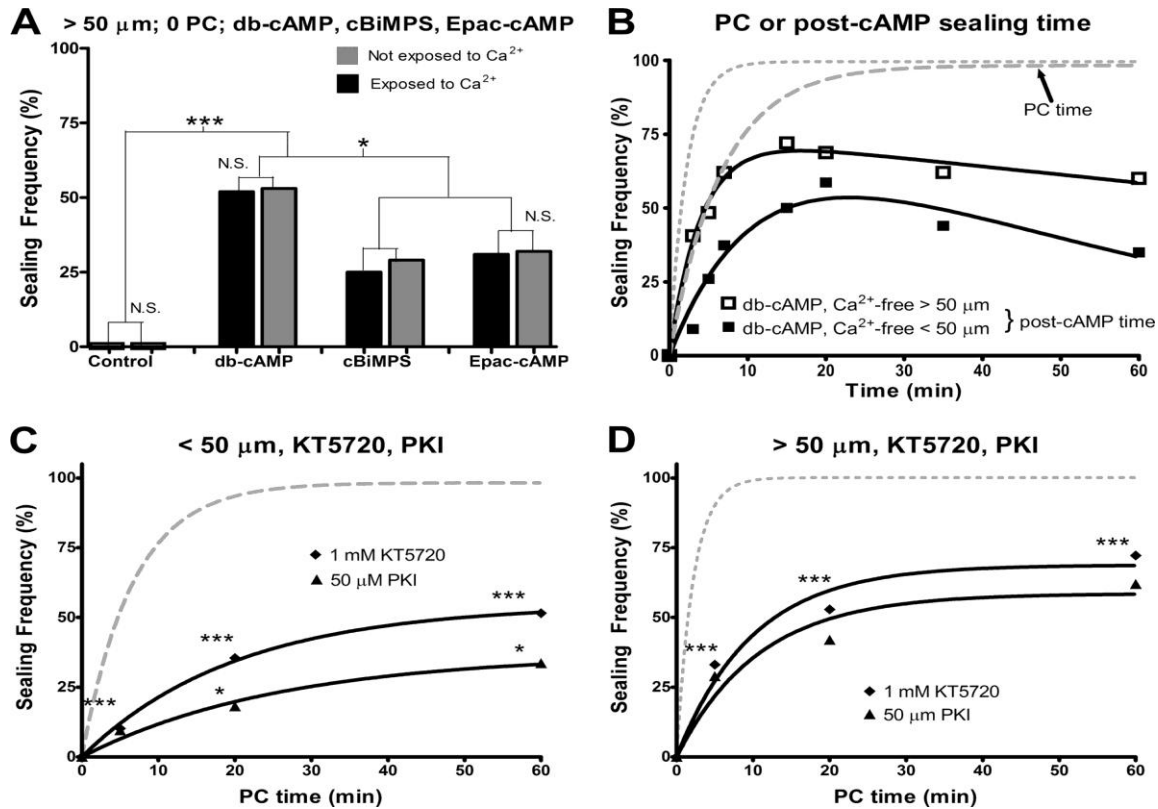


Figure 2.3 A: Sealing frequency (%) of B104 cells transected >50 μm from the soma in Ca^{2+} -free saline or Ca^{2+} -free saline containing one of the cAMP analogs and assessed for sealing at 0 min PC in either Ca^{2+} saline (black bars) or Ca^{2+} -free saline with 0.5 mM EGTA (gray bars). **B,** Sealing frequency (%) versus post-cAMP addition time (min) for cells transected nearer to or farther from the soma (solid lines). Cells were transected in Ca^{2+} free saline, after which db-cAMP without Ca^{2+} (squares) was added to the Petri dish. Cells that were bathed in 1 mM db-cAMP following neurite transection were never exposed to extracellular Ca^{2+} . Control sealing frequency (%) versus PC time (min) plotted following neurite transection nearer to (dashed line) or farther from the soma (dotted line) as described for Figure 2A. **C, D:** Sealing frequency (%) versus PC time (min) following neurite transection nearer to (**C**) or farther from (**D**) the soma in 1 mM KT5720 (diamonds) or 50 μM PKI (triangles).

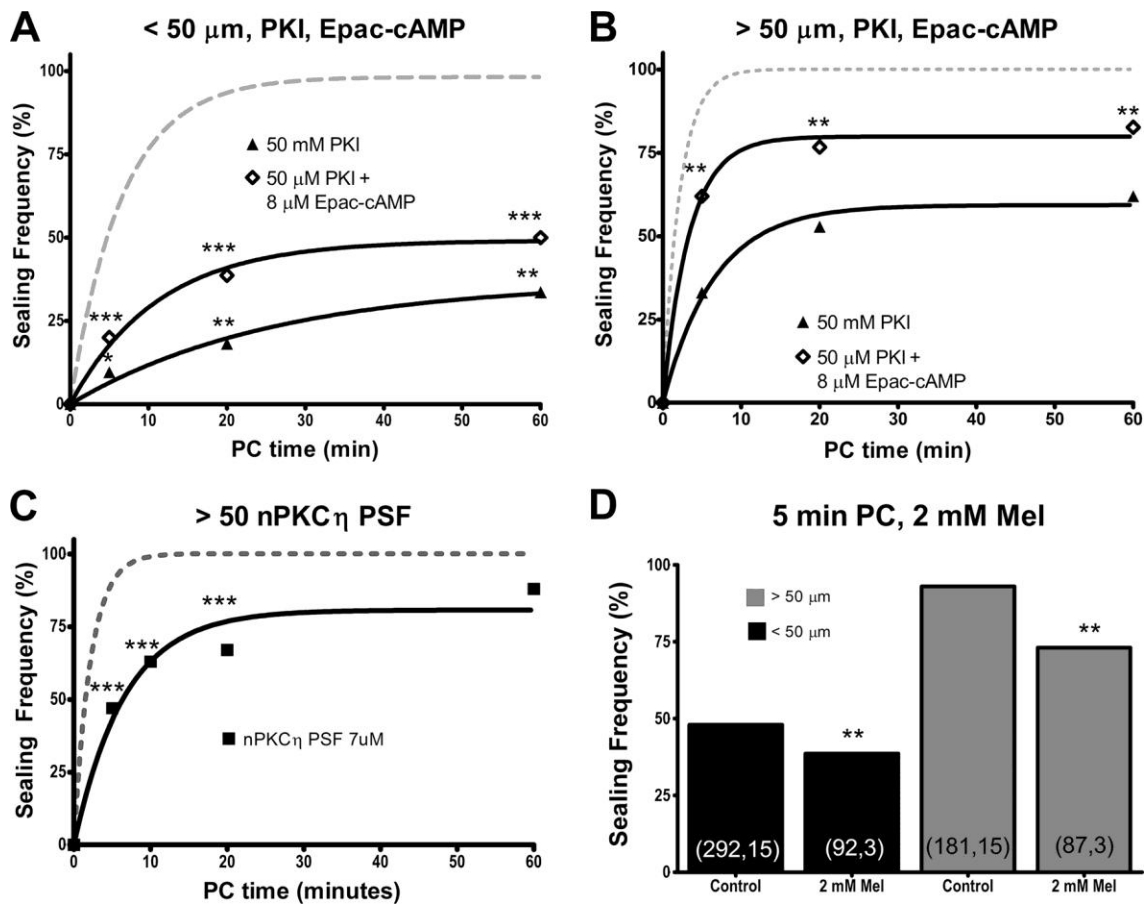


Figure 2.4. A–C: Sealing frequency (%) versus PC time (min) following neurite transection nearer to (A) or farther from (B, C) the soma in 8 μM Epac-cAMP and 50 μM PKI (unfilled diamonds), 50 μM PKI (filled triangles) or nPKC pseudosubstrate fragment (PSF; solid line, filled squares). D, Sealing frequency of cells transected nearer to (black bars) or farther from (gray bars) the soma in 2 mM melatonin (Mel) or Ca^{2+} -free solution (control) and assessed for sealing at 5 min PC.

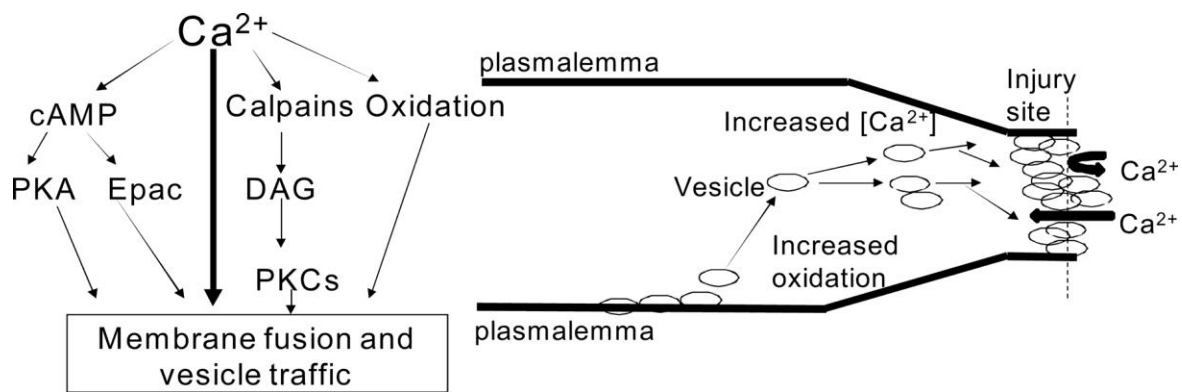


Figure 2.5: Model of plasmalemmal sealing. Ca^{2+} flowing inward through the damage site activates multiple parallel (redundant) pathways that increase cAMP concentration (Figs. 2B,C, 3A,B) by activating Ca^{2+} -dependent adenylate cyclases (Dunn et al., 2009). Ca^{2+} influx also activates calpain (Eddleman et al., 1997), whose protease action rearranges the cytoskeleton, partially constricting the cut ends of a transected axon or neurite, and also increases DAG availability by activating phospholipases. Ca^{2+} influx at sites of plasmalemmal damage also leads to increased cytosolic oxidation, facilitating plasmalemmal sealing (McNeil, 2009). Production of membrane-bound structures, usually vesicles, is stimulated by cAMP activation of PKA and Epac (Hatakeyama et al., 2007), DAG activation of nPKCs (Steinberg, 2008), and cytosolic oxidation (Cai et al., 2009a,b). These vesicles are targeted to and fuse with the damage site by: (1) PKA phosphorylation of SNARE and SNARE-related proteins important for vesicle traffic (Deák et al., 2006; Menegon et al., 2006; Bonanomi et al., 2007) (Figs. 2B,C, 3A,C,D); (2) Epac, which activates proteins important for vesicle motility (Fujimoto et al., 2002) (Figs. 2B,C, 4A,B); (3) nPKC phosphorylation (Uberall et al., 1997; Tsai et al., 2007) (Fig. 4C); and (4) oxidative activation of vesicle motility proteins (van Diepen et al., 2005; Cai et al., 2009a,b) (Fig. 4D).

Supplemental Tables:

Table 2.1 A: Number of cells and dishes used to obtain the data points for all figures for cells transected nearer to (< 50 μ m) the soma.

Test substance	PC Time (min)										
	0	1	2.5	4	5	6	7	10	20	60	
Control	165,3	117,5	168,4	149,2	272,15	174,2	239,3	146,9	102,5	115,2	
db-cAMP	208,3	261,3			216,6			145,2	98,3	157,2	
cBiMPS	175,2	127,2			112,2			161,2	124,2	167,2	
Epac-cAMP	98,2	147,2			403,5			252,3	151,2	104,2	
DMSO					231,5			218,2	96,2		
KT5720					235,5			140,5	123,2		
PKI					167,5			88,2	137,2		
Epac-cAMP + PKI					110,2			181,2	135,2		

Table 2.1 B: Number of cells and dishes used to obtain the data points for all figures for cells transected farther from (> 50 μ m) the soma:

Test substance	PC Time (min)										
	0	1	2.5	4	5	6	7	10	20	60	
Control	112,3	67,5	71,4	118,2	143,15	110,2	147,3	126,9	56,5	91,2	
db-cAMP	88,3	123,3			89,6			61,2	53,3	71,2	
cBiMPS	129,2	57,2			48,2			128,2	97,2	86,2	
Epac-cAMP	112,2	40,2			102,5			108,2	90,2	123,2	
DMSO					103,5			48,2	87,2		
KT5720					130,5			121,5	90,2		
PKI					137,5			49,2	91,2		
Epac-cAMP + PKI					100,2			99,2	104,2		
nPKC η PSF									108,3		

Supplemental Table 2.1 Legend: **PC Time:** Time (min) when Texas Red dextran was added to the Ca²⁺-containing saline. **Numbers (n, N):** Pooled number of B104 cells (n) with a transected neurite examined in a set of identically treated Petri dishes (N) at a given PC time. Gray areas in **Table 1A** and **B** with no values indicate the PC times for a given test substance that were not investigated in this study.

Supplemental List of Plasmalemmal Sealing references by preparation:

Animals:

Invertebrates:

Cockroach Giant axons:

Yawo and Kuno, 1985;

Earthworm Medial giant axons:

Krause, et al., 1994; Ballinger, et al., 1997; Blanchette, et al., 1999; Lichstein, et al., 2000

Squid Giant Axons:

Krause, et al., 1994; Eddleman, et al., 1997, 1998; Godell, et al., 1997; Detrait, et al., 2000a

Sea Urchin Eggs:

Steinhardt, et al., 1994; Bi, et al., 1995; Terasaki, et al., 1997; Bi, et al., 1997; McNeil, et al., 2001; McNeil and McNeil, 2005;

Crayfish Medial Giant axons:

Eddleman, et al., 1997, 1998; Godell, et al., 1997; Detrait, et al., 2000a;

Starfish Oocytes:

Terasaki, et al., 1997

Mammals:

Rat Sciatic nerves:

Lore, et al., 1999; Marzullo, et al., 2003; Stavisky, et al., 2005; Britt, et al., 2010

Intestinal Endothelial/Epithelial cells:

Saito, et al., 1999; Miyake, et al., 2001, 2006; Paclik, et al., 2008; Garcia-Fernandez, et al., 2009;

Fibroblast:

Togo, et al., 1999; Togo, et al., 2000; Reddy, et al., 2001; Chakrabarti, et al., 2003; McNeil, et al., 2003; Togo, et al., 2003, 2004; Togo and Steinhardt, 2004; Shen, et al., 2005; Mellgren, et al., 2007; Mellgren, et al., 2009;

Guinea Pig spinal cord:

Shi and Pryor, 2000; Nehrt, et al., 2007; Cho, et al., 2010; Nerht, et al., 2010;

B104 Cells:

Detrait, et al., 2000b; Yoo, et al., 2003, 2004; Nguyen, et al., 2005;

PC12 Cells:

Yoo, et al., 2003, 2004; Detrait, et al., 2000b;

Cos7 cells (African Green Monkey):

Togo and Steinhardt, 2003;

S91 cells (mouse melanoma):

Togo and Steinhardt, 2003;

Mouse Skeletal Muscle:

Bansal, et al., 2003; Chakrabarti, et al., 2003; Bansal and Campbell, 2004; Cai, et al., 2009a, b; Mellgren, et al., 2009;

Rabbit corneal cells:

Shen and Steinhardt, 2005;

Cardiomyocytes:

Han, et al., 2007; Wang, et al., 2009

Rat Kidney Cells:

Idone, et al., 2008;

HeLa Cells:

Idone, et al., 2008

A549 (Lung cancer cells):

Kawai, et al., 2008;

Mast cells:

Shaik, et al., 2009;

Plants:

Arabidopsis:

Yamazaki, et al., 2008; Schapir, et al., 2009

Supplemental List of Plasmalemmal sealing references by molecule/protein/substance:

Actin/Microtubules:

Miyake, et al., 2001; Togo, 2004, 2006;

Annexins:

McNeil, et al., 2006

Arf1/Golgi: Togo, 2004;

Ca²⁺: Yawo and Kuno, 1985; Steinhardt, et al., 1994; Krause, et al., 1994; Bi, et al., 1995; Bi, et al., 1997; Terasaki, et al., 1997; Eddleman, et al., 1997; Godell, et al., 1997; Eddleman, et al., 1998; Blanchette, et al., 1999; Lore, et al., 1999; Saito, et al., 1999; Togo, et al., 1999; Shi and Pryor, 2000; Togo, et al., 2000; Detrait, et al., 2000a; Detrait, et al., 2000b; Miyake, et al., 2001; Reddy, et al., 2001; Bansal, et al., 2003; Chakrabarti, et al., 2003; Marzullo, et al., 2003; McNeil, et al., 2003; Togo, et al., 2003; Yoo, et al., 2003; Lennon, et al., 2003; Bansal and Campbell, 2004; Togo, et al., 2004; Togo and Steinhardt, 2004; Yoo, et al., 2004; McNeil and McNeil, 2005; Nguyen, et al., 2005; Shen, et al., 2005; Stavisky, et al., 2005; Miyake, et al., 2006; Nehrt, et al., 2007; Han, et al., 2007; Mellgren, et al., 2007; Kawai, et al., 2008; Idone, et al., 2008; Paclik, et al., 2008; Yamazaki, et al., 2008; Cai, et al., 2009a; Cai, et al., 2009b; Garcia-Fernandez, et al., 2009; Mellgren, et al., 2009; Schapir, et al., 2009; Wang, et al., 2009; Britt, et al., 2010; Nerht, et al., 2010

Calmodulin: Steinhardt, et al., 1994; Bi, et al., 1997;

Calpains: Xie and Barret, 1991; Godell, et al., 1997; Howard, et al., 1999; Yoo, et al., 2003; Mellgren, et al., 2006; Mellgren and Huang, 2007; Mellgren, et al., 2007

Dysferlin: Bansal, et al., 2003; Lennon, et al., 2003; Bansal and Campbell, 2004;

Fetuin A: Mellgren and Huang, 2007

Kinesin: Steinhardt, et al., 1994; Bi, et al., 1997;

Lysosomes:

Reddy, et al., 2001; Idone, et al., 2008

MG53: Cai, et al., 2009a,b

PKA: Togo, et al., 2003, 2004; Shen and Steinhardt, 2005;
PKC: Togo, et al. 1999, 2000; Togo, 2004, 2006; Shen and Steinhardt, 2005;
PEG: Britt, et al., 2010; Nehrt, et al., 2010;
Silica nanoparticle-PEG matrix: Cho, et al., 2010
SNAP-25: Steinhardt, et al., 1994; Bi, et al., 1995;
Synaptobrevin: Steinhardt, et al., 1994; Bi, et al., 1995; Detrait, et al., 2000a; Yoo, et al., 2003; Shen, et al., 2005;
Synaptotagmin: Detrait, et al., 2000a,b; Reddy, et al., 2001; Chakrabarti, et al., 2003; Yoo, et al., 2003; Shen, et al., 2005; Yamazaki, et al., 2008;
Synaptophilin: Yoo, et al., 2003, 2004;
Syntaxin: Bi, et al., 1995; Detrait, et al., 2000a,b; Yoo, et al., 2003

For full references, see page 190

Chapter 3: Pathways for plasmalemmal repair mediated by PKA, Epac and cytosolic oxidation in rat B104 cells *in vitro* and sciatic axons *ex vivo*

Running Title: PKA, Epac, and cytosolic oxidation pathways of sealing

Abstract

Plasmalemmal repair (sealing) is necessary for survival of damaged eukaryotic cells. We previously reported that Ca^{2+} influx through plasmalemmal disruptions affects various substances (cAMP, PKA, Epac, PKC) and cytosolic oxidation to increase sealing, as assessed by formation of a dye barrier. We now report that Botulinum toxins (BoNT) A&E that cleave SNAP-25 and Tetanus toxin (TeNT) or BoNT B that cleave synaptobrevin all decrease sealing in rat B104 hippocampal cells and/or sciatic axons. Brefeldin A (Bref A), which inhibits Golgi vesicular trafficking and N-ethylmaleimide (NEM), which inhibits N-ethylmaleimide-Sensitive-Factor (NSF), also decrease sealing. Epac, but not PKA or cytosolic oxidation, partly overcomes the decrease in sealing produced by BoNT A, E, B and TeNT. PKA and increased cytosolic oxidation, but not Epac, can partly overcome the decrease produced by Bref A. PKA, Epac, and/or cytosolic oxidation cannot overcome the NEM-dependent decrease in sealing. Substances (NEM, Bref A, PKI, db-cAMP) that affect plasmalemmal sealing in B104 cells *in vitro* have similar effects on plasmalemmal sealing in rat sciatic nerves *ex vivo*. From these and other data, we propose a plasmalemmal sealing model having four redundant, parallel pathways mediated by 1) PKA, 2) Epac, 3) cytosolic oxidation, that all converge on NSF and 4) previously reported PKC pathway. Our data are consistent with hypotheses that the evolutionary origin of these pathways for vesicle interactions

and membrane fusion was to seal plasmalemmal damage and that similar pathways are found in all eukaryotic cells.

Introduction

Rapid (within minutes) repair of a damaged plasmalemma is necessary for survival of all eukaryotic cells. Sealing is especially important in neurons, which typically do not proliferate as readily as other cell types. *In vitro*, hippocampal-derived B104 cells with plasmalemmal damage nearer to the soma are less likely to rapidly repair that damage (Spaeth, et al., 2010), and thus are less likely to survive, compared to cells with a neurite transected farther from the soma (Nguyen, et al., 2005). *In vivo*, spinal motor neurons with axons transected nearer to their soma are also less likely to survive and therefore less likely to regenerate (Ramon y Cajal, 1928).

Eukaryotic cells repair (seal) plasmalemmal damage by a Ca^{2+} -dependent accumulation of vesicles that interact with each other and with nearby, undamaged membrane to rapidly form a plug that continuously decreases the influx/efflux of substances of smaller and smaller molecular weight (Krause et al., 1994; Bittner and Fishman, 2000; Yoo, et al., 2004). Formation of a vesicular plug requires cAMP activation of PKA and Epac (Spaeth, et al., 2010), and membrane fusion proteins, including SNAP-25, synaptobrevin, and syntaxin, involved in vesicle-mediated release of neurotransmitters, (Bi, et al., 1995; Detrait, et al., 2000a,b; Yoo, et al., 2003) and Arf 1, involved in Golgi vesicular trafficking (Togo, 2006). Cytosolic oxidation also may

increase sealing (Spaeth, et al., 2010), potentially by activating Tri-Partite Motif (TRIM) proteins (Cai, et al., 2009a,b).

In this paper, we report that sealing in B104 cells is increased by H₂O₂ that directly increases cytosolic oxidation, consistent with previous reports that sealing is decreased by reducing agents such as melatonin (Spaeth et al., 2010). Sealing is decreased by toxins BoNT A and E (cleave SNAP-25), and BoNT B and TeNT (cleave synaptobrevin), which decrease neurotransmitter release. Sealing is also decreased by Bref A, which inhibits Golgi-vesicular trafficking, and NEM, which inhibits NSF, a protein involved in membrane fusion for both neurotransmitter release (Kuner, et al., 2007) and Golgi vesicular trafficking (Morgans and Brandstatter, 1999). The increase in sealing due to cBiMPS activation of PKA, or H₂O₂ is prevented by BoNT A, E, B or TeNT cleavage of proteins involved in neurotransmitter release. The increase in sealing due to Epac-cAMP activation of Epac is prevented by Bref A inhibition of Golgi vesicular traffic, and partly prevented by BoNT A and TeNT. The increase in sealing induced by cBiMPS, Epac-cAMP or H₂O₂ is prevented by NEM inhibition of NSF. Substances that affect sealing of B104 cells *in vitro* also affect sealing of rat sciatic nerves *ex vivo*, consistent with our hypotheses that sealing occurs by similar pathways in all eukaryotic cells.

These and other data suggest a model of sealing involving at least four redundant, parallel, partly independent pathways: two cAMP-dependent sealing pathways (PKA and Epac) and an oxidation pathway that all converge on NSF, and a recently reported PKC pathway (Spaeth, et al., 2010).

Methods

B104 cells: B104 cells derived from a CNS neuroblastoma (Bottenstein and Sato, 1979) have often been used as a model system to study neuronal function *in vitro* (Toda, *et al.*, 1999; Tan, *et al.*, 2003; Yoo, *et al.*, 2003, 2004; Nguyen, *et al.*, 2005; Miller, *et al.*, 2006). These cells have easily identifiable cell bodies and neurites, allowing each precisely transected cell to be uniquely and individually identified (Detrait, *et al.*, 2000b; Yoo, *et al.*, 2003, 2004; Spaeth, *et al.*, 2010). Data on sealing of B104 cells is consistent with similar data on sealing from at least 20 other preparations from many phyla and different cell types *in vitro* and *in vivo* (Spaeth, *et al.*, 2010).

Cell culture: As previously described (Spaeth, *et al.*, 2010), B104 cells were grown in 75cm² vented cap flasks (BD-Falcon, Franklin Lakes, NJ) in a humidified incubator at 37°C in 5% CO₂ in 4 mL of “cell growth media,” which consists of a 1:1 mixture of Dulbecco’s Modified Eagle’s Media and Ham’s F12 (DMEM:F12, HyClone, Logan, UT), supplemented for growth with 10% heat inactivated fetal bovine serum (FBS, Hyclone, Logan, UT) and 1% antibiotics (10,000 Units of Penicillin/mL and 10 mg/mL of streptomycin, Sigma-Aldrich, St. Louis, MO). The cell growth media was changed every 2 days. Cultures were passaged at 80% confluency and cells were then either sub-cultured in a vented cap flask or seeded at approximately 2000 cells/cm² in cell growth media on Petri dishes coated with Poly-D-lysine (Sigma-Aldrich, St. Louis, MO) to prevent cells from detaching during solution changes and/or neurite transections. After 24 hours, the growth media was replaced with serum-free DMEM:F12 (Hyclone, Logan,

UT) to allow the B104 cells to differentiate. B104 neurites were transected 24-48 hours after replacing the cell growth media with serum-free DMEM:F12.

Transection of neurites of B104 cells: Prior to transecting neurites, the solution (DMEM:F12) in the Petri dish was washed out twice with a Ca^{2+} -free phosphate buffered saline (referred to as “ Ca^{2+} -free saline”, PBS -/-, HyClone, Logan, UT). All neurites were transected in Ca^{2+} -free saline using a sharpened, pulled-glass micro-capillary tube ("micro-knife"), which was placed on a micro-manipulator (Narishige Instruments, East Meadow, NY) and quickly drawn across the surface of the Petri dish, etching a score line that showed the path of the knife. We were able to uniquely and individually identify each transected cell by the relation of the transected neurite to its soma and to the score mark on the plate (see Spaeth et al., 2010).

Microscopy and Imaging: For all experiments, B104 cells were observed under an inverted Zeiss ICM-405 fluorescent microscope (Zeiss, West Germany) with a 40X, long focal distance lens. Transected cells were imaged through a hole cut out of the bottom of a plastic dish covered by a thin glass coverslip using a Leica DM IRBE outfitted with a 40x lens and a Leica DFC350 FX fluorescence camera at the UT Core Microscopy facility. Individually identified cells with neurites obviously transected within $< 50 \mu\text{m}$ of the soma were counted as transected “nearer to” the soma, and those with neurites transected at $> 50 \mu\text{m}$ of the soma were counted as transected “farther from” the soma. No further observations were made on any cell whose transection distance was not clearly definable.

Assessment of plasmalemmal sealing: We transected 10 – 130 uniquely identifiable cells within 10 min in a Petri dish containing Ca^{2+} -free saline. The Ca^{2+} -free saline was then replaced with a phosphate buffered saline containing 1 mM Ca^{2+} (“ Ca^{2+} -saline”, PBS+/+, HyClone, Logan, UT) to initiate the sealing process (Detrait *et al.*, 2000b; Yoo *et al.*, 2003; Spaeth *et al.*, 2010). The time elapsed after exposing cells to Ca^{2+} -saline is defined as the “post- Ca^{2+} addition time” (PC time).

At various PC times (0-60 min PC), 3kD Texas Red dextran (Molecular Probes, Eugene, OR) was added to the Ca^{2+} -saline to assess the formation of a plasmalemmal seal. For all experiments, the dye was thoroughly washed out with Ca^{2+} -saline after a 10 min exposure to Texas Red dextran and sealing was assessed. Transected cells that excluded Texas Red dextran were counted as “sealed”. Cells that did not exclude Texas Red dextran were counted as “not sealed”. Nearby undamaged cells did not take up Texas Red dextran. We consistently used 3 kDa Texas Red dextran to assess sealing in all other experiments reported herein to avoid any variation in sealing time due to differences in dye molecular weight (Eddleman *et al.*, 2000; Spaeth *et al.*, 2010).

Pharmacological Reagents: All pharmacological agents were added to Ca^{2+} -free saline before neurite transection and were dissolved in distilled water, unless otherwise noted. We used 8 μM Sp-5,6-Dichloro-1- β -D-ribofuranosylbenzimidazole-3',5'-monophosphorothioate, referred to as cBiMPS, (Biomol, Plymouth Meeting, PA; 419.2 Da) to activate PKA. We used 8 μM 8-(4-Chlorophenylthio) -2'-O-methyladenosine-cAMP, referred to as Epac-cAMP (Tocris Biosciences, Ellisville, MO; 507.82 Da) to activate Epac, and di-butyryl cyclic adenosine monophosphate, referred to as db-cAMP

(Biomol, Plymouth Meeting, PA; 398 Da) to activate both PKA and Epac. We used TeNT (Biomol, Plymouth Meeting, PA) and BoNT B (BB Tech, Dartmouth, NH) to cleave synaptobrevin. We used BoNT A and E (BB Tech, Dartmouth, NH) to cleave SNAP-25. We used NEM (Biomol, Plymouth Meeting, PA) to inhibit NSF, and Bref A (Biomol) to reduce trans-Golgi trafficking.

Western Blotting: Once the cells in vented cap flasks reached 80% confluency, they were removed from the surface of the flask using 1% Trypsin (Sigma-Aldrich), and collected in a pellet by gentle (4000 rpm) centrifugation. The pellet was re-suspended in 500 μ L M-Per mammalian protein extraction buffer (Fisher, Pittsburgh, PA). A broad protease cocktail inhibitor was added to prevent protein degradation (Fisher). Cells were gently shaken on a rotating table at 4° C for 30 minutes, and then vortexed for 1-2 minutes. Samples were denatured using Running Buffer/Lane marker (Fisher) and run on 4% stacking, 20% separating gels (Promega). Since Epac isoforms are relatively heavy, lower molecular weight proteins were run off the gel to insure proper separation of higher molecular weight proteins. Proteins were electro-transferred onto nitrocellulose membranes (Fisher). The membranes were pre-blotted with 5% BSA (Fisher) and probed with primary antibodies for Epac1, Epac2, or PKA (AbCam). The blots were washed in TBST (0.1% Tween 20 in TBS) and incubated in anti-donkey IgG-HRP at a dilution of 1:10,000. The blots were washed and developed with Super Signal (Fisher, Pittsburgh, PA).

Statistics: For each experimental treatment group, at a given PC time, the data was pooled for all cells (n) from all Petri dishes (N). See Supplemental Table 3.1 A and

B for n, N values for each data set at each PC time point in all figures presented in this paper. “Sealing frequency” is defined as the percent of a set of individually-transected and uniquely identified cells that exclude 3 kDa Texas Red dye (sealed) at a given PC time. The Cochran-Mantel-Haenszel χ^2 (CMH χ^2) test for independence was used to determine whether the differences between the sealing frequency at a given PC time for different experimental treatments was statistically significant ($p < 0.05$), as previously described (Agresti, 1996; Detrait, *et al.*, 2000b; Yoo, *et al.*, 2003, 2004; Spaeth *et al.*, 2010).

GraphPad Prism was used to fit the sealing frequency for all PC times of a given control or test substance to a one phase exponential equation (Spaeth *et al.*, 2010). The solid and dashed lines on all graphs calculated by GraphPad Prism represent the exponential equations fitted to the sealing frequencies at all PC times for all data sets. The maximum sealing frequency (plateau) was always reached within 60 min PC.

Sealing rate constants (k) were calculated by GraphPad Prism and used to calculate time constants ($\tau = 1/k$) equal to the PC time to achieve 63.2% of the observed maximum (plateau) sealing (Spaeth *et al.*, 2010). Rate or time constants for two experimental conditions were normalized and compared using Fisher’s Z transformation (FZT, Table 3.1). Two sealing rate or time constants were considered significantly different if p was < 0.05 , using a Z-table. R^2 values were also calculated for the exponential equation defining each time constant to determine how closely the exponential equations modeled the observed data (Table 3.1).

Sealing of cut rat sciatic axons *ex vivo*: All experimental procedures were approved by the University of Texas at Austin's Institutional Animal Care and Use Committee. Prior to surgical procedures, all animals were housed in groups of three in polycarbonate cages with sawdust bedding, maintained on a 12:12 dark:light cycle and given food and water *ad libitum*.

Surgical Procedures: As previously described (Britt, et al., 2010), rats were anesthetized with intraperitoneal injections of ketamine (90 mg/kg) and xylazine (10 mg/kg). An incision about 1.5 cm long was made in the left hindlimb quadriceps muscle to expose axons in the sciatic nerve. Exposed sciatic nerves were bathed with Ca^{2+} -free Krebs's physiological saline (Ca^{2+} -free saline in mM: 124 NaCl, 5 KCl, 1.2 KH_2PO_4 , 1.3 MgSO_4 , 26 NaHCO_3 , 10 Na ascorbate, 10 dextrose, pH 7.35), cleaned of connective tissue, and removed from the rat by cutting a nerve segment more distally and then more proximally with micro-scissors.

Nerve treatments: We have previously reported (Lore et al, 1999; Britt et al., 2010) that transected rat sciatic axons seal their cut ends when placed in Krebs physiological saline containing Ca^{2+} and do not seal in Ca^{2+} -free Krebs. Hence, some sciatic nerve segments with axons cut at both ends were placed in Petri dishes containing Ca^{2+} Krebs (n=2; positive control), or Ca^{2+} Krebs containing 1mM NEM (n=5), 10 μM Bref A (n=3), or 50 μM PKI (n=2) to inhibit sealing. Other sciatic nerve segments were placed in Petri dishes containing Ca^{2+} -free Krebs (n=3; negative control), or Ca^{2+} -free Krebs containing 1 mM db-cAMP (n=3) to enhance sealing. Texas Red dye (Molecular Probes) was then added to all dishes, which were then refrigerated for 14 hours at 4°C.

We examined the nerves for axonal uptake or exclusion of fluorescent dye using a Zeiss ICM-405 inverted fluorescent microscope. Images of axons in sciatic nerves were taken using a Leica DM IRBE with a 20X objective outfitted with a Leica DFC350 FX fluorescence camera.

Results

Plasmalemmal sealing *in vitro* in rat B104 cells with singly transected neurites

As previously described (Spaeth et al., 2010), neurites of B104 cells are transected in Ca^{2+} -free saline or in Ca^{2+} -free saline containing a test substance, or combination of test substances. After 10 minutes, the Ca^{2+} -free saline is replaced with Ca^{2+} -containing saline (1 mM Ca^{2+}) and dye is added at various post- Ca^{2+} (PC) times to evaluate sealing frequency defined as the percent of a set of individually-transected and uniquely identified cells that exclude 3 kD Texas Red dye (seal) at a given PC time. Sealing frequency data are fitted to a single phase exponential equation. Sealing rates are calculated from the exponential equation, as described in Methods.

Consistent with previous reports (Spaeth, et al., 2010), B104 cells transected nearer to the soma always seal at a lower frequency and rate compared to cells transected farther from the soma for all control or experimental protocols. Furthermore, sealing frequency is determined by PC time and not the time elapsed since neurite transection, the length of time cells are exposed to dye, the time at which cells are imaged after dye is washed out of the dish, or any residual Ca^{2+} remaining in Ca^{2+} -free saline or Ca^{2+} release from nearby cells.

Epac1 and 2 and PKA are expressed in B104 cells

Increased Epac or PKA activity induced by cBiMPS and Epac-cAMP has been reported to significantly increase the sealing frequency and rate compared to control sealing (Spaeth, et al., 2010). Since Epac-cAMP non-specifically activates Epac isoforms 1&2 (Christenson, et al., 2003), we investigated which Epac isoform B104 cells might express. Western blots (Fig. 3.1 A) show that Epac isoforms 1&2 are both expressed in B104 cells, as is PKA (Fig. 3.1 B).

Sealing is increased by cBiMPS, Epac-cAMP, db-cAMP and H₂O₂

Figure 3.2 A, B confirms (Spaeth, et al., 2010) that 8 μ M cBiMPS, and 8 μ M Epac-cAMP each significantly increase the sealing frequency ($p < 0.01$ CMH χ^2) and rate ($p < 0.01$, FZT, Table 3.1) for cells transected nearer to, or farther from, the soma compared to control sealing. [See Table 3.1 for k , τ , R^2 values, and comparisons of significance levels between experimental and control rates of sealing for transections nearer to, or farther from, the soma.] Similar results are observed for cells transected in 1mM db-cAMP (Fig. 3.1 A,B). Since an anti-oxidant, melatonin, decreases plasmalemmal sealing (Spaeth, et al., 2010), we hypothesized that increasing cytosolic oxidation should increase plasmalemmal sealing. Figure 3.2 A, B shows that cells transected nearer to, or farther from, the soma in 10 μ M H₂O₂ seal at a significantly ($p < 0.05$, CMH χ^2) higher frequency and significantly ($p < 0.05$, FZT, Table 3.1) faster rate

compared to control sealing. At 5 min PC, 100 μM H_2O_2 produces the same increase in sealing as does 10 μM H_2O_2 (see below).

These data also confirm our previous report (Spaeth, et al., 2010) that 8 μM cBiMPS, or 8 μM Epac-cAMP increase sealing at 0 min PC (i.e., dye added before adding Ca^{2+}) for cells transected nearer to, or farther from, the soma (Fig. 3.2 C,D). However, 10 μM H_2O_2 does not increase sealing nearer to, or farther from, the soma at 0 min PC compared to control sealing (Fig. 3.2 C,D). These data suggest that, in contrast to PKA and Epac activation, the oxidation dependent increase in sealing requires extracellular Ca^{2+} .

Sealing is decreased by BoNT A/E, B, TeNT, Bref A, and NEM

BoNT A decreases sealing: Since SNAP-25, a protein involved in vesicle-mediated neurotransmitter release (Hayashi, et al., 1994; Bronk, et al., 2007), is present at higher concentrations along axolemmal walls than at nerve terminals (Tao-cheng, *et. al.*, 1995), SNAP-25 might also be involved in plasmalemmal sealing in B104 cells. Figure 3.3 shows that B104 cells transected nearer to (Fig. 3.3 A), or farther from (Fig. 3.3 B), the soma in 1 μM BoNT A, which specifically cleaves SNAP-25 (Blasi, et al., 1993; Chapman, et al., 1994), seal at a significantly ($p < 0.001$, CMH χ^2) lower frequency and significantly slower rate ($p < 0.001$, FZT, Table 3.1) compared to control sealing (Fig. 3.3 A). Similar results are observed at 5 min PC following neurite transection in BoNT E, which cleaves SNAP-25, but recognizes a different sequence of SNAP-25 amino acids than BoNT A (Blasi, et al., 1993) (see Supplemental Fig. 3.1 A). Cells transected in 25

μM BoNT A do not exhibit decreased plasmalemmal sealing compared to 1 μM BoNT A, suggesting that 1 μM BoNT A produces the maximum effect of BoNT A to decrease sealing (Supplemental Fig. 3.1 A,B).

TeNT and BoNT B decrease sealing: TeNT specifically cleaves synaptobrevin (Link, et al., 1992), a protein involved in vesicle-mediated neurotransmitter release (Hayashi, et al., 1994). TeNT also decreases plasmalemmal sealing in neuronally-derived B104 cells transected at unspecified distances from their soma (Yoo et al, 2003) and in other types of eukaryotic cells (Bi, et al., 1995; Togo, 2004). We now show that B104 cells transected nearer to (Fig. 3.3 C), or farther from (Fig. 3.3 D), the soma in 100 nM TeNT seal at a significantly ($p < 0.001$, CMH χ^2) lower frequency and significantly slower rate ($p < 0.05$, FZT, Table 3.1) compared to control sealing. Similar results are observed at 5 min PC for cells transected in BoNT B, which cleaves synaptobrevin at a different location (Supplemental Fig. 3.1 C, D). When TeNT data from nearer to and farther from the soma are combined, the resulting data are not significantly ($p > 0.05$, CMH χ^2) different from TeNT data from B104 cells for which transection distance from the soma is not taken into account (Yoo, *et. al.*, 2003). Cells transected in 500 nM TeNT do not exhibit decreased plasmalemmal sealing compared to 100 nM TeNT, suggesting that 100 nM TeNT produces the maximum effect of TeNT to decrease sealing (Supplemental Fig. 3.2 A,B).

Bref A decreases sealing: Bref A, which inhibits Golgi vesicular trafficking (Fujiwara, et al., 1988), and decreases plasmalemmal sealing in fibroblasts (Togo, 2006) also decreases plasmalemmal sealing in B104 cells. Figure 3.4 A shows that B104 cells

transected nearer to the soma in 10 μ M Bref A seal at a significantly lower frequency ($p < 0.05$, CMH χ^2) at all PC times, and significantly slower rate ($p < 0.05$, FZT, Table 3.1) compared to control sealing. Similar results are observed for cells transected farther from the soma (Fig. 3.4 B). Transecting cells in 50 μ M Bref A, or pretreating cells with 10 μ M Bref A for 60 min prior to transection, does not further decrease plasmalemmal sealing, suggesting that 10 μ M Bref A added immediately before neurite transection (i.e. no pre-treatment) produces the maximum effect of Bref A to decrease sealing (see Supplemental Fig. 3.2 C, D).

NEM decreases sealing: Since NSF is involved in vesicle-mediated neurotransmitter release (Schweizer, et al., 1998; Parnas, et al., 2006), as well as membrane fusion of Golgi-derived vesicles (Garcia, et al., 1995) and NEM specifically inhibits NSF (Rodriguez, et al., 1994), NEM might be expected to decrease sealing of B104 cells after neurite transection. Figure 3.4 C,D shows that cells transected nearer to, or farther from, the soma in 1mM NEM seal at a significantly lower frequency ($p < 0.001$, CMH χ^2) and significantly slower rate ($p < 0.001$, FZT, Table 3.1) compared to control sealing. Furthermore, NEM decreases sealing frequencies at all PC times significantly ($p < 0.01$, CMH) more than BoNT A, BoNT E (Fig. 3.3 A,B) or TeNT/BoNT B (Fig. 3.3 C,D). Cells transected in 10 mM NEM do not exhibit further decreases in plasmalemmal sealing compared to 1 mM NEM, suggesting that 1 mM NEM produces the maximum effect of NEM to decrease sealing (Supplemental Fig. 3.3 A,B).

Three pathways that enhance plasmalemmal sealing

To investigate each of three possible pathways that enhance plasmalemmal sealing (Epac, PKA, cytosolic oxidation), we examine whether enhanced sealing following activation of a given pathway is prevented or decreased by a bacterial toxin that decreases vesicle-mediated neurotransmitter release (TeNT or BoNT A, B, or E) or Golgi vesicular trafficking (Bref A). If the increase in sealing is decreased or prevented by a given toxin, then we infer that the inhibited/cleaved target protein of the given toxin is downstream of the substance that activated that pathway.

A PKA pathway for plasmalemmal sealing

Activated PKA enhancement of plasmalemmal sealing is decreased by BoNT A/E cleavage of SNAP-25 and TeNT or BoNT B cleavage of synaptobrevin: Cells transected nearer to (Fig. 3.3 A), or farther from (Fig. 3.3 B), the soma in 8 μ M cBiMPS + 1 μ M BoNT A do not seal at a significantly different frequency ($p > 0.05$, CMH χ^2) or rate ($p > 0.05$, FZT, Table 3.1) compared to cells transected in 1 μ M BoNT A. If 1 μ M BoNT E is used instead of 1 μ M BoNT A, then cells transected nearer to, or farther from, the soma in 8 μ M cBiMPS + 1 μ M BoNT E do not seal at a significantly ($p > 0.05$, CMH χ^2) different frequency compared to cells transected only in 1 μ M BoNT E at 5 min PC (Supplemental Fig. 3.1 A, B). Furthermore, cells transected in 8 μ M cBiMPS + 1 μ M BoNT E do not seal at a significantly ($p > 0.05$, CMH χ^2) different frequency compared to cells transected in 8 μ M cBiMPS + 1 μ M BoNT A (Supplemental Fig. 3.1 A, B).

Cells transected nearer to the soma in 8 μ M cBiMPS + 100 nM TeNT do not seal at a significantly different frequency ($p < 0.01$, CMH χ^2), or rate ($p < 0.01$, FZT) compared

to cells transected only in 100 nM TeNT (Fig. 3.3 C). With the exception of 5 min PC, cells transected farther from the soma in 8 μ M cBiMPS + 100 nM TeNT do not seal at a significantly ($p < 0.01$, CMH χ^2) different frequency compared to cells transected only in 100 nM TeNT (Fig. 3.3 D). All these data suggest that PKA-dependent sealing utilizes proteins involved in vesicle-mediated neurotransmitter release.

Activated PKA enhancement of sealing is not decreased by Bref A inhibition of vesicle-mediated Golgi trafficking: Cells transected nearer to (Fig. 3.4 A), or farther from (Fig. 3.4 B), the soma in 8 μ M cBiMPS + 10 μ M Bref A do not seal at a significantly different frequency ($p > 0.05$, CMH χ^2), or rate ($p > 0.05$, FZT, Table 3.1), compared to control sealing. These data suggest that PKA-dependent sealing does not require proteins involved in Golgi vesicular trafficking.

An Epac pathway for plasmalemmal sealing

Activated Epac enhancement of plasmalemmal sealing is decreased by BoNT A, E cleavage of SNAP-25 and TeNT or BoNT B cleavage of synaptobrevin: B104 cells transected 8 μ M Epac-cAMP + 1 μ M BoNT A nearer to (Fig. 3.3 A), or farther from (Fig. 3.3 B), the soma seal at a significantly ($p < 0.001$, CMH χ^2) lower frequency and significantly slower rate ($p < 0.01$, FZT, Table 3.1) compared to control sealing. Cells transected nearer to (Fig. 3.3 A), or farther from (Fig. 3.3 B), the soma in 8 μ M Epac-cAMP + 1 μ M BoNT A seal at a significantly greater frequency ($p < 0.01$, CMH χ^2) and significantly faster rate ($p < 0.05$, FZT, Table 3.1) compared to cells transected only in 1 μ M BoNT A. If 1 μ M BoNT E is used instead of 1 μ M BoNT A, then cells transected

nearer to, or farther from, the soma in 8 μ M Epac-cAMP + 1 μ M BoNT E also seal at a significantly ($p < 0.05$, CMH χ^2) higher frequency compared to cells transected only in 1 μ M BoNT E at 5 min PC (Supplemental Fig. 3.1 A, B).

Cells transected nearer to, or farther from, the soma in 8 μ M Epac-cAMP + 100 nM TeNT seal at a significantly greater frequency ($p < 0.001$, CMH χ^2) and significantly faster rate ($p < 0.01$, FZT) compared to cells transected only in 100 nM TeNT (Fig. 3.3 C, D). However, this Epac-dependent increase in sealing following TeNT cleavage of synaptobrevin does not restore sealing to control levels. All these data suggest that an Epac-dependent sealing utilizes proteins involved in vesicle-mediated neurotransmitter release, although this may not be the only pathway enhanced by activating Epac (e.g., a vesicle mediated pathway for Golgi trafficking: see below).

Activated Epac enhancement of plasmalemmal sealing is decreased by Bref A inhibition of vesicle-mediated Golgi trafficking: At 20 min PC, cells transected farther from the soma in 8 μ M Epac-cAMP + 10 μ M Bref A seal at a significantly greater frequency compared to cells transected only in 10 μ M Bref A. However, for all other PC times, cells transected nearer to (Fig. 3.4 A), or farther from (Fig. 3.4 B), the soma in 8 μ M Epac-cAMP + 10 μ M Bref A do not seal at a significantly different frequency ($p > 0.05$, CMH χ^2) or rate ($p > 0.05$, FZT, Table 3.1) compared to cells transected only in 10 μ M Bref A. These data suggest that the Epac-dependent plasmalemmal sealing utilizes proteins involved in Golgi vesicular trafficking – as well as vesicle-mediated neurotransmitter release described above.

Cells transected nearer to (Fig. 3.5 A), or farther from (Fig. 3.5 B), the soma in 8 μ M Epac-cAMP + 1 μ M BoNT A + 10 μ M Bref A do not seal at a significantly ($p>0.05$, CMH χ^2) different frequency or rate ($p>0.05$, FZT, Table 3.1) compared to cells transected only in 1 μ M BoNT A. Furthermore, cells transected nearer to, or farther from, the soma in 8 μ M Epac-cAMP + 100 nM TeNT + 10 μ M Bref A do not seal at a significantly different frequency ($p>0.05$, CMH χ^2) or rate ($p>0.05$, FZT) compared to cells transected only in 100 nM TeNT (Fig. 3.5 C, D). These data are consistent with the hypothesis that Epac activation enhances sealing via isoforms of proteins involved in vesicle-mediated neurotransmitter release and Golgi vesicular trafficking.

A cytosolic oxidation pathway for plasmalemmal sealing

Enhancement of plasmalemmal sealing by cytosolic oxidation is decreased by BoNT A cleavage of SNAP-25 or TeNT cleavage of synaptobrevin: At 5 min PC, cells transected nearer to the soma in 10 μ M H₂O₂ + 1 μ M BoNT A do not seal at a significantly ($p>0.05$, CMH χ^2) different frequency compared to cells transected only in 1 μ M BoNT A (Fig. 3.6A). Similarly, at 5 min PC, cells transected nearer to, or farther from, the soma in 10 μ M H₂O₂ + 100 nM TeNT do not seal at a significantly ($p>0.05$, CMH χ^2) different frequency compared to cells transected only in 100 nM TeNT (Fig. 3.6 B). Similar data were observed for cells transected farther from the soma (Supplemental Fig. 3.4 A, B). These data suggest that a cytosolic oxidation-dependent plasmalemmal sealing utilizes proteins involved in vesicle-mediated neurotransmitter release.

Enhancement of plasmalemmal sealing by cytosolic oxidation is not decreased by Bref A inhibition of Golgi traffic: At 5 min PC, cells transected nearer to the soma in 10 μ M H₂O₂ + 10 μ M Bref A seal at a significantly ($p < 0.05$, CMH χ^2) higher frequency compared to cells transected only in BoNT A (Fig. 3.6C). Similar data were observed for cells transected farther from the soma (Supplemental Fig. 3.4C). These data suggest that a cytosolic oxidation-dependent plasmalemmal sealing may not utilize proteins involved in Golgi vesicular trafficking.

PKA, Epac, and cytosolic oxidation pathways each converge on NSF

Since NSF is involved in membrane fusion for both vesicle-mediated neurotransmitter release (Parnas, et al., 2006) and Golgi vesicular trafficking (Garcia, et al., 1995), we investigated whether activated PKA, activated Epac, or cytosolic oxidation can overcome the NEM-dependent decrease in sealing. Cells transected nearer to the soma in 8 μ M cBiMPS + 1 mM NEM, or in 8 μ M Epac-cAMP + 1 mM NEM, do not seal at a significantly different frequency ($p < 0.001$, CMH χ^2) or rate ($p > 0.05$, FZT, Table 3.1) compared to cells transected only in 1 mM NEM (Fig. 3.4 C, D). Similarly, at 5 min PC, cells transected nearer to, or farther from, the soma in 10 μ M H₂O₂ + 1 mM NEM do not seal at a significantly ($p > 0.05$) different frequency compared to cells transected only in 1 mM NEM (Fig. 3.6 D, F).

Additionally, simultaneous activation of application of db-cAMP to activate PKA and Epac, and H₂O₂ to increase cytosolic oxidation, did not overcome NEM inhibition of NSF. Cells transected nearer to, or farther from, the soma in 1 mM db-cAMP + 10 μ M

H₂O₂ + 1 mM NEM do not seal at a significantly different frequency ($p < 0.05$, CMH χ^2) at 5 min PC compared to cells transected in 1 mM NEM (Fig. 3.6 E, F). These data suggest that sealing mediated by PKA, Epac, or cytosolic oxidation all converge on NSF.

If NSF activity is downstream of PKA, Epac and cytosolic oxidation during plasmalemmal sealing, then BoNT A, E, B or Bref A should not further decrease the NEM-dependent decrease in plasmalemmal sealing. At 5 min PC, cells transected nearer to, or farther from, the soma in 1 μ M BoNT A + 1 μ M BoNT E + 1 μ M BoNT B + 1 mM NEM do not seal at a significantly ($p > 0.05$, CMH χ^2) different frequency compared to cells transected only in 1 mM NEM (Fig. 3.6 E, F). Furthermore, at 5 min PC, cells transected nearer to, or farther from, the soma in 10 μ M Bref A + 1 mM NEM do not seal at a significantly ($p > 0.05$, CMH χ^2) different frequency compared to cells transected only in 1 mM NEM (Fig. 3.6 E, F).

Plasmalemmal sealing *ex vivo* in rat sciatic nerves with doubly transected axons

NEM, Bref A, and PKI decrease and db-cAMP increases plasmalemmal sealing: We have previously reported (Yoo et al., 2003, 2004 or Spaeth et al., 2010) that B104 cells with transected neurites seal in Ca²⁺-containing media and do not seal in Ca²⁺-free media. Since toxins or inhibitors targeted to cAMP-dependent proteins decrease, and cAMP-analogs increase, plasmalemmal sealing in B104 cells *in vitro* (Figs. 3.2 - 3.6), these same substances might be expected to have similar effects on plasmalemmal sealing *in vivo* or *ex vivo*. To test this hypothesis, we cut rat sciatic nerves as previously described (Britt, et al., 2010), and placed them in a Petri dish containing Texas Red (3

kDa) dye in Ca^{2+} -free Krebs (negative control, n=4) and 1 mM db-cAMP (n=3), or Ca^{2+} Krebs (positive control, n=2) and 1 mM NEM (n=5), or 10 μM Bref A (n=3), or 50 μM PKI (n=2), as described in Methods.

As we have previously described (Lore et al., 1999; Britt et al, 2010) for cut rat sciatic nerves bathed in Ca^{2+} -free Krebs *ex vivo*, dye is taken up at unsealed cut axonal ends and is visible intra-axonally throughout the entire segment. Consistent with these two previous reports for nerve segments bathed in Ca^{2+} -containing Krebs, dye is not taken up at sealed cut ends and is excluded from sciatic axons. We now report that following incubation in Ca^{2+} Krebs containing 1 mM NEM (n=5) (Fig. 3.1D), 10 μM Bref A (n=3) or 50 μM PKI (n=2), axons filled with dye, presumably through unsealed cut ends. Following incubation in Ca^{2+} -free Krebs and 1 mM db-cAMP, axons did not fill with dye (Fig. 3.1C), similar to nerve segments bathed in Ca^{2+} Krebs. All these data are consistent with an interpretation that Ca^{2+} , or 1mM db-cAMP, rapidly induces plasmalemmal sealing of cut axonal ends and that 1 mM NEM, 10 μM Bref A, and 50 μM PKI decrease plasmalemmal sealing *ex vivo* in transected rat sciatic axons (Fig. 3.1), as also demonstrated for transected B104 neurites *in vivo* (Figs. 3.2 - 3.6).

Discussion

Overview of plasmalemmal sealing in eukaryotic cells/preparations

In all preparations studied to date, plasmalemmal sealing occurs by Ca^{2+} -dependent accumulation and fusion of many (perhaps all) available membrane-bound structures (Bittner and Fishman, 2000; Fishman and Bittner, 2003), including lysosomes

(Reddy, et al., 2001), mitochondria (Pfenniger, et al., 2009), membrane derived from myelin (Ballinger et al., 1999), endocytotic vesicles from nearby, adjacent undamaged plasmalemma (Eddleman, et al., 1998, 1999) and pre-existing vesicle pools (Steinhardt, et al., 1994). These membrane-bound structures fuse with each other (Mellgren, et al., 2006) and nearby, undamaged membrane (Eddleman, et al., 1998; Detrait, et al., 2000a) to decrease, and eventually restrict, the influx of extracellular ions, including Ca^{2+} . If not rapidly prevented by a vesicle-mediated plasmalemmal seal, the damage-induced increases in $[\text{Ca}^{2+}]_i$ and cytosolic oxidation lead to cell death (Nguyen et al., 2005; Cai, et al., 2009a,b).

Effects of toxins on plasmalemmal sealing of damaged eukaryotic cells

In sea urchin eggs, BoNT A cleavage of SNAP-25, or TeNT cleavage of synaptobrevin completely inhibits sealing (Steinhardt, et al., 1994; Bi, et al., 1995). In B104 cells, BoNT A cleavage of SNAP-25, or TeNT cleavage of synaptobrevin decreased (Figs. 3.2, 3.3), but did not completely eliminate sealing, even at higher concentrations of either toxin (Supplemental Figs. 3.2, 3.3). The residual amount of plasmalemmal sealing observed in B104 cells following treatment with BoNT A/E or TeNT/BoNT B may be due to some or all of the following reasons: 1) lack of inhibition of other sealing pathways, such as cytosolic oxidation (Cai, et al., 2009a,b; Spaeth, et al., 2010), 2) protein isomers involved in vesicle-mediated release of neurotransmitters that are not cleaved, or are resistant to neurotoxins, such as TI-VAMP (Galli, et al., 1998), 3) proteins used for Golgi vesicular trafficking (Nebenfuhr, et al., 2002). For example, a

population of SNAP-25 or synaptobrevin is protected from toxin cleavage due to inclusion into pre-fusion 20S SNARE complex (Singh, et. al., 2000) or insertion into Golgi derived vesicles (Proux-Gillardeaux, et al., 2005).

Bref A specifically inhibits Arf1, which eliminates Golgi vesicular trafficking (Fujiwara, et al., 1988; Nebenfuhr, et al., 2002), and decreases sealing (Fig. 3.4 A, B), consistent with previous reports from mouse-derived fibroblasts (Togo, 2006). These data are also consistent with previous observations that plasmalemmal sealing may utilize all available membrane-bound structures (Bittner and Fishman, 2000; Fishman and Bittner, 2003).

Four pathways of plasmalemmal sealing

In this paper, we examine three partly independent, redundant pathways of plasmalemmal sealing mediated by PKA, Epac, and cytosolic oxidation. Damage-induced Ca^{2+} influx through a plasmalemmal damage site oxidizes the cytosol (McNeil, 2009), and activates Ca^{2+} -dependent adenylate cyclases (Dunn, et al., 2009), thus increasing [cAMP], which activates both PKA and Epac (Gilman, 1970; de Rooij, et al., 1998). PKA, Epac, and cytosolic oxidation then activate parallel, somewhat independent, pathways of plasmalemmal sealing. We also know of (Spaeth et al., 2010), and include in our model (Fig. 3.7), the probable existence of a fourth parallel pathway mediated by Ca^{2+} activation of PKC. [Other pathways that enhance plasmalemmal sealing may also exist.] We suggest that eukaryotic cells have evolved at least four redundant pathways to insure that plasmalemmal damage is rapidly repaired, and that isoforms of proteins

involved in plasmalemmal sealing are conserved in all eukaryotic preparations studied to date (Spaeth, et al., 2010).

A PKA pathway for plasmalemmal sealing

The PKA pathway (Fig. 3.7) utilizes proteins involved in vesicle-mediated neurotransmitter release (Fig. 3.3), but does not utilize proteins involved in Golgi vesicular trafficking (Fig. 3.4 A, B). These data from B104 cells are consistent with reports that active PKA, localized to Golgi cisternae, does not increase Golgi vesicular trafficking to the plasmalemma (Mavillard, et al., 2009) and that, siRNA or small molecule inhibition of PKA in HeLa cells does not disrupt anterograde Golgi vesicular trafficking, despite structural changes to Golgi cisternae (Bejerano, et al., 2006). These data are also consistent with reports that PKA phosphorylates SNAP-25 and activates pathways that require synaptobrevin (Yoshihara, et al., 1999, 2000; Nagy, et al., 2004; Bronk, et al., 2007). Since syntaxin is also involved in plasmalemmal sealing (Yoo, et al., 2003) and interacts with SNAP-25 and synaptobrevin during 20S SNARE formation (Sudhof, 2004), we suggest that syntaxin is also part of the PKA-dependent pathway of sealing (Fig. 3.7).

An Epac pathway for plasmalemmal sealing

The Epac pathway (Fig. 3.7) utilizes proteins involved in vesicle-mediated release of neurotransmitters and Golgi vesicular trafficking (Fig. 3.4 A,B; 3.5A-D). These data

are consistent with recent reports of Epac activity. For example, Epac increases neurotransmission in rat hippocampal slices (Ster, et al., 2009) and PC12 cells (Hatekeyama, et al., 2009) by activating SNAP-25 (Vikman, et al., 2006) and other proteins important for Ca^{2+} -dependent exocytosis, such as Rab3A (Branham, et al., 2009). Epac also increases membrane fusion events in non-neuronal preparations, such as insulin secretion in pancreatic cells (Wu, et al., 2002). Epac increases trans-Golgi vesicular trafficking via Rap1 (de Rooij, et al., 1998) by increasing both Rap1 GTPase activity (Niimura, et al., 2009) and Rap1 translocation from Golgi cisternae to the plasma membrane (Wu, et al, 2002). Finally, Bref A greatly reduces Rap1 GTPase activity and Rap1 translocation to the plasmalemma (Wu, et al., 2002; Niimura, et al., 2009), and decreases plasmalemmal sealing (Figs. 3.4, 3.5). These data suggest Bref A may inhibit Epac activity.

A cytosolic oxidation pathway for plasmalemmal sealing

Plasmalemmal damage likely leads to cytosolic oxidation (Cai, et al., 2009; McNeil, 2009) due to influx of extracellular substances, including Ca^{2+} , and/or efflux of intracellular substances. H_2O_2 increases vesicle-mediated processes, such as LTP in hippocampal (Thiels, et al., 2000) or spinal axons (Lee, et al, 2010), perhaps due to an H_2O_2 -dependent release of Ca^{2+} stores from endoplasmic reticulum (Gerich, et al., 2009). The release of Ca^{2+} from internal stores does not increase $[\text{Ca}^{2+}]_i$ to levels necessary to initiate plasmalemmal sealing (Yoo, et al., 2004). However, the release of Ca^{2+} from internal stores may increase the rate of sealing after its initiation by enhancing other

pathways, such as vesicle-mediated release of neurotransmitters. Cytosolic oxidation also activates Tri-partite motif (TRIM) proteins (Cai, et al., 2009a,b), Galectins (Horie, et al., 2004), and initiates oxy-sterol formation (Ma, et al., 2010), all of which increase vesicle formation and exocytosis, and likely affect sealing. Our data suggest (Fig. 3.6A-D) that cytosolic oxidation enhances plasmalemmal sealing via proteins involved in neurotransmitter release, but not Golgi vesicular trafficking (Fig. 3.7).

PKA, Epac and Cytosolic oxidation pathways of plasmalemmal sealing all converge on NSF

All three plasmalemmal sealing pathways examined in this paper almost certainly converge on NSF since enhancement of plasmalemmal sealing by all three pathways cannot overcome NEM inhibition of NSF (Fig. 3.4 C, D). These data are consistent with reports suggesting that vesicle-mediated neurotransmitter release (Rodriguez, et al., 1994) and Golgi vesicular trafficking both utilize NSF (Garcia, et al., 1995). However, plasmalemmal sealing still persists in B104 cells following NEM inhibition of NSF, suggesting that other sealing pathways (e.g., PKC) might not use NSF and thereby account for the residual (unblocked) sealing. Alternatively, some NSF isoforms may be resistant to NEM due to their insertion into membranes, docking in 20S SNARE complexes, and/or location in endosomal compartments not accessible by NEM (Rodriguez, et. al., 1994).

Significance and clinical relevance of understanding pathways that enhance sealing

Increased [cAMP]_i increases PKA and Epac activities, both of which increase survival and axonal outgrowth following injury, even in non-permissive growth substrates of the central nervous system (Cai, et al., 1999; Qui, et al., 2002; Shewan and Murray, 2008). Damaged-induced increases in [cAMP]_i enhances plasmalemmal sealing *in vitro* (Fig. 3.2) and *ex vivo* (Fig. 3.1 C,D) – and therefore almost certainly *in vivo*. Repairing plasmalemmal damage, which increases the probability of neuron survival (Nguyen, et al., 2005), also increases the probability of axon regeneration for those neurons that survived a plasmalemmal disruption (Ramon y Cajal, 1928).

Similar to activation of competing pathways initiated by Ca²⁺ influx at sites of plasmalemmal damage, cytosolic oxidation initiates various competing pathways, some leading to plasmalemmal sealing and cell survival and others to cell death. Influx/ efflux of Ca²⁺, and other substances, at a site of plasmalemmal damage oxidizes the cytosol, activate proteins that maintain the cytosolic reducing environment (McNeil, 2009), induces vesicle accumulation (Cai, et al., 2009 a,b) and enhances plasmalemmal sealing (Fig. 3.2 A, B; 3.6 A-D). Reducing proteins, (e.g., glutathiones, super-oxide dismutases (Sods); Circu and Aw, 2009) help maintain a reducing intracellular environment, and increase cell survival following traumatic injury (Celsi, et al., 2010). However, disruption of the intracellular redox environment, leads to cell death, and is possibly involved in, the etiology of some neurodegenerative diseases. For example, improper functioning Sod1 correlates strongly to ALS and neuronal death (Barber and Shaw, 2009). Therefore, a better understanding of the role of Ca²⁺ influx and cytosolic oxidation following traumatic injury should provide clinically relevant insights into the

etiology of neurodegenerative disorders—and subsequent treatments for their prevention or amelioration.

Tables and Figures:

Table 3.1: Sealing constants (τ , k) and R^2 for exponential fits of sealing PC times:

Test Substance	τ (min) < 50 μm	k (min^{-1}) < 50 μm	R^2 < 50 μm	τ (min) > 50 μm	k (min^{-1}) > 50 μm	R^2 > 50 μm
Control	5.95	0.168	0.9865	2.16	0.461	0.9970
8 μM cBiMPS	1.24**	0.805**	0.9413	0.497**	2.01**	0.8231
8 μM Epac-cAMP	2.89**	0.345**	0.9141	0.628**	1.59**	0.7933
1 mM db-cAMP	1.98**	0.503**	0.9877	0.622**	1.61**	0.9976
10 μM H_2O_2	2.69**	0.372**	0.9605	1.70*	0.589*	0.9998
1 μM BoNT A	14.12***	0.0708***	0.9899	5.82**	0.1718**	0.9968
1 μM BoNT A + 8 μM cBiMPS	14.14***	0.0707***	0.9609	4.84**	0.2065**	0.9917
1 μM BoNT A + 1 μM Epac-cAMP	3.37	0.2963	0.9811	3.05	0.3278	0.9958
100 nM TeNT	18.52***	0.0540***	0.9624	3.39*	0.2949*	0.9972
100 nM TeNT + 8 μM cBiMPS	14.91***	0.0671***	0.9632	3.46*	0.2980*	0.9973
100 nM TeNT + 8 μM Epac-cAMP	5.49	0.1821	0.9902	2.77	0.3609	0.9992
10 μM Bref A	8.53*	0.1172*	0.9587	4.01*	0.2491*	0.9587
10 μM Bref A + 8 μM cBiMPS	7.85*	0.1274*	0.9760	3.14*	0.3182*	0.9670
10 μM Bref A + 8 μM Epac-cAMP	10.15**	0.0985**	0.9703	2.18	0.4595	0.9703
1 μM BoNT A + 10 μM Bref A + 8 μM Epac-cAMP	9.97**	0.1003**	0.9788	4.74**	0.2109**	0.9862
100 nM TeNT + 10 μM Bref A + 8 μM Epac-cAMP	14.27***	0.0701**	0.9691	3.33*	0.3006*	0.9953
1 mM NEM	9.46**	0.1057**	0.9984	2.92	0.3423	0.9882
1 mM NEM + 8 μM cBiMPS	9.62**	0.1040**	0.9915	5.31**	0.1883**	0.9912
1 mM NEM + 8 μM Epac-cAMP	14.35***	0.0697***	0.9933	5.78**	0.1730**	0.9580

Table 3.1: Statistical comparisons of rate constants (k , min^{-1}) or exponential time constants (τ , min) for sealing of B104 cells transected nearer to (< 50 μm), or farther from (> 50 μm), the soma. Cells transected nearer to the soma and bathed in a given test substance always sealed at a slower rate compared to cells transected farther from the soma and bathed in the same test substance. **$R^2 < 50 \mu\text{m}$ or $R^2 > 50 \mu\text{m}$:** Goodness of fit values obtained from a single-exponential model to fit the sealing frequency at all PC times for control sealing, or for sealing in a given test substance. Asterisks indicate the level of significant difference between sealing time constants or rate constants for a given test-substance compared to control sealing. Significance levels for this and all other tables and figures are indicated beside each value as follows: no asterisk = $p > 0.05$ and < 0.95 , single asterisk (*) = $p < 0.05$, double asterisk (**) = $p < 0.01$, and triple asterisk (***) = $p < 0.00$

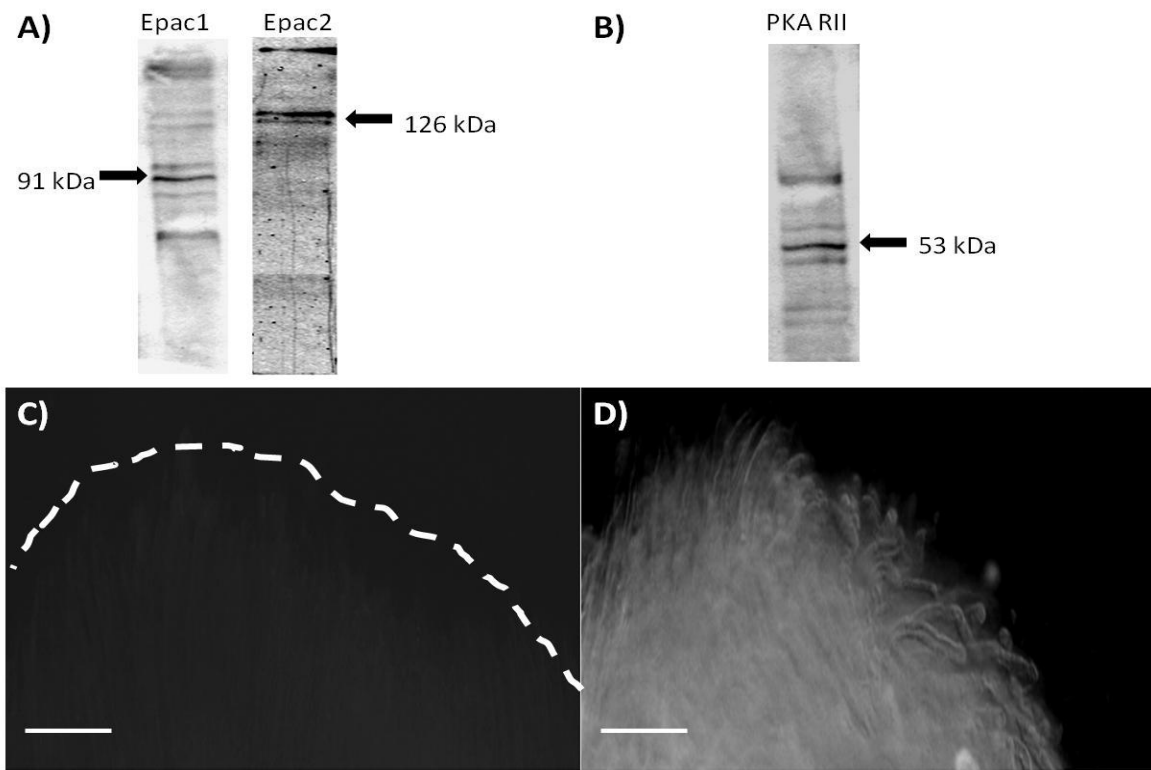


Figure 3.1 A, B: Representative western blots of B104 cell lysates (approximately 5 μ g of protein per lane) for Epac1&2 (**A**) and PKA (**B**). Additional bands likely represent splice variants of Epac or PKA, or SDS-resistant protein complexes containing Epac or PKA. **C-D:** Images of sciatic nerves used for sealing studies. **C:** Cut nerve ends treated with db-cAMP, followed by addition of Ca^{2+} -free saline excluded dye. **D:** Cut nerve ends treated with NEM, followed by Ca^{2+} addition did not exclude dye. Scale bar = 50 μ m for all figures.

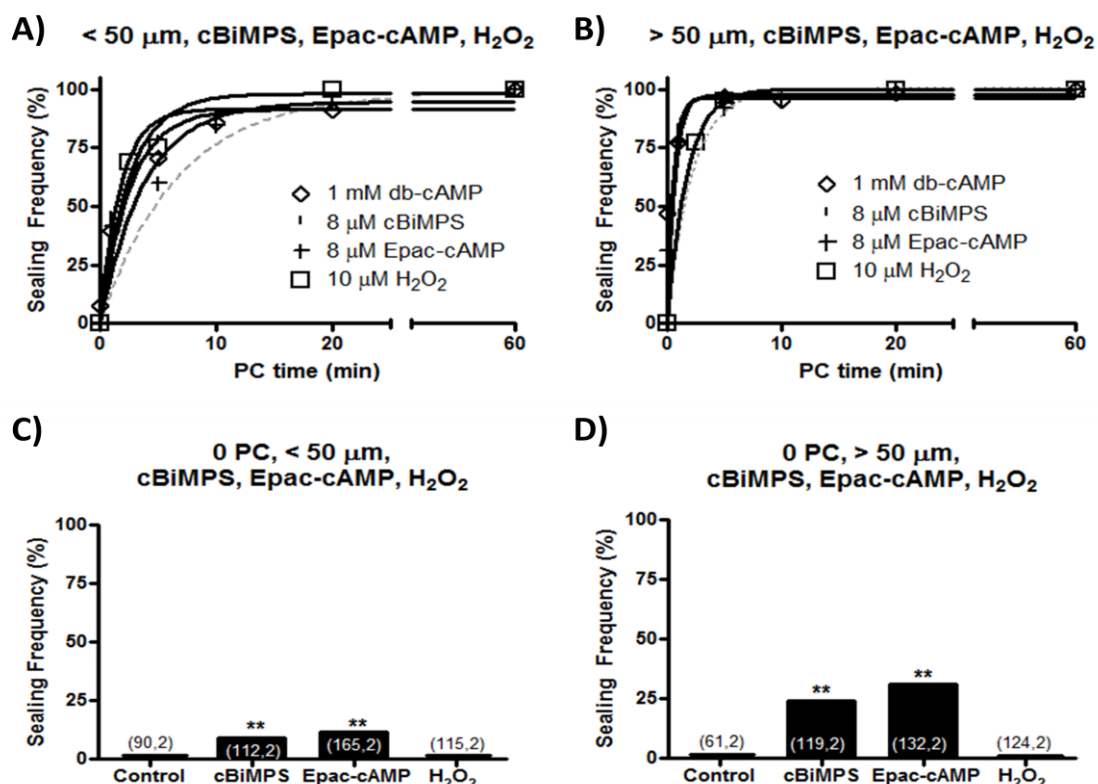


Figure 3.2 A,B: Sealing frequency (%) plotted versus PC time (min) for cells transected nearer to (A) or farther from (B) the soma in 8 μM cBiMPS (black line, dashed symbols), 8 μM Epac-cAMP (black line, crosses), 1 mM db-cAMP (black line, open diamonds) or 10 μM H_2O_2 (black line, open squares). In this and subsequent figures, dotted or dashed lines represent the frequency for control sealing and solid lines for test substances fitted to **Equation 1** by GraphPad Prism (See **Methods**). In **A**, **B**, and subsequent figures, the x-axis is interrupted between 25 min and 60 min PC so that differences in sealing frequencies from 0-20 min PC can be observed more easily. In **A**, **B** and subsequent figures, control sealing curves are plotted as dashed (< 50 μm) or dotted (>50 μm) lines to compare the effects of test substances (e.g., 1 μM BoNT A) to control sealing. The total number of cells transected to obtain each data point (n) varied from 58 to 272 on a total number (N) of Petri dishes (2 to 15). These numbers (n, N) are given in **Supplemental Table 3.1 A & B** for all figures these values are not shown for. **C,D:** Cells assessed for sealing at 0 PC following transection in 8 μM cBiMPS, 8 μM Epac-cAMP, or 10 μM H_2O_2 .

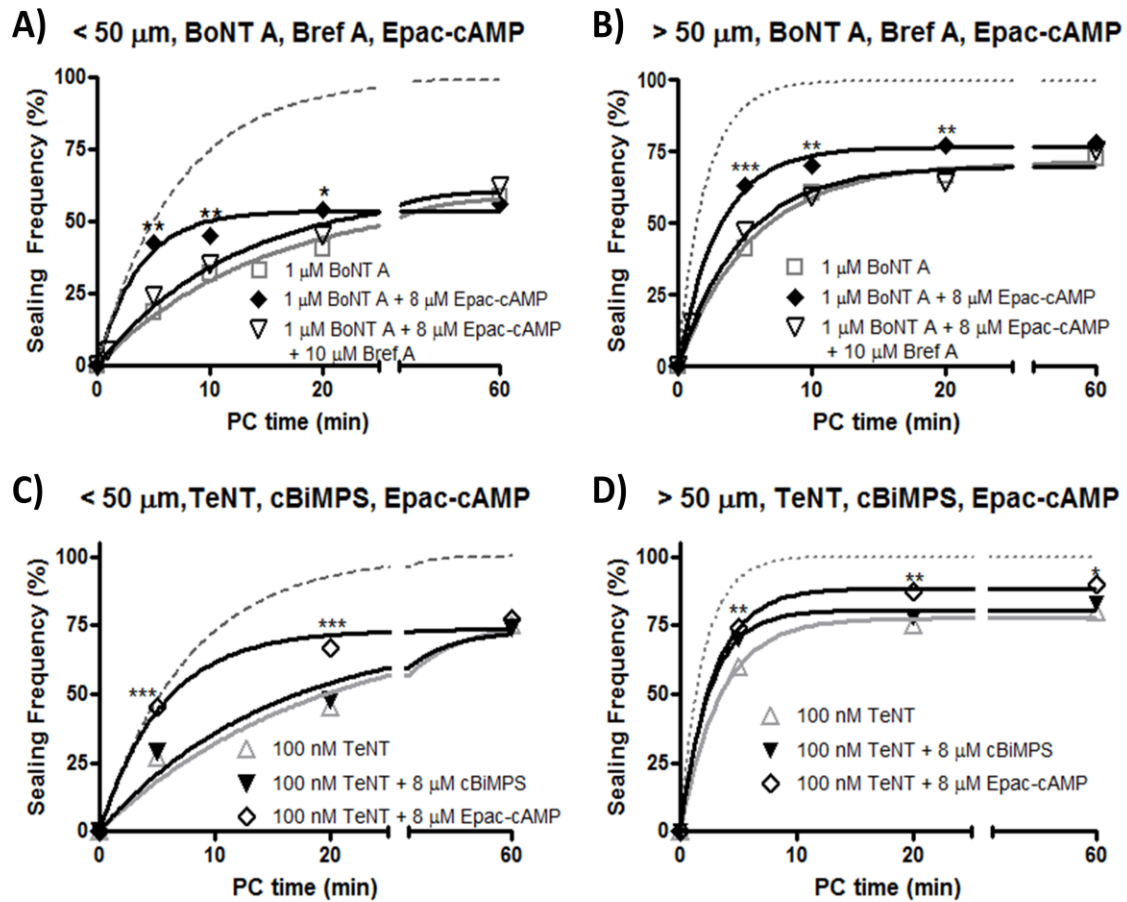


Figure 3.3 A-D: Sealing frequency (%) plotted against PC time (min) for cells transected nearer to (A, C), or farther from (B, D) the soma in 1 μM BoNT A (gray line, open squares), 1 μM BoNT A + 8 μM cBiMPS (black line, open triangles), 1 μM BoNT A + 8 μM Epac-cAMP (black line, filled diamonds), 100 nM TeNT (gray line, open triangles), 100 nM TeNT + 8 μM cBiMPS (black line, inverted filled triangles), or 100 nM TeNT + 8 μM Epac-cAMP (black line, open diamonds).

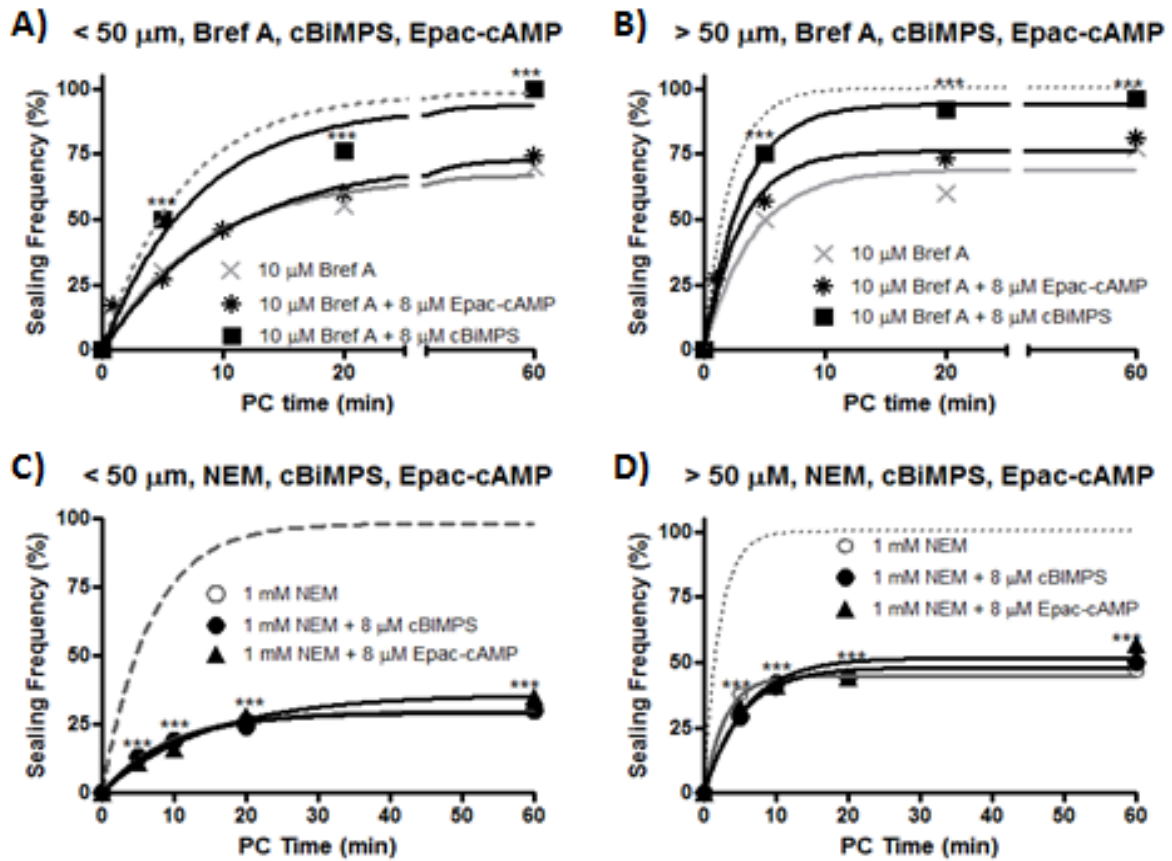


Figure 3.4 A-D: Sealing frequency (%) plotted against PC time (min) for cells transected nearer to (A, C), or farther from (B, D) the soma in 10 μ M Bref A (gray lines, crosses), 10 μ M Bref A + 8 μ M cBiMPS (black line, filled squares), 10 μ M Bref A + 8 μ M Epac-cAMP (black line, asterisks), 1 mM NEM (gray line, open circles), 1 mM NEM + 8 μ M cBiMPS (black line, filled circles), 1 mM NEM + 8 μ M Epac-cAMP (black line, filled triangles).

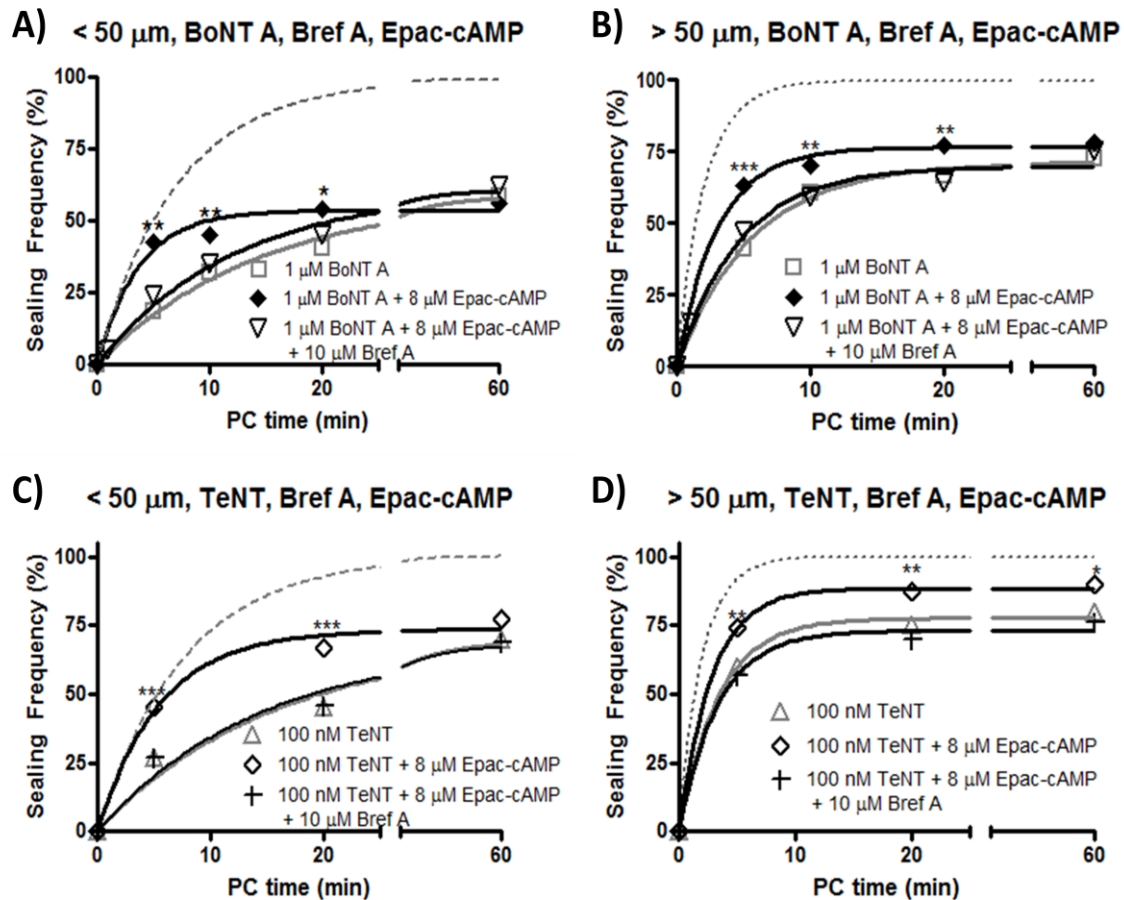


Figure 3.5 A-D: Sealing frequency (%) plotted against PC time (min) for cells transected nearer to (A, C), or farther from (B, D) the soma in 1 μM BoNT A (gray line, open squares) + 1 μM BoNT A + 8 μM Epac-cAMP (black line, filled diamonds), 1 μM BoNT A + 8 μM Epac-cAMP + 10 μM Bref A (black line, inverted open triangles), 100 nM TeNT (gray line, open triangles), 100 nM TeNT + 8 μM Epac-cAMP (black line, open diamonds), 100 nM TeNT + 8 μM Epac-cAMP + 10 μM Bref A (black line, crosses).

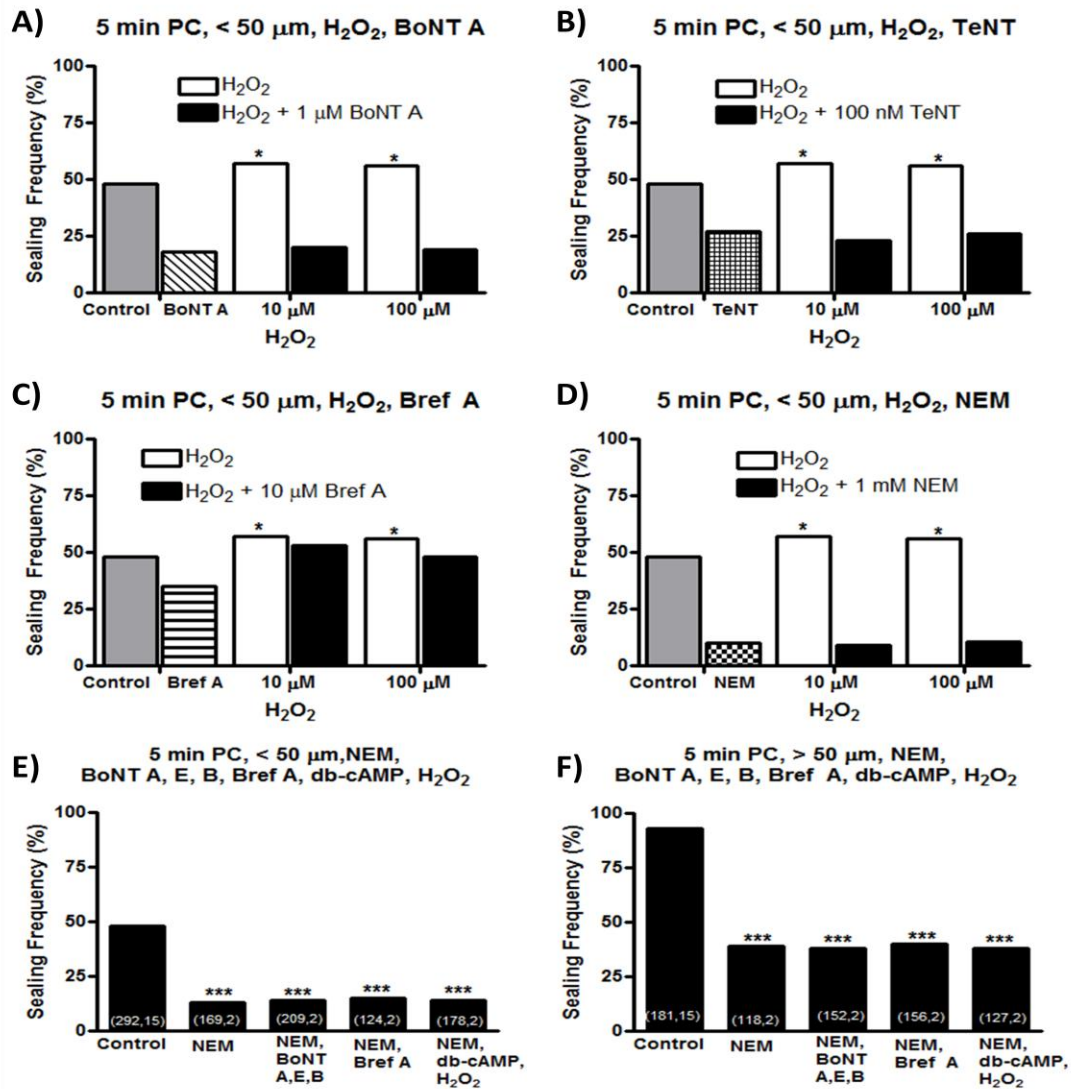


Figure 3.6 A-D: Cells assessed for sealing at 5 min PC, and transected nearer to the soma in 10 μ M H_2O_2 or 100 μ M H_2O_2 (white bars) compared to control sealing (gray bars). **A:** Cells transected in 1 μ M BoNT A (diagonal bars), 10 μ M H_2O_2 + 1 μ M BoNT A or 100 μ M H_2O_2 + 1 μ M BoNT A (black bars). **B:** Cells transected in 100 nM TeNT (plaid bars), 10 μ M H_2O_2 + 100 nM TeNT or 100 μ M H_2O_2 + 100 nM TeNT (black bars). **C:** Cells transected in 10 μ M Bref A (horizontal lines), 10 μ M H_2O_2 + 10 μ M Bref A or 100 μ M H_2O_2 + 1 μ M Bref A (black bars). **D:** Cells transected in 1 mM NEM (diagonal bars), 10 μ M H_2O_2 + 1 mM NEM or 100 μ M H_2O_2 + 1 mM NEM (black bars). **E-F:** Cells transected nearer to (E), or farther from (F) the soma in 1 mM NEM + 1 μ M BoNT A + 1 μ M BoNT B + 1 μ M BoNT E; 1 mM NEM + 10 μ M Bref A, or 1 mM NEM + 1 mM db-cAMP + 10 μ M.

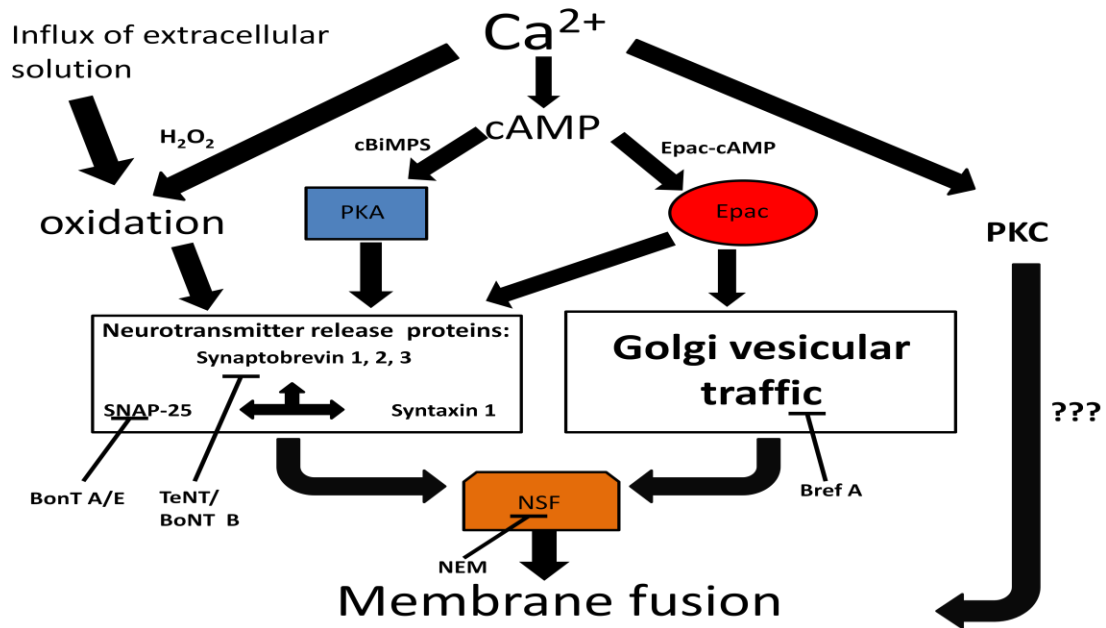


Figure 3.7: A Model of plasmalemmal sealing: Immediately after plasmalemmal damage, Ca^{2+} influx at the damage site activates four parallel, partly redundant pathways of plasmalemmal sealing mediated by PKA, Epac, cytosolic oxidation, and PKCs. PKA and Epac pathways are activated by Ca^{2+} -dependent increases in cAMP concentration. The PKA pathway of sealing (activated in this study by cBiMPS) likely only uses proteins required for synaptic neurotransmitter release, such as SNAP-25, that is cleaved by BoNT A&E and synaptobrevin isoforms, that are cleaved by TeNT & BoNT B, except synaptobrevin 3, that is insensitive to toxins (Galli, et al., 1998). One predicted target of PKA-dependent sealing is syntaxin 1, which binds SNAP-25 (Sudhof, et al., 2004), since inhibition of syntaxin decreases sealing in B104 cells, PC12 cells and invertebrate axons (Detrait, et al., 2000a; Yoo, et al., 2003). The Epac pathway of sealing (activated in this study by Epac-cAMP) utilizes proteins required for synaptic neurotransmitter release, in addition to Golgi vesicular traffic (inhibited by Bref A), possibly through Rab3-dependent exocytosis (Branham, et al., 2009). The cytosolic oxidation pathway, activated by both Ca^{2+} influx and influx of extracellular solution and efflux of intracellular solution, in this study activated further by H_2O_2 , uses proteins required for synaptic neurotransmitter release, potentially after activation of TRIM (tri-partite motif) proteins (Cai, et al., 2009a,b). The pathway of cytosolic oxidation cannot initiate membrane fusion without damage-induced influx of extracellular Ca^{2+} (Fig. 2C,D). All three sealing pathways (PKA, Epac, cytosolic oxidation) require NSF. Any sealing that remains following inhibition of all of these pathways may be due to damage-induced activation of PKCs (indicated by “???”).

Supplemental Figures and Tables:

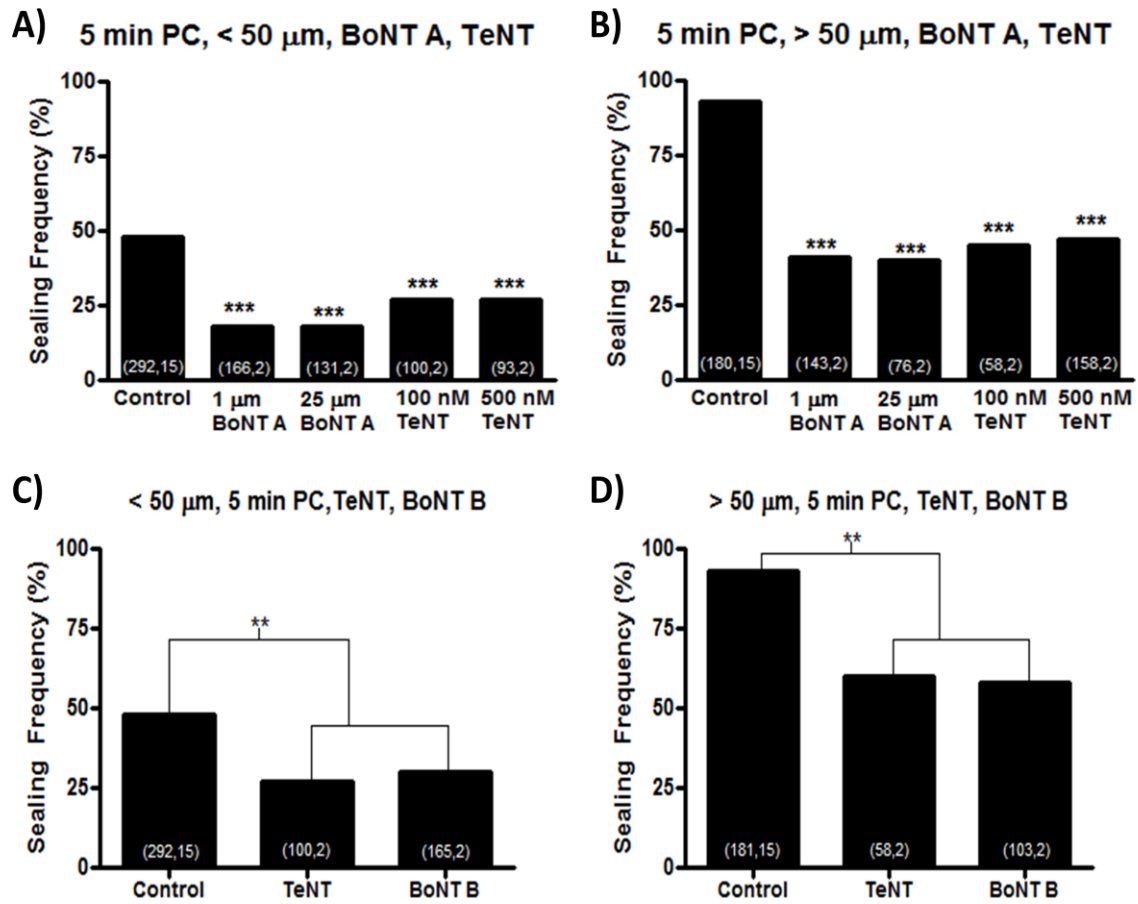
Table 3.1 A: Number of cells and dishes used to obtain the data points for all figures for cells transected nearer to (< 50 μ m) the soma:

Test substance	PC Time (min)						
	0	1	5	10	20	60	
Control	90,2	117,5	272,15	146,9	102,5	115,2	
cBiMPS	112,2	133,2	156,2	169,2	132,2	174,2	
Epac-cAMP	165,2	155,2	158,2	160,2	139,2	149,2	
H ₂ O ₂	115,2		187,2	145,2	153,2	162,1	
BoNT A			166,3	135,2	157,2	170,2	
BoNT A + cBiMPS			181,2	103,2	113,2	150,2	
BoNT A + Epac-cAMP			212,2	104,2	193,2	217,3	
TeNT			100,3		149,3	118,2	
TeNT + cBiMPS			149,2		133,2	144,2	
TeNT + Epac-cAMP			83,2		154,2	167,2	
Bref A			134,2		87,2	60,2	
Bref A + cBiMPS			167,2		144,2	172,2	
Bref A + Epac-cAMP			122,2	161,2	148,2	167,2	155,2
Bref A + BoNT A				149,2		132,2	111,2
Bref A + TeNT				167,2		154,2	151,1
BoNT A + Bref A + Epac-cAMP		132,2	155,2	93,2	142,2	147,2	
TeNT + Bref A + Epac-cAMP	145,2	108,2		80,2	85,2		
NEM		169,2	137,2	116,2	106,2		
NEM + cBiMPS		103,5	165,2	119,2	105,2		
NEM + Epac-cAMP		96,2	185,2	108,2	117,2		

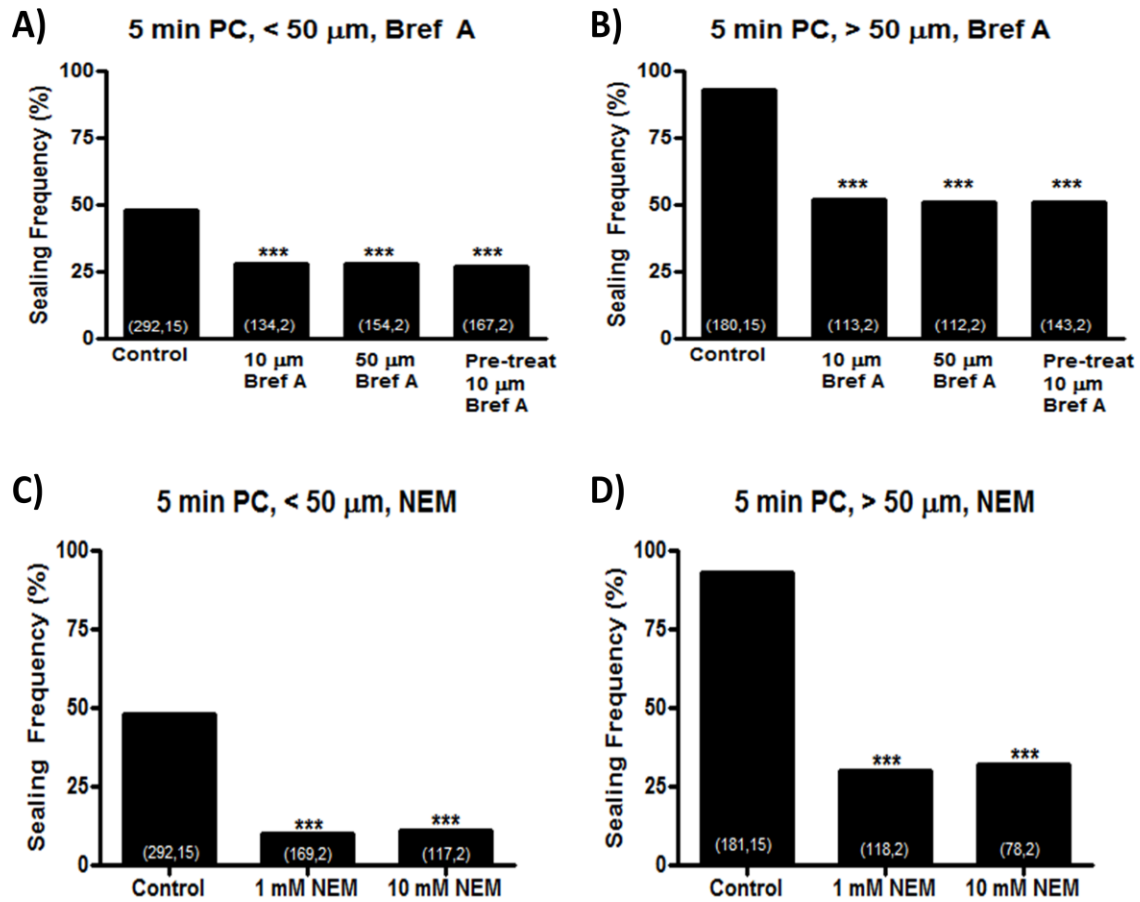
Table 3.1 B: Number of cells and dishes used to obtain the data points for all figures for cells transected farther from (> 50 μ m) the soma:

Test substance	PC Time (min)						
	0	1	5	10	20	60	
Control	61,2	117,5	272,15	146,9	102,5	115,2	
cBiMPS	119,2	132,2	139,2	129,2	101,2	115,2	
Epac-cAMP	132,2	111,2	123,2	120,2	119,2	125,2	
H ₂ O ₂	124,2		134,2	113,2	107,2	99,2	
BoNT A			143,3	86,2	131,2	134,2	
BoNT A + cBiMPS			131,2	75,2	81,2	130,2	
BoNT A + Epac-cAMP			146,2	66,2	101,2	159,3	
TeNT			63,2		77,2	108,2	
TeNT + cBiMPS			70,2		111,2	94,2	
TeNT + Epac-cAMP			58,2		87,2	102,2	
Bref A			113,2		73,2	131,2	
Bref A + cBiMPS			156,2		76,2	143,2	
Bref A + Epac-cAMP			101,2		141,2	133,2	127,2
Bref A + BoNT A					103,2	114,2	98,2
Bref A + TeNT					142,2	96,2	107,2
BoNT A + Bref A + Epac-cAMP			95,2	104,2	91,2	97,2	123,2
TeNT + Bref A + Epac-cAMP			89,2	119,2		78,2	90,2
NEM				118,2	96,2	90,2	85,2
NEM + cBiMPS		85,6		135,2	106,2	86,2	
NEM + Epac-cAMP	113,2	124,2		92,2	134,2		

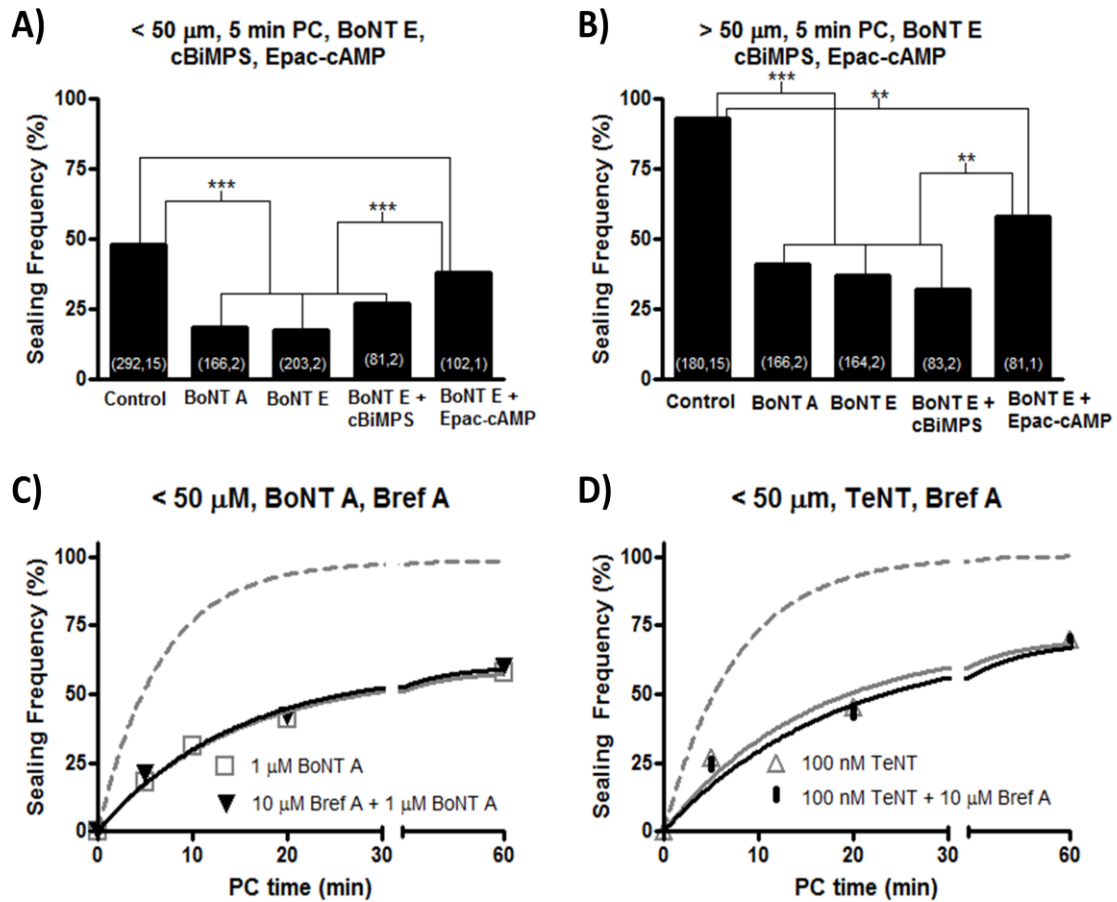
Supplemental Table 3.1 Legend: **PC Time:** Time (min) when Texas Red dextran was added to the Ca²⁺-containing saline. **Numbers (n, N):** Pooled number of B104 cells (n) with a transected neurite examined in a set of identically treated Petri dishes (N) at a given PC time. Gray areas in **Table 1A** and **B** with no values indicate the PC times for a given test substance that were not investigated in this study.



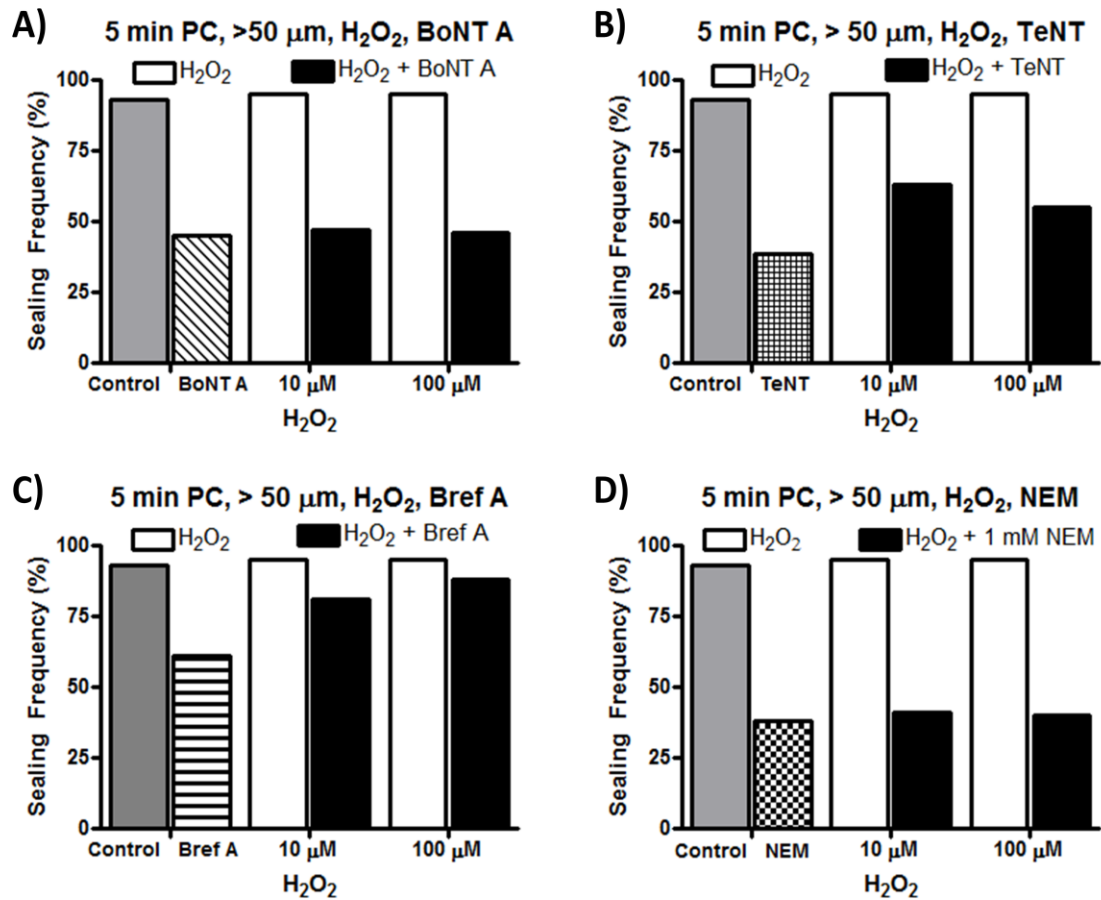
Supplemental Figure 3.1 A-B: Cells assessed for sealing at 5 min PC following transection in 1 μ M BoNT A, 25 μ M BoNT, 100 nM TeNT, or 500 nM TeNT or Ca^{2+} -free saline (control). **C,D:** Cells assessed for sealing at 5 min PC following transection in 100 nM TeNT or 1 μ M BoNT B.



Supplemental Figure 3.2 A,B: Cells assessed for sealing at 5 min PC following transection in 10 μ M Bref A, 50 μ M Bref A, or 1 hour pre-treatment with 10 μ M Bref A, followed by transection in 10 μ M Bref A. **C,D:** Cells assessed for sealing at 5 min PC following transection in 1 mM NEM or 10 mM NEM.



Supplemental Figure 3.3 A,B: Cells assessed for sealing at 5 min PC following transection in 1 μM BoNT A, 1 μM BoNT E, 1 μM BoNT E + 8 μM cBiMPS, or 1 μM BoNT E + 8 μM Epac-cAMP. **C,D:** Cells transected nearer to the soma in (C) 1 μM BoNT A (gray open squares), or 1 μM BoNT A and 10 μM Bref A (inverted black, filled triangles) or (D) 100 nM TeNT (gray open triangles), 100 nM TeNT + 10 μM Bref A (black vertical dashes).



Supplemental Figure 3.4 A-D: Cells assessed for sealing at 5 min PC, and transected farther from the soma in 10 μM H_2O_2 or 100 μM H_2O_2 (white bars) compared to control sealing (gray bars). **A:** Cells transected in 1 μM BoNT A (diagonal bars), 10 μM H_2O_2 + 1 μM BoNT A or 100 μM H_2O_2 + 1 μM BoNT A (black bars). **B:** Cells transected in 100 nM TeNT (plaid bars), 10 μM H_2O_2 + 100 nM TeNT or 100 μM H_2O_2 + 100 nM TeNT (black bars). **C:** Cells transected in 10 μM Bref A (horizontal lines), 10 μM H_2O_2 + 10 μM Bref A or 100 μM H_2O_2 + 1 μM Bref A (black bars). **D:** Cells transected in 1 mM NEM (diagonal bars), 10 μM H_2O_2 + 1 mM NEM or 100 μM H_2O_2 + 1 mM NEM (black bars).

Chapter 4: Cytosolic oxidation enhances plasmalemmal repair of B104 cells

Running Title: **Oxidation enhances plasmalemmal repair**

Abstract:

Immediately after plasmalemmal damage, Ca^{2+} and other ions in the extracellular solution flow into the cell, and cytoplasmic ions and other substances flow out of the cell. We now report that plasmalemmal damage produces cytosolic oxidation as assayed by methylene blue (MB) color change. Direct oxidation of the cytosol using a wide range (10 μM to 50 mM) of H_2O_2 concentrations increases plasmalemmal sealing at 1 to 10 min post calcium addition (PC time). However, after 10 min PC, 100 μM , 5 mM, and 50 mM H_2O_2 produce a decline in sealing associated with plasmalemmal disruption even in previously uninjured cells. Reducing agents or anti-oxidants decrease sealing.

Introduction

To survive traumatic injury, a cell must repair the plasmalemmal damage (Yoo, et al., 2004). Repairing plasmalemmal damage is particularly important for neurons, which do not proliferate as readily as many other cell types. All eukaryotic cell types, including neurons, repair plasmalemmal damage by a Ca^{2+} -dependent accumulation of various membrane-bound vesicles at the damage site (see Bittner and Fishman, 2003). The movement, interactions, and membrane fusion of such vesicles are controlled by multiple intracellular pathways including those mediated by cAMP activation of PKA and Epac, DAG activation of PKC, and possibly cytosolic oxidation (Spaeth, et al., 2010).

However, cytosolic oxidation has also been reported to produce deleterious effects on all cells, especially neurons (Sugawara, et al., 2002). In this paper, we investigate the possibility that oxidation increases plasmalemmal sealing, since an anti-oxidant decreases sealing (Spaeth, et al., 2010), and cytosolic oxidation increases vesicle accumulation in many different cell types (Cai, et al., 2009a,b,c; Horie, et al., 1999, 2004; Thiels, et al., 2000; Knapp and Klann, 2002; Gerich, et al., 2009).

Methods

We evaluated plasmalemmal repair (sealing) by a dye exclusion of individually transected neurites of rat hippocampal B104 cells (Spaeth, et al., 2010), which extend neurites with axonal-like properties (Bottenstein and Sato, 1979) (Fig. 4.1 A,C). Neurites of uniquely identifiable rat hippocampal B104 cells were transected in a Petri dish using a sharpened glass micro-capillary tube fastened to a micromanipulator for 10 minutes in Ca^{2+} -free saline, at which time cells are bathed in saline containing 1 mM Ca^{2+} (Ca^{2+} containing saline). As previously reported (Spaeth, et al., 2010) the time elapsed after Ca^{2+} addition is referred to as “post- Ca^{2+} time” (PC time). At various PC times, extracellular dye (Texas Red dextran, 3 kDa) is added to the Petri dish. We interpret transected cells that exclude dye as having formed a dye barrier seal (sealed), which is a precursor to the eventual repair of the plasmalemmal damage. Cells that take up dye have not formed a dye barrier (not sealed) (Fig. 4.1 B,D). “Sealing frequency” is defined as the percent of a set of individually-transected and uniquely identified B104 cells that

exclude Texas Red dextran. Sealing frequencies at a given PC time point are compared using the Cochran-Mantel-Haenzsel χ^2 test (CMH χ^2) (Agresti, 1996).

Results

We directly tested whether cytosolic oxidation occurs after plasmalemmal damage by observing the color change of MB from clear (reduced) to blue (oxidized). For cells transected nearer to (453 cells, 6 plates), or farther from (435 cells, 6 plates), the soma in 100 μ M MB, all (100%) cells turned blue within a few seconds of neurite transection. Furthermore, nearby, undamaged cells were not blue.

Since plasmalemmal damage leads to cytosolic oxidation we directly oxidized the cytosol with H_2O_2 to investigate whether oxidation increases sealing. At PC times between 0 and 10 min, cells transected in 10 μ M (filled diamonds), 100 μ M (inverted open triangles), 5 mM (filled triangles), and 50 mM H_2O_2 (open diamonds) all sealed at a significantly ($p < 0.05$, CMH χ^2) greater frequency compared to control sealing (Fig. 4.2 A,B). Control sealing curves (no experimental compound added to either Ca^{2+} -free saline or Ca^{2+} -containing saline) are plotted as dashed (nearer to the soma) or dotted (farther from the soma) lines. Solid lines connecting individual sealing frequencies represent an exponential equation fitted to the data using GraphPad Prism. Exponential equations for each data set are used to calculate the rate of sealing, which is the time required for sealing to reach 63.2% of the maximum observed sealing frequency. The sealing rate for cells transected nearer to, or farther from the soma in any $[\text{H}_2\text{O}_2]$ was not significantly ($p > 0.05$, FZT) faster compared to control sealing (Table 4.1).

H₂O₂ could not increase sealing in the absence of Ca²⁺. At 0 min PC, when dye was added before Ca²⁺, no (0%) cells transected nearer to, or farther from, the soma in 10 μ M, 100 μ M, 5 mM, and 50 mM H₂O₂ sealed, similar to control sealing (0%, Fig. 4.2 A,B). These data suggest that oxidation-dependent sealing requires Ca²⁺.

After 10 min PC for cells transected in 50 mM H₂O₂, 15 min PC for cells transected in 5 mM H₂O₂, or 30 min PC for cells transected in 100 μ M H₂O₂, the sealing frequency significantly ($p < 0.05$, CMH χ^2) declined compared to control sealing (Fig. 4.2 A,B). The rate for the decline of sealing is the time required for sealing to decrease from the maximum observed sealing frequency to 37.8% of the minimum observed sealing frequency. The observed decline in sealing exhibited a faster rate ($p < 0.05$, FZT) for higher concentrations of H₂O₂ compared to lower concentrations of H₂O₂ (Table 4.2).

The decline in sealing frequency from the maximum observed sealing frequency for cells transected in 100 μ M, 5 mM, or 50 mM H₂O₂ was associated with cells exhibiting signs plasmalemmal swelling and breakdown, or “blebbing” a condition associated with plasmalemmal damage (Yoo, et al., 2004) that often precedes cell death. Cells that exhibited signs of “blebbing” almost always filled with dye, whether or not they were transected (Fig. 4.1C,D, cell marked with arrow). These data are consistent with reports that cytosolic oxidation is toxic to neurons. For example, exposing PC12 or primary murine neurons to 5 mM H₂O₂ eliminates mTor activity, leading to apoptosis within 30 minutes of treatment (Chen, et al., 2010). Improper intracellular scavenging of ROS due to a genetic deletion of Sod1 leads to neuronal impairment, even in uninjured neurons (Thiels, et al., 2000), whereas increasing Sod1-activity is neuroprotective

following traumatic injury (Sugawara, et al., 2002) or ischemia (Endo, et al., 2007). Such oxidative neuronal death is a factor in many neurodegenerative disorders, especially Sod1-dependent ALS, which involves a decreased cytosolic ability to buffer the ROS release from mitochondria (Celsi, et al., 2004).

A similar decline in sealing frequency or plasmalemmal breakdown was not observed for cells transected in 10 μM H_2O_2 up to 60 min PC, suggesting that lower $[\text{H}_2\text{O}_2]$ (10 μM) may be beneficial for repairing plasmalemmal damage.

PKA inhibition by the small peptide inhibitor PKI decreases sealing (Spaeth, et al., 2010) (confirmed at 5 min PC in Fig. 4.3 A,B). To investigate whether the H_2O_2 -dependent increase in sealing could be decreased, or prevented, by PKI inhibition of PKA, cells were transected in both 50 μM PKI and various $[\text{H}_2\text{O}_2]$. At 5 min PC, cells transected in 10 μM H_2O_2 + 50 μM PKI, 100 μM H_2O_2 + 50 μM PKI or 5 mM H_2O_2 + 50 μM PKI sealed at a significantly ($p < 0.001$, CMH χ^2) lower frequency compared to control sealing, but not a significantly ($p > 0.05$, CMH χ^2) greater frequency compared to cells transected in only 50 μM PKI (Fig. 4.3 A,B). Since PKI inhibition of PKA blocks the H_2O_2 -dependent increase in sealing, the H_2O_2 -dependent increase in sealing requires PKA. These data are consistent with reports that H_2O_2 increases PKA activity (Brennan, et al., 2006; Humphries, et al., 2007) while simultaneously decreasing the activity of various phosphatases that reverse the effects of PKA phosphorylation (Humphries, et al., 2007). Although PKA is typically activated by cAMP (Gilman, et al., 1970), including during plasmalemmal sealing (Spaeth, et al., 2010), PKA may also be activated by H_2O_2 in a concentration-dependent manner independent of cAMP (Brennan, et al., 2006).

Since oxidation increases sealing (Fig. 4.2 A,B), and the anti-oxidant Melatonin (Mel) decreases sealing (Spaeth, et al., 2010), we investigated whether using the reducing agent DTT to prevent damage induced cytosolic oxidation would decrease sealing. At 5 min PC, cells transected in 10 mM DTT or 50 mM DTT sealed at a significantly lower frequency compared to control sealing (Fig. 4.3 A,B). Similar results were observed for cells transected in 100 μ M Methylene Blue (MB), which acts as an anti-oxidant.

We also transected cells in Ca^{2+} -free saline containing no other substance, then added Ca^{2+} -saline containing either 10 mM DTT, 50 mM DTT, 2 mM Mel or 100 μ M MB. At 5 min PC, cells treated with 50 mM DTT, 2 mM Mel or 100 μ M MB following transection soma sealed at a significantly ($p < 0.05$, CMH χ^2) lower frequency compared to control sealing (Fig. 4.3 C,D). However, the observed decrease in sealing was not as great as when cells were transected in Ca^{2+} -free saline containing DTT, Melatonin, or MB. Transecting cells in Ca^{2+} -free saline containing 10 mM DTT, 50 mM DTT, 2 mM Mel or 100 μ M MB, then treated with Ca^{2+} saline containing 10 mM DTT, 50 mM DTT, 2 mM Mel or 100 μ M MB sealed at a significantly lower frequency compared to control sealing (Fig. 4.3 E,F). These data suggest that the intracellular Redox environment influences plasmalemmal sealing. Furthermore, we would predict that other oxidizing agents would increase sealing, and other reducing agents/anti-oxidants or free radical scavenging substances would decrease sealing.

Discussion

Repairing plasmalemmal damage is very important for neurons, which do not proliferate as readily as other cell types (Cai, et al., 2009a,b,c), especially following traumatic injury. Additionally, neurons exhibit extreme sensitivity to cytosolic oxidation, whereas muscle or other non-neuronal cell types fail to exhibit the same sensitivity to cytosolic oxidation. However, recent data, including our current data, suggest that cytosolic oxidation may also have beneficial effects, including enhancing repair of plasmalemmal damage (Cai, et al., 2009a,b,c), and axonal regeneration (Ignaki, et al., 2000).

H₂O₂ might increase sealing frequency by activating pathways involved in vesicle accumulation, since vesicle accumulation is important for sealing (Krause, et al., 1994; Steinhardt, et al., 1994; Cai, et al., 2009b). For example, low [H₂O₂], or cytosolic oxidation, increases vesicle mediated synaptic potentiation in hippocampal slices (Knapp and Klann, 2002), LTP in spinal axons (Lee, et al., 2010), as well as providing additional membrane sources during axon extension in invertebrates (van Diepen, et al., 2005) and mammals (Horie, et al., 1999, 2004) and vesicle accumulation muscle cells (Cai, et al., 2009a,b,c), and increased exocytosis through oxy-sterol formation in pancreatic cells (Ma, et al., 2010). These and other data on H₂O₂- dependent vesicle accumulation demonstrates a new understanding of the role of cytosolic oxidation, and may provide key insights into the etiology of oxidation dependent neurodegenerative disorders.

Chapter 4 Figures and Tables:

Table 4.1A: Rates of increasing sealing

Test Substance	τ (min) < 50 μm	k (min^{-1}) <50 μm	R^2 < 50 μm	τ (min) > 50 μm	k (min^{-1}) > 50 μm	R^2 > 50 μm
Control	5.95	0.168	0.9865	2.16	0.461	0.9970
10 μM H_2O_2	5.14	0.195	0.9774	2.11	0.475	0.9998
100 μM H_2O_2	4.78	0.209	0.9807	2.88	0.347	0.9998
5 mM H_2O_2	6.65	0.151	0.9291	1.59	0.628	0.9733
50 mM H_2O_2	1.51**	0.661**	0.9291	1.59	0.628	0.9733

Table 4.1B: Rates of declining sealing

Test Substance	τ (min) < 50 μm	k (min^{-1}) <50 μm	R^2 < 50 μm	τ (min) > 50 μm	k (min^{-1}) > 50 μm	R^2 > 50 μm
Control	N.A.	N.A.	N.A.	N.A.	N.A.	N.A.
10 μM H_2O_2	N.A.	N.A.	N.A.	N.A.	N.A.	N.A.
100 μM H_2O_2	24.45** *	0.041***	0.9807	2.7E+3**	3.65E-5**	0.9677
5 mM H_2O_2	8.70*	0.115*	0.9291	7.23	0.138	0.9989
50 mM H_2O_2	4.68	0.214	0.9999	6.4	0.155	0.9913

Table 4.1A,B: Statistical comparisons of rate constants (k , min^{-1}) or exponential time constants (τ , min) for sealing of B104 cells transected nearer to (< 50 μm), or farther from (> 50 μm), the soma. Cells transected nearer to the soma and bathed in a given test substance always sealed at a slower rate compared to cells transected farther from the soma and bathed in the same test substance. **R^2 < 50 μm or R^2 > 50 μm :** Goodness of fit values obtained from a single-exponential model to fit the sealing frequency at all PC times for control sealing, or for sealing in a given test substance. Asterisks indicate the level of significant difference between sealing time constants or rate constants for a given test-substance compared to control sealing. Significance levels for this and all other tables and figures are indicated beside each value as follows: no asterisk = $p > 0.05$ and < 0.95 , single asterisk (*) = $p < 0.05$, double asterisk (**) = $p < 0.01$, and triple asterisk (***) = $p < 0.001$. **Rate of increasing sealing:** Rate calculated for sealing frequencies from 0 PC until the maximum observed sealing frequency occurred. **Decline of sealing:** Rate calculated for sealing frequencies from the PC time of the maximum observed sealing until 60 min PC.

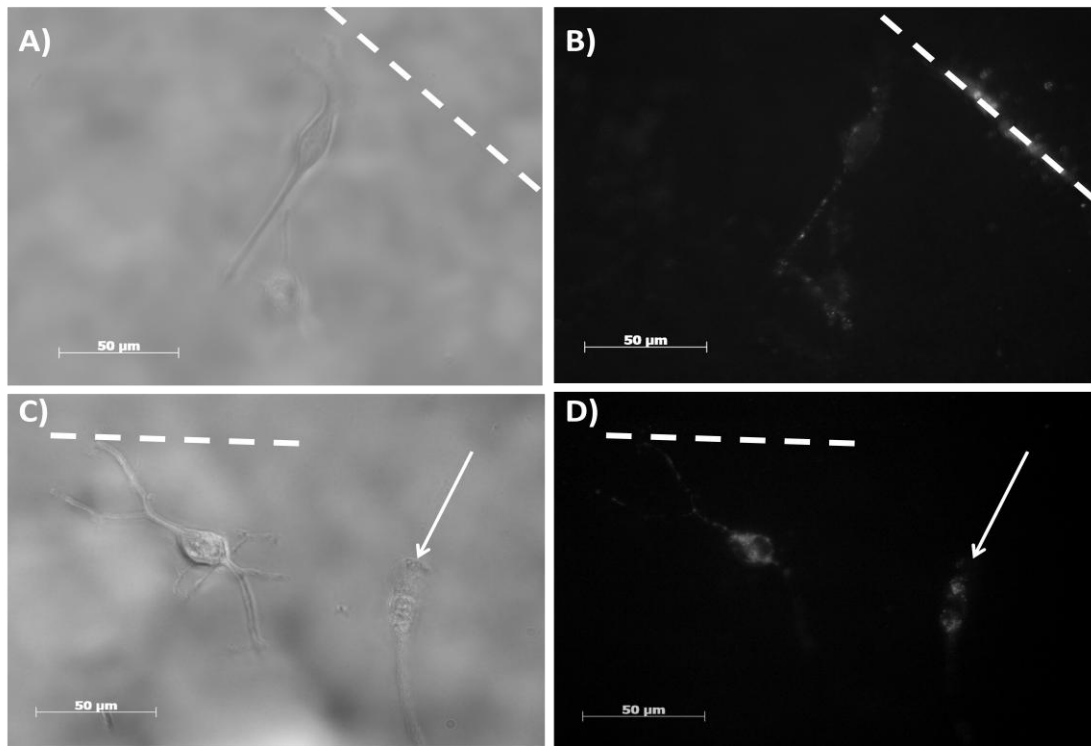


Figure 4.1A-D: Brightfield (**A, C**) and fluorescence (**B, D**) images typical of those used to assess dye uptake or exclusion by B104 cells having a transected neurite. Brightfield images (**A, C**) taken after transecting a neurite, marked by a score line, (white dashed line), in Ca^{2+} -free saline. After 10 min in Ca^{2+} -free saline, the cells were bathed in Ca^{2+} -saline for 5 min, at which time Texas-Red dextran was added to the Ca^{2+} -saline. The cells were then imaged Texas Red (**B, D**) emission. The presence of Texas Red emission (**B, D**) shows these cells did not exclude dye, and therefore did not form a plasmalemmal seal. Uninjured cells typically did not take up dye, indicating their plasmalemma remained intact, however the uninjured cell marked with an arrow in **C** and **D** exhibits signs of plasmalemmal breakdown (swelling), and fills with dye (**D**). Scale bars in all panels represent 50 μm .

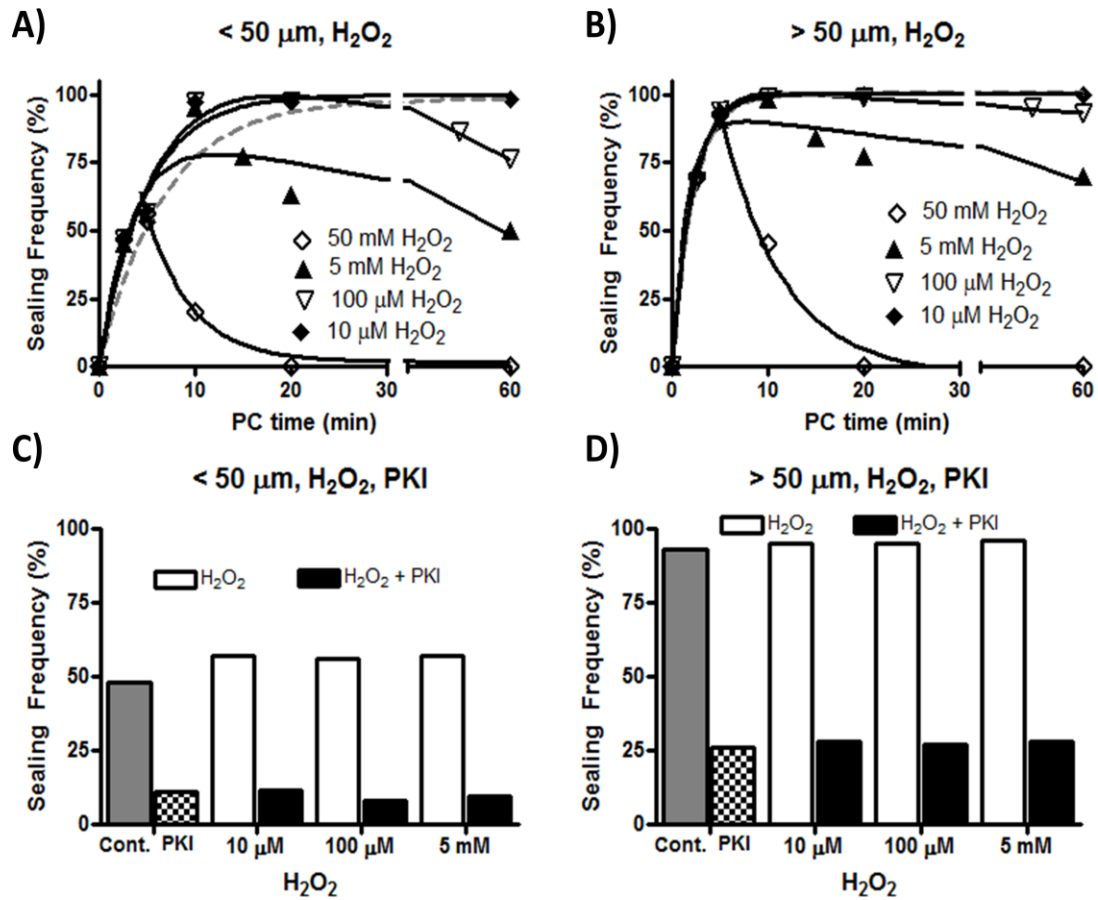


Figure 4.2: Cells transected nearer to (A) or farther from (B) the soma in 10 μM H_2O_2 (filled diamonds), 100 μM H_2O_2 (inverted open triangles), 5 mM H_2O_2 (filled triangles), or 50 mM H_2O_2 (open diamonds). Dotted or dashed lines represent the sealing frequency for control sealing and solid lines for test substances fitted to **Equation 1** by GraphPad Prism (See **Methods**). In A, B control sealing curves are plotted as dashed (< 50 μm) or dotted (> 50 μm) lines to compare the effects of various [H_2O_2] to control sealing. C, D: Cells assessed for sealing at 5 min PC. Cells were transected nearer to (C) or farther from (D), the soma in: 10 μM H_2O_2 , 100 μM H_2O_2 , or 5 mM H_2O_2 (white bars), 50 μM PKI (checkered bars), or a given [H_2O_2] and 50 μM PKI (black bars) compared to control sealing (gray bars).

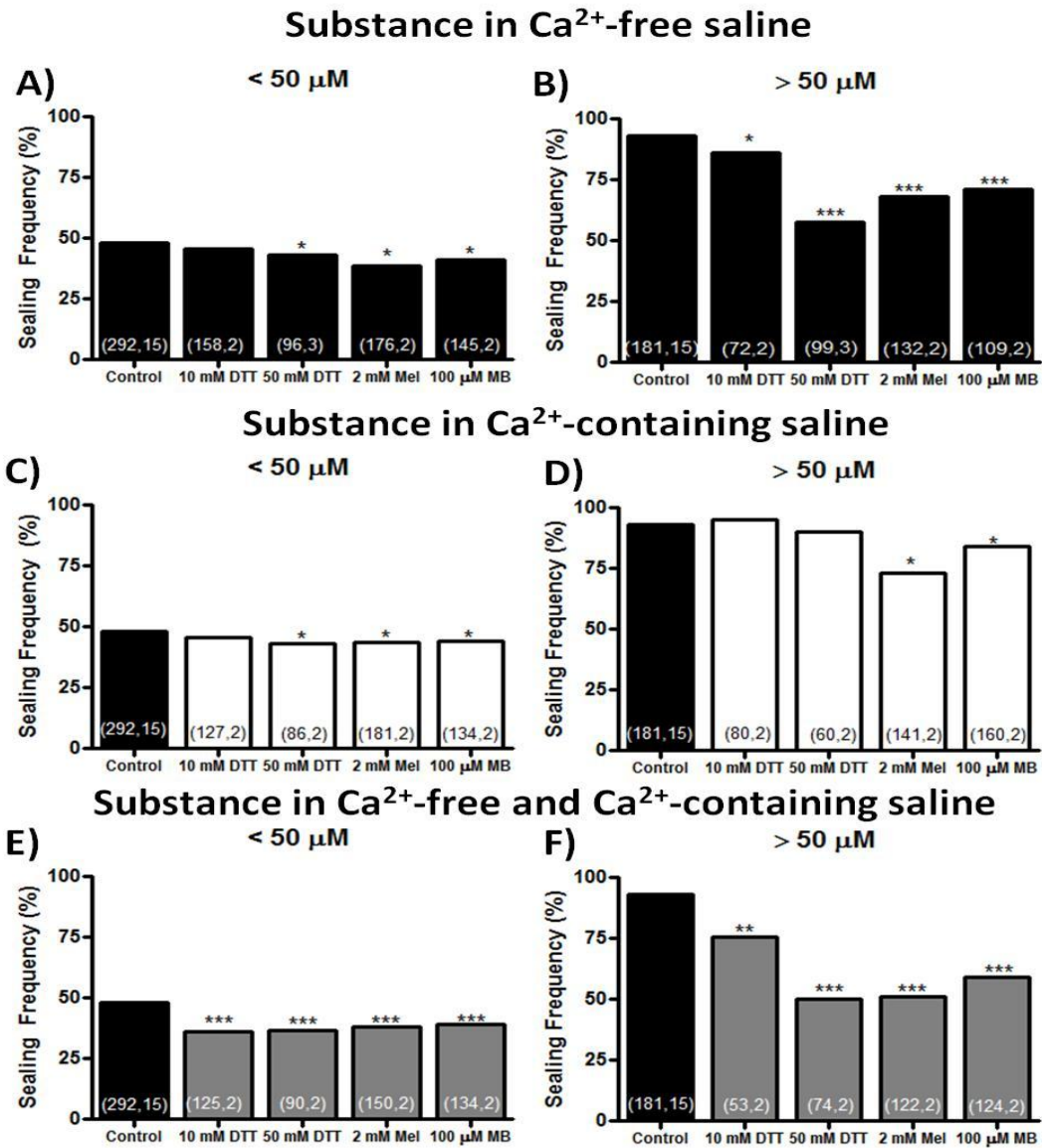


Figure 4.3: A,B: Cells transected nearer to (A) or farther from (B) the soma in Ca^{2+} free saline containing 10 mM DTT, 50 mM DTT, 2 mM Mel or 100 μM MB (black bars). C,D: Cells transected nearer to (C) or farther from (D) the soma in Ca^{2+} free saline, followed by the addition of Ca^{2+} saline containing 10 mM DTT, 50 mM DTT, 2 mM Mel or 100 μM MB (white bars). E,F: Cells transected nearer to (E) or farther from (F) the soma in Ca^{2+} free saline containing 10 mM DTT, 50 mM DTT, 2 mM Mel or 100 μM MB, followed by the addition of Ca^{2+} saline containing 10 mM DTT, 50 mM DTT, 2 mM Mel or 100 μM MB (gray bars). The numbers in parenthesis in each bar represent the number of cells transected, and the number of Petri dishes used to obtain that many cells.

Chapter 4 Supplementary Methods:

B104 cells: B104 cells derived from a CNS neuroblastoma (Bottenstein and Sato, 1979) have often been used as a model system to study neuronal function *in vitro* (Toda, *et al.*, 1999; Tan, *et al.*, 2003; Yoo, *et al.*, 2003, 2004; Nguyen, *et al.*, 2005; Miller, *et al.*, 2006). These cells have easily identifiable cell bodies and neurites, allowing each precisely transected cell to be uniquely and individually identified (Detrait, *et al.*, 2000b; Yoo, *et al.*, 2003, 2004; Spaeth, *et al.*, 2010). Data on sealing of B104 cells is consistent with similar data on sealing from at least 20 other preparations from many phyla and different cell types *in vitro* and *in vivo* (Spaeth, *et al.*, 2010).

Cell culture: As previously described (Spaeth, *et al.*, 2010), B104 cells were grown in 75cm² vented cap flasks (BD-Falcon, Franklin Lakes, NJ) in a humidified incubator at 37°C in 5% CO₂ in 4 mL of “cell growth media,” which consists of a 1:1 mixture of Dulbecco’s Modified Eagle’s Media and Ham’s F12 (DMEM:F12, HyClone, Logan, UT), supplemented for growth with 10% heat inactivated fetal bovine serum (FBS, Hyclone, Logan, UT) and 1% antibiotics (10,000 Units of Penicillin/mL and 10 mg/mL of streptomycin, Sigma-Aldrich, St. Louis, MO). The cell growth media was changed every 2 days. Cultures were passaged at 80% confluency and cells were then either sub-cultured in a vented cap flask or seeded at approximately 2000 cells/cm² in cell growth media on Petri dishes coated with Poly-D-lysine (Sigma-Aldrich, St. Louis, MO) to prevent cells from detaching during solution changes and/or neurite transections. After 24 hours, the growth media was replaced with serum-free DMEM:F12 (Hyclone, Logan,

UT) to allow the B104 cells to differentiate. B104 neurites were transected 24-48 hours after replacing the cell growth media with serum-free DMEM:F12.

Transection of neurites of B104 cells: Prior to transecting neurites, the solution (DMEM:F12) in the Petri dish was washed out twice with a Ca^{2+} -free phosphate buffered saline (referred to as “ Ca^{2+} -free saline”, PBS -/-, HyClone, Logan, UT). All neurites were transected in Ca^{2+} -free saline using a sharpened, pulled-glass micro-capillary tube ("micro-knife"), which was placed on a micro-manipulator (Narishige Instruments, East Meadow, NY) and quickly drawn across the surface of the Petri dish, etching a score line that showed the path of the knife. We were able to uniquely and individually identify each transected cell by the relation of the transected neurite to its soma and to the score mark on the plate (Fig. 1).

Microscopy and Imaging: For all experiments, B104 cells were observed under an inverted Zeiss ICM-405 fluorescent microscope (Zeiss, West Germany) with a 40X, long focal distance lens. Transected cells were imaged (Fig 4.1) through a hole cut out of the bottom of a plastic dish covered by a thin glass coverslip using a Leica DM IRBE outfitted with a 40x lens and a Leica DFC350 FX fluorescence camera at the UT Core Microscopy facility. Individually identified cells with neurites obviously transected within $< 50 \mu\text{m}$ of the soma were counted as transected “nearer to” the soma (Fig. 4.1 A,B), and those with neurites transected at $> 50 \mu\text{m}$ of the soma were counted as transected “farther from” the soma (Fig. 4.1 C,D). No further observations were made on any cell whose transection distance was not clearly definable.

Assessment of plasmalemmal sealing: We transected 10 – 130 uniquely identifiable cells within 10 min in a Petri dish containing Ca^{2+} -free saline. The Ca^{2+} -free saline was then replaced with a phosphate buffered saline containing 1 mM Ca^{2+} (“ Ca^{2+} -saline”, PBS+/+, HyClone, Logan, UT) to initiate the sealing process (Detrait, *et al.*, 2000b; Yoo, *et al.*, 2003; Spaeth, *et al.*, 2010). The time elapsed after exposing cells to Ca^{2+} -saline is defined as the “post- Ca^{2+} addition time” (PC time).

At various PC times (0-60 min PC), 3kD Texas Red dextran (Molecular Probes, Eugene, OR) was added to the Ca^{2+} -saline to assess the formation of a plasmalemmal seal. For all experiments, the dye was thoroughly washed out with Ca^{2+} -saline after a 10 min exposure to Texas Red dextran and sealing was assessed. Transected cells that excluded Texas Red dextran were counted as “sealed” (Fig. 4.1 B,D). Cells that did not exclude Texas Red dextran were counted as “not sealed” (not pictured). We consistently used 3 kDa Texas Red dextran to assess sealing in all other experiments reported herein to avoid any variation in sealing time due to differences in dye molecular weight (Eddleman, *et al.*, 2000; Spaeth, *et al.*, 2010).

Pharmacological Reagents: All pharmacological agents were dissolved in distilled water, unless otherwise noted. We used H_2O_2 (Fisher, Pittsburgh, PA) to produce cytosolic oxidation, and Di-thio-threitol (DTT, 154.25 Da, Sigma, St. Louis, MO), Melatonin (Mel, 232.28 Da), and Methylene Blue (MB, 373.91 Da, a generous gift from Dr. Gonzalez-Lima, UT-Austin) to decrease cytosolic oxidation. We used the small peptide PKI (kDa, 14-22 fragment, a generous gift from Drs. Michael Markham and Harold Zakon, UT-Austin) to inhibit PKA.

Statistical analysis: For each experimental treatment group, at a given PC time, the data was pooled for all cells (n) from all Petri dishes (N). “Sealing frequency” is defined as the percent of a set of individually-transected and uniquely identified cells that exclude 3 kD Texas Red dye (sealed) at a given PC time. The Cochran-Mantel-Haenszel χ^2 (CMH χ^2) test for independence was used to determine whether the differences between the sealing frequency at a given PC time for different experimental treatments was statistically significant ($p < 0.05$), as previously described (Agresti, 1996; Detrait, *et al.*, 2000b; Yoo, *et al.*, 2003, 2004; Spaeth, *et al.*, 2010).

GraphPad Prism was used to fit the sealing frequency for all PC times of a given control or test substance to a one phase exponential equation (Spaeth, *et al.*, 2010). The solid and dashed lines on all graphs calculated by GraphPad Prism represent the exponential equation fitted to the sealing frequencies at various PC times.

Sealing rate constants (k) were calculated by GraphPad Prism and used to calculate time constants ($\tau = 1/k$) equal to the PC time to achieve 63.2% of the observed maximum sealing (rising phase; Spaeth, *et al.*, 2010), or the time to achieve 33.8% of the observed minimum sealing frequency (decline phase). Rate or time constants for two experimental conditions were normalized and compared using Fisher’s Z transformation (FZT, Table 1). Two sealing rate or time constants were considered significantly different if p was < 0.05 , using a Z-table. R^2 values were also calculated for the exponential equations defining each time constant to determine how closely the exponential equations modeled the observed data (Table 4.1 A,B).

Chapter 5: Polyethylene Glycol Rapidly Restores Axonal Integrity and Improves Behavioral Recovery After Sciatic Nerve Crush Injury*

Significant portions of this chapter have been previously published as part of Britt, et al., 2010

Abstract

The inability to rapidly (within minutes to hours) improve behavioral function after severance of peripheral nervous system axons is an ongoing clinical problem. We have previously reported that polyethylene glycol (PEG) can rapidly restore axonal integrity (PEG-fusion) between proximal and distal segments of cut- and crush-severed rat axons in vitro and in vivo. We now report that PEG-fusion not only re-establishes the integrity of crush-severed rat sciatic axons as measured by the restored conduction of compound action potentials (CAPs) and the intra-axonal diffusion of fluorescent dye across the lesion site, but also leads to more rapid recovery of appropriate hindlimb motor behaviors. Improvement in recovery occurred during the first week as assayed by a foot fault (FF) asymmetry test and between post-operatives weeks 2 and 3 for the Sciatic Functional Index (SFI). That is, the FF test was the more sensitive indicator of early behavioral recovery, showing significant postoperative improvement of motor behavior in PEG-treated animals at 24–48 h. In contrast, the SFI more sensitively measured longer-term postoperative behavioral recovery and deficits at 4–8 wk, perhaps reflecting the development of fine (distal) motor control. These and other data show that PEG-fusion not only rapidly restores physiological and morphological axonal continuity, but also more quickly improves behavioral recovery.

Introduction

Crush-severance is the most common form of traumatic injury to PNS axons in humans (Bozkurt et al. 2007, 2008). Crush- (or cut-) severance injuries completely disrupt the axolemma at the lesion site and also produce smaller plasmalemmal holes proximal and distal to the severance site (Fig. 1B; Bittner et al. 1986; Lore et al. 1999). Distal segments of severed mammalian PNS and CNS axons undergo Wallerian degeneration within 12–72 h (Ramón y Cajal 1928; Waller 1850). If proximal PNS axonal segments survive axotomy, regeneration by outgrowth can occur at rates of 1–2 mm/day (Hadlock et al. 2005; Ramón y Cajal 1928). Thus acute (within days) recovery in mammals is nonexistent. Chronic behavioral recovery is delayed and often very inadequate or nonexistent because PNS outgrowths take months to years to reach denervated target tissues in larger mammals such as humans and those target tissues are often nonspecifically reinnervated (Bozkurt et al. 2007, 2008; Das and Wallace 1986; Ingoglia and Murray 2001).

In the last several decades, various procedures have improved the number and specificity of PNS axons that reestablish connections following severance, but not the outgrowth rate or time for PNS axons to reestablish those connections. For example, nerve grafts (Jeng and Coggeshall 1986; Lago et al. 2007), connective tissue matrices (Bozkurt et al. 2007; Herbert et al. 1996; Lore et al. 1999), and nerve growth guides (Aebischer et al. 1990; Kalbermatten et al. 2009) have all been reported to improve the extent of regeneration by severed PNS axons, but not the rate or time at which PNS axons reestablish their connections.

We now describe the further use of an unconventional technique to improve the time to reinnervate and specificity of acute and chronic repair of mammalian PNS axons by directly applying polyethylene glycol (PEG) solutions to the lesion site of severed axons (Fig. 5.1, B–E).

This PEG-fusion technique and its rationales are as follows: Ca^{2+} influx through partially constricted axonal ends and nearby small holes produced by the trauma of crush-severance (Fig. 5.1B) induces vesicles derived from nearby undamaged membranes (Eddleman et al. 1997), lysosomes (Reddy et al. 2003), and/or myelin delaminations (Ballinger et al. 1997) to migrate, accumulate, and pack tightly at the damage site. These membrane-bound structures interact with each other and nearby, undamaged membrane to continuously reduce the influx and efflux of ions and other substances until a complete seal is formed in 10–20 min (Bittner and Fishman 2000). Eventually, the plasmalemma is completely repaired (Fig. 5.1A) and vesicles are no longer observed 24 h after severance (Lichstein et al. 1999). Vesicle interactions are practically impossible to image in vivo in small-diameter unmyelinated or myelinated mammalian axons, but biochemical and dye exclusion data show that the same proteins and processes are involved with time courses similar to those in invertebrates (Bittner and Fishman 2000; Detrait et al. 2000a,b; Nguyen et al. 2005; Yoo et al. 2003, 2004).

Bathing recently severed invertebrate or mammalian axons in Ca^{2+} -free hypotonic salines containing EGTA opens severed axonal ends, flushes out most previously formed vesicles, and prevents new vesicle formation (Fig. 5.1, B and C). PEG applied in pure H_2O to proximal and distal ends of severed axons removes waters of hydration from

membrane proteins so that plasmalemmal lipids flow together at points where axonal open ends are closely apposed (Fig. 5.1D; Krause and Bittner 1990; Krause et al. 1991; Lore et al. 1999). That is, two open, largely vesicle free, axonal ends can be more easily fused by PEG than two constricted ends filled with vesicles. [For decades, hybrid cell lines have been made by using PEG solutions to remove waters of hydration from membrane-bound proteins, thereby allowing membrane lipids to fuse when cell plasmalemmas are closely apposed (Ahkong et al. 1987).] The subsequent application of Ca^{2+} -containing isotonic saline to the lesion site induces vesicles to seal any remaining plasmalemmal holes (Fig. 5.1E). Crush-severed nerves that are PEG-fused may be mechanically weak at the lesion site because severance (Fig. 5.1B) disrupts the extracellular matrix (ECM) that normally prevents intact axons (Fig. 5.1A) from tearing when stretched or stressed by joint or muscle movements.

In the present study, we confirm that PEG applied directly to the lesion site rapidly restores morphological and physiological continuity to crush-severed PNS axons. We report for the first time that this PEG-fusion technique rapidly (within 24–48 h) improves behavioral function in rats with crush-severed sciatic axons as measured by a modified foot fault (FF) test (Schallert et al. 2002; Yang et al. 2006). Only behavioral measures in this or any other study reported to date indicate whether PEG-fusion or any other technique to enhance regeneration has reconnected proximal and distal axonal ends of individual mammalian axons with sufficient specificity to enable the restoration of some or all of their original functions.

Methods

Subjects: All experimental procedures were approved by the University of Texas at Austin's Institutional Animal Care and Use Committee.

Our experimental group was composed of crush-severed axons that received a PEG treatment. Our control groups and their rationales were composed of crush [-severed] controls treated with distilled water to examine whether our vehicle affects any of our three measures of nerve repair. Sham controls examined whether the injuries to skin and adjacent muscles impair any measure of nerve repair. Cut [-severed] controls examined whether any measure of repair occurs naturally when a rat sciatic nerve receives a very severe and less common injury, in which the ends of proximal and distal sciatic nerve axons separate by about 2 mm and are not surgically reapposed.

One set of experimental and control groups totaling 40 adult male Sprague–Dawley rats (250–350 g) received in vivo compound action potential (CAP) measurements to both sciatic nerves (80 nerves total: 18 PEG-crush; 21 crush; 4 distilled water crush; 6 cut; 31 sham-operated) to assess axonal continuity immediately followed by in vitro intraaxonal dye diffusion assessments of axonal continuity (Table 1). Another set of experimental and control groups totaling 39 adult male Sprague–Dawley rats (250–350 g) received in vivo CAP measurements to assess axonal continuity of one (left) sciatic nerve (39 nerves: 13 PEG-crush; 9 crush; 9 distilled water crush; 4 cut; 4 sham-operated) and were examined postoperatively for 8 wk using two behavioral tests (Table 1). All animals were housed in groups of three in polycarbonate cages with sawdust

bedding, maintained on a 12:12-h dark:light cycle and given unrestricted access to food and water.

Surgical procedures: Rats were anesthetized with intraperitoneal injections of ketamine (90 mg/kg) and xylazine (10 mg/kg). An incision about 1.5 cm long was made in the hindlimb posterior-thigh muscles to expose the sciatic nerve. Exposed sciatic nerves were bathed with hypotonic Ca^{2+} -free Krebs's physiological saline containing 0.5 mM EGTA (Ca^{2+} -free saline, in mM: 99 NaCl, 5 KCl, 1.2 KH_2PO_4 , 1.3 MgSO_4 , 26 NaHCO_3 , 10 Na ascorbate, 10 dextrose, pH 7.35, 295 milliosmolar) and cleaned of connective tissue. Animals in the sham-operated group received no nerve injury following exposure of the sciatic nerve via incision. The sciatic nerve was bathed with isotonic Ca^{2+} -containing saline (in mM: 124 NaCl, 5 KCl, 1.2 KH_2PO_4 , 1.3 MgSO_4 , 26 NaHCO_3 , 110 Na ascorbate, 10 dextrose, 2 CaCl_2 , pH 7.35, 345 milliosmolar) before closing the incision.

Sciatic crush-severance injuries were made with Dumont #5 forceps. Experimenters carrying out the crush were blind to the assignment of postcrush treatment to eliminate possibility of bias in the force used to make the crush in the PEG versus non-PEG treatments. Following crush injury, the severed ends of the crushed sciatic axons remained closely apposed within their endo-, peri-, and epineural sheaths. The epineural sheath of the sciatic nerve was nicked with microscissors to allow better access of PEG or other solutions to axonal tissues.

Experimental animals in the PEG-crush group received a topical application of a 50% solution (w/w) of 2 kDa PEG dissolved in distilled water following crush injury.

PEG was applied from a micropipette positioned so that the PEG-containing solution flowed in a narrow stream (about 1 mm wide) over the crushed axons at the lesion site and allowed to bathe the injured nerve for about 1.5 min. Control animals in the crush injury group received no further treatment. Control animals in the distilled water crush group received a vehicle treatment of distilled water applied as previously described for the PEG-treated group. Control animals in the cut group received a sciatic nerve transection with microdissection scissors so that the proximal and distal ends retracted for 1–2 mm and were not reapposed or further treated, which produced a complete severance of all axons and their epineural sheaths. After assessing CAP conduction (see following text), the skin incision was closed with staples in all rats that later received behavioral tests.

All experimental and control animals used for behavioral testing received a 5 mg/kg subcutaneous injection of ketoprofen after surgery. Pharmacokinetic studies show that ketoprofen is almost completely excreted within 24 h (Kantor 1986). Our first behavioral analysis was conducted at 24 h postoperation and therefore ketoprofen should have very little, if any, residual effect on behavioral performance.

Electrophysiological recording of CAPs across a lesion site: As one measure of axonal continuity through a lesion site, conventional *in vivo* extracellular stimulation and recording of CAPs (extracellular recordings of action potentials generated by sciatic nerve axons) were performed for animals ($n = 40$) immediately used to examine morphological continuity by *in vitro* intraaxonal dye diffusion (Lore et al. 1999) as well as for animals ($n = 39$) used to examine behavioral measures of reinnervation specificity

for 8 postoperative weeks. Nickel-tipped hook electrodes were placed beneath the sciatic nerve to stimulate and record CAPs, which were visualized on an oscilloscope display. Preoperative electrophysiological assessments of axonal continuity were made by recording CAPs of ≥ 0.5 mV, conducted through the site of the proposed cut or crush injury.

After cutting or crushing the sciatic nerve between the stimulating and recording electrodes, complete severance of all axons was confirmed by an inability to record any detectable CAPs conducted through the lesion site (Lore et al. 1999). After any treatment, the sciatic nerve was always stimulated to determine whether any detectable CAPs conducted through the lesion site. During preoperative and postoperative CAP recordings, the nerve was frequently moistened with Ca^{2+} -free saline. Some animals received a sham operation consisting of exposure of the sciatic nerve via incision and application of Ca^{2+} -containing saline. Since these control animals in a sham-operated group received no neural injury, one CAP measurement was taken during each sham operation and that CAP amplitude was plotted as both a pre- and postoperative CAP (see Fig. 5.2).

Intra-axonal dye diffusion across a lesion site: As described earlier and in Table 5.1, one group of experimental animals received crush-severance injury followed by treatment with PEG and other groups of control animals received a sham, cut-severance, crush-severance, or crush-severance injury plus distilled water. The effectiveness of all these procedures was assessed by a CAP confirmation assay.

To examine intra-axonal diffusion of dye through the lesion site after performing

a CAP confirmation assay, we excised a 3-4 cm length of the sciatic nerve (including the lesion site) from each animal as described in Lore et al. (1999). We removed most of the epineural sheath and placed the nerve in a watertight well made of Vaseline on a 60 × 15 mm petri dish. For all sham operations and crush-severed nerves (PEG-treated, distilled water treated, and no treatment), the proximal end of the sciatic nerve was placed within the Vaseline well containing Ca²⁺-free saline and 20 μL of hydrophilic dye (Texas Red dextran; Molecular Probes). The remainder of the nerve, including the crush site, was bathed in Ca²⁺-free saline. For cut nerves, two Vaseline wells were made; one well contained the proximal end of the nerve bathed in Ca²⁺-free saline and 20 μL of 15% Texas Red dextran (Molecular Probes), whereas the distal segment of the nerve was anchored within the second well such that the transected segments were 1–2 mm apart. The petri dishes containing nerves in Vaseline wells were refrigerated for 14 h at 4°C and usually examined for intraaxonal diffusion of fluorescent dye beyond the crush or transection site using a Zeiss ICM-405 inverted fluorescence microscope. Some nerves were imaged using a Leica DM IRBE with a ×20 objective outfitted with a Leica DFC350 FX fluorescence camera.

Behavioral tests

Behavioral assessments were performed by experienced testers blind to the treatment condition during the dark portion of each animal's daily light cycle in which rats are more active. Animals were handled daily for 7 days prior to the start of behavioral testing. After receiving a CAP continuity assay of their left sciatic nerves, experimental and control groups of rats were behaviorally evaluated at 24, 48, and 72 h

after surgery, and then at weekly postoperative intervals for 8 wk. Animals were first tested at 24 h postoperatively to allow animals to recover from anesthesia.

Foot-fault test: Animals were allowed to roam freely on a wire mesh grid (45 × 30 cm, with 2.5 × 2.5 cm openings) elevated 1.5 cm above a solid base floor. Trials for each animal were recorded for 50 total steps per hindlimb. [In some cases, the animal was injured enough that 50 steps would not be reached. To eliminate undue stress, in these few instances, animals were removed from the grid after 5 min]. A foot fault was scored when a misstep resulted in the hindlimb falling through an opening in the grid. If the hindlimb misstepped, but was pulled back before touching the floor beneath the grid, the movement was scored as a partial fault and given a fault score of one. A full fault occurred when the animal's hindlimb touched the floor beneath the grid for support. Full faults were given a fault score of two. A composite fault score was calculated (see the following equations) for each of the injured and uninjured hindlimbs of every animal at each postoperative time. The composite fault score was further divided by 50 (total number of steps/limb) to obtain a fault percentage for each hindlimb. The percentage of faults by the injured hindlimb was subtracted from the percentage of faults by the uninjured hindlimb, yielding an asymmetry score for each animal at a given postoperative time according to the following three equations (Equation 5.1, 5.2, 5.3):

$$\text{Composite FF Score} = (\# \text{Partial faults} \times 1) + (\# \text{Full faults} \times 2) \quad (1)$$

$$\% \text{ FF} = \text{Composite FF Score} / 50 (\text{total number of steps}) \times 100\% \quad (2)$$

$$\text{FF Asymmetry Score} = \% \text{ FF (uninjured limb)} - \% \text{ FF (injured limb)} \quad (3)$$

FF asymmetry tests were conducted two times at 1–5 days prior to surgery and their scores averaged to obtain preoperative baseline values plotted at 0 postoperative days.

Sciatic Functional Index: Footprints have been used previously to measure gait quality in rat models of Parkinson's disease (Schallert et al. 1978) and sciatic nerve severance by the Sciatic Functional Index (SFI; de Medinaceli et al. 1982). Rats were trained to traverse an elevated (3-4 feet) wooden beam (4 inches wide) ending in their home cage. After a few habituation trials, during which rats frequently stopped and paused en route to their home cage, rats traversed the beam to the home cage without hesitation. For each trial run, a white strip of paper was secured to the wooden beam to collect footprints (two trials per rat at a given postoperative time). Animals had their injured and uninjured hind paws inked with black and red ink, respectively, and were placed near the end of the wooden beam farthest from the home cage. Three consecutive footprints from each limb (for a total of six consecutive prints) were used to measure (in millimeters) the following: NPL, normal footprint length; EPL, experimental footprint length; NTS, normal toe spread between toes one and five; ETS, experimental toe spread; NIT, normal intermediary toe spread between toes two and four; and EIT, experimental intermediary toe spread (Carlton and Goldberg 1986). SFI scores were then computed for each animal at a given postoperative time using the following formula (Carlton and Goldberg 1986) (Equation 5.4):

$$SFI = \left(\frac{NPL - EPL}{EPL} + \frac{ETS - NTS}{NTS} + \frac{EIT - NIT}{NIT} \right) \times 73$$

SFI scores of about -100 indicate complete impairment of behaviors mediated by the sciatic nerve and scores of about 0 indicate normal use/complete recovery of behaviors mediated by the sciatic nerve (de Medinaceli et al. 1982; Mackinnon et al. 1989). SFI tests were conducted three times at 1–5 days prior to surgery and their scores averaged to obtain preoperative baseline values plotted at 0 postoperative days.

Video recordings: We recorded foot fault (FF) tests using a Canon XL1 with a shutter speed of 1/420 s (videos available online at Journal of Neurophysiology website). Foot fault tests were recorded during the light phase of the animals' reverse dark/light cycle in the presence of experimenters scoring the animals' behavior (videos SV5.1–SV5.4). Open field observations were recorded in the dark using the camera's night vision setting, sacrificing some resolution in the videos for increased locomotor activity (videos SV5.5–SV5.6). The video recordings show qualitative differences in behavior between experimental groups.

Statistical analyses: Student's t-test was used to assess differences ($P < 0.05$) in preoperative CAP amplitudes versus postoperative CAP amplitudes. ANOVA was used to assess differences in SFI and FF asymmetry scores and Tukey's test was used for post hoc analysis to adjust for multiple comparisons. Hindlimb motor behaviors were subjected to a linear regression t-test to determine whether the regression line slopes of two treatment groups differed significantly ($P < 0.05$) over the 8-wk observational period following surgery.

Results

CAP assessments of axonal continuity

To evaluate the ability of PEG-fused axons to conduct action potentials across the lesion site in vivo, we measured pre- and postinjury CAP amplitudes for all treatment groups. Peak CAP amplitudes of ≥ 0.5 mV were easily detectable with hook electrodes.

For dye diffusion experimental and control groups ($n = 40$ rats, 80 nerves), we recorded CAPs in vivo (Fig. 5.2) from both sciatic nerves and immediately assessed these nerves for morphological continuity by observing intraaxonal dye diffusion in vitro (Fig. 5.2). As previously described, sham-operated animals received no neural injury and only one CAP measurement was taken during each sham operation. Sham-operated CAP data are shown as identical pre- and postoperative means. Prior to any cut or crush injury, in vivo CAP amplitudes of these sciatic nerves ranged from 1 to 5 mV and the mean preoperative CAP across all treatment groups was 2.4 ± 0.09 mV. Preoperative CAP amplitudes were not significantly different between treatment groups. No postoperative CAP was detectable immediately following crush injury, cut injury, or treatment with distilled water following crush injury (Fig. 5.2). The mean postoperative CAP following PEG-fusion of crush-severed axons was 2.0 ± 0.22 mV. This average postoperative CAP was significantly ($p < 0.005$) reduced compared with the preoperative CAP amplitude for this PEG-fused group or the average preoperative CAP amplitude pooled for all experimental groups used to assess intraaxonal dye diffusion. The observation that the postoperative CAP is 72 or 89% of preoperative or control CAPs, respectively, indicates that the two halves of many crush-severed sciatic axons are joined by PEG application.

We also observed preoperative CAP amplitudes ranging from 1 to 6 mV whose average values were not significantly different between any two groups (Fig. 5.2) in recordings from animals ($n = 40$) that were subsequently tested for behavioral recovery at 24 h to 8 wk postoperatively. The mean preoperative CAP across all treatment groups was 3.2 ± 0.22 mV (cut, $n = 4$; crush, $n = 9$; distilled water crush, $n = 9$; PEG-crush, $n = 13$; sham, $n = 4$). CAPs from sham-operated animals were treated as described earlier. CAPs conducted across the lesion site were not detected immediately following cut or crush injuries in the absence of PEG application. Crush-severed nerves did not have a detectable CAP with or without subsequent treatment with distilled water. After a crush injury, all 32 PEG-treated nerves, except one, had successful PEG-fusion as measured by conduction of CAPs of ≥ 0.5 mV through the lesion site (Fig. 5.2).

The mean postoperative CAP after successful PEG-fusion of crush-severed sciatic nerves was 1.9 ± 0.23 mV (Fig. 5.2) and was significantly ($p < 0.001$) reduced compared with the preoperative CAP for this PEG-fused group (2.87 ± 0.29 mV) or the average preoperative CAP pooled for all experimental groups (3.27 ± 0.36 mV). The significant reduction in postoperative mean CAP amplitude for PEG-treated nerves indicates that not all crush-severed sciatic axons are immediately repaired by PEG application. The observation that the postoperative CAP amplitude is 57 or 50% of preoperative or control CAPs, respectively, again indicates that the two halves of many crush-severed sciatic axons are joined by our PEG-fusion technique, although the specificity of those connections is not tested by this measure.

Intra-axonal dye diffusion assessments of axonal continuity

For one set of experimental and control groups for which in vivo CAPs were measured (Fig. 5.2, black and red bars), we evaluated the morphological continuity of axons in the sciatic nerve in vitro by observing the intraaxonal diffusion of Texas Red, a hydrophilic fluorescent dye (Fig. 5.3). The lesion site was readily visible as a distinct gap in low-power fluorescence images. Small amounts of dye-labeled connective tissue elements at the cut edges and some extraaxonal autofluorescence were sometimes visible in distal nerve segments. In all sham (uninjured) nerve segments ($n = 31$, Fig. 5.3A), the dye was visible intra-axonally throughout the entire segment (Fig. 5.3B). Dye did not diffuse intraaxonally across the lesion site in any nerves following crush injury ($n = 21$, Fig. 5.3, A and C), cut injury ($n = 6$, Fig. 5.3, A and E), or crush injury with distilled water treatment ($n = 4$, Fig. 5.3 A; image not shown). In contrast, for 17 of 18 total nerves (94%) that were crushed and subsequently treated with PEG, dye diffused across the lesion site (Fig. 5.3, A and D). All these CAP and intra-axonal dye data are consistent with the interpretation that crush- or cut-severance completely disrupts physiological and morphological continuity between axonal segments proximal and distal to the lesion site and that PEG application usually rapidly restores physiological and morphological continuity to many crush-severed axons.

Foot fault asymmetry scores

FF asymmetry scores (averages \pm SE) were obtained twice for each animal prior to any operative procedures and at postoperative times of 24, 48, and 72 h and weekly for

8 wk. We observed no significant differences in baseline scores between any experimental groups. Sham-operated animals did not show any obvious behavioral deficit as measured by FF asymmetry score at any postoperative time, indicating that muscle injury during surgery did not produce detectable impairment in hindlimb motor behaviors (Fig. 5.4). Animals with cut sciatic nerves exhibited a mean FF asymmetry score of -72 ± 6.5 at 24 h following surgery and did not improve over the course of the study. The FF asymmetry scores did not differ significantly ($p > 0.05$) for animals with crush-severed sciatic nerves that received no further treatment ($n = 9$) compared with that of animals that subsequently received distilled water as a vehicle control ($n = 9$; data not shown). Thus FF asymmetry scores were pooled from crush and crush nerves treated with distilled water ($n = 18$).

PEG-crush animals performed better than crush animals when measured at 24 h after surgery and this difference persisted until postoperative week 4. One-way ANOVA showed significant differences in behavior function (as measured by FF) across all groups [$F(3,24) = 29.4$, $p < 0.001$], with post hoc assessments demonstrating that PEG-crush animals performed significantly ($p < 0.05$) better between 24 h and 3 wk postoperation compared with crush group animals. At 4–8 wk after surgery, PEG-crush and crush group animals did not differ significantly in their behavior; i.e., recovery was so complete that the behaviors of intact PEG-fused and sham-operated animals were indistinguishable ($p > 0.05$). Crush and PEG-crush animals showed improved hindlimb motor behavior relative to cut animals at 24 h following surgery ($p < 0.05$). At 48 and 72 h postoperation, cut group animals performed similarly to crush group animals (Fig. 5.4). Crush group

animals continued to significantly improve relative to cut group animals from 72 h through 8 wk postoperation ($p < 0.01$). Sham-operated animals performed significantly better from 24 h through 3 wk postoperation compared with cut, crush, and PEG-crush group animals ($p < 0.01$).

We also compared the time course of recovery of FF asymmetry scores for different groups (lines connecting data points in Fig. 5.4) by regression analysis. The rate of recovery of crush and PEG-crush animals was significantly [$t(18) = 3.64$, $P < 0.001$; $F(13) = 3.69$, $p < 0.01$] faster compared with cut group animals, which did not show any improvement for 8 wk postoperation. The time course of recovery for PEG-crush animals was also significantly improved compared with untreated crush animals [$t(27) = 2.13$, $p < 0.05$; Fig. 5.4].

Video recordings of representative animals from each of the experimental groups and three control groups at 3 postoperative weeks showed that experimental animals with PEG-treated crush-severed sciatic nerves navigated an FF grid noticeably better (video SV5.1) than control animals with crush-severed sciatic nerves that were not PEG-treated (video SV5.2). In these videos, cut group animals occasionally refrained from using the injured limb for portions of the trial (video SV5.3) and missteps of the cut-injured limb were almost all exclusively full faults. Sham-operated animals did not show any deficit throughout the FF test in video SV4 and other video recordings. In videos of open field trials, behavioral recovery of animals with PEG-treated crush-severed sciatic nerves (video SV5.6) was noticeably better than that of animals with crush-severed sciatic nerves that were not PEG-treated (video SV5.5).

Sciatic Functional Index

Mean SFI scores (\pm SE) were obtained three times for each animal prior to any operative procedures and at postoperative times of 24 h, 48 h, 72 h, 1 wk, and weekly thereafter for 8 wk (Fig. 5.5). Baseline preoperative scores did not differ significantly between any experimental or control groups. Sham-operated animals did not show any behavioral deficit at any postoperative time as measured by the SFI, indicating that muscle injury during surgery did not result in behavioral impairment (Fig. 5.5). Cut group animals exhibited a mean SFI score of -92 ± 0.95 and did not show any improvement in behavior for the duration of the study, as previously reported (de Medinaceli et al. 1982; Hare et al. 1992).

We observed no significant difference at any postoperative time between animals with crush-severed sciatic nerves that received no treatment ($n = 9$) compared with animals that received distilled water treatment ($n = 9$; data not shown). These results were consistent with results from electrophysiological measures (CAPs; Fig. 5.2), morphological measures (intraaxonal dye diffusion; Fig. 5.3), and FF asymmetry measures (Fig. 5.4). Therefore data from crush and distilled water crush group animals were pooled.

One-way ANOVA of SFI results showed differences between groups were significant [$F(3,40) = 18.78$, $p < 0.001$], with post hoc assessments demonstrating no significant difference in the time course of recovery between PEG-crush and crush group animals, although further inspection did show that PEG-crush animals performed

significantly [$t(27) = 2.12$, $p < 0.05$] better 3 wk postoperation compared with crush group animals. Over the 8-wk postoperative testing period, crush group animals showed significant improvement in behavior as measured by the SFI compared with cut group animals ($p < 0.05$). Additionally, sham-operated animals performed significantly better on the SFI test than did both crush group animals ($p < 0.01$) and PEG-crush animals ($p < 0.01$) throughout the study.

We compared the time course of recovery of SFI scores for the experimental and various control groups (lines connecting data points in Fig. 5.5) by regression analysis. No significant difference was found between the recovery of PEG-crush and crush group animals. Both crush and PEG-crush animals showed significant [$t(18) = 3.35$, $p \leq 0.01$; $t(13) = 3.69$, $p < 0.01$, respectively] improvement in behavior relative to animals with sciatic nerve cuts.

Discussion

Assessments of CAP amplitude (Fig. 5.2) and intraaxonal dye diffusion (Fig. 5.3) show that direct application of PEG to crush-severed sciatic nerves usually (97% of all attempts) rapidly restores physiological and morphological continuity to at least some axons in the sciatic nerve. In fact, continuity may be restored to many proximal and distal axonal halves (with unknown specificity) since CAP amplitudes of PEG-fused nerves on average are 50 to 89% of CAP amplitudes of intact-control or sham-operated nerves. FF asymmetry scores (Fig. 5.4) provide quantitative assessment of hindlimb motor behavior and show significantly faster recovery of functional behavior associated with direct

application of PEG to crush-severed sciatic nerves. This finding for FF asymmetry scores is consistent with our measures of physiological and morphological continuity.

Video observations of FF trials and of open field trials also show rapid behavioral improvement associated with direct application of PEG to crush-severed sciatic nerves. That is, all data are consistent with the interpretation that PEG rejoins proximal and distal axonal halves (PEG-fusion) with sufficient specificity to allow significantly faster improvement in hindlimb motor behaviors mediated by the sciatic nerve.

Direct PEG application to crush-severed axons produces significant reversal of behavioral deficits within 24–48 h and does not prevent further improvement in behaviors at later (3 to 8 weeks) postoperative times. The shorter-term behavioral recoveries at 24–48 h are likely produced by PEG-fused axons. Longer-term behavioral recoveries at 3 to 8 wk may well be produced by crush-severed sciatic axons that were not PEG-fused and then grew out at 1–2 mm/day to appropriately reinnervate denervated muscles.

One of the difficulties in assessing behavioral outcome and treatment success following neural injury is that animals readily adopt compensatory behavioral strategies that can mask their true deficits (Schallert et al. 2000, 2002, 2006). A modified FF test eliminates much of this problem (Hernandez and Schallert 1988). When injured rats walk on a grid surface, the impaired hindlimb frequently slips through the openings. In the absence of a platform underlying the grid surface, rats typically learn motor strategies that reduce the number of slips, which obscure adequate evaluation of the degree of deficit. Previous reports have indicated such compensation occurs, often involving a shift in the burden of weight support and locomotion to the uninjured limbs (Dellon and

Dellon 1991). Placing a solid platform just beneath the grid surface provides a “crutch” floor that the rats can use for support when their impaired hindlimb slips through the grid openings, allowing for a more sensitive detection of deficits (Schallert et al. 2002; Yang et al. 2006). Unoperated or sham-operated rats rarely use the underlying solid floor surface during exploration of the grid. In contrast, rats with sciatic nerve injuries frequently use the floor for support.

The SFI is a computational assessment of three variables that measure print length, intermediary toe spread (digits 2–4), and total toe spread (digits 1–5). Previous studies have shown that the most useful parameter for overall evaluation of sciatic function is total toe spread (Bain et al. 1989; Bervar 2000). This factor deviates the most from control values, making it highly sensitive to long-term deficits in fine distal control. Proximal muscles are innervated more quickly than distal muscles and SFI scores may be more heavily influenced by toe use and toe spread controlled by distal muscle groups compared with FF asymmetry scores. Thus the SFI might be expected to show significant behavioral improvement later than FF asymmetry scores and detect more chronic deficits, as we have reported.

Our data suggesting that PEG-fusion can more rapidly improve behavioral recovery following a crush injury to the sciatic nerve in the rat extend previous studies indicating that PEG induces both physiological (measured by the restored conduction of action potentials through the lesion site) and morphological continuity (intra-axonal diffusion of fluorescent dyes across the lesion site) between the cut or crushed ends of mammalian myelinated axons (Lore et al. 1999). Other recent studies assessing

behavioral recovery following PEG treatment of cut- or crush-severed axons have focused on injury models of CNS axons. Subcutaneous injections of PEG have been reported to partially restore the cutaneous trunci muscle reflex in guinea pigs following a crush injury to the midthoracic spinal cord (Borgens and Bohnert 2001). Rats receiving an intravenous injection of PEG following a spinal cord compression injury at T4 showed improved locomotor performance relative to saline-treated control groups as measured by the Basso–Beattie–Bresnahan open-field hindlimb motor scale (Ditor et al. 2007). A computer-managed open-field behavioral test has also been used in a recent study reporting improved exploratory behavior in animals receiving a subcutaneous injection of PEG following traumatic brain injury compared with untreated animals (Koob et al. 2008).

The PEG-fusion technique modified for *in vivo* use may have immediate clinical implications to improve the acute and chronic repair of PNS crush-severance injuries as measured by physiological, morphological, and behavioral assays described herein. For example, after nerve crush functional recovery is often poor if regenerating motor axons are too far from the denervated target tissue. Prolonged denervation of muscle leads to a deterioration of the intramuscular nerve sheaths, which are the normal target pathways for regenerating motor axons (Fu and Gordon 1995; Mackinnon et al. 1991). The loss of intramuscular nerve sheaths greatly reduces the number of motor axons that are able to reinnervate muscle fibers. In addition, muscle fibers do not fully recover from atrophy due to prolonged denervation (Fu and Gordon 1995). It is possible that the repair of at least some axons by PEG-fusion can have a trophic integrity-maintenance effect on target

muscles that might keep them more receptive to reinnervation for a longer time, which could promote a more optimal chronic outcome. That is, initial functional recovery mediated by PEG-fusion of some axons might later be increased by reinnervation of denervated muscle fibers by newly formed synapses made by other, non-PEG-fused regenerated axons that reach the muscle at 4–8 wk.

Finally, we have worked on solving two basic problems considering the clinical use of PEG to repair bundles of crush-severed PNS axons (e.g., sciatic or other peripheral nerves). First, severed distal stumps need be induced to survive until they can be PEG-fused. We can now consistently (80–100% success rate) induce severed mammalian CNS or PNS axons to survive for 3–10 days by cooling (Marzullo et al. 2001; Sea et al. 1995) or injections of cyclosporin A (Sunio and Bittner 1997) and such surviving axons can be PEG-fused (Lore et al. 1999; Marzullo et al. 2001; Stavisky et al. 2003, 2005). The ability to extend the time needed to use PEG-fusion techniques on crush-severed PNS axons is important because such injuries usually occur in a nonclinical setting and medical treatment may be delayed for hours to days. Second, crush-severed axons that are PEG-fused in mammals *in vivo* have poor mechanical strength at the lesion site (Fig. 5.1E) and may pull apart after animals recover from anesthesia, thereby preventing chronic recovery (Bittner and Fishman 2000; Lore et al. 1999). Crush-severed axons PEG-fused in invertebrates *in vivo* show both acute and chronic repair of severed axons if the animal is immobilized by cooling for 24–48 h or if a PEG hydrogel is applied to add mechanical strength to the ECM at the lesion site (Lore et al. 1999). Unfortunately, this hydrogel by itself has acute cytotoxic effects in mammalian neurons and behavior-

impairing effects (unpublished observations). Other tissue adherents (e.g., fibrin glues or biogels) applied to the ECM at the site of PEG-fusion might provide additional mechanical strength in vivo (Fig. 5.1F). Alternatively, techniques to immobilize the joints crossed by the affected axons might enhance the PEG-fusion technique. If successful, such techniques would also be immediately applicable for clinical use, although a concern might be that this procedure could be detrimental because optimal behavioral outcome may require adequate motor experience (Bittner et al. 2000; Kleim et al. 2003). However, intense motor rehabilitation targeting movements impaired by the injury could be combined with PEG and other axon-mending or degeneration-preventing interventions to improve restoration of function.

Treatment Group	Number of Rats, CAP Confirmation Assays
<i>A. Dye diffusion groups</i>	
PEG-crush	9, 18
Crush	11, 21
Distilled water crush	2, 4
Cut	3, 6
Sham-operated	15, 31
	Total = 40 rats, 80 CAP confirmation assays
<i>B. Behavioral groups</i>	
PEG-crush	14, 13
Crush	9, 9
Distilled water crush	9, 9
Cut	4, 4
Sham-operated	4, 4
	Total = 40 rats, 39 CAP confirmation assays

Table 5.1: Number of rats and nerves assayed for CAP confirmation of axonal continuity for each experimental and control treatment group followed by dye diffusion or behavioral assessment. For sham-operated and PEG-crush groups, CAP confirmation was the conduction of CAPs through the lesion site. For crush, distilled water crush, and cut groups, CAP confirmation was the absence of CAPs conducted through the lesion site. Dye diffusion data were collected more quickly than behavioral data and both sciatic nerves could be used. Thus more rats were assayed for CAPs and dye diffusion than for CAPs and behavior. Experimental groups (PEG-crush) and control groups (sham-operated, crush) were analyzed in several subgroups to ensure that CAPs did not vary over time due to changes in surgical or assay conditions. That is, there was no significant difference in CAP amplitude between the first and last subgroups of animals tested. Fewer measurements were needed in the cut or distilled water control groups than originally expected to obtain statistically significant differences because there was no variation in CAP amplitude for any control group with cut or crush injuries (CAPs were never detected, i.e., were 0 mV). The smaller number of rats in cut and distilled water crush treatment groups conducted later in this study reflects this observation. CAP confirmation for PEG-crush animals required the conduction of CAPs through the lesion site and 31 PEG-fused sciatic nerves met this criterion. One PEG-crush sciatic nerve in the behavioral PEG-crush treatment group did not meet this criterion and that animal was removed from the study. That is, PEG-fusion was successful in 31 (97%) of 32 attempts.

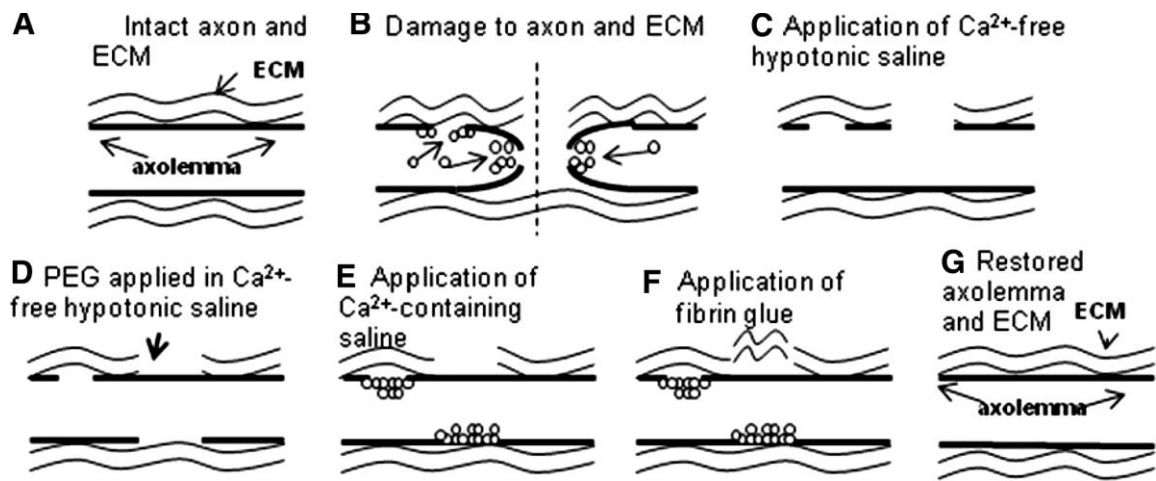


Figure 5.1: Mechanisms of axonal repair by polyethylene glycol (PEG) and increasing strength of extracellular matrix (ECM) by fibrin glue.

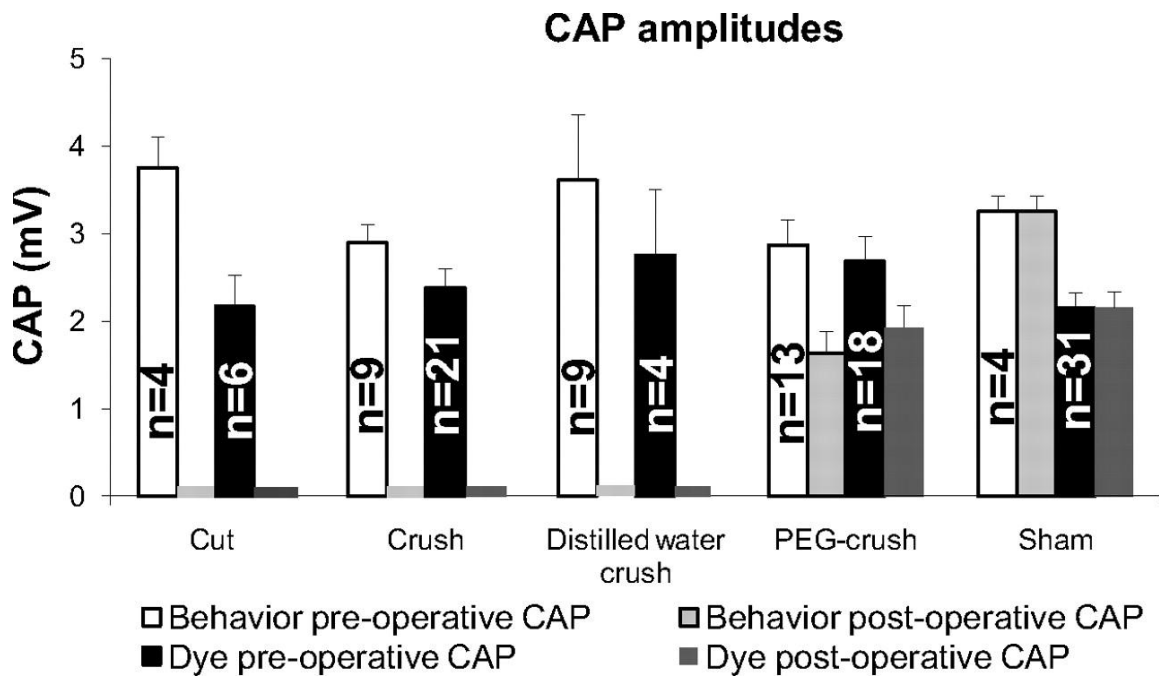


Figure 5.2: Compound action potential (CAP) amplitudes of rat sciatic nerves recorded preoperatively (white and black bars) and postoperatively (blue and red bars) for each group (cut, crush, distilled water-crush, PEG-crush, and sham) used in dye diffusion (black and red bars) or behavioral (white and blue bars) assays. Colored bars on the x-axis indicate a CAP amplitude of 0 mV for all animals. All CAP and other data in this and other figures (except Fig. 3) are plotted as means \pm SE.

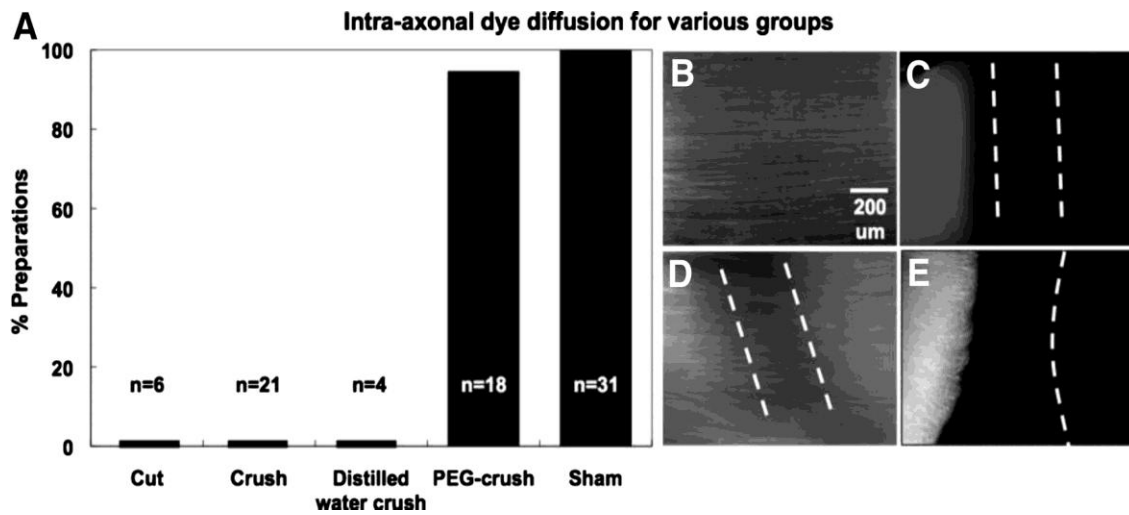


Figure 5.3: Graph showing percentage of sciatic nerve preparations exhibiting intra-axonal dye diffusion across a lesion site following cut, crush, distilled water crush, PEG-crush, or sham operations (A). Fluorescence images showing intra-axonal dye diffusion across a lesion site following (B) sham, (C) crush, (D) PEG-crush, and (E) cut operations in sciatic nerves. In C and D, dotted lines are drawn to show the location and extent of the lesion. In E, the dotted line indicates the edge of the distal segment (not visible because it contained no dye). In each image the proximal portion of sciatic nerve is on the left and the distal portion of sciatic nerve is on the right. Scale bar: 200 μm for B–E.

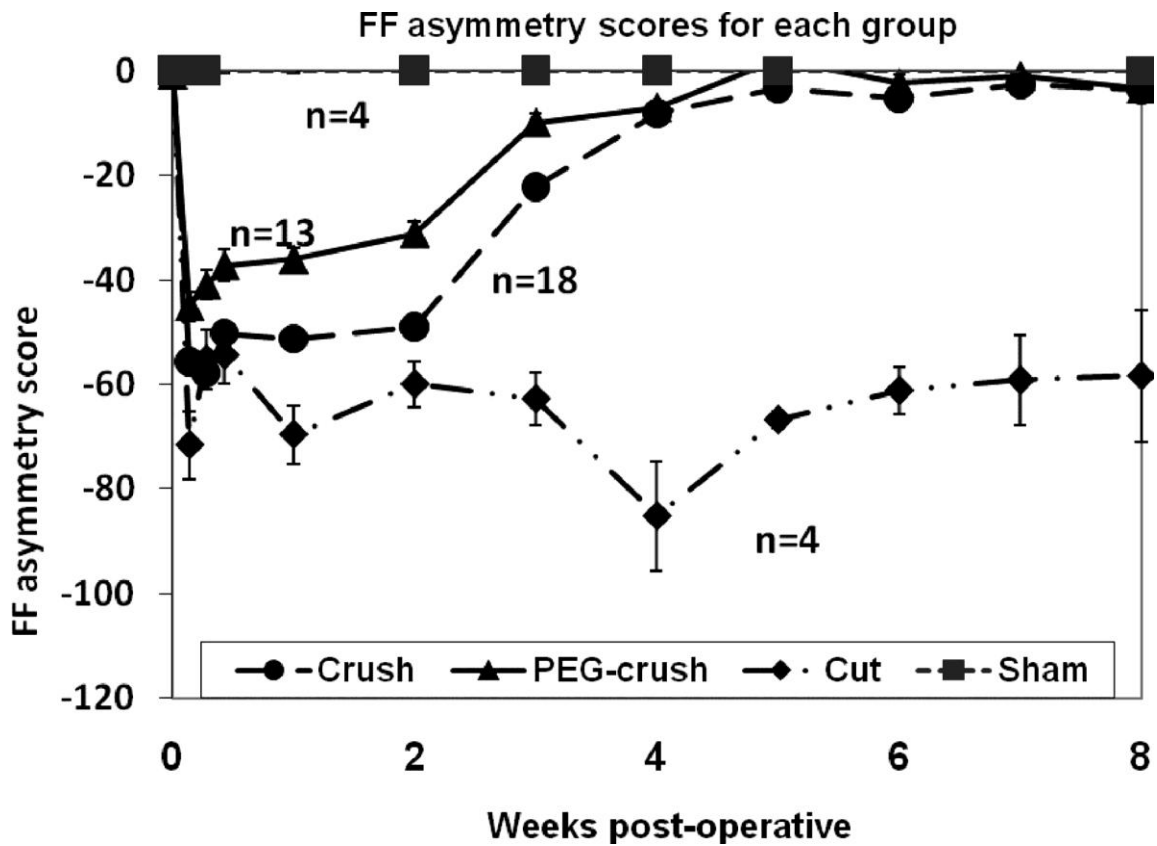


Figure 5.4: Mean foot fault (FF) asymmetry scores from 0 to 8 postoperative weeks for cut (solid line, diamonds), crush (dashed line, circles), PEG-crush (solid line, triangles), or sham-operated (dotted line, squares) groups. Baseline scores were obtained twice for each animal prior to surgery and are plotted at the 0 wk time point. SE values are so close to the plotted mean values at some time points that the error bars are within the space occupied by the symbol showing the mean value.

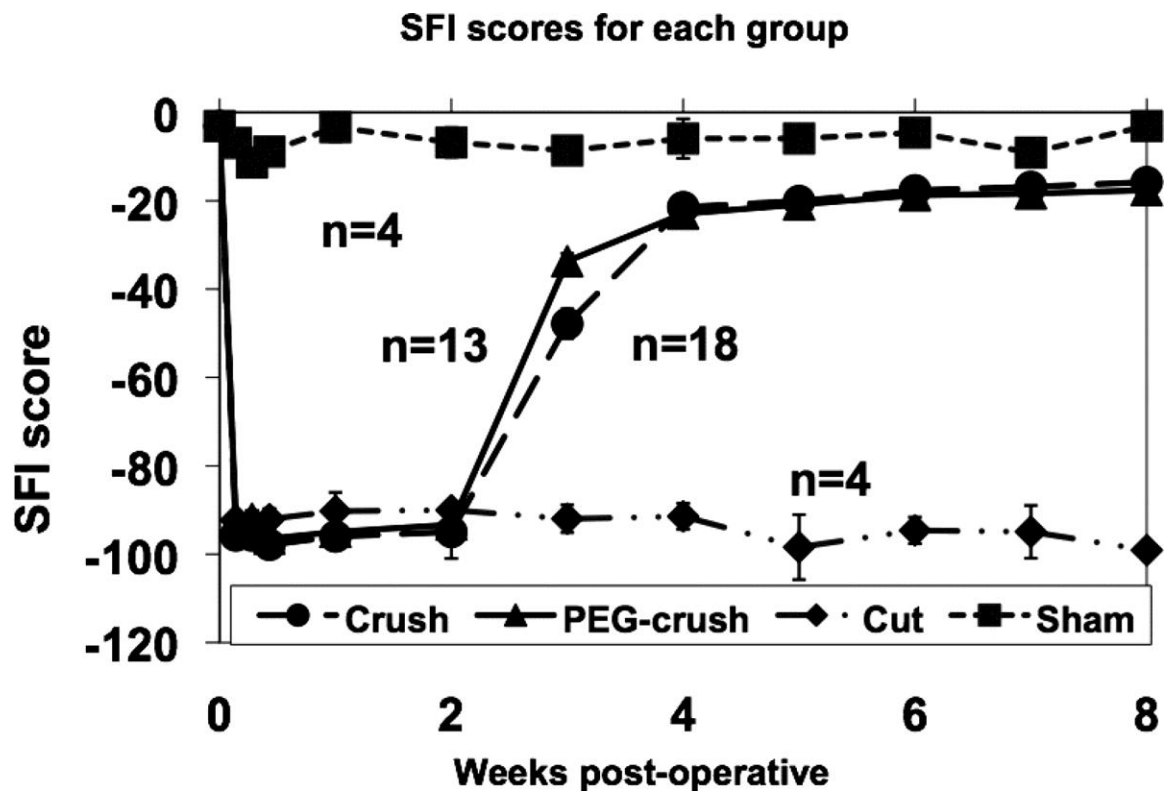


Figure 5.5: Sciatic Functional Index (SFI) results from 0–8 postoperative wk for cut (solid line, diamonds), crush (dashed line, circles), PEG-crush (solid line, triangles), or sham-operated (dotted line, squares) groups. Baseline scores were obtained 3 times for each animal prior to surgery and plotted at the 0 wk time point.

Chapter 6: Polyethylene glycol repair of severed axons: behavioral recovery and in vitro mechanisms

Abstract:

The fusogenic compound polyethylene glycol (PEG) rapidly reconnects severed axons; however behavioral recovery following PEG treatment is modest. To improve behavioral recovery, we applied the antioxidants melatonin (MEL) or methylene blue (MB) to crush-severed sciatic nerves prior to PEG treatment. Treatment with PEG and these antioxidants, especially MB, produced significantly greater behavioral recovery and axonal conduction compared to treatment with PEG alone. Additionally PEG rapidly sealed transected axonal-like neurites of B104 cells in the absence of calcium or in the presence of various substances that inhibit or enhance plasmalemmal sealing, suggesting that PEG has beneficial effects beyond reconnecting axons. These and other data suggest that PEG together with certain antioxidants may have a clinical use to rapidly produce behavioral recovery of crush-severed nerves.

Introduction

Behavioral recovery following axonal severance in mammals is often slow and poor because surviving proximal outgrowths regenerate at 1-2 mm/day and many distal target tissues are partially or non-specifically innervated (Ramon y Cajal, 1928; Das and Wallace, 1986; Ingoglia and Murray, 2001; Bozkurt et al, 2008). The membrane-fusogenic compound polyethylene glycol (PEG) rapidly (within minutes) reconnects the

proximal and distal axonal halves of mammalian sciatic and spinal axons (Lore, et al., 1999). Such PEG-fusions have rapidly restored axonal morphological and physiological continuity, but have only shown modest (but significant) improvements in behavioral recovery (Britt et al., 2010).

Ca^{2+} -dependent plasmalemmal sealing almost certainly influences PEG fusion, since unsealed axons (in Ca^{2+} -free saline) are easier to PEG-fuse than sealed axons (in Ca^{2+} -containing saline) (Lore, et al., 1999). However, bathing the nerve in Ca^{2+} -free saline may not eliminate all interstitial Ca^{2+} , and some sealing may still occur, decreasing the probability of PEG-fusion. We recently reported (Spaeth, et al., 2010) that various substances can decrease plasmalemmal sealing, such as the antioxidant melatonin (Mel), which decreases plasmalemmal sealing of B104 cells (Spaeth et al., 2010), enhances PEG-fusion in sciatic nerves *in vitro* (Stavisky et al., 2005), and exhibits neuroprotective properties (Chen, et al., 2009). Other antioxidants, such as methylene blue (MB), exhibit neuroprotective properties and improve behavioral recovery, such as after striatal lesions (Rojas et al., 2009). Thus, co-application of substances that decrease plasmalemmal sealing and are neuroprotective may increase PEG fusion-induced behavioral recovery.

Results

For both morphological and behavioral experiments, crush-severance injuries were made using Dumont #5 forceps, while cut-severance injuries were made using dissection scissors. Exposed sciatic nerves were continuously bathed with Ca^{2+} -free saline prior to any injury and treatment given. The epineural sheaths of crush-injured nerves were

nicked with microscissors to allow direct exposure of axonal tissues to MEL, MB, and PEG solutions. All of these treatment compounds were applied locally to the injury site of anesthetized animals using a syringe fitted with a pulled glass micropipette.

To assess axonal morphological continuity for crush-severed sciatic nerves treated with Mel+PEG, MB+PEG, Mel, or MB, we excised 3-4 cm lengths of sciatic nerves and placed the proximal end in a water-tight Vaseline well containing Ca^{2+} -free saline and 20 μL of Texas Red. We observed the intra-axonal diffusion of Texas Red, a hydrophilic fluorescent dye (Fig. 6.1), from the proximal to distal end of the nerve segment following overnight incubation at 4°C . Dye diffused across all sham nerve segments (Fig. 6.1E). Similarly, dye diffused across the lesion site in crush-injured nerves incubated overnight in Ca^{2+} -free hypotonic saline (Fig. 6.1F), crush-injured nerves treated with MB+PEG (Fig. 6.1G), crush-injured nerves treated with MEL+PEG and crush-injured nerves treated with PEG alone (as previously reported in Britt et al., 2010). In contrast, dye did not diffuse across the lesion site for crush-injured nerves incubated overnight in Ca^{2+} -containing saline (Fig. 6.1H), crush-injured nerves treated with MB, or cut-injured nerves. These intra-axonal dye diffusion data are consistent with the interpretation that crush- or cut-severance completely disrupts continuity between axonal segments proximal and distal to the lesion site, and that PEG application rapidly restores morphological continuity to many crush-severed axons. Additionally, these data suggest that MEL and MB do not interfere with the ability of PEG to rapidly restore axonal continuity following crush injury.

To assess physiological continuity for crush-severed sciatic nerves treated with Mel+PEG, MB+PEG, Mel, or MB *in vivo*, hook electrodes were placed above or below sciatic nerve segments to externally measure the ability to conduct compound action potentials (CAPs) across a lesion site (Lore et al., 1999; Stavisky et al., 2005; Britt et al., 2010). Prior to any injury, CAP amplitudes ranged from 1-5 mV, and the mean pre-operative CAP across all treatment groups was 3.7 ± 0.11 mV (Fig. 6.2A). Post-operative CAPs were only observed in animals treated with PEG. The mean post-operative CAP for crush+MB+PEG was 3.4 ± 0.22 mV, while the mean post-operative CAP for crush+MEL+PEG was 2.0 ± 0.22 mV. CAPs conducted across the lesion site were not detected immediately following cut or crush injuries in the absence of PEG application or in cut+PEG controls.

As one measure of behavioral recovery for animals with crush-severed sciatic nerves treated with Mel+PEG, MB+PEG, Mel, or MB, we used the Sciatic functional index (SFI). SFI is a composite score computed from various footprint measurements and is frequently used to measure return of distal function in rat models of sciatic nerve severance (de Medinaceli et al., 1982). Mean SFI scores \pm SEM were obtained three times for each animal prior to any operative procedures and at post-operative times of 24 hours, 48 hours, 72 hours, one week and weekly thereafter for six weeks (Fig. 6.2B).

One way ANOVA of SFI scores with post-hoc assessments demonstrated that crush+MB+PEG animals behaved significantly ($F [3,36] = 15.33, p < 0.001$) better compared to all other groups except sham group animals from 72 hours post-operation until 3 weeks post-operation. Additionally, crush+MB+PEG and crush+Mel+PEG

animals demonstrate improved SFI performance during post-operative weeks 4-6 compared to all other groups, including crush+PEG. This improved recovery was not different from sham animals (Fig. 6.2B).

A modified foot fault (FF) test was also used to assess behavioral function for animals with crush-severed sciatic nerves treated with Mel+PEG, MB+PEG, Mel, or MB. During FF testing, the animal freely roams on an elevated wire grid (45cm x 30cm, with 2.5cm x 2.5cm openings) 1.5cm above a solid floor. A foot fault was scored when a misstep resulted in the hindlimb falling through an opening in the grid. If the hindlimb misstepped, but was pulled back before touching the floor beneath the grid, the movement was scored as a partial fault and given a fault score of one. A full fault occurred when the animal's hindlimb touched the floor beneath the grid for support. Full faults were given a fault score of two. A composite foot fault asymmetry score was then calculated as previously reported (Britt et al., 2010). FF asymmetry scores were obtained twice for each animal prior to any operative procedures and at post-operative times of 24, 48, and 72 hours, and weekly for six weeks. We observed no significant differences in baseline scores between any experimental groups. We have previously shown sham-operated animals did not exhibit any obvious behavioral deficit as measured by FF asymmetry score at any post-operative time (Britt et al., 2010; Fig. 6.2C).

One way ANOVA of FF scores with post-hoc assessments demonstrated that crush+MB+PEG animals performed significantly ($F [3,36] = 20.9, p < 0.001$) better relative to all other experimental groups from 24 hours through three weeks post-operation. At four to six weeks after surgery, crush+Mel+PEG and crush+MB+PEG

animals did not differ significantly in their FF score compared to injured, (i.e sham) animals ($p>0.05$) (Fig. 6.2 C). Additionally, crush+MB+PEG animals demonstrate functional improvement through week three compared to both crush+MB and crush animals ($p<0.05$). However, by week four, these three experimental groups do not differ significantly in their behavior ($p>0.05$).

Since some of the PEG-induced behavioral recovery could be a result of PEG-induced sealing of damage plasmalemma (instead of PEG-fusion of axonal halves), we next investigated how PEG affects plasmalemmal sealing. Plasmalemmal repair (sealing) was evaluated using dye exclusion in rat sciatic nerves (Britt, et al, 2010) or B104 cells (Spaeth, et al., 2010). Sciatic nerves were removed from the rat, treated with 10 mM PEG, and placed in Ca^{2+} -free or Ca^{2+} -containing (1mM) saline containing Texas red dextran (3kDa). Neurites of individually identified rat hippocampal B104 cells were typically transected for 9 min in a Petri dish containing Ca^{2+} -free saline using a sharpened glass micro-capillary tube fastened to a micromanipulator. After neurite transection, various [PEG] were added to the Petri dish for 1 min, and washed out with Ca^{2+} -free saline, to mimic PEG application *in vivo*. Extracellular dye (Texas Red dextran, 3 kDa) was added to assess dye exclusion. We interpret cells (or sciatic nerves) that excluded dye as having formed a dye barrier seal (sealed), which is a precursor to the eventual repair of the plasmalemmal damage. Cells that took up dye have not formed a dye barrier (not sealed). “Sealing frequency” is the percent of a set of individually-transected and uniquely identified B104 cells that exclude Texas Red dextran.

Sciatic nerves segments removed from rats and placed in Ca^{2+} -containing saline excluded dye (sealed) (Fig. 6.3A), whereas sciatic nerve segments placed in Ca^{2+} -free saline did not seal (Fig. 6.3B). Sciatic nerve segments removed from the rat, treated with PEG at their cut ends, and placed in Ca^{2+} -free saline always sealed (Fig. 6.3C). Thus, in the absence of a distal half, PEG seals proximal axons, even in Ca^{2+} free saline. Since PEG seals plasmalemmal damage in sciatic axons, we modified our previously described sealing protocol in B104 cells (Spaeth, et al., 2010) to examine the extent and mechanism of PEG-sealing.

Various PEG concentrations ([PEG]) are reported to increase behavioral recovery in mammals (Ballinger, et al., 1999; Lore, et al., 1999; Borgens and Bohnert, 2001; Borgens, et al., 2002; Donaldson, et al., 2002) and plasmalemmal repair (Nehrt, et al., 2010). Thus, we investigated how different [PEG] affect plasmalemmal sealing. After transecting neurites of a population of B104 cells, various [PEG] were added to the Petri dish. Cells were subsequently maintained in Ca^{2+} -free saline containing Texas Red dextran, and sealing assessed. Low [PEG] (below 800 μM) did not affect sealing, similar to no PEG treatment (control sealing) (Fig. 6.3A). [PEG] between 1 mM and 50 mM significantly ($p < 0.001$) increased sealing compared to control sealing, and 10 mM and 50 mM [PEG] sealed nearly all transected cells, and nearby, uninjured cells did not fill with dye (Fig. 6.3A). Very high [PEG] (100 mM, 250 mM, 500 mM) caused cells to fill with dye, even those not transected, suggesting that too much PEG leads to plasmalemmal damage (Fig. 6.3A). Similar results were observed if cells were maintained in Ca^{2+} -containing saline after transection (Fig. 6.3B). These data suggest that 10 mM and 50

mM PEG produced the maximal effect of PEG on sealing without producing plasmalemmal damage, and that PEG-sealing at these concentrations does not require Ca^{2+} . However, PEG cannot substitute for Ca^{2+} , since sealing declined 20 min after PEG addition for damaged cells never exposed to Ca^{2+} (Fig. 6.3 F). We also transected cells in Ca^{2+} -containing sealing and added dye immediately after transection, or after PEG washout. Transected cells treated with 10 mM PEG sealed at a significantly ($p < 0.01$) higher frequency compared to cells not treated with PEG (Fig. 6.3 G). Considering all of our data, PEG increases sealing (i.e. membrane fusion) in B104 cells in Ca^{2+} -free and Ca^{2+} -containing salines.

We next investigated the stability of PEG-induced sealing by observing whether PEG-sealing was maintained for up to 60 min in Ca^{2+} -containing saline following PEG treatment. Sealing was evaluated as the time post- Ca^{2+} addition (PC time). Transected cells treated with 10 mM PEG and maintained in Ca^{2+} -containing saline sealed at a significantly greater frequency before 20 min PC ($p < 0.001$) compared to control sealing (i.e. cells not treated with PEG and maintained in Ca^{2+} -containing saline, dotted or dashed lines) (Fig. 6.4 A,B). At 60 min PC, nearly all cells treated with 10 mM PEG sealed, similar to control sealing. These data suggest that 10 mM PEG treatment did not harm B104 cells bathed in Ca^{2+} for 60 min after PEG application.

We previously reported that 2 mM Melatonin (Mel) significantly decreases the sealing frequency of B104 cells at 5 min PC (Spaeth, et al., 2010). At additional PC times, 2 mM Mel (open squares) also significantly decreased sealing compared to control (dotted/dashed lines, no data points shown) (Fig. 6.4 A,B). Similar results were observed

for cells transected nearer to, or farther from, the soma in MB (open triangles) (Fig. 6.4 A,B). These data suggest that anti-oxidants decrease Ca^{2+} -dependent sealing.

PKA, Epac, membrane fusion proteins, such as SNAP-25, synaptobrevin, syntaxin, NSF, Golgi-vesicular traffic, and cytosolic oxidation strongly influence plasmalemmal sealing (Krause, et al., 1994; Steinhardt, et al., 1994; Bi, et al., 1995; Detrait, et al, 2000a,b; Yoo, et al., 2003; Cai, et al., 2009a,b; Spaeth, et al., 2010). We investigated whether the PEG-dependent increase in sealing utilizes any previously discovered proteins or pathways whose inhibition or cleavage decreases sealing.

At 0 PC, cells transected in substances that inhibit sealing, followed by 10 mM PEG application and maintained in Ca^{2+} free saline, did not seal at significantly ($p > 0.05$, CMH χ^2) different frequency compared to cells transected in only Ca^{2+} -free saline (i.e. no test substance added) and treated with 10 mM PEG (Fig. 6.4 C,D). Similar results were observed if cells were maintained in Ca^{2+} -containing saline after PEG treatment (Fig. 6.4 E,F). These data suggest that PEG-sealing (and thus PEG-fusion) does not require PKA, Epac, membrane fusion proteins, Golgi-vesicular traffic, or cytosolic oxidation.

Discussion

Both SFI and FF tests show that MB+PEG-treated animals exhibit improved behavior much more rapidly than other treatment groups (Fig. 6.2; as early as 72 hours post-operation for SFI scores, as early as 24 hours post-operation for FF scores), as well as behavioral function that eventually improves to uninjured (sham) levels (Fig. 6.2; week 4 post-operation in both SFI and FF tests). Such early and lasting return of function

to more distal target tissues (such as those involved with aspects of plantar stepping assessed by SFI) - as well as the restoration of physiological and morphological continuity - suggest that coapplication of MB and PEG (or Mel and PEG) is a more effective treatment following axon severance than PEG alone.

Application of MB or Mel may increase behavioral recovery of PEG-fused nerves in two ways. First by preventing sealing of damaged axons even more than Ca^{2+} -free saline, MB or Mel may allow a greater number of axons to fuse. This hypothesis is consistent with the observed increase in PEG-fusion CAPs for nerves treated with MB (Fig 6.2) or Mel (Stavisky, et al., 2005). Second, as neuroprotective anti-oxidants, MB or Mel may increase survival of all damaged axons, including PEG-fused axons. PEG may provide additional protection for those axons not PEG fused by quickly sealing the plasmalemmal damage site. Since sealing is often neuroprotective (Yoo, et al., 2004), PEG-sealed proximal axons may have a higher likelihood of survival, and increased probability of regeneration, thereby accounting for some of the behavioral recovery following PEG treatment. Furthermore, PEG-dependent membrane fusion (and sealing) is unaffected by substances that decrease or increase sealing, whether or not Ca^{2+} is present (Fig 6.4). These data suggest that behavioral recovery from axonal severance can be improved using a combination of antioxidants and PEG-based solutions.

Chapter 6: Figures

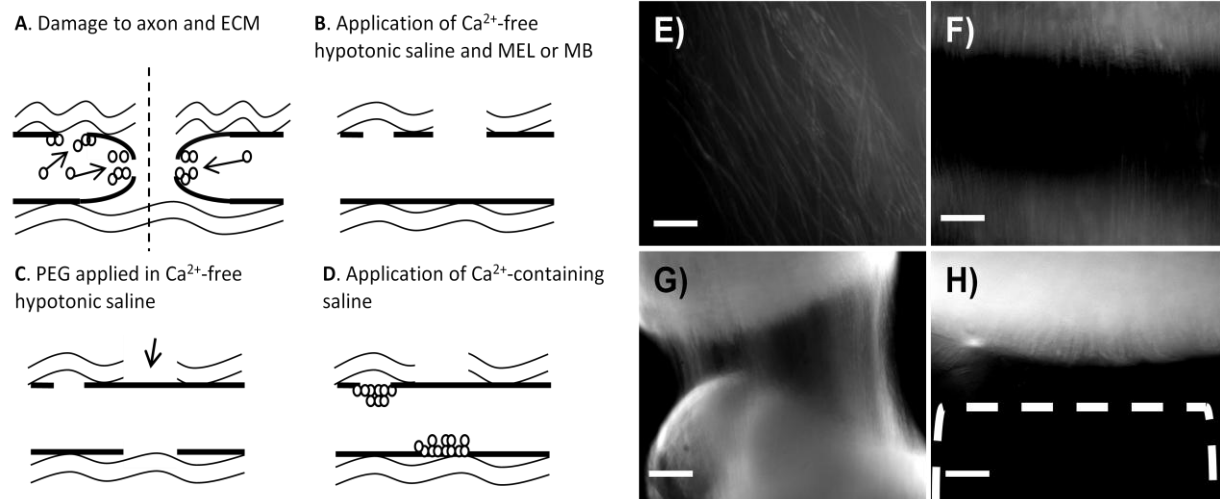


Figure 6.1: Mechanisms of axonal repair by PEG and fluorescence images of control and experimental groups. A-D illustrate mechanisms of our PEG-fusion technique, as well as application of compounds such as MEL or MB (B). E-H) Intra-axonal dye diffusion across a lesion site following E) sham-operated sciatic nerves in Ca^{2+} -containing and F-H) crush-severed in Ca^{2+} -free hypotonic saline. F) Crush-severed in Ca^{2+} -free hypotonic saline. G) Crush+MB+PEG and H) Crush in Ca^{2+} -containing saline operations in sciatic nerves. In H), a dotted line is drawn to show the location of the distal portion of the nerve segment (not visible because it contained no dye). In each image the proximal portion of sciatic nerve is located above the distal portion of sciatic nerve in the photograph. Scale bar: 50 μm for A-D.

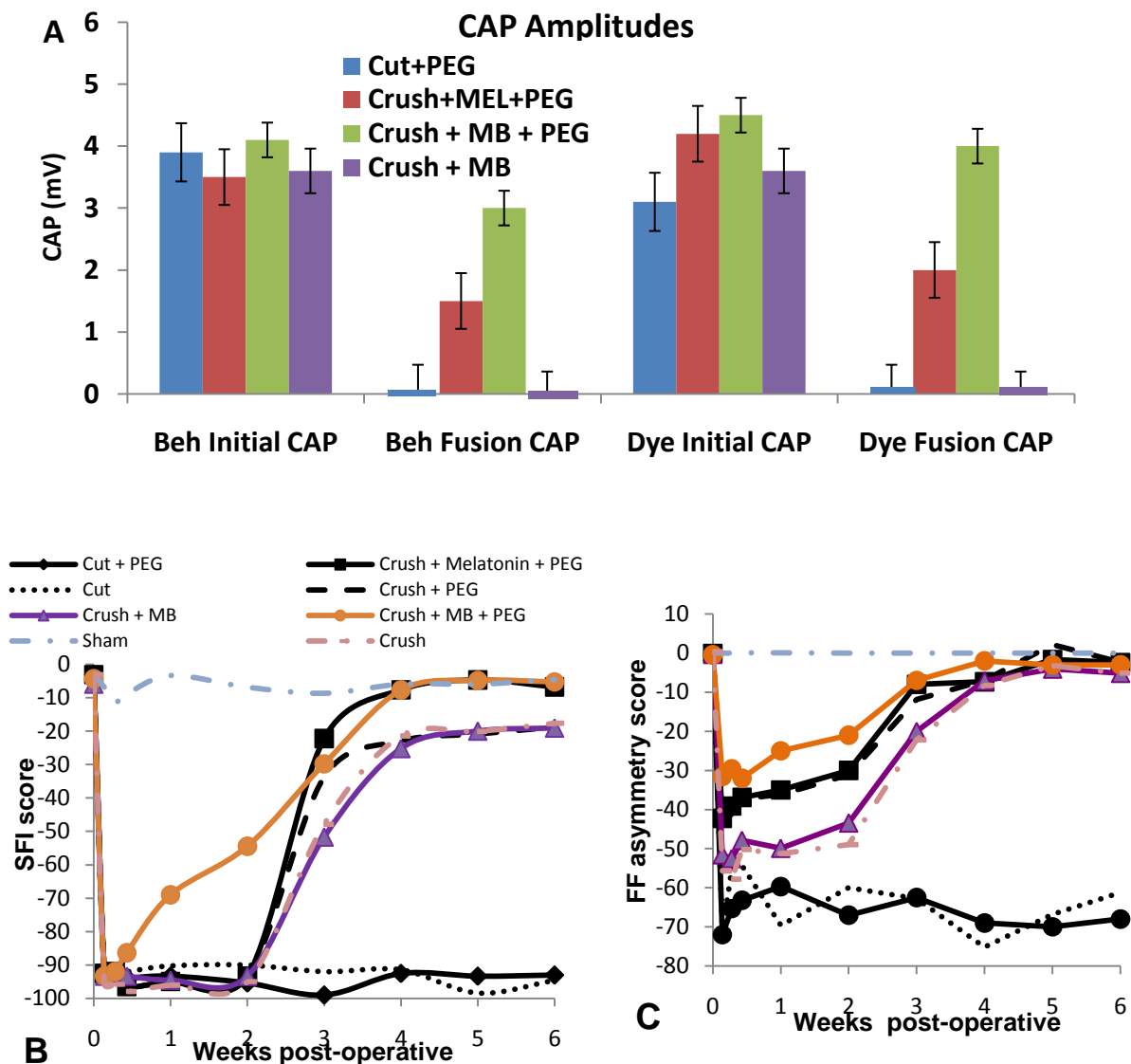


Figure 6.2: CAP amplitudes, SFI scores, and FF asymmetry scores for each group. A) CAP amplitudes of rat sciatic nerves recorded pre-operatively and post-operatively for each group (cut+PEG, crush+Mel+PEG, crush+MB+PEG, crush+MB) used in dye diffusion or behavioral assays. Colored bars on the X-axis indicate a CAP amplitude of 0mV for all animals. CAP data are plotted as means \pm SEM. B) SFI results from 0 – 6 post-operative weeks for all experimental and control treatment groups. Baseline scores were obtained three times for each animal prior to surgery and plotted at the 0 week time point. C) Mean foot fault asymmetry scores from 0 – 6 post-operative weeks for all experimental and control treatment groups. Baseline scores were obtained twice for each animal prior to surgery and are plotted at the 0 week time point. SEM values are so close to the plotted mean values at some time points that the error bars are within the space occupied by the symbol showing the mean value.

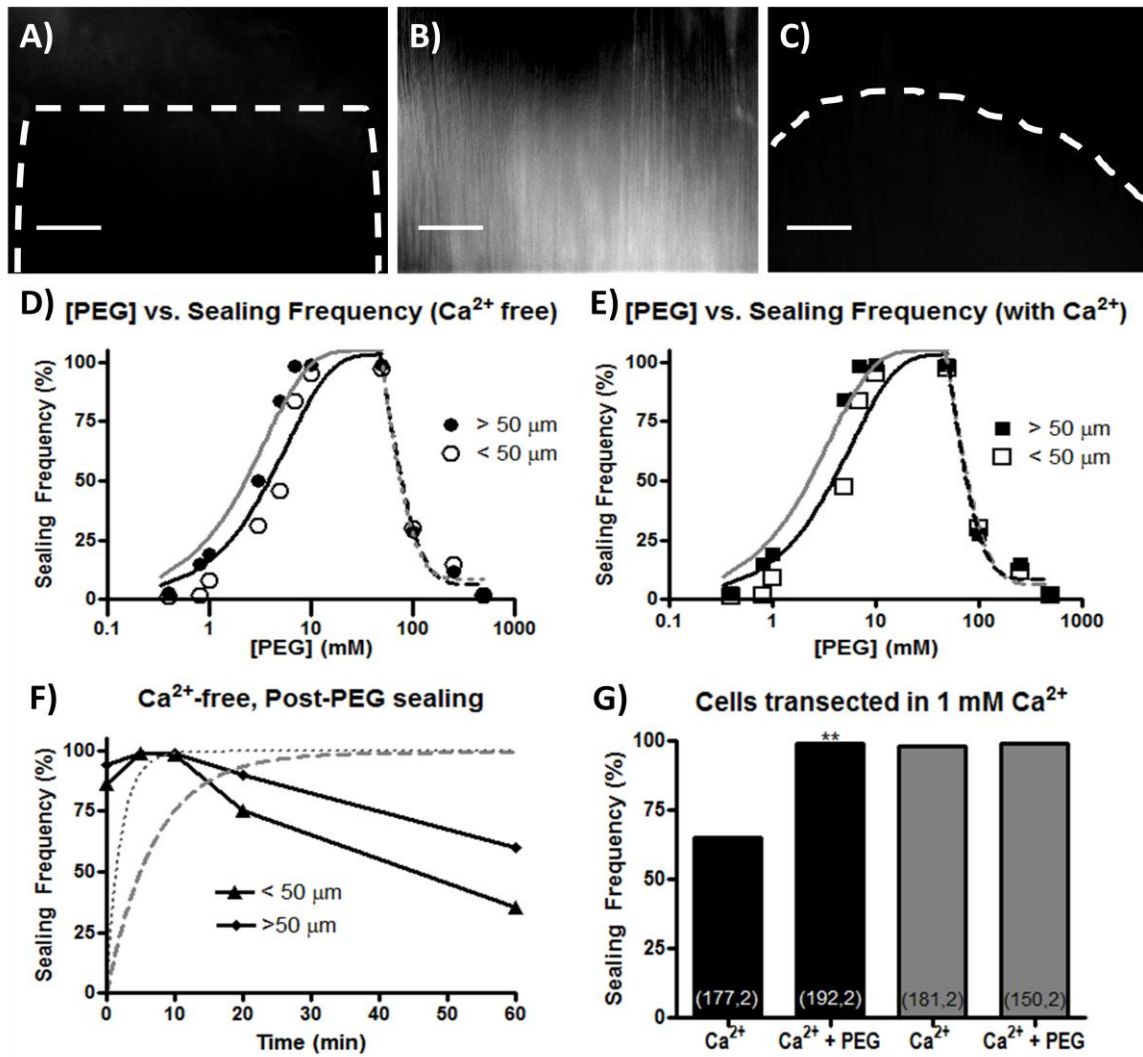


Figure 6.3: A-C: Images of sciatic nerves removed from rats and placed in Ca^{2+} -containing saline (A), Ca^{2+} free saline (B), or treated with PEG at both ends and placed in Ca^{2+} free saline (C). Texas Red dextran was added to the saline for all nerves. D,E: Cells transected in Ca^{2+} -free saline for 9 min, treated with various [PEG] for 1 min, dye added immediately after PEG washout, and maintained in Ca^{2+} free saline (D) or Ca^{2+} -containing saline. F,G: Cells transected Ca^{2+} -free saline nearer to (F) or farther from (G) the soma in 2 mM Mel (open squares) or 100 μM MB (open circles), or treated with 10 mM PEG immediately after transection (open triangles). Cells were maintained in Ca^{2+} -containing saline, and dye added at various post- Ca^{2+} (PC) times.

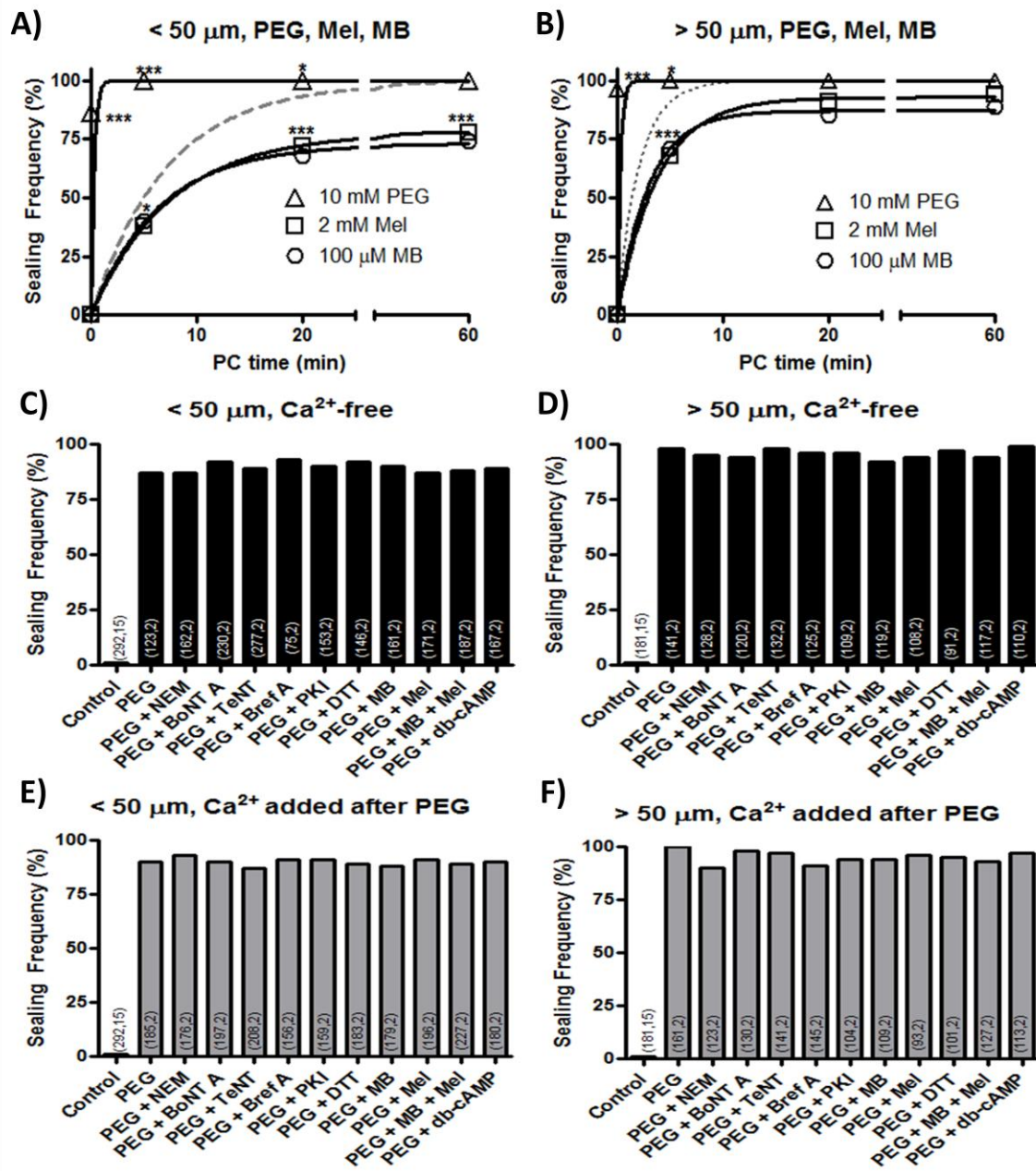


Figure 6.4: A,B: Cells transected in Ca^{2+} -containing saline nearer to (black bars) or farther from (gray bars) the soma and either not treated (marked Ca^{2+}) or treated with PEG (+PEG). Dye was immediately added after transection, or PEG washout, and cells maintained in Ca^{2+} -containing saline. C-F: Cells transected nearer to (C,E) or farther from (D,F) the soma in Ca^{2+} -free saline only ("Control" or "PEG") or Ca^{2+} -free saline containing an inhibitor of a molecular sealing pathway. All plates, except Control, were treated with PEG, and dye added immediately after PEG washout. Cells were maintained in Ca^{2+} -free saline (C,D) or Ca^{2+} containing saline (E,F).

Chapter 6 Supplementary Materials and Methods:

Animal Subjects: All experimental procedures were approved by the University of Texas at Austin's Institutional Animal Care and Use Committee.

Our experimental groups are: Crush-severed axons that are treated with MEL+PEG and crush-severed axons treated with MB+PEG. Our control groups and their rationales are: Crush-severed controls treated with MB to examine whether the compound affects any of our three measures of nerve repair. Figure 2 includes data from previous work in our lab to illustrate reliability between studies as well as similar studies conducted by others (see Britt, et al., 2010). Additionally, these data are reported to compare the effects of MB + PEG and MEL + PEG treatments to the application of PEG alone following crush injury of the sciatic nerve.

One set of experimental and control groups totaling 18 adult male Sprague-Dawley rats (250-350 g) received *in vivo* CAP measurements to both sciatic nerves (35 nerves total: 5 sham; 5 crush/ Ca^{2+} -free; 5 crush/ Ca^{2+} -containing; 5 crush+MB+PEG, 5 crush+MEL+PEG, 5 crush+MB, 5 cut +PEG) to assess axonal continuity immediately followed by *in vitro* intra-axonal dye diffusion assessments of axonal continuity (as described in Britt et al., 2010). Another set of experimental and control groups totaling 35 adult male Sprague-Dawley rats (250-350 g) received *in vivo* CAP measurements to assess axonal continuity of one (left) sciatic nerve (35 nerves: 10 crush+MB+PEG; 10 crush+MEL+PEG, 10 crush +MB, 5 cut+PEG) and were examined postoperatively for six weeks using two behavioral tests. All animals were housed in groups of three in

polycarbonate cages with sawdust bedding, maintained on a 12:12 dark:light cycle and given food and water *ad libitum*.

Surgical Procedures: Rats were anesthetized with intraperitoneal injections of ketamine (90 mg/kg) and xylazine (10 mg/kg). An incision about 1.5 cm long was made in the hindlimb posterior-thigh muscles to expose the sciatic nerve. Exposed sciatic nerves were bathed with hypotonic Ca^{2+} -free Krebs's physiological saline containing 0.5 mM EGTA (Ca^{2+} -free saline in mM: 99 NaCl, 5 KCl, 1.2 KH_2PO_4 , 1.3 MgSO_4 , 26 NaHCO_3 , 10 Na ascorbate, 10 dextrose, pH 7.35, 295 milli-osmolar), and cleaned of connective tissue. Animals in the sham-operated group received no nerve injury following exposure of the sciatic nerve *via* incision. The sciatic nerve was bathed with isotonic Ca^{2+} -containing saline (in mM; 124 NaCl, 5 KCl, 1.2 KH_2PO_4 , 1.3 MgSO_4 , 26 NaHCO_3 , 110Na ascorbate, 10 dextrose, 2 CaCl_2 , pH 7.35, 345 milli-osmolar) before closing the incision.

Sciatic crush-severance injuries were made with Dumont # 5 forceps. Experimenters carrying out the crush were blind to the assignment of post-crush treatment to eliminate possibility of bias in the force used to make the crush in the various experimental and control treatments. Following crush injury, the epineural sheath of the sciatic nerve was nicked with microscissors to allow better access of MB, MEL and PEG solutions to axonal tissues.

Experimental animals in groups treated with PEG received a topical application of a 50% solution (w/w) of 2 kD PEG dissolved in distilled water following crush injury. PEG was applied from a micropipette positioned so that the PEG-containing solution

flowed in a narrow stream (about 1 mm wide) over the crushed axons at the lesion site and allowed to bathe the injured nerve for about 1.5 min. Similarly, MB and MEL treatments were given locally to the lesion site via a micropipette. Control animals in the cut + PEG group received a sciatic nerve transection with micro-dissection scissors so that the proximal and distal ends retracted for 1-2 mm and were not re-apposed or further treated, which produced a complete severance of all axons and their epineural sheaths. PEG was then applied to the lesion site between the proximal and distal segments. After assessing CAP conduction (see below), the skin incision was closed with staples in all rats that later received behavioral tests.

As previously reported (Britt et al., 2010) all experimental and control animals used for behavioral testing received a 5 mg/kg subcutaneous injection of ketoprofen after surgery.

Electrophysiological recording of CAPs across a lesion site: As one measure of axonal continuity through a lesion site, conventional *in vivo* extracellular stimulation and recording of CAPs (extracellular recordings of action potentials generated by sciatic nerve axons) was performed for animals (n=18) immediately used to examine morphological continuity by *in vitro* intra-axonal dye diffusion (Lore et al. 1999) as well as for animals (n=35) used to examine behavioral measures of re-innervation specificity for 6 post-operative weeks.

Intra-axonal dye diffusion across a lesion site: To examine intra-axonal diffusion of dye through the lesion site after performing a CAP confirmation assay, we excised a 3-4 cm length of the sciatic nerve (including the lesion site) from each animal

as previously described (Lore et al., 1999; Britt et al., 2010). The proximal end of the sciatic nerve was placed within the Vaseline well containing Ca^{2+} -free saline and 20 μL of hydrophilic dye (Texas red dextran, Molecular Probes). The remainder of the nerve, including the crush site, was bathed in Ca^{2+} -containing saline. For cut+PEG nerves, two Vaseline wells were made; one well contained the proximal end of the nerve bathed in Ca^{2+} -free saline and 20 μL of 15% Texas Red Dextran (Molecular Probes), while the distal segment of the nerve was anchored within the second well such that the transected segments were 1-2 mm apart. The petri dishes containing nerves in Vaseline wells were refrigerated for 14 hours at 4°C, and usually examined for intra-axonal diffusion of fluorescent dye beyond the crush or transection site using a Zeiss ICM-405 inverted fluorescence microscope. Some nerves were imaged using a Leica DM IRBE with a 20X objective outfitted with a Leica DFC350 FX fluorescence camera.

Behavioral tests : Behavioral assessments were performed by experienced testers blind to the treatment condition during the dark portion of each animal's daily light cycle in which rats are more active. Animals were handled daily for seven days prior to the start of behavioral testing. After receiving a CAP continuity assay of their left sciatic nerves, experimental and control groups of rats were behaviorally evaluated at 24, 48, and 72 hours after surgery, and then at weekly post-operative intervals for 6 weeks. Animals were first tested at 24 hours post-operatively to allow animals to recover from anesthesia.

Foot-fault Test: Animals were allowed to roam freely on a wire mesh grid (45 cm x 30 cm, with 2.5 cm x 2.5 cm openings) elevated 1.5 cm above a solid base floor.

Trials for each animal were recorded for 50 total steps per hindlimb. A foot fault was scored when a misstep resulted in the hindlimb falling through an opening in the grid. If the hindlimb misstepped, but was pulled back before touching the floor beneath the grid, the movement was scored as a partial fault and given a fault score of one. A full fault occurred when the animal's hindlimb touched the floor beneath the grid for support. Full faults were given a fault score of two. A composite foot fault asymmetry score was then calculated as previously reported (Britt et al., 2010)

Sciatic Functional Index: Rats were trained to traverse a wooden beam ending in their home cage. After a few habituation trials, during which rats frequently stopped and paused en route to their home cage, rats traversed the beam to the home cage without hesitation. For each trial run, a white strip of paper was secured to the wooden beam to collect footprints (two trials per rat at a given post-operative time). Animals had their injured and uninjured hind paws inked with black and red ink, respectively, and were placed near the end of the wooden beam farthest from the home cage. Three consecutive footprints from each limb (for a total of six consecutive prints) were used to measure (in millimeters) the following: NPL: normal footprint length; EPL: experimental footprint length; NTS: normal toe spread between toes one and five; ETS: experimental toe spread; NIT: normal intermediary toe spread between toes two and four; EIT: experimental intermediary toe spread (Carlton and Goldberg 1986). SFI scores were then computed for each animal at a given post-operative time as previously described (Britt et al., 2010).

B104 cells: B104 cells derived from a CNS neuroblastoma (Bottenstein and Sato, 1979) have often been used as a model system to study neuronal function *in vitro* (Toda,

et al., 1999; Tan, *et al.*, 2003; Yoo, *et al.*, 2003, 2004; Nguyen, *et al.*, 2005; Miller, *et al.*, 2006). These cells have easily identifiable cell bodies and neurites, allowing each precisely transected cell to be uniquely and individually identified (Detrait, *et al.*, 2000b; Yoo, *et al.*, 2003, 2004; Spaeth, *et al.*, 2010). Data on sealing of B104 cells is consistent with similar data on sealing from at least 20 other preparations from many phyla and different cell types *in vitro* and *in vivo* (Spaeth, *et al.*, 2010).

Cell culture: As previously described (Spaeth, *et al.*, 2010), B104 cells were grown in 75cm² vented cap flasks (BD-Falcon, Franklin Lakes, NJ) in a humidified incubator at 37°C in 5% CO₂ in 4 mL of “cell growth media,” which consists of a 1:1 mixture of Dulbecco’s Modified Eagle’s Media and Ham’s F12 (DMEM:F12, HyClone, Logan, UT), supplemented for growth with 10% heat inactivated fetal bovine serum (FBS, Hyclone, Logan, UT) and 1% antibiotics (10,000 Units of Penicillin/mL and 10 mg/mL of streptomycin, Sigma-Aldrich, St. Louis, MO). The cell growth media was changed every 2 days. Cultures were passaged at 80% confluency and cells were then either sub-cultured in a vented cap flask or seeded at approximately 2000 cells/cm² in cell growth media on Petri dishes coated with Poly-D-lysine (Sigma-Aldrich, St. Louis, MO) to prevent cells from detaching during solution changes and/or neurite transections. After 24 hours, the growth media was replaced with serum-free DMEM:F12 (Hyclone, Logan, UT) to allow the B104 cells to differentiate. B104 neurites were transected 24-48 hours after replacing the cell growth media with serum-free DMEM:F12.

Transection of neurites of B104 cells: Prior to transecting neurites, the solution (DMEM:F12) in the Petri dish was washed out twice with a Ca²⁺-free phosphate buffered

saline (referred to as “Ca²⁺-free saline”, PBS -/-, HyClone, Logan, UT). All neurites were transected in Ca²⁺-free saline, unless otherwise noted, using a sharpened, pulled-glass micro-capillary tube ("micro-knife"), which was placed on a micro-manipulator (Narishige Instruments, East Meadow, NY) and quickly drawn across the surface of the Petri dish, etching a score line that showed the path of the knife. We were able to uniquely and individually identify each transected cell by the relation of the transected neurite to its soma and to the score mark on the plate (see Spaeth et al., 2010).

Microscopy and Imaging: For all experiments, B104 cells were observed under an inverted Zeiss ICM-405 fluorescent microscope (Zeiss, West Germany) with a 40X, long focal distance lens. Transected cells were imaged through a hole cut out of the bottom of a plastic dish covered by a thin glass coverslip using a Leica DM IRBE outfitted with a 40x lens and a Leica DFC350 FX fluorescence camera at the UT Core Microscopy facility. Individually identified cells with neurites obviously transected within < 50 μm of the soma were counted as transected “nearer to” the soma, and those with neurites transected at > 50 μm of the soma were counted as transected “farther from” the soma. No further observations were made on any cell whose transection distance was not clearly definable.

Assessment of plasmalemmal sealing: To assess plasmalemmal repair, we transected 10 – 130 uniquely identifiable cells within 10 min in a Petri dish containing Ca²⁺-free saline. The Ca²⁺-free saline was then typically replaced with a phosphate buffered saline containing 1 mM Ca²⁺ (“Ca²⁺-saline”, PBS+/, HyClone, Logan, UT) to initiate the sealing process (Detrait *et al.*, 2000b; Yoo *et al.*, 2003; Spaeth et al., 2010).

The time elapsed after exposing cells to Ca^{2+} -saline is defined as the “post- Ca^{2+} addition time” (PC time).

At various PC times (0-60 min PC), 3kD Texas Red dextran (Molecular Probes, Eugene, OR) was added to the Ca^{2+} -saline to assess the formation of a plasmalemmal seal. For all experiments, the dye was thoroughly washed out with Ca^{2+} -saline after a 10 min exposure to Texas Red dextran and sealing was assessed. Transected cells that excluded Texas Red dextran were counted as “sealed”. Cells that did not exclude Texas Red dextran were counted as “not sealed”. Nearby undamaged cells did not take up Texas Red dextran. We consistently used 3 kDa Texas Red dextran to assess sealing in all other experiments reported herein to avoid any variation in sealing time due to differences in dye molecular weight (Eddleman et al., 2000; Spaeth et al., 2010).

Pharmacological Reagents: All pharmacological agents were added to Ca^{2+} -free saline before neurite transection and were dissolved in distilled water, unless otherwise noted. We used 8 μM Sp-5,6-Dichloro-1- β -D-ribofuranosylbenzimidazole-3',5'-monophosphorothioate, referred to as cBiMPS, (Biomol, Plymouth Meeting, PA; 419.2 Da) to activate PKA. We used 8 μM 8-(4-Chlorophenylthio) -2'-O-methyladenosine-cAMP, referred to as Epac-cAMP (Tocris Biosciences, Ellisville, MO; 507.82 Da) to activate Epac, and di-butyryl cyclic adenosine monophosphate, referred to as db-cAMP (Biomol, Plymouth Meeting, PA; 398 Da) to activate both PKA and Epac. We used TeNT (Biomol, Plymouth Meeting, PA) and BoNT B (BB Tech, Dartmouth, NH) to cleave synaptobrevin. We used BoNT A and E (BB Tech, Dartmouth, NH) to cleave

SNAP-25. We used NEM (Biomol, Plymouth Meeting, PA) to inhibit NSF, and Bref A (Biomol) to reduce trans-Golgi trafficking.

Statistics: Students' t-test was used to assess differences ($p < 0.05$) in pre-operative CAP amplitudes vs. post-operative CAP amplitudes. ANOVA was used to assess differences in SFI and FF asymmetry scores, and Tukey's test was used for post-hoc analysis to adjust for multiple comparisons.

For all cell culture data: At a given PC time, the data was pooled for all cells (n) from all Petri dishes (N) for each experimental treatment group. "Sealing frequency" is defined as the percent of a set of individually-transected and uniquely identified cells that exclude 3 kD Texas Red dye (sealed) at a given PC time. The Cochran-Mantel-Haenszel χ^2 (CMH χ^2) test for independence was used to determine whether the differences between the sealing frequency at a given PC time for different experimental treatments was statistically significant ($p < 0.05$), as previously described (Agresti, 1996; Detrait, *et al.*, 2000b; Yoo, *et al.*, 2003, 2004; Spaeth *et al.*, 2010).

GraphPad Prism was used to fit the sealing frequency for all PC times of a given control or test substance to a one phase exponential equation (Spaeth *et al.*, 2010). The solid and dashed lines on all graphs calculated by GraphPad Prism represent the exponential equations fitted to the sealing frequencies at all PC times for all data sets. The maximum sealing frequency (plateau) was always reached within 60 min PC.

Sealing rate constants (k) were calculated by GraphPad Prism and used to calculate time constants ($\tau = 1/k$) equal to the PC time to achieve 63.2% of the observed maximum (plateau) sealing (Spaeth *et al.*, 2010). Rate or time constants for two

experimental conditions were normalized and compared using Fisher's Z transformation (FZT). Two sealing rate or time constants were considered significantly different if p was <0.05 , using a Z-table. R^2 values were also calculated for the exponential equation defining each time constant to determine how closely the exponential equations modeled the observed data.

Chapter 7: Discussion

In this thesis, I investigated the molecular mechanisms of plasmalemmal sealing, and how an understanding of sealing can lead to behavioral recovery by enhancing PEG-fusion of proximal and distal severed axonal halves *in vivo*.

Plasmalemmal Sealing summary

Following traumatic injury, plasmalemmal sealing (repair) is required for any cell, including neurons, to survive the injury. Since sealing is so important for survival, eukaryotic cells have evolved multiple, redundant pathways to ensure plasmalemmal sealing occurs. In all preparations studied to date (see Supplemental sealing list), plasmalemmal sealing (repair) requires damage induced Ca^{2+} influx leading to an accumulation of vesicles at, or near, the damage site. These vesicles undergo Ca^{2+} -dependent fusion to each other and/or nearby, undamaged membrane to decrease, and eventually restrict, the inward flow of extracellular solution, and the outward flow of cytosol. In addition to the activation of Ca^{2+} -dependent sealing pathways (Spaeth, et al., 2010) plasmalemmal damage also shifts the intracellular reducing potential towards oxidation (Chapter 6). Repair of plasmalemmal damage is critical for survival, and all cells (including neurons) will use any available source of vesicles (Bittner and Fishman, 2003), including those vesicles stimulated by damage-induced cytosolic oxidation (Cai, et al., 2009b). Furthermore, since sealing requires (isoforms of) the same proteins in all preparations investigated, the molecular mechanisms of sealing are likely conserved in all

eukaryotic cells. Plasmalemmal sealing is particularly important for neurons, which do not proliferate as readily as other cell types.

We used the most reliable measure of plasmalemmal repair (dye exclusion) to assay plasmalemmal sealing (Blanchette, et al., 1999; Detrait, et al., 2000a,b). Other measures of sealing, such as intracellular recordings of membrane potential or input resistance (Krause, et al., 1995), vibrating probe measurements of cell currents (Eddelman, et al., 2000), preloading cells with Ca^{2+} sensitive dyes or fluorescence extinction of membrane bound dyes (Togo, 2004, 2006; Cai, et al., 2009b) all have much more ambiguous interpretations as measures of plasmalemmal sealing. Similarly, electron microscopic images in any preparation have insufficient resolution to assess the status of plasmalemmal repair, (Fishman and Bittner, 2003), and the harsh fixative chemicals often destroy most, if not all, membrane bound structures (Bittner lab, unpublished observations).

Since plasmalemmal sealing occurs by an accumulation of intracellular vesicles, larger plasmalemmal disruptions likely seal more slowly than smaller plasmalemmal disruptions. B104 cells provide a method for investigating disruption size, since neurites of B104 cells, similar to other neuronal cell types (Lucas, et al., 1985; 1990), likely decrease in diameter as they extend away from the cell body. Therefore, plasmalemmal disruptions nearer to the soma are larger than plasmalemmal disruptions farther away from the soma. As predicted, nearly all sealing data in B104 cells shows that cells transected nearer to the soma seal at a lower frequency, and slower rate, compared to cells transected farther from the soma. (The only exception is PEG-dependent sealing,

since greater than 90% of cells transected in some [PEG] seal, even before Ca^{2+} is added).

Pathways of plasmalemmal sealing

To date, most sealing studies investigate individual proteins (see Krause, et al., 1994; Steinhardt, et al., 1994; Bi, et al., 1995; Detrait, et al., 2000a,b; Yoo, et al., 2003; Mellgren and Huang, 2006; Mellgren, et al., 2007; Cai, et al., 2009a,b,c). However, none of these reports provide evidence how these pathways interact to produce a plasmalemmal seal. This thesis provides both general (Spaeth, et al., 2010, Chapter 2) and more specific (Chapter 3, 4) models of plasmalemmal sealing based on new data and previous reports of sealing and vesicle trafficking/membrane fusion from various preparations from many different phyla. These data suggest that Ca^{2+} -dependent sealing requires PKA, Epac, cytosolic oxidation, and nPKCs. PKA, Epac, and cytosolic oxidation pathways require (isoforms of) membrane fusion and vesicle trafficking proteins required for neurotransmitter release and Golgi trafficking. [No pathways of PKC-dependent sealing were investigated further.] Furthermore, direct investigation of the phenomena of oxidative dependent sealing, using oxidizing agents and reducing agents/antioxidants, demonstrated for the first time that H_2O_2 increases sealing, but is dependent on Ca^{2+} , SNAP-25, synaptobrevin, NSF, and PKA activity. These data are consistent with the role of cAMP activation of PKA and Epac in vesicle exocytosis and membrane fusion (see Sudhof, 2004; Hochbaum, et al., 2005) and H_2O_2 in vesicle accumulation (Thiels, et al., 2000; Ma, et al. 2010).

Proteins targeted by toxins/inhibitors affect sealing

To investigate pathways of sealing, I first confirmed that specific cleavage of proteins required neurotransmitter release, or Golgi-vesicular trafficking decrease sealing. Specifically, BoNT A/E cleavage of SNAP-25, TeNT/BoNT B cleavage of synaptobrevin, Bref A inhibition of Golgi-vesicular traffic, and NEM inhibition of NSF all decrease, but do not eliminate, plasmalemmal sealing, even when used in combination. These data confirm previous reports that sealing requires (isoforms of) proteins required for neurotransmitter release (SNAP-25, synaptobrevin, NSF) and Golgi-vesicular traffic (Arf1, NSF) (Steinhardt, et al., 1994; Krause, et al., 1994; Bi, et al., 1995; Yoo, et al., 2003; for full list, see Spaeth, et al., 2010 Supplementary List of Sealing references).

The observation that cleavage/inhibition of any of these proteins individually, or in combination, does not completely eliminate sealing is consistent with reports that these toxins/inhibitors do not completely eliminate neurotransmitter release. For example, BoNT A cleavage of SNAP-25, or TeNT cleavage of synaptobrevin, decrease, but cannot completely eliminate, evoked neurotransmitter release (Link, et al., 1992; Chapman, et al., 1994). These data suggest that many redundant pathways act in concert to produce membrane fusion, and inhibition of a protein from one pathway can be overcome, in part, by another pathway (see below). Thus, multiple, redundant pathways exist to ensure sealing occurs.

Part of the remaining sealing in B104 cells following transection in a toxin may also be partly due to the inability of a given toxin to cleave all intracellular target proteins

(Singh, 2000). For example, some SNAP-25 or synaptobrevin may be sequestered in vesicles during constitutive secretion, and are therefore not accessible to neuro-toxins (Chapman, et al., 1994). Additionally, toxin resistant isoforms of membrane fusion proteins, such as TI-vAMP (toxin insensitive vesicle associated membrane protein/synaptobrevin3) (Galli, et al., 2005) may produce some fusion in the presence of a neurotoxin that cleaves synaptobrevin.

NEM inhibition of NSF produces the greatest decrease in sealing, but NEM does not eliminate sealing. These data are also similar to previous data investigating the role of NSF during synaptic transmission (Garcia, et al., 1995) or Golgi-vesicular traffic (Rodriguez, et al., 1994). NSF produces membrane fusion (Babcock, et al., 1998; Kuner, et al., 2007), but is also involved in SNARE disassembly following membrane fusion (Parnas, et al., 2006). Thus, NSF leads to recycling of synaptic vesicle proteins, increasing the efficacy of later fusion events shortly after the first round of vesicle fusion (Hanson, et al., 1995). The decrease in sealing due to NEM inhibition of NSF may therefore also lead to a depletion of available membrane fusion proteins, and therefore less sealing, provided sealing requires many rounds of membrane fusion, as suggested by McNeil and colleagues (2009).

PKA and Epac pathways of sealing

Based on our new model of sealing, following plasmalemmal damage, Ca^{2+} influx increases [cAMP] (Spaeth, et al., 2010), potentially by activating Ca^{2+} -dependent adenylate cyclases (Dunn, et al, 2009). Plasmalemmal damage also leads to cytosolic

oxidation. Increased [cAMP]_i activates PKA and Epac, which have both redundant and independent roles during sealing (Spaeth, et al., 2010; Chap. 3, Figs. 2-5). For example, PKA- and oxidation-dependent sealing require (isoforms of) proteins involved in neurotransmitter release, but not Golgi-vesicular traffic (Chap. 3, Figs. 2-6). Epac-dependent sealing, in contrast, only partly requires (isoforms of) proteins involved in neurotransmitter release, but depends on Golgi-vesicular trafficking (Chap. 3, Figs 2-5). These data are consistent with recent reports suggesting that PKA and Epac pathways have both redundant and independent roles (Borland, et al., 2009). Finally, all three sealing pathways converge on NSF, since NEM blocks all three of these pathways, activated individually or all at the same time. These NEM data are consistent with a role for NSF as one of the last membrane fusion steps required during neurotransmitter release (Kuner, et al., 2007).

The observation that cAMP-dependent sealing requires (isoforms of) proteins required for neurotransmitter release is consistent with the role of cAMP, PKA, and Epac during multiple vesicle trafficking events. cAMP is an important molecule for regulating exocytosis in many preparations, from invertebrates (Yoshihara, et al., 1999, 2000) to mammals (Hatekeyama, et al., 2007) in neuronal (Chierzi, et al., 2005) and non-neuronal preparations (Hatekeyama, et al., 2007). These cAMP stimulated vesicles are then likely used for plasmalemmal sealing. Consistent with a role for cAMP activated PKA and Epac isoforms in plasmalemmal sealing, these proteins also increase exocytosis and membrane fusion during neurotransmitter release (for review, see Sudhof, 2004), large core vesicle exocytosis (Hatakeyama, et al., 2007), granule vesicle exocytosis (Ster, et al.,

2009), insulin exocytosis in pancreatic cells (Kwan, et al, 2007), and the acrosome reaction in spermatozoa (Branham, et al., 2009).

Oxidation-dependent pathways of plasmalemmal sealing

The oxidation-dependent enhancement of sealing requires Ca^{2+} , SNAP-25, synaptobrevin, NSF (Chapter 3), and PKA (Chapter 4). These data suggest that cytosolic oxidation occurs before PKA activation during plasmalemmal sealing. Part of the role of the oxidation-dependent sealing pathway may be to further increase $[\text{Ca}^{2+}]_i$ by releasing intracellular Ca^{2+} stores, since a wide range of $[\text{H}_2\text{O}_2]$ stimulate sarcoplasmic reticulum Ca^{2+} release (Gerich, et al., 2009). H_2O_2 cannot increase sealing in the absence of extracellular Ca^{2+} , however these data are consistent with reports suggesting that intracellular Ca^{2+} is not sufficient to initiate plasmalemmal sealing (Yoo, et al., 2004). These data demonstrating the importance of cytosolic oxidation during plasmalemmal sealing are consistent with previous reports in mouse muscle cells (Cai, et al., 2009a,b,c). Intracellular Ca^{2+} stores may increase an already occurring sealing process by further activating PKA, thus explaining, in part, how H_2O_2 may increase sealing.

Proteins predicted to affect sealing

Based on the models presented in Chapters 2 and 3, other proteins not yet investigated would be predicted to strongly influence plasmalemmal sealing. Some of these proteins and reasons why they are important targets for sealing are described below. Additional proteins that may influence sealing almost certainly exist, however they may

be less critical than some of the proteins presented here. Confirmation of the role of these proteins, and/or the discovery of additional proteins important for sealing may provide clinically relevant pharmacological targets for more quickly repairing plasmalemmal damage, thereby increasing survival of damaged cells, and decreasing the severity of the traumatic injury that produced the plasmalemmal damage.

Syntaxin decreases sealing when cleaved by BonT C1 (Yoo, et al., 2003).

Syntaxin isoforms typically bind SNAP-25 during neurotransmitter release (Chapman, et al., 1994), forming a binding site for synaptobrevin (Sudhof, 1995). Since both SNAP-25 and synaptobrevin are required for PKA and oxidation dependent sealing (Spaeth, et al., 2010) syntaxin is also likely required for PKA and oxidation dependent sealing. Furthermore, since Epac activity partly overcomes SNAP-25 and synaptobrevin cleavage, Epac may also partly overcome syntaxin cleavage.

α -SNAP (soluble N-ethyl maleimide attachment protein) is required for SNARE-dependent membrane fusion in multiple intracellular compartments, including during neurotransmitter release (Hanson, et al., 1995) and Golgi-vesicular traffic (Peter, et al., 1998) following PKA phosphorylation (Hirling and Scheller, 1996). α -SNAP produces membrane fusion by binding to SNARE proteins and NSF (Babcock, et al., 1998), and also by holding syntaxin in the correct conformation for binding to SNAP-25 (Hanson, et al., 1995). Thus, α -SNAP (and related isoforms) are likely important for plasmalemmal sealing.

mUNC/Sec family members are required for membrane fusion in all intracellular compartments, such as Golgi cisternae (Sec 1; Garcia, et al., 1995), granule exocytosis

(mUnc-13; Kwan, et al., 2007), or neurotransmitter release (mUnc-18; Deak, et al., 2009). mUnc/Sec family members drive cAMP-dependent exocytosis. For example, Epac isoforms likely bind to mUnc-13 during insulin secretion (Kwan, et al., 2007), and mUnc-18 is required for Ca^{2+} -dependent, cAMP stimulated, evoked transmitter release (Burgoyne, et al., 2009). In fact, inhibition or genetic deletion of mUnc-18 completely eliminates evoked neurotransmitter release (Burkhardt, et al., 2008), in direct contrast to cleavage/inhibition or deletion of SNAP-25, synaptobrevin, or syntaxin (Sudhof, 2004), which decrease, but do not eliminate, transmitter release. The role of mUnc family members during membrane fusion may be to hold syntaxin in an open conformation until SNAP-25 can bind (Deak, et al., 2009). Thus, without mUnc-18, syntaxin cannot bind SNAP-25, and vesicle bound synaptobrevin cannot bind to the SNAP-25 – syntaxin heterodimer (Rizo, et al., 2005), thereby preventing membrane fusion.

Rab3A/rabphilin may be the central modulators of Ca^{2+} -dependent vesicle exocytosis (see Sudhof, 2004). Rab3A is a vesicle bound GTPase that moves vesicles along the actin cytoskeleton (Branham, et al., 2009). Furthermore, Rab3A activity is increased by Epac activation (Branham, et al., 2009), suggesting that Epac may be a guanine exchange factor (GEF) for Rab3A, as well as the GEF for Rap1 (de Rooij, et al., 1998). Rabphilin is a Rab3A binding protein that increases Rab GTPase activity following PKA phosphorylation (Deak, et al., 2006). Thus, both Epac and PKA may both increase sealing through activating Rab3A.

Intracellular axon guidance: Plasmalemmal sealing likely requires all membrane bound vesicular sources, and thus proteins required for trafficking vesicles and

vesicle bound proteins to the leading edge of axons during growth cone extension may also be involved in sealing. Many proteins required for vesicle trafficking during growth cone extension are activated by cAMP-dependent processes (especially PKA and Epac) (Moore and Kennedy, 2006; Cutinho-Budd, et al., 2008; Shewan and Murray, 2008). For example, intracellular PKA activity determines whether a growth cone will be attracted to, or repelled from, and extracellular cue, such as a semaphorins or netrins (Moore and Kennedy, 2006; Tojima, et al., 2007). PKA leads to growth cone turning via increasing vesicle accumulation towards, or away from, the extracellular cue (Tojima, et al., 2007), and leads to insertion of DCC, an important receptor for growth cone turning, into the plasmalemma (Bouchard, et al., 2004). Epac may have a more prominent role than PKA during growth cone extension (Murray and Shewan, 2008) by activating axonal growth in the absence of PKA activity. Thus, additional proteins required for sealing will likely be found by investigating proteins required for growth cone extension and turning.

Tri-partite Motif (TRIM) proteins increase oxidative-dependent sealing in muscle muscle (Cai, et al., 2009b). Many neuronal TRIM proteins lead to increased vesicle traffic, and are likely candidates for oxidation-dependent vesicle accumulation during plasmalemmal sealing. The most prominent candidate is TRIM72, which increases vesicle accumulation during growth cone extension and turning (Van Diepen, et al., 2005).

Other proteins (cGMP, Galectins) and pathways (oxysterols): Additional oxidation-dependent pathways may also increase vesicle accumulation leading to

plasmalemmal sealing, possibly in synergy with TRIM proteins. We recently demonstrated that a cyclic nucleotide (cAMP) increases sealing (Spaeth, et al., 2010). Other cyclic nucleotides may also influence sealing. MB, in addition to buffering cytosolic oxidation, also inhibits soluble guanylyl cyclase (sGC) activity, thereby decreasing cGMP production. Since MB decreases sealing, cGMP pathways, possibly through PKG, may also be important for sealing. Membrane cholesterol also oxidize, following plasmalemmal damage, forming oxy-sterols, which increase exocytosis in PC12 cells (Ma, et al., 2010). Sugar binding proteins, known as lectins, also become oxidized following traumatic injury (Ignaki, et al., 2000). Galectin1, a canonical lectin family member with broad neuronal expression (Horie, et al., 1999) increases axonal regeneration following traumatic injury in dorsal root ganglion cells from mice or rat (Ignaki, et al., 1999; Horie, et al., 1999, 2004) by stimulating vesicle accumulation at growing axonal ends (Horie, et al., 2004).

Evolutionary origin of proteins required for plasmalemmal sealing

Since eukaryotic cells likely evolved a plasmalemmal membrane before membrane-enclosed organelles (Gerhart and Kirchner, 1997), we suggest that the first evolved role of membrane fusion proteins activated by PKA, Epac, PKC, or cytosolic oxidation was likely to seal plasmalemmal damage. Membrane fusion proteins were likely then co-opted in eukaryotic evolution for use in Golgi trafficking, then growth cone extension and subsequently, as suggested by Südhof and Rothman (2009), for transmitter release. Therefore, a better understanding of the molecular pathways of plasmalemmal

sealing is likely to increase our understanding of vesicle interactions and membrane fusion in the Golgi apparatus, exocytosis, synaptic transmission and growth cone extension.

Role of Plasmalemmal sealing in PEG fusion

Plasmalemmal sealing plays an important role in the rapid repair and reconnection of severed axons by PEG. We bathe crush-severed axons in Ca^{2+} -free saline prior to PEG application, which increases successful PEG-fusion of proximal and distal severed axonal halves (90%) compared to when axons are bathed in Ca^{2+} -containing saline prior to PEG application (40%) (Britt, et al., 2010; Lore, et al., 1999). These data suggest that unsealed axons are easier to PEG-fuse than sealed axons. Additionally, PEG-fusion *in vitro* can be further improved by treating crush- or cut-severed nerves with Melatonin, prior to PEG treatment (Stavisky, et al., 2005). These data are consistent with recent data suggesting that Melatonin decreases plasmalemmal sealing (Spaeth, et al., 2010).

Chapter 5 demonstrates that PEG fusion *in vivo* immediately restores morphological continuity (dye diffusion across the lesion site), electrophysiological ability (as measured by compound action potentials (CAPs) across the lesion site), and improves behavioral function in crush-severed mammalian axons (Britt, et al., 2010). Additionally, PEG fusion rapidly increases behavioral recovery to uninjured levels, and that recovery is maintained for the duration of the testing period (Britt, et al., 2010), demonstrating that PEG may have potential therapeutic use following traumatic nerve injury. These mammalian data are consistent with morphological, electrophysiological,

and behavioral data from invertebrates (Lore, et al., 1999). However, the observed increase in behavioral recovery of crush-severed nerves following PEG treatment did not strictly correlate to the electrophysiological or morphological data. Both CAPs and dye diffusion were observed immediately after PEG treatment, but behavioral recovery took longer to observe (72 hours for the Foot Fault Asymmetry test, 3 weeks for the Sciatic Functional Index).

PEG induced behavioral recovery was enhanced by treating crush-severed sciatic nerves with anti-oxidants that decrease sealing: Methylene Blue (MB) and Melatonin (Mel). These data are consistent with the discovery that treating nerves with Ca^{2+} -free saline prior to crush severance and PEG application significantly increases the success of PEG-fusion (Lore, et al., 1999). Thus, substances that decrease Ca^{2+} -dependent sealing may increase PEG fusion. Increased PEG fusion may account for the increase in CAP amplitude for crush severed nerves treated with MB or Mel prior to PEG application. Furthermore, since plasmalemmal sealing produces cytosolic oxidation (as assessed by MB color change in B104 cells, Chapter 4) which is toxic to neurons, preventing some damage induced cytosolic oxidation may improve survival of all damaged or severed axons within mammalian nerves (Chen, et al., 2009; Rojas, et al., 2009), whether they were PEG-fused, PEG-sealed, or unaffected by PEG.

Some of the observed behavioral recovery following PEG treatment may be due to PEG sealing proximal axonal halves, thereby preventing these axons from dying, and decreasing the distance they need to cover to re-innervate distal muscle targets, as demonstrated in Chapter 6. Furthermore, the PEG sealing data strongly suggest that at

high enough concentrations, PEG may fuse opposing plasmalemmal leaflets without the requirement of membrane fusion proteins, or other pathways of vesicle accumulation (Chapter 6). These data are consistent with data from *in vitro* membrane preparations, where PEG overcomes the activation energy required to fuse opposing membranes together *in vitro*, thereby mimicking membrane fusion *in vivo* (Lee and Lentz, 1998).

Conclusion and potential clinical relevance

Plasmalemmal damage is an inevitable result of traumatic injury, and often leads to cell death if the plasmalemmal hole is not quickly repaired. Repair (sealing) of plasmalemmal damage is particularly important for neurons, which do not proliferate as readily as other cell types, and loss of neurons produces very severe symptoms, such as paralysis, loss of sensation, memory loss, or neuropathic pain (and many others). In this thesis, I provide both a general and specific model for how Ca^{2+} -dependent, vesicle mediated plasmalemmal repair occurs. These models provide potential targets for future clinical studies into ameliorating the effects of plasmalemmal damage.

Traumatic injury to nerves often leads to axonal severance. Using PEG based solutions, proximal and distal axons are rapidly reconnected, which increases behavioral recovery compared to those animals not treated with PEG. Since plasmalemmal repair directly affects PEG fusion, combinatorial treatments of PEG and substances that inhibit sealing (such as MB, or Mel) or increase axon survival (db-cAMP) may further increase behavioral recovery. Future studies will combine PEG and these (and other) substances

to provide clinically relevant methods for rapidly repairing axonal severance and plasmalemmal damage following traumatic injury.

References

- Aebischer P, Guenard V, Valentini RF (1990) The morphology of regenerating peripheral nerves is modulated by the surface microgeometry of polymeric guidance channels. *Brain Res* 531: 211–218.
- Agresti A (1996) An introduction to categorical data analysis, pp 60–64. New York: Wiley.
- Ahkong QF, Desmazes JP, Georgescauld D, Lucy JA (1987) Movements of fluorescent probes in the mechanism of cell fusion induced by poly(ethylene glycol). *J Cell Sci* 88: 389–398.
- Arellano M, Valdivieso MH, Calonge TM, Coll PM, Duran A, Perez P (1999) *Schizosaccharomyces pombe* protein kinase C homologues, pck1p and pck2p, are targets of rho1p and rho2p and differentially regulate cell integrity. *J Cell Sci* 112:3569–3578.
- Atamna H., Nguyen A., Schultz C., Boyle K., Newberry J., Kato H., Ames BN. Methylene blue delays cellular senescence and enhances key mitochondrial biochemical pathways. *FASEB J.* 22(3): 703-712.
- Babcock M., Macleod GT., Leither J., Pallanack L. (2004). Genetic analysis of Soluble N-ethylmaleimide-sensitive factor attachment protein function in *Drosophila* reveals positive and negative secretory roles. *J Neurosci.* 24(16): 3964-3973.
- Bain JR, Mackinnon SE, Hunter DA (1989) Functional evaluation of complete sciatic, peroneal, and posterior tibial nerve lesions in the rat. *Plast Reconstr Surg* 83: 129–136.
- Ballinger ML, Blanchette AR, Krause TL, Smyers ME, Fishman HM, Bittner GD (1997) Delaminating myelin membranes help seal the cut ends of severed earthworm giant axons. *J Neurobiol* 33:945–960.
- Bansal D, Campbell KP (2004) Dysferlin and the plasma membrane repair pathway in muscular dystrophy. *Trends Cell Biol* 14:206–213.
- Bansal D, Miyake K, Vogel SS, Groh S, Chen CC, Williamson R, McNeil PL, Campbell KP. (2003) Defective membrane repair in dysferlin-deficient muscular dystrophy. *Nature.* 423(6936):168-72.
- Barros F, Gómez-Varela D, Vilorio CG, Palomero T, Giráldez T, de la Peña P (2009) Modulation of human erg K⁺ channel gating by activation of a G protein-coupled receptor and protein kinase C. *J Physiol* 511:333–346.

Bejarano E, Carera M, Vega L, Hidalgo J, Velasco A (2006) Golgi structural stability and biogenesis depend on associated PKA activity. *J of Cell Sci* 119, 3764-3774.

Bervar M (2000) Video analysis of standing: an alternative footprint analysis to assess functional loss following injury to the rat sciatic nerve. *J Neurosci Methods* 102:109–116.

Bi GQ, Alderton JM, Steinhardt RA. (1995) Calcium regulated exocytosis is required for cell membrane sealing. *J Cell Biol* 131(6 pt. 2):1747-58

Bi GQ, Morris RL, Liao G, Alderton JM, Scholey JM, Steinhardt RA. (1997) Kinesin- and myosin-driven steps of vesicle recruitment for Ca^{2+} -regulated exocytosis. *J Cell Biol* 138:999–1008

Bittner GD, Ballinger ML, Raymond MA (1986) Reconnection of severed nerve axons with polyethylene glycol. *Brain Res* 367: 351–355.

Bittner GD, Fishman HM (2000a) Axonal sealing following injury. In: Axonal regeneration in the central nervous system (Ingoglia N, Murray M, eds), pp 337. New York: Dekker.

Bittner GD, Schallert T, Peduzzi JD (2000b) Degeneration, trophic interactions and repair of severed axons: a reconsideration of some common assumptions. *Neuroscientist* 6: 88–109.

Blasi J, Chapman ER, Link E, Binz T, Yamasaki S, De Camilli P, Sudhof TC, Niemann H, Jahn R (1993) Botulinum neurotoxin A selectively cleaves the synaptic protein SNAP-25. *Nature* 365(6442): 160-163.

Blanchette AR, Ballinger ML, Fishman HM, Bittner GD (1999) Calcium entry initiates processes that restore a barrier to dye entry in severed earthworm giant axons. *Neurosci Lett* 272:147–150.

Bonanomi D, Rusconi L, Colombo CA, Benfenati F, Valtorta F (2007) Synaptophysin I selectively specifies the exocytic pathway of synaptobrevin 2/VAMP2. *Biochem J* 404:525–534.

Borgens RB, Bohnert D (2001) Rapid recovery from spinal cord injury after subcutaneously administered polyethylene glycol. *J Neurosci Res* 6: 1179–1186.

Borgens RB, Shi R, Bohnert D (2002) Behavioral recovery from spinal cord injury following delayed application of polyethylene glycol. *J Exp Biol* 205: 1–12.

Borland G, Smith BO, Yarwood SJ (2009) EPAC proteins transduce diverse cellular actions of cAMP. *Br J Pharmacol* 158(1):70-86.

Bos JL. (2006). Epac proteins: multi-purpose cAMP targets. *Trends Biochem Sci.* 31(12): 680-686.

Bottenstein JE, Sato GH (1979) Growth of a rat neuroblastoma cell line in serum-free supplemented medium. *Proc Natl Acad Sci USA* 76:514–517.

Bouchard JF., Moore SW., Tritsch NX., Roux PP., Shekarabi M., Barker PA., Kennedy TE. (2004). Protein kinase A activation promotes plasma membrane insertion of DCC from an intracellular pool: A novel mechanism regulating commissural axon extension. *J Neurosci.* 24(12): 3040-3050.

Bozkurt A, Brook GA, Moellers S, Lassner F, Sellhaus B, Weis J, Woeltje M, Tank J, Beckmann C, Fuchs P, Damink LO, Schügner F, Heschel I, Pallua N (2007) In vitro assessment of axonal growth using dorsal root ganglia explants in a novel three-dimensional collagen matrix. *Tissue Eng* 12: 2971–2979.

Bozkurt A, Deumens R, Scheffel J, O'Dey DM, Weis J, Joosten EA, Führmann T, Brook GA, Pallua N (2008) Catwalk gait analysis in assessment of functional recovery after sciatic injury. *J Neurosci Methods* 173: 91–98.

Branham MT, Bustos MA, De Blas GA, Rehmann H, Zarelli VE, Treviño CL, Darszon A, Mayorga LS, Tomes CN (2009) Epac activates the small G proteins Rap1 and Rab3A to achieve exocytosis. *J Biol Chem* 284:24825–24839.

Brennan J.P, Bardswell SC, Burgoyne JR, Fuller W, Schroder E, Wait R, Begum S, Kentish JC, Eaton P (2006) Oxidant-induced activation of Type I protein kinase A is mediated by RI subunit interprotein disulfide bond formation. *J Biol Chem* 281(33): 21827-36.

Britt JM, Kane JR, Spaeth CS, Zuzek A, Robinson GL, Gbanaglo MY, Estler CJ, Boydston EA, Schallert T, Bittner GD (2010) Polyethylene glycol rapidly restores axonal integrity and improves the rate of motor behavior recovery after sciatic crush injury. *J Neurophysiol* 104:695–703.

Bronk P, Deák F, Wilson MC, Liu X, Südhof TC, Kavalali ET (2007) Differential effects of SNAP-25 deletion on Ca^{2+} -dependent and Ca^{2+} -independent neurotransmission. *J Neurophysiol* 98:794–806.

Burdick JA, Ward M, Liang E, Young MJ, Langer R (2006) Stimulation of neurite outgrowth by neurotrophins delivered from degradable hydrogels. *Biomaterials* 3: 452–459.

Burgoyne RD., Barclay JW., Ciufo LF., Graham ME., Handley MTW., Morgan A. (2009). The functions of Munc18-1 in regulated exocytosis. *Ann NY Acad Sci.* 11152:76-86.

Burkhardt P., Hatendorf DA., Weis WI., Fasshaur D. (2008). Munc18a controls SNARE assembly through its interaction with the syntaxin N-peptide. *EMBO.* 27: 923-933.

Cai D, Qiu J, Cao Z, McAtee M, Bregman BS, Filbin MT (2001) Neuronal cyclic AMP controls the developmental loss in ability of axons to regenerate. *J Neurosci* 21:4731–4739.

Cai C, Masumiya H, Weisleder N, Matsuda N, Nishi M, Hwang M, Ko JK, Lin P, Thornton A, Zhao X, Pan Z, Komazaki S, Brotto M, Takeshima H, Ma J (2009a) MG53 nucleates assembly of cell membrane repair machinery. *Nat Cell Biol* 11:56–64.

Cai C, Weisleder N, Ko JK, Komazaki S, Sunada Y, Nishi M, Takeshima H, Ma J (2009b) Membrane repair defects in muscular dystrophy are linked to altered interaction between MG53, caveolin-3 and dysferlin. *J Biol Chem* 284:15894–15902.

Cai C, Masumiya H, Weisleder N, Pan Z, Nishi M, Komazaki S, Takeshima H, Ma J (2009c) MG53 regulates membrane budding and exocytosis in muscle cells. *J Biol Chem* 284(5): 3314-22.

Carlton JM, Goldberg NH (1986) Quantitating integrated muscle function following reinnervation. *Surg Forum* 37: 611–612.

Celsi F, Ferri A, Casciati A, D'Ambrosi N, Rotilio G, Costa A, Volente C, Carri MT (2004) Overexpression of superoxide dismutase 1 protects against Beta-amyloid peptide toxicity: effect of estrogen and copper chelators. *Neurochem Inter* 44: 25-33.

Chakrabarti, S., Kobayshi, KS., Flavell RA., Marks CB., Miyake K., Liston DR., Fowler KT., Gorelick FS., Andrews NW. (2003). Impaired membrane resealing and autoimmune myositis in synaptotagmin VII-deficient mice. *J Cell Biol.* 162(4):543-549.

Chen H., Hung Y., Chen T., Huang S., Wang Y., Lee W., Wu T., Lee E. (2009). Melatonin improves presynaptic protein SNAP-25 expression and dendritic spine density and enhances functional and electrophysiological recovery following transient focal cerebral ischemia in rats. *J Pineal Res.* 47:260-270.

Chapman ER, An S, Barton N, Jahn R (1994) SNAP-25, a t-SNARE which binds to both syntaxin and synaptobrevin via domains that may form coiled coils. *J Biol Chem* 269(44):27427-32.

Chierzi S, Ratto GM, Verma P, Fawcett JW (2005) The ability of axons to regenerate their growth cones depends on axonal type and age, and is regulated by calcium, cAMP and ERK. *Eur J Neurosci* 21:2051–2062.

Cho Y, Shi R, Ivanisevic A, Borgens RB. (2010) Functional silica nanoparticle-mediated neuronal membrane sealing following traumatic spinal cord injury. *J Neurosci Res*. 88(7):1433-44.

Christensen AE, Selheim F, de Rooij J, Dremier S, Schwede F, Dao KK, Martinez A, Maenhaut C, Bos JL, Genieser HG, Døskeland SO (2003) cAMP analog mapping of Epac1 and cAMP kinase. *J Biol Chem* 278:35394–35402.

Circu ML, Moyer MP, Harrison L, Aw TY (2009) Contribution of glutathione status to oxidant-induced mitochondrial DNA damage in colonic epithelial cells. *Free Rad Biol Med* 47:1190–1198.

Coffield JA., Yan X. (2009). Neuritogenic actions of botulinum neurotoxin A on cultured motor neurons. *J Pharmacol Exp Ther*. 330(1): 352-358.

Coutinho-Budd JC., Ezerman EB., Forehand CJ. (2008). The effect of cAMP signaling on the longitudinal extension of spinal sensory neurons in the chicken embryo. *J Anat*. 213: 547-554.

Dalton GD, Dewey WL (2006) Protein kinase inhibitor peptide (PKI): a family of endogenous neuropeptides that modulate neuronal cAMP-dependent protein kinase function. *Neuropeptides* 40:23–34.

Das GD, Wallace RB (1986) *Neural Transplantation and Regeneration*. New York: Springer.

Davies SP, Reddy H, Caivano M, Cohen P (2000) Specificity and mechanism of action of some commonly used protein kinase inhibitors. *Biochem J* 351:95–105.

Deák F, Ok-Ho Shin OH, Tang J, Hanson P, Ubach J, Jahn R, Rizo J, Kavalali ET, Südhof TS (2006) Rabphilin regulates SNARE-dependent re-priming of synaptic vesicles for fusion. *EMBO J* 25:2856–2866.

Dellon ES, Dellon AL (1991) Functional assessment of neurologic impairment: track analysis in diabetic and compression neuropathies. *Plast Reconstr Surg* 88: 686–694.

de Medinaceli L, Freed WJ, Wyatt RJ (1982) An index of the functional condition of rat sciatic nerve based on measurements made from walking tracks. *Exp Neurol* 77: 634–643.

de Rooij, J, Zwartkruis, FJ, Verheijen, MH, Cool, RH, Nijman, SM, Wittinghofer, A, Bos, JL (1998) Epac is a Rap1 guanine-nucleotide exchange factor directly activated by cAMP. *Nature* 396, 474–77

Detrait E, Eddleman CS, Yoo S, Fukuda M, Nguyen MP, Bittner GD, Fishman HM (2000a) Axolemmal repair requires proteins that mediate synaptic vesicle fusion. *J Neurobiol* 44:382–391.

Detrait ER, Yoo S, Eddleman CS, Fukuda M, Bittner GD, Fishman HM (2000b) Plasmalemmal repair of severed neurites of PC12 cells requires Ca^{2+} and synaptotagmin. *J Neurosci Res* 62:566–573.

Ditor DS, John SM, Roy J, Marx JC, Kittner C, Weaver LC (2007) Effects of polyethylene glycol and magnesium sulfate administration on clinically relevant neurological outcomes after spinal cord injury in the rat. *J Neurosci Res* 7: 1458–1467.

Donaldson J, Shi R, Borgens R (2002) Polyethylene glycol rapidly restores physiological functions in damaged sciatic nerves of guinea pigs. *Neurosurgery* 1: 147–156.

Dunn TA, Storm DR, Feller MB (2009) Calcium-dependent increases in protein kinase-A activity in mouse retinal ganglion cells are mediated by multiple adenylate cyclases. *PLoS One* 4:e7877.

Dworkin S., Malaterre J., Hollande F., Darcy PK., Ramsay RG., Mantamadiotis T. (2009). cAMP response element binding protein is required for mouse neural progenitor cell survival and expansion. *Stem Cells*. 27(6):1347-1357.

Eddleman CS, Ballinger ML, Smyers ME, Godell CM, Fishman HM, Bittner GD (1997) Repair of plasmalemmal lesions by vesicles. *Proc Natl Acad Sci U S A* 94:4745–4750.

Eddleman CS, Ballinger ML, Smyers ME, Fishman HM, Bittner GD (1998) Endocytotic formation of vesicles and other membranous structures induced by Ca^{2+} and axolemmal injury. *J Neurosci* 18:4029–4041.

Eddleman CS, Bittner GD, Fishman HM (2000) Barrier permeability at cut axonal ends progressively decreases until an ionic seal is formed. *Biophys J* 79:1883–1890.

Endo H., Nito C., Kamada H., Yu F., Chan PH. (2007). Reduction in oxidative stress by superoxide dismutase overexpression attenuates acute brain injury after subarachnoid

hemorrhage via activation of Akt/glycogen synthase kinase-3 β survival signaling. *J Cereb Blood Flow Metab.* 27(5): 975-82

Enserink JM, Christensen AE, de Rooij J, van Triest M, Schwede F, Genieser HG, Døskeland SO, Blank JL, Bos JL (2002) A novel Epac-specific cAMP analog demonstrates independent regulation of Rap1 and ERK. *Nat Cell Biol* 4:901–906.

Fishman HM, Bittner GD (2003) Vesicle-mediated restoration of a plasmalemmal barrier after axonal injury. *News Physiol Sci* 18:115–118.

Fu SY, Gordon T (1995) Contributing factors to poor functional recovery after delayed nerve repair: prolonged denervation. *J Neurosci* 15: 3876–3885.

Fujimoto K, Shibasaki T, Yokoi N, Kashima Y, Matsumoto M, Sasaki T, Tajima N, Iwanaga T, Seino S (2002) Piccolo, a Ca²⁺ sensor in pancreatic beta-cells: involvement of cAMP-GEFII-Rim2-Piccolo complex in cAMP-dependent exocytosis. *J Biol Chem* 277:50497–50502.

Fujiwara T., Oda K., Yokota S., Takatsuki A., Ikehara Y. (1988). Brefeldin A causes disassembly of the Golgi complex and accumulation of secretory proteins in the endoplasmic reticulum. *J Biol Chem.* 263(34):18545-52.

Galli T, Zahraoui A, Vaidyanathan VV, Raposo G, Tian JM, Karin M, Niemann H, Louvard D (1998) A Novel tetanus neurotoxin-insensitive vesicle associated membrane protein in SNARE complexes of the apical plasma membrane in epithelial cells. *Mol Cell Biol.* 9:1437:1448.

Garcia EP, McPherson PS, Chilcote TJ, Takei K, De Camilli P (1995) rbSec1A and B colocalize with syntaxin 1 and SNAP-25 throughout the axon, but are not in a stable complex with syntaxin. *J Cell Biol* 129:105–120.

Garcia-Fernandez B., Campos I., Geiger J., Santos A.C., Jacinto A. (2009). Epithelial resealing. *International Journal of Developmental Biology*, 8-10, 1549-1556.

Gatlin JC, Estrada-Bernal A, Sanford SD, Pfenninger KH (2006) Myristoylated, alanine-rich C-kinase substrate phosphorylation regulates growth cone adhesion and pathfinding. *Mol Biol Cell* 17:5115–5130.

Gelinas JN., Banko JL., Peters MM., Klann E., Weeber EJ., Nguyen PV. (2008) Activation of exchange protein activated by cyclic-AMP enhances long-lasting synaptic potentiation in the hippocampus. *Learn Mem.* 15(6): 403-411.

Gerhart J, Kirchner M (1997) Cells, embryos and evolution, pp 642. Malden, MA: Blackwell Science.

Gerich FJ, Funke F, Hildebrandt B, Fasshaur M, Muller M (2009) H₂O₂-mediated modulation of cytosolic signaling and organelle function in the rat hippocampus. *Eur J Physiol* 458:937-952.

Gervasi N., Hepp R., Tricoire L., Zhang J., Lambolez B., Paupardin-Tritsch D., Vincent P. (2007). Dynamics of protein kinase A signaling at the membrane, in the cytosol, and in the nucleus of neurons in mouse brain slices. *J Neurosci.* 27(11): 2744-50.

Glantz SB., Amat JA., Rubin CS. (1992). cAMP signaling in neurons: patterns of neurons expression and intracellular localization for a novel protein, AKAP 150, that anchors the regulatory subunit of cAMP-dependent protein kinase II beta. *Mol Biol Cell.* 3(11): 1215-1228.

Godell CM, Smyers ME, Eddleman CS, Ballinger ML, Fishman HM, Bittner GD (1997) Calpain activity promotes the sealing of severed giant axons. *Proc Natl Acad Sci U S A* 94:4751–4756.

Hadlock TA, Heaton J, Cheney M, Mackinnon SE (2005) Functional recovery after facial and sciatic nerve crush injury in the rat. *Arch Facial Plast Surg* 1: 17–20.

Han R, Bansal D, Miyake K, Muniz VP, Weiss RM, McNeil PL, Campbell KP. (2007) Dysferlin-mediated membrane repair protects the heart from stress-induced left ventricular injury. *J Clin Invest.* 117(7):1805-13

Hannila SS, Filbin MT (2008) The role of cyclic AMP signaling in promoting axonal regeneration after spinal cord injury. *Exp Neurol* 209:321–332.

Hanson PI., Otto H., Barton N., Jahn R. (1995). The N-ethylmaleimide-sensitive fusion proteins and α -SNAP induce a conformational change in syntaxin. *J Biol Chem.* 270(28): 16955-16961.

Hare GM, Evans PJ, Mackinnon SE, Best TJ, Bain JR, Szalai JP, Hunter DA (1992) Walking track analysis: a long-term assessment of peripheral nerve recovery. *Plast Reconstr Surg* 2: 251–258.

Hatakeyama H, Takahashi N, Kishimoto T, Nemoto T, Kasai H (2007) Two cAMP pathways differentially regulate exocytosis of large dense core and small vesicles in mouse β cells. *J Physiol* 582:1087–1098.

Hayashi T, McMahon H, Yamasaki S, Binz T, Hata Y, Sudhof TC, Niemann H (1994) Synaptic vesicle membrane fusion complex: action of clostridial neurotoxins on assembly. *EMBO J.* 13(21):5051-5061.

Herbert CB, Bittner GD, Hubbell JA (1996) Effects of fibrinolysis on neurite growth from dorsal root ganglia cultured in two- and three-dimensional fibrin gels. *J Comp Neurol* 365: 381–391.

Hernandez TD, Schallert T (1988) Seizures and recovery from experimental brain damage. *Exp Neurol* 102: 318–324.

Hochbaum D, Hong K, Barila G, Ribeiro-Neto F, Altschuler DL (2008) Epac, in synergy with cAMP-dependent protein kinase (PKA), is required for cAMP-mediated mitogenesis. *J Biol Chem* 283:4464–4468.

Holz GG., Kang G., Harbeck M., Row MW., Chepurny OG. (2006). Cell physiology of the cAMP sensor Epac. *J Physiol.* 577(1): 5 - 15.

Horie H, Inagaki Y, Sohma Y, Nozawa R, Okawa K, Hasegawa M, Muramatsu N, Kawano H, Horie M, Koyama H, Sakai I, Takeshita K, Kowada Y, Takano M, & Kadoya T. (1999). Galectin-1 regulates initial axonal growth in peripheral nerves after axotomy. *Journal of Neuroscience.* 19(22), 9964-9974.

Horie H, Kadoya T, Hikawa N, Sango K, Inoue H, Takeshita K, Asawa R, Hiroi T, Sato M, Yoshioka T, Ishikawa Y (2004) Oxidized Galectin-1 stimulates macrophages to promote axonal regeneration in peripheral nerves after axotomy. *J Neurosci* 24(8):1873-1880

Hucho TB., Dina OA., Levine JD. Epac mediates a cAMP-to-PKC signaling in inflammatory pain: an isolectin B4(+) neuron-specific mechanism. *J Neurosci.* 25(26): 6119-6126.

Idone V, Tam C, Andrews NW. (2008). Two-way traffic on the road to plasma membrane repair. *Trends in Cell Biology*, 11, 552-559.

Ignaki Y, Sohma Y, Horie H, Nozawa R, Kadoya T (2000) Oxidized galectin-1 promotes axonal regeneration in peripheral nerves but does not possess lectin properties. *Eur J Biochem* 267(10): 2955-64.

Ingoglia N, Murray M (2001) Axonal Regeneration in the Central Nervous System. New York: Marcel Dekker.

Jenq CB, Coggeshall RE (1986) The effects of an autologous transplant on patterns of regeneration in rat sciatic nerve. *Brain Res*364: 45–56.

Kadoya T, Horie H (2005) Structural and functional studies of Galectin-1: a novel axonal regeneration promoting activity for oxidized Galectin-1. *Curr Drug Targets* 6(4):375-83.

Kalbermatten DF, Pettersson J, Kingham PJ, Pierer G, Wiberg M, Terenghi G (2009) New fibrin conduit for peripheral nerve repair. *J Reconstr Microsurg*1: 27–33.

Kandel ER, Schwartz JH, Jessel T (1991) Principles of neural science, Ed 3. New York: McGraw-Hill.

Kantor TG (1986) Ketoprofen: a review of its pharmacologic and clinical properties. *Pharmacotherapy*6: 93–103.

Kleim JA, Jones TA, Schallert T (2003) Motor enrichment and the induction of plasticity before and after brain injury. *Neurochem Res*28: 1757–1769.

Knapp LT., Klann E. (2002). Potentiation of hippocampal synaptic transmission by superoxide requires the oxidative activation of protein kinase C. *22*(3): 674-683.

Koob AO, Colby JM, Borgens RB (2008) Behavioral recovery from traumatic brain injury after membrane reconstruction using polyethylene glycol. *J Biol Eng*2: 1–9.

Korshunova I, Novitskaya V, Kiryushko D, Pedersen N, Kolkova K, Kropotova E, Mosevitsky M, Rayko M, Morrow JS, Ginzburg I, Berezin V, Bock E (2007) GAP-43 regulates NCAM-180 mediated neurite outgrowth. *J Neurochem* 100:1599–1612.

Krause TL, Bittner GD (1990) Rapid morphological fusion of severed myelinated axons by polyethylene glycol. *Proc Natl Acad Sci USA*87: 1471–1475.

Krause TL, Marquis RM, Lyckman AW, Ballinger ML, Bittner GD (1991) Rapid artificial restoration of electrical continuity across a crush lesion of a giant axon. *Brain Res*561: 350–353.

Krause TL, Fishman HM, Ballinger ML, Bittner GD (1994) Extent and mechanism of sealing in transected giant axons of squid and earthworms. *J Neurosci* 14:6638–6651.

Krause TL, Magarshak Y, Fishman HM, Bittner GD. (1995) Membrane potential and input resistance are ambiguous measures of sealing of transected cable-like structures. *Biophys J.* 68(3):795-9.

Kuner T, Li Y, Gee KR, Bonewald LF, Augustine GJ (2007) Photolysis of a caged peptide reveals rapid action of N-ethylmaleimide sensitive factor before neurotransmitter release. *PNAS* 105(1): 347-352.

Kwan EP, Xie L, Sheu L, Ohtsuka T, Gaisano HY (2007) Interaction between Munc13–1 and RIM is critical for glucagon-like peptide-1 mediated rescue of exocytotic defects in Munc13–1 deficient pancreatic beta-cells. *Diabetes* 56:2579–2588.

Lago N, Rodriguez FJ, Guzman MS, Jaramillo J, Navarro X (2007) Effects of motor and sensory nerve transplants on amount and specificity of sciatic nerve regeneration. *J Neurosci Res* 12: 2800–2812.

Lassot I, Robbins I, Kristiansen M, Rahmeh R, Jaudon F, Magiera MM, Mora S, Vanhille L, Lipkin A, Pettmann B, Ham J, & Desagher S (2010). Trim17, a novel E3 ubiquitin-ligase, initiates neuronal apoptosis. *Cell Death and Differentiation* 17(12):1928-41

Lee KY, Chung K, & Chung JM (2010) Involvement of reactive oxygen species in long term potentiation of spinal cord dorsal horn. *Journal of Neurophysiology* 103(1), 382-391.

Lee JK., Lentz BR. (1998). Secretory and viral fusion may share mechanistic events with fusion between curved lipid bilayers. *PNAS*. 95: 9274-9279.

Lennon, N. J., Kho, A., Bacskai, B. J., Perlmutter, S. L., Hyman, B. T. and Brown, R. H., Jr (2003). Dysferlin interacts with annexins A1 and A2 and mediates sarcolemmal wound-healing. *J. Biol. Chem.* 278, 50466-5047.

Lichstein JW, Ballinger ML, Blanchette AR, Fishman HM, Bittner GD (2000) Structural changes at cut ends of earthworm giant axons in the interval between dye barrier formation and neuritic outgrowth. *J Comp Neurol* 416:143–157.

Link E, Edelmann L, Chou JH, Binz T, Yamasaki S, Eisel U, Baumert M, Sudhof TC, Niemann H, Jahn R (1992) Tetanus toxin action: inhibition of neurotransmitter release linked to synaptobrevin proteolysis. *Biochem Biophys Res Commun* 189(2):1017-1023.

Liu C, Takahashi M, Yanping L, Song S, Dillon TJ, Shinde U, Stork PJS (2008) Ras is required for the cyclic AMP-dependent activation of Rap1 via Epac2. *Mol Cell Biol* 28(32):7109-7125.

Liu XF, Xie X, Miki T (2006) Inhibition of protein kinase C zeta blocks the attachment of stable microtubules to kinetochores leading to abnormal chromosome alignment. *Cell Signal* 18:2314–2323.

Lore AB, Hubbell JA, Bobb DS Jr., Ballinger ML, Loftin KL, Smith JW, Smyers ME, Garcia HD, Bittner GD (1999) Rapid induction of functional and morphological continuity between severed ends of mammalian or earthworm myelinated axons. *J Neurosci* 19: 2442–2454.

Loewy AD, Schader RE (1977) A quantitative study of retrograde neuronal changes in Clarke's column. *J Comp Neurol* 171:65–81.

Lucas JH, Gross GW, Emery DG, Gardner CR (1985) Neuronal survival or death after dendrite transection close to the perikaryon: correlation with electrophysiologic, morphologic, and ultrastructural changes. *Cent Nerv Syst Trauma* 2:231–255.

Lucas JH, Emery DG, Higgins ML, Gross GW (1990) Neuronal survival and dynamics of ultrastructural damage after dendrotomy in low calcium. *J Neurotrauma* 7:169–192.

Ma, M, Zhang J, Akhlaq, AF, Chen P, Ong, W (2010) Effects of cholesterol oxidation products on exocytosis. *Neurosci. Lett* 476:36-41.

Mackinnon SE, Dellon AL, O'Brien JP (1991) Changes in nerve fibre numbers distal to a nerve repair in the rat sciatic model. *Muscle Nerve* 14: 1116–1122.

Mackinnon SE, Dellon AL, O'Brien JP, Goldberg N, Hunter DA, Seiler WA 4th., Carlton J (1989) Selection of optimal axon ratio for nerve regeneration. *Ann Plast Surg* 23: 129–134.

Marzullo TC, Britt J, Stavisky RC, Bittner GD (2002) Cooling enhances in vitro survival fusion-repair of severed axons taken from the peripheral and central nervous systems of rats. *Neurosci Lett* 327: 9–12.

McLean J, Batt J, Doering LC, Rotin D, Bain JR (2002) Enhanced rate of nerve regeneration and directional errors after sciatic nerve injury in receptor protein tyrosine phosphatase knock-out mice. *J Neurosci* 22: 5481–5491.

McNeil A, McNeil PL. (2005) Yolk granule tethering: a role in cell resealing and identification of several protein components. *J Cell Sci.* 118(Pt 20):4701-8.

McNeil AK, Rescher U, Gerke V, McNeil PL. (2006) Requirement for annexin A1 in plasma membrane repair. *J Biol Chem.* 281(46):35202-7.

McNeil P (2009) Membrane repair redux: redox of MG53. *Nat Cell Biol* 11(1):7-9

McNeil PL, Vogel SS, Miyake K, Terasaki M. (2000). Patching plasma membrane disruptions with cytoplasmic membrane. *J Cell Sci.* 113 (Pt 11):1891-902.

Mellgren RL, Zhang W, Miyake K, McNeil PL (2007) Calpain is required for the rapid, calcium-dependent repair of wounded plasma membrane. *J Biol Chem* 282:2567–2575.

Mellgren RL, Huang X (2007) Fetuin A stabilizes m-calpain and facilitates plasma membrane repair. *J Biol Chem*. 282(49):35868-77

Mellgren RL, Miyake K, Kramerova I, Spencer MJ, Bourg N, Bartoli M, Richard I, Greer PA, McNeil PL. (2009). Calcium-dependent plasma membrane repair requires m- or mu-calpain, but not calpain-3, the proteasome, or caspases. *Biochimica and Biophysica Acta*, 12, 1886-1893.

Menegon A, Bonanomi D, Albertinazzi C, Lotti F, Ferrari G, Kao HT, Benfenati F, Baldelli P, Valtorta F (2006) Protein kinase A-mediated synapsin I phosphorylation is a central modulator of Ca²⁺-dependent synaptic activity. *J Neurosci* 26:11670–11681.

Millán-Plano S, Piedrafita E, Miana-Mena FJ, Fuentes-Broto L, Martínez-Ballarín E, López-Pingarrón L, Sáenz MA, García JJ (2010) Melatonin and structurally-related compounds protect synaptosomal membranes from free radical damage. *Int J Mol Sci* 11:312–328.

Miller MW, Mooney SM, Middleton FA (2006) Transforming growth factor β 1 and ethanol affect transcription and translation of genes and proteins required for cell adhesion molecules in B104 neuroblastoma cells. *J Neurochem* 97:1182–1190.

Miyake K, McNeil PL (1995) Vesicles accumulate and exocytosis is induced at sites of plasma membrane disruption. *J Cell Biol* 131:1737–1745

Miyake K, McNeil PL, Suzuki K, Tsunoda R, Sugai N. (2001) An actin barrier to resealing. *J Cell Sci*. 2001 Oct;114(Pt 19):3487-94.

Miyake K, Tanaka T, McNeil PL. (2006). Disruption-induced mucus secretion: repair and protection. *PLoS Biol*. 4(9):e276.\

Moore SW., Kennedy TE. (2006). Protein kinase A regulates the sensitivity of spinal commissural axon turning to netrin-1 but does not switch between chemoattraction and chemorepulsion. *J Neurosci*. 26(9): 2419-2423.

Morgans C, Brandstatter JH (2000) SNAP-25 is present on the Golgi apparatus of retinal neurons. *NeuroReport* 11(117):85-88.

Murray AJ, Shewan DA (2008) Epac mediates cyclic AMP-dependent axon growth, guidance and regeneration. *Mol Cell Neurosci* 38:578–588.

- Nagy G, Reim K, Matti U, Brose N, Binz T, Rettig J, Neher E, Sørensen JB (2004) Regulation of releasable vesicle pool sizes by protein kinase A-dependent phosphorylation of SNAP-25. *Neuron* 41:417–429.
- Nebenfuhr A, Ritzenhaler C, Robinson DG (2002) Brefeldin A: Deciphering an enigmatic inhibitor of secretion. *Plant Phys* 130:1102-1108.
- Nehrt A, Haman K, Ouyang H, Shi (2010) Polyethylene glycol enhances axolemmal resealing following transection in cultured cells and in ex vivo spinal cord. *J Neurotrauma* 27:151–161.
- Nehrt A, Rodgers R, Shapiro S, Borgens R, Shi R. (2007) The critical role of voltage-dependent calcium channel in axonal repair following mechanical trauma. *Neuroscience*. 146(4):1504-12
- Nguyen MP, Bittner GD, Fishman HM (2005) Critical interval of somal calcium transient after neurite transection determines B104 cell survival. *J Neurosci Res* 81:805–816.
- Niimura M, Miki T, Shibasaki T, Fujimoto W, Iwanaga T, Seino S (2009) Critical role of the N-terminal cyclic AMP binding domain of Epac2 in its subcellular location and function. *J Cell Physiol* 219:652-658.
- Olyer GA., Higgins GA., Hart RA., Battenberg E., Billingsley M., Bloom FE., Wilson MC. (1989). The identification of a novel synaptosomal-associated protein, SNAP-25, differentially expressed by neuronal subpopulations. *J Cell Biol.* 109(6): 3039-52.
- Paclik D, Lohse K, Wiedenmann B, Dignass AU, Sturm A. (2008). Galectin-2 and -4, but not galectin-1, promote intestinal epithelial wound healing in vitro through a TGF-beta-independent mechanism. *Inflammatory Bowel Disease*, 10, 1366-1372.
- Parnas I, Rashkovan G, O'Connor V, El-Far O, Betz H, Parnas H (2006) Role of NSF in neurotransmitter release: a peptide microinjection study at the crayfish neuromuscular junction. *J Neurophys* 96:1053-1060.
- Peter F., Wong SW., Subramaniam VN., Tang BL., Hong W. (1998). A-SNAP, but not γ -SNAP, is required for ER-Golgi transport after vesicle budding and the Rab1-requiring step, but before the EGTA-sensitive step. *J Cell Sci.* 111: 2625-2633.
- Qiu J, Cai D, Dai H, McAtee M, Hoffman PN, Bregman BS, Filbin MT (2002) Spinal axon regeneration induced by elevation of cyclic AMP. *Neuron* 34:895–903.
- Radogna F., Nuccitelli S., Mengoni F., Ghibelli L. (2009) Neuroprotection by melatonin on astrocytoma cell death. *Ann. N.Y. Acad. Sci.* 1171, 509-513.

Ramón y, Cajal S (1928) Estudios sobre la degeneración y regeneración del sistema nervioso (Degeneration and Regeneration of the Nervous System), translated from Spanish by May RM. London: Oxford Univ. Press; original Spanish version (2 volumes), 1913–1914.

Reddy A, Caler EV, Andrews NW (2001) Plasma membrane repair is mediated by Ca^{2+} -regulated exocytosis of lysosomes. *Cell* 106:157–169.

Rizo J., Chen X., Arac D. (2005). Unraveling the mechanisms of synaptotagmin and SNARE function in neurotransmitter release. *TRENDS in Cell Biol.* 16(7): 339-350.

Rodriguez L, Stirling CJ, Woodman PG (1994) Multiple N-ethylmaleimide-sensitive components are required for endosomal vesicle fusion. *Mol Biol Cell* 5:773-783.

Rojas JC., Simola N., Kermath BA., Kane JR., Schallert T.,Gonzalez-Lima F. (2009) Striatal neuroprotection with methylene blue. *Neurosci.* 163(3): 877-889.

Saito K, Miyake K, McNeil PL, Kato K, Yago K, Sugai N. (1999). Plasma membrane disruption underlies injury of the corneal endothelium by ultrasound. *Exp Eye Res.* 68(4):431-7.

Schapire A.L., Valpuesta V., Botella M.A. (2009). Plasma membrane repair in plants. *Trends in Plant Science*, 14,12,645-652.

Shaik GM, Dráberová L, Heneberg P, Dráber P. (2009). Vacuolin-1-modulated exocytosis and cell resealing in mast cells. *Cell Signaling*, 8,1337-1345.

Schallert T, Whishaw IQ, Ramirez VD, Teitelbaum P (1978) Compulsive, abnormal walking caused by anticholinergics in akinetic, 6-hydroxydopamine-treated rats. *Science* 4336:1461–1463.

Schallert T, Fleming SM, Bland ST (2000) Functional recovery after brain injury: role of neurotrophic factors and behavior-driven structural events. In: *Pharmacology of Cerebral Ischemia*, edited by Krieglstein J, Klumpp S. Stuttgart, Germany: Medpharm Scientific Publishers, p. 329–344.

Schallert T, Woodlee MT, Fleming SM (2002) Disentangling multiple types of recovery from brain injury. In: *Pharmacology of Cerebral Ischemia*, edited by Krieglstein J, Klumpp S. Stuttgart, Germany: Medpharm Scientific Publishers, p. 201–216.

Schallert T (2006) Behavioral tests for preclinical intervention assessment. *NeuroRx*3: 497–504.

Schlaepfer WW (1973) Effects of nerve constriction on oxygenated excised segments of rat peripheral nerve. *J Neuropathol Exp Neurol* 32:203–217.

Schlaepfer WW, Bunge RP (1973) Effects of calcium ion concentration on the degeneration of amputated axons in tissue culture. *J Cell Biol* 59:456–470.

Schweizer FE, Dresbach T, DeBello WM, O'Connor V, Augustine GJ, Betz H (1998) Regulation of neurotransmitter release kinetics by NSF. *Science* 279:1203–1206.

Sedj S, Rose T, Rupnik M (2005) cAMP increase Ca^{2+} -dependent exocytosis through both PKA and Epac2 in mouse melanotrophs from pituitary slices. *J Physiol* 567:799–813.

Sehrawat S., Cullere X., Patel S., Italiano J Jr., Mayadas TN. (2008). Role of Epac1, an exchange factor for Rap GTPases in endothelial microtubule dynamics and barrier function. *83(4): 972-981.*

Shen SS., Steinhardt RA (2005). The mechanisms of membrane resealing in rabbit corneal epithelial cells. *Curr Eye Res.* 30(7):543-54.

Shen SS., Tucker WC., Chapman ER., Steinhardt RA. (2005). Molecular regulation of membrane resealing in 3T3 fibroblasts. *J Biol Chem.* 280(2): 1652-1660.

Shi R, Borgens RB (1999) Acute repair of crushed guinea pig spinal cord by polyethylene glycol. *J Neurophysiol* 81:1572–1580.

Shi R, Borgens RB. (2001) Anatomical repair of nerve membranes in crushed mammalian spinal cord with polyethylene glycol. *J Neurocytol.* 29(9):633-43.

Singh BH (2000) Intimate details of the most poisonous poison. *Nature Struct Biol* 7(8):671–620.

Sisková Z, Baron W, de Vries H, Hoekstra D (2006) Fibronectin impedes "myelin" sheet-directed flow in oligodendrocytes: a role for a beta 1 integrin-mediated PKC signaling pathway in vesicular trafficking. *Mol Cell Neurosci* 33:150–159.

Sivasankaran R, Pei J, Wang KC, Zhang YP, Shields CB, Xu XM, He Z (2004) PKC mediates inhibitory effects of myelin and chondroitin sulfate proteoglycans on axonal regeneration. *Nat Neurosci* 7:261–268.

Sollner T., Whiteheart SW., Brunner M., Erdjument-Bromage H., Geromanos S., Tempst P., Rothman JE. (1993). SNAP receptors implicated in vesicle targeting and fusion. *Nature.* 362: 318-324.

- Spaeth CS, Boydston EA, Figard LR, Zuzek A, Bittner GD (2010). A model for sealing plasmalemmal damage in neurons and other eukaryotic cells. *J Neurosci* 30(47):15790-15800.
- Spira ME, Benbassat D, Dormann A (1993) Resealing of the proximal and distal cut ends of transected axons: electrophysiological and ultrastructural analysis. *J Neurobiol* 24:300–316.
- Stavisky RC, Britt JM, Zuzek A, Truong E, Bittner GD (2005) Melatonin enhances the in vitro and in vivo repair of severed sciatic axons. *Neurosci Lett* 382: 98–101.
- Steinberg SF (2008) Structural basis of protein kinase C isoform function. *Physiol Rev* 88:1341–1378.
- Steinhardt RA, Bi G, Alderton JM (1994) Cell membrane resealing by a vesicular mechanism similar to neurotransmitter release. *Science* 263:390–393.
- Ster J, de Bock F, Bertaso F, Abitbol K, Daniel H, Bockaert J, Fagni L (2009) Epac mediates PACAP-dependent long-term depression in the hippocampus. *J Physiol* 587:101–113.
- Südhof TC, Rothman JE (2009) Membrane fusion: grappling with SNARE proteins. *Science* 323:474–477.
- Tan ZY, Chen J, Shun HY, Feng XH, Ji YH (2003) Modulation of BmK AS, a scorpion neurotoxic polypeptide, on voltage-gated Na⁺ channels in B104 neuronal cell line. *Neurosci Lett* 340:123–126.
- Tanji K, Kamitani T, Mori F, Kakita A, Takahashi H, & Wakabayashi K (2010) TRIM9, a novel brain-specific E3 ubiquitin ligase, is repressed in the brain of Parkinson's disease and dementia with Lewy bodies. *Neurobiological Disorders* 38(2), 210-218.
- Tao-Cheng JH, Du J, McBain CJ (2000) Snap-25 is polarized to axons and abundant along the axolemma: an immunogold study of intact neurons. *J Neurocytol* 29:67–77.
- Taylor SS., Kim C., Vigil D., Haste NM., Yang J., Wu J., Anand GS. (2005) Dynamics of signaling by PKA. *Biochem Biophys Acta*. 1745(1-2): 25-37.
- Taylor SS., Radzio-Andzelm E., Hunter T. (1995) How do protein kinases discriminate between serine/threonine and tyrosine? Structural insights from the insulin receptor protein-tyrosine kinase. *FASEB J*. 9(13): 1255-1266.

Terasaki M, Miyake K, McNeil PL (1997) Large plasma membrane disruptions are rapidly resealed by Ca^{2+} -dependent vesicle-vesicle fusion events. *J Cell Biol* 139: 63–74.

Thiels E, Urban NN, Gonzalez-Burgos GR, Kanterewicz BI, Barrionuevo G, Chu CT, Oury TD, & Klann E. (2000). Impairment of long-term potentiation and associative memory in mice that overexpress extracellular superoxide dismutase. *Journal of Neuroscience* 20(20), 7631-7639.

Toda M, Shirao T, Uyemura K (1999) Suppression of an actin-binding protein, drebrin, by antisense transfection attenuates neurite outgrowth in neuroblastoma B104 cells. *Brain Res Dev Brain Res* 114:193–200.

Togo T, Alderton JM, Bi GQ, Steinhardt RA. (1999) The mechanism of facilitated cell membrane resealing. *J Cell Sci.* 112 (Pt 5):719-31.

Togo T, Krasieva TB, Steinhardt RA. (2000) A decrease in membrane tension precedes successful cell-membrane repair. *Mol Biol Cell.* 11(12):4339-46.

Togo T, Alderton JM, Steinhardt RA (2003) Long-term potentiation of exocytosis and cell membrane repair in fibroblasts. *Mol Biol Cell* 14:93–106.

Togo T (2004) Long term potentiation of wound-induced exocytosis and plasma membrane repair is dependent on cAMP-response element-mediated transcription via a protein kinase C- and p38 MAPK-dependent pathway. *J Biol Chem* 279(43):44996:5003.

Togo T (2006) Disruption of the plasma membrane stimulates rearrangement of microtubules and lipid traffic toward the wound site. *J. Cell Sci* 119(13): 2780:2786.

Tojima T., Akiyama H., Itofusa R., Li Y., Katayama H., Miyawaki A., Kamiguchi H. (2007). Attractive axon guidance involves asymmetric membrane transport and exocytosis in the growth cone. *Nat Neurosci.* 10(1): 58-66.

Tsai SY, Yang LY, Wu CH, Chang SF, Hsu CY, Wei CP, Leu SJ, Liaw J, Lee YH, Tsai MD (2007) Injury-induced Janus kinase/protein kinase C-dependent phosphorylation of growth-associated protein 43 and signal transducer and activator of transcription 3 for neurite growth in dorsal root ganglion. *J Neurosci Res* 85:321–331.

Tsao JW, George EB, Griffin JW (1999) Temperature modulation reveals three distinct stages of Wallerian degeneration. *J Neurosci* 19: 4718–4726.

Uberall F, Giselsbrecht S, Hellbert K, Fresser F, Bauer B, Gschwendt M, Grunicke HH, Baier G (1997) Conventional PKC- α , novel PKC- ϵ and PKC- θ , but not

atypical PKC-lambda are MARCKS kinases in intact NIH 3T3 fibroblasts. *J Biol Chem* 272:4072–4078.

van Diepen MT, Spencer GE, van Minnen J, Gouwenberg Y, Bouwman J, Smit AB, van Kesteren RE (2005) The molluscan RING-finger protein L-TRIM is essential for neuronal outgrowth. *Mol Cell Neurosci* 29:74–81.

Vikman J., Svensson H., Huang YC., Kang Y., Andersson SA., Gaisano HY., Eliasson L. (2009). Truncation of SNAP-25 reduces the stimulator action of cAMP on rapid exocytosis in insulin secreting cells. *Am J Physiol Endocrinol Metab.* 297(2): E452-61.

Waller A (1850) Experiments on the section of the glossopharyngeal and hypoglossal nerves of the frog, and observations of the alterations produced thereby in the structure of their primitive fibres. *Philos Trans R Soc Lond B Biol Sci* 140: 423–439.

Wu C, Chun-Fai L, Mobley C (2001) Nerve Growth factor activates persistent Rap1 signaling in Endosomes. *J of Neurosci* 21(15):5405-5416.

Xie XY, Barrett JN. (1991) Membrane resealing in cultured rat septal neurons after neurite transection: evidence for enhancement by Ca^{2+} -triggered protease activity and cytoskeletal disassembly. *J Neurosci.* 11(10):3257-67.

Yamazaki T, Kawamura Y, Minami A, Uemura M. (2008). Calcium-dependent freezing tolerance in *Arabidopsis* involves membrane resealing via synaptotagmin SYT1. *Plant Cell*, 12,3389-3404.

Yawo H, Kuno M (1985). Calcium dependence of membrane sealing at the cut end of the cockroach giant axon. *J Neurosci* 5:1626 –1632

Yang H, Preston M, Chopp M, Jiang F, Zhang X, Schallert T (2006) Mass-related traumatic tissue displacement and behavior: a screen for treatments that reduce harm to bystander cells and recovery of function. *J Neurotrauma* 23: 721–732.

Yoo S, Nguyen MP, Fukuda M, Bittner GD, Fishman HM (2003) Plasmalemmal sealing of transected mammalian neurites is a gradual process mediated by Ca^{2+} -regulated proteins. *J Neurosci Res* 74:541–551.

Yoo S, Bottenstein JE, Bittner GD, Fishman HM (2004) Survival of mammalian B104 cells following neurite transection at different locations depends on somal Ca^{2+} concentration. *J Neurobiol* 60:137–153.

Yoshihara M, Ueda A, Zhang D, Deitcher DL, Schwarz TL, Kidokoro Y (1999) Selective effects of neuronal-synaptobrevin mutations on transmitter release evoked by sustained versus transient Ca^{2+} increases and by cAMP. *J Neurosci* 19:2432–2441.

Yoshihara M, Suzuki K, Kidokoro Y (2000) Two independent pathways mediated by cAMP and protein kinase A enhance spontaneous transmitter release at *Drosophila* neuromuscular junctions. *J Neurosci* 20:8315–8322.

Vita

Christopher Spaeth was born in Allentown, PA, and attended Southern Lehigh High school. Upon graduation, he attended Villanova University, located in the suburbs of Philadelphia, earning a Bachelor's degree in Comprehensive Science and a minor in Russian Language. While attending Villanova, he worked in the lab of Dr. Randy Strich at Fox Chase Cancer Center, where he became interested in intracellular signaling pathways. In August of 2004, he entered graduate school at the University of Texas at Austin.

Permanent address: 3355 Blackburn Street, Dallas, Texas 75204

This dissertation was typed by the author.